



National Library
of Canada

Bibliothèque nationale
du Canada

Canadian Theses Service

Service des thèses canadiennes

Ottawa, Canada
K1A 0N4

NOTICE

The quality of this microform is heavily dependent upon the quality of the original thesis submitted for microfilming. Every effort has been made to ensure the highest quality of reproduction possible.

If pages are missing, contact the university which granted the degree.

Some pages may have indistinct print, especially if the original pages were typed with a poor typewriter ribbon or if the university sent us an inferior photocopy.

Previously copyrighted materials (journal articles, published tests, etc.) are not filmed.

Reproduction in full or in part of this microform is governed by the Canadian Copyright Act, R.S.C. 1970, c. C-30.

AVIS

La qualité de cette microforme dépend grandement de la qualité de la thèse soumise au microfilmage. Nous avons tout fait pour assurer une qualité supérieure de reproduction.

S'il manque des pages, veuillez communiquer avec l'université qui a conféré le grade.

La qualité d'impression de certaines pages peut laisser à désirer, surtout si les pages originales ont été dactylographiées à l'aide d'un ruban usé ou si l'université nous a fait parvenir une photocopie de qualité inférieure.

Les documents qui font déjà l'objet d'un droit d'auteur (articles de revue, tests publiés, etc.) ne sont pas microfilmés.

La reproduction, même partielle, de cette microforme est soumise à la Loi canadienne sur le droit d'auteur, SRC 1970, c. C-30.

THE UNIVERSITY OF ALBERTA

A STUDY OF THE IMPACT OF INSTABILITY ON THE IMMISCIBLE DISPLACEMENT
OF ONE FLUID BY ANOTHER

by

HEMANTA KUMAR SARMA

A THESIS

SUBMITTED TO THE FACULTY OF GRADUATE STUDIES AND RESEARCH

IN PARTIAL FULFILMENT OF THE REQUIREMENTS FOR THE DEGREE

OF DOCTOR OF PHILOSOPHY

IN

PETROLEUM ENGINEERING

DEPARTMENT OF MINING, METALLURGICAL AND PETROLEUM ENGINEERING

EDMONTON, ALBERTA

SPRING, 1988

Permission has been granted to the National Library of Canada to microfilm this thesis and to lend or sell copies of the film.

The author (copyright owner) has reserved other publication rights, and neither the thesis nor extensive extracts from it may be printed or otherwise reproduced without his/her written permission.

L'autorisation a été accordée à la Bibliothèque nationale du Canada de microfilmer cette thèse et de prêter ou de vendre des exemplaires du film.

L'auteur (titulaire du droit d'auteur) se réserve les autres droits de publication; ni la thèse ni de longs extraits de celle-ci ne doivent être imprimés ou autrement reproduits sans son autorisation écrite.

ISBN 0-315-42950-X

THE UNIVERSITY OF ALBERTA

RELEASE FORM

NAME OF AUTHOR

HEMANTA KUMAR SARMA

TITLE OF THESIS

A STUDY OF THE IMPACT OF INSTABILITY ON THE
IMMISCIBLE DISPLACEMENT OF ONE FLUID BY
ANOTHER

DEGREE FOR WHICH THESIS WAS PRESENTED DOCTOR OF PHILOSOPHY

YEAR THIS DEGREE GRANTED SPRING, 1988

Permission is hereby granted to THE UNIVERSITY OF ALBERTA LIBRARY
to reproduce single copies of this thesis and to lend or sell such copies for private,
scholarly or scientific research purposes only.

The author reserves other publication rights, and neither the thesis nor extensive
extracts from it may be printed or otherwise reproduced without the author's written
permission.

(SIGNED) 

PERMANENT ADDRESS:

Maripur Anandapur

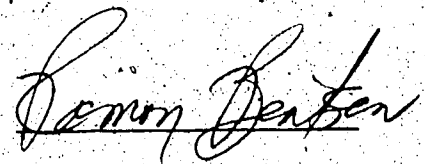
P.O. NITYANANDA - 781-329

Dist.: Barpeta, Assam, India

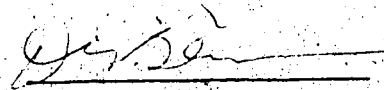
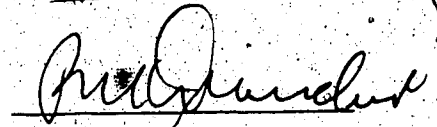
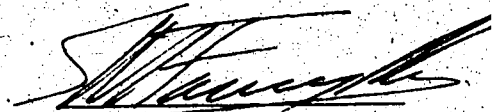
DATED March 28, 1988.

THE UNIVERSITY OF ALBERTA
FACULTY OF GRADUATE STUDIES AND RESEARCH

The undersigned certify that they have read, and recommend to the Faculty of Graduate Studies and Research, for acceptance, a thesis entitled "A Study of the Impact of Instability on the Immiscible Displacement of One Fluid by Another" submitted by Hemanta Kumar Sarma in partial fulfilment of the requirements for the degree of Doctor of Philosophy in Petroleum Engineering.



Supervisor



External Examiner

Date March 28, 1988.

TO
MY PARENTS,

AND

THE EVER SMILING, ENERGETIC AND ENTHUSIASTIC LITTLE ONES

ABSTRACT

Recovery efficiency is dependent upon whether a displacement is stable or unstable. A modified stability theory, which takes into account a linear time function, is presented in this study. The modified theory is validated by comparing theoretical results with those obtained experimentally. It is demonstrated that the modified theory predicts correctly the stability boundary, and it is shown that the theory can be used to predict the breakthrough recovery for both stable and pseudostable displacements.

Accurate estimates of relative permeability are dependent upon the functional forms used to fit the experimental data. Appropriate functional forms for cumulative-oil and pressure-drop histories have been postulated by taking proper account of the constants of integration for the two differential equations describing the system. These functional forms have been validated by using them to fit the experimental data acquired in this study.

The external-drive method has been validated by comparing it with the steady-state method. Further validation of the method is undertaken by measuring the saturation and pressure gradients at the outlet end of the core and comparing these values with those predicted using external-drive theory. Moreover, dynamic capillary pressures measured during the course of a displacement are compared with those measured under equilibrium conditions for the same sand-fluid system.

Because of the rapid changes in saturation which take place in the immediate vicinity of a displacement front, it is not possible to estimate relative permeabilities over the entire saturation range of interest when using the external-drive method. It is demonstrated that this limitation can be removed, if data from an unstabilized and/or unstable displacement are used. Further, it is shown that use of such data is permissible, provided: (i) saturation profiles and pressure gradients in both phases can be measured directly, (ii) the external-drive theory is modified to account for the existence of capillary pressure gradients, and (iii) the analysis is carried out from a Lagrangian rather than an Eulerian point of view. Relative permeability curves obtained over the entire range of saturation of interest by using this method are presented for both unstabilized and unstable runs.

ACKNOWLEDGEMENTS

I wish to express my sincere gratitude and thanks to Dr. Ramón G. Bentsen, under whose supervision this study was carried out. Thanks are also due to: Dr. Donald L. Flock, who made numerous suggestions and made available some of the equipment needed for this study, Dr. S.M. Farouq Ali and Prof. P.M. Dranchuk for various suggestions and discussions during the course of study.

Special thanks are extended to Mrs. Barbara Bentsen, who painstakingly reviewed the manuscript at various stages of its preparation. Technical support received from Messrs Robert (Bob) Smith, Robert Stefaniuk, Jacques Gibeau, John Czuroski, and Doug Booth during the course of this study, is thankfully acknowledged.

I also wish to express my appreciation to the Natural Sciences and Engineering Research Council of Canada and to the Alberta Oil Sands Technology and Research Authority for the financial assistance which made this study possible. Moreover, thanks are extended to Imperial Oil Limited for providing the oils used in this study.

Last but not least, very special thanks and gratitude to the members of my family, and relatives, whose constant encouragement, good wishes and, sacrifices have immensely contributed towards the successful culmination of this study. I must also thank my wife, Madhumita, who joined me towards the end of this study, and shared with me the moments of joy, happiness, and most important, the moments of frustration, agony and stress. Their understanding and patience have been always my source of encouragement.

H.K.S.

Table of Contents

Chapter		Page
1.	INTRODUCTION	1
2.	LITERATURE REVIEW	4
2.1	Stability Studies	4
2.2	Stabilization	9
2.3	Relative Permeabilities	12
2.3.1	Steady-State Method	13
2.3.2	External-Drive Method	13
2.3.3	Lagrangian Approach	15
2.3.4	Dynamic Method	16
2.3.5	Effects of Capillary and Viscous Forces	16
2.3.6	Relative-Permeability Hysteresis	20
2.4	Capillary Pressure	21
2.4.1	Laboratory Methods to Measure Capillary Pressure	21
2.4.1.1	Restored-State Method	22
2.4.1.2	Mercury-Injection Method	23
2.4.1.3	Centrifuge Method	23
2.4.1.4	Dynamic Method of Capillary Pressure	24
2.4.2	Capillary Pressure Hysteresis	24
2.5	Microwave Theory	25
2.5.1	Dielectric Behaviour	26
3.	STATEMENT OF THE PROBLEM AND OBJECTIVES	28
4.	THEORY	30
4.1	Modification of Stability Theory	30
4.1.1	Introduction	30
4.1.2	Capillary Pressure Potential	31
4.1.3	Macroscopic Capillary Pressure	32

4.1.4	Equation for Pseudosurface	36
4.1.5	Perturbation Velocities	37
4.1.6	Time Function	38
4.1.7	Compatibility Conditions	41
4.1.8	Velocity of Penetrating Fingers	43
4.1.9	Most Probable Finger Width	44
4.1.10	Stability Criterion	46
4.1.10.1	Pseudointerfacial Tension	47
4.1.11	Breakthrough Recovery	47
4.1.11.1	Stable Displacements	47
4.1.11.2	Pseudostable Displacements	48
4.2	Stabilization	49
4.3	Estimation of Relative Permeabilities	50
4.3.1	Introduction	50
4.3.2	Basic Equations	50
4.3.3	Estimation of Fractional Flow and Saturation	51
4.3.4	Reciprocal Mobility	53
4.4	Cumulative Oil Recovery	55
4.5	Time to Breakthrough	55
4.6	Maximum Time	56
4.7	Lagrangian Method for Estimating Relative Permeabilities	57
4.7.1	Introduction	57
4.7.2	Basic Equations	58
4.7.3	Reciprocal Mobility	59
4.7.4	Fractional Flow	60
4.8	Distance Travelled by a Particular Saturation	61
4.9	Estimation of Water Saturations During Waterflood	62

5.	EXPERIMENTAL EQUIPMENT, MATERIALS AND PROCEDURE	65
5.1	Equipment	65
5.1.1	Stability Experiments	65
5.1.2	Relative Permeability and Capillary Pressure Experiments	65
5.1.2.1	Interface System	69
5.1.2.2	Microwave Instrumentation	71
5.2	Materials	74
5.3	Experimental Procedure	74
5.3.1	Stability Experiments	74
5.3.2	Relative Permeability and Capillary Pressure Experiments	77
6.	EXPERIMENTAL RESULTS	79
6.1	Validation of the Modified Stability Theory	79
6.1.1	Introduction	79
6.1.2	Results	86
6.1.2.1	Stability Boundary	86
6.1.2.2	Breakthrough Recovery	87
6.2	Estimation of Relative Permeabilities Using the External-Drive Technique	91
6.2.1	Introduction	91
6.2.2	Data Analysis	91
6.2.3	Results	95
6.2.4	Discussion of Results	100
6.2.4.1	Jones-Roszelle Data	100
6.2.4.2	Miller Data	104
6.2.4.3	Run 62	105
6.3	Further Validation of the External-Drive Technique	106
6.3.1	Introduction	106
6.3.2	Data Analysis	108

6.3.3	Results	108
6.3.4	Discussion of Results	116
6.3.4.1	Saturation Profiles	116
6.3.4.2	Saturations at Outlet End	116
6.3.4.3	Material Balance	119
6.3.4.4	Capillary Pressure Data	119
6.3.4.5	Reciprocal Mobility	120
6.3.4.6	Relative Permeability Curves	122
6.3.4.7	Buckley-Leverett Saturation Profiles	122
6.4	Lagrangian Method for Estimating Relative Permeabilities	123
6.4.1	Introduction	123
6.4.2	Data Analysis	123
6.4.3	Results	125
6.4.4	Discussion of Results	134
6.4.4.1	Saturation Profiles	134
6.4.4.2	Capillary Pressure Data	139
6.4.4.3	Pressure Gradients	140
6.4.4.4	Stabilization	142
6.4.4.5	Relative Permeability Curves	146
6.5	Unstable Displacements	147
6.5.1	Introduction	147
6.5.2	Results	147
6.5.3	Discussion of Results	159
6.5.3.1	Saturation Profiles	159
6.5.3.2	Fractional Flow Curves	165
6.5.3.3	Capillary Pressure Curves	166
6.5.3.4	Relative Permeability Curves	166

6.5.3.5 Impact of Instability	168
7. SUMMARY AND CONCLUSIONS	171
7.1 Modification of Stability Theory and Its Experimental Verification	171
7.2 Estimation of Relative Permeabilities Using the External-Drive Technique	172
7.3 Lagrangian Method for Estimating Relative Permeabilities	174
7.4 Validation of Concepts of Relative Permeability and Capillary Pressure for Unstable Displacements	175
7.5 Suggestions for Future Study	176
REFERENCES	178
APPENDIX A: Derivation of Equation Describing the Pseudosurface Separating Oil From Water	186
APPENDIX B: Functional Equations Used to Fit Data	188
APPENDIX C: Programs for Data Acquisition, Retrieval and Interpretation	193
APPENDIX D: Program to Evaluate Saturation at the Front, S_{wf}	220
APPENDIX E: Typical Routine for Use of BMDP Statistical Package	222

List of Tables

Table	Page
1. Physical Dimensions of Coreholders	67
2. Porosities and Absolute Permeabilities of Sandpacks	75
3. Fluid Properties @ 21°C	76
4. Predicted Breakthrough Recoveries as Functions of Initial Oil-in-Place	80
5. Displacement Data for LAGO Displacements ($M=2.53$)	81
6. Displacement Data for MCT-5 + LAGO Displacements ($M=4.06$)	82
7. Displacement Data for MCT-5 Displacements ($M=8.13$)	83
8. Displacement Data for MCT-10 Displacements ($M=29.72$)	84
9. Summary of Core Data	96
10. Parameters Obtained From Fitting of Cumulative-Oil Recovery Data	97
11. Parameters Obtained From Fitting of Pressure Function	98
12. Comparison of Observed and Calculated Breakthrough Time, K_{wor} and S_{or}	99
13. Summary of Experimental Data (Run 63)	107
14. Fluid Properties @ 21°C for Run 63	121
15. Summary of Experimental Data (Run 64)	126
16. Summary of Experimental Data (Runs 65 - 67)	148
B.1 Parameters for Q_w versus S_w Fit (Run 64)	189
B.2 Parameters for P_o versus x Fit (Run 64)	189
B.3 Parameters for f_w versus S_w Fit	190
B.4 Parameters for K_{ro} versus S_w Fit	191
B.5 Parameters for K_{rw} versus S_w Fit	192

List of Figures

Figure	Page
1. Schematic Diagram of Experimental Equipment (Stability Experiments)	66
2. Schematic Diagram of Experimental Equipment (Relative Permeability and Capillary Pressure Experiments)	68
3. Schematic Diagram of Microwave Instrumentation	72
4. Breakthrough Recovery As A Function Of Instability Number	85
5. Cumulative-Oil History and Reciprocal Mobilities (Run 62)	92
6. Estimation of Breakthrough Point from Fluid Recovery Data (Run 62)	94
7. Relative Permeability Curves for Oil and Water (Jones-Roszelle Data)	101
8. Relative Permeability Curves for Oil and Water (Miller Data)	102
9. Relative Permeability Curves for Oil and Water (Run 62)	103
10. Dynamic Saturation Profiles During a Stable Displacement (Run 63)	109
11. Comparison of Measured and Predicted S_{w2} (Run 63)	111
12. Comparison of N_p Determined from Weighing and Microwave Scan	112
13. Capillary Pressure-Saturation Curve (Run 63)	112
14. Comparison of Measured and Predicted Reciprocal Mobility at the Outlet End (Run 63)	114
15. Comparison of Relative Permeabilities Using P_o and P_w (Run 63)	115
16. Comparison of Measured and Predicted Saturation Profiles (Run 63)	117
17. Dynamic Saturation Profiles During an Unstabilized Waterflood (Run 64)	127
18. Water Saturation versus Time at the Midpoint of the Core (Run 64)	128
19. Capillary Pressure-Saturation Curve for an Unstabilized Run (Run 64)	130
20. Pressure Gradient along the Core at Time 1020 seconds (Run 64)	131
21. Reciprocal Mobility versus Displacement Time at the Midpoint of the Core (Run 64)	132
22. Volume of Injected Water, $Q_w(S_w)$, versus Time for Various Values of S_w (Run 64)	133
23. f_w versus S_w during an Unstabilized Waterflood @880 and 1020 seconds (Run 64)	135
24. Comparison of f_w versus S_w Curves Obtained Using the Lagrangian and the	

Eulerian Approach (Run 64)	136
25. Comparison of Measured and Predicted Saturation Profiles at Time = 1020 seconds for an Unstabilized Displacement (Run-64)	137
26. Relative Permeability Curves Using Lagrangian and Eulerian Approaches (Run 64)	138
27. Dynamic Saturation Profiles during an Unstable Displacement (Run 65)	149
28. Dynamic Saturation Profiles during an Unstable Displacement (Run 66)	150
29. Dynamic Saturation Profiles during an Unstable Displacement (Run 67)	151
30. Average Slope of Saturation Profiles as Function of the Ratio of Capillary Number to Mobility Ratio	153
31. Average Slope of Saturation Profiles as a Function of the Instability Number	154
32. Residual Oil Saturation as a Function of the Reciprocal Capillary Number	155
33. Fractional Flow Curves for Runs 63 and 65 Using Water - MCT-5 System	156
34. Fractional Flow Curves for Runs 66 and 67 Using Water - MCT-10 System	157
35. Capillary Pressure-Saturation Curves for Different Flow Regimes for Water-MCT-5 System	158
36. Capillary Pressure-Saturation Curves for for Water-MCT-10 System	160
37. Relative Permeability Curves for Runs 63 and 65 Using Water - MCT-5 System	161
38. Relative Permeability Curves for Unstable Runs Using Water-MCT-10 System (Runs 66 and 67)	162
39. Comparison of Relative Permeabilities Obtained by Using Lagrangian and Eulerian Methods (Run 66)	163

NOMENCLATURE

a_o, a_w	initial amplitude of disturbance for oil and water fingers, respectively, m [ft]
a_2, a_3, a_4, a_5	parameters in the functional form equation for cumulative oil production history
A	cross-sectional area of core, m ² [ft ²]
A_c	area under capillary pressure curve, kPa [psi]
A_{ls}	lump sum absorbance due to core material, sand and oil
A_T	total absorbance
A_{sw}	surface area of water finger, m ² [ft ²]
A_w	absorbance due to water
b	width of porous medium, m [ft]
b_2, b_3, b_4, b_5	parameters in the functional form equation for average reciprocal mobility
b_w	width of a water finger, m [ft]
c	velocity of light, m/s [ft/sec]
c_1, c_2, c_3, c_4	parameters in the functional form equation for volume of injected water
\bar{c}	solution concentration
C, C_x, C_y	arbitrary constants of proportionality in x- and y-directions
$C(M)$	constant of proportionality as defined by Equation 137
d_1, d_2, d_3, d_4	parameters in the functional form equation for pressure in the oil phase
D_x, D_y	arbitrary constants of proportionality in x- and y-directions
e_1, e_2, e_3, e_4	parameters in the functional form equation for relative permeability to water
f	frequency of microwave signals, Hz
f_o, f_w	fractional flow to oil and water, respectively

f_{o2}, f_{w2}	fractional flow to oil and water at the outlet, respectively
F_w	non-capillary fractional flow to water as defined by Buckley-Leverett theory
g	acceleration due to gravity, m/s^2 [ft/sec ²]
g_1, g_2, g_3, g_4	parameters in the functional form equation for fractional flow of water
h	thickness of porous medium, m [ft]
h_1, h_2, h_3, h_4	parameters in the functional form equation for relative permeability to oil
h_w	thickness of a water finger, m [ft]
I_o	incident microwave power, mW
I_{sr}	dimensionless velocity (instability number) for rectangular system
I_x	attenuated microwave power after traversing a distance x , mW
\bar{k}	absorption coefficient
k	absolute permeability, m^2 [d]
k_e	extinction coefficient
k_o	effective permeability to oil, m^2 [darcy]
k_{oiw}	permeability to oil at connate water saturation, m^2 [d],
k_{ro}	relative permeability to oil
k_{rw}	relative permeability to water
k_w	effective permeability to water, m^2 [darcy]
k_{wor}	permeability to water at residual oil saturation, m^2 [d],
L	length of porous medium, m [ft]
m_1, m_2	mode numbers: 0, 1, 2, 3, ...
M	endpoint mobility ratio
N_c	capillary number
N_g	gravitational number
N_p	cumulative oil production, m^3 [ft ³]

n_w	time constant, sec ⁻¹
p	pressure, kPa [psi]
p_o	pressure in oil phase, kPa [psi]
p_w	pressure in water phase, kPa [psi]
P_c	macroscopic capillary pressure, kPa [psi]
$P_c(t)$	microscopic capillary pressure, kPa [psi]
$(P_{co})_w$	macroscopic capillary pressure in the region where water is flowing, kPa [psi]
$(P_{cw})_o$	macroscopic capillary pressure in the region where oil is flowing, kPa [psi]
$(P_{cw})_{oe}$	equilibrium macroscopic capillary pressure in the region where oil is flowing, kPa [psi]
q	volumetric injection rate, m ³ /s [cu ft/sec]
Q_i	pore volumes of displacing fluid injected
Q_w	volume of injected water defined by Equation 120, m ³ [ft ³]
R_{bt}	breakthrough recovery, fraction of initial oil-in-place
R_{sw}	the rate at which new surface is being created, m ² /s [ft ² /sec]
r_{th}	average macroscopic mean radius, m [ft]
S_{or}	residual oil saturation
S_w	water saturation
S_w^*	specific water saturation
\bar{S}_w	average water saturation
S_{w2}	water saturation at outlet end
S_{wi}	initial water saturation
t	real time, sec
t^*	specific time, sec
t_a	time of arrival at the midpoint of the core
t_{bt}	breakthrough time of displacing fluid at the outlet end, sec

t_m	maximum time required to displace total recoverable oil, sec
T_{1v}	vertical component of force (tension) in x-direction, N.m [lbf-ft]
T_{2v}	vertical component of force (tension) in y-direction, N.m [lbf-ft]
v	superficial velocity, m/s [ft/sec]
\vec{v}_o	oil superficial velocity vector, m/s [ft/sec]
V_p	pore volume of the sandpack, m ³ [ft ³]
$(v_{wm}^*)_o$	velocity at which the tip of water finger is propagating, m/s [ft/sec]
$(v_{om}^*)_w$	velocity at which the tip of oil finger is propagating, m/s [ft/sec]
v_{ox}, v_{oy}, v_{oz}	x, y, and z components in oil superficial velocity vector, respectively, m/s [ft/sec]
$(v_{ox}^*)_w, (v_{oy}^*)_w, (v_{oz}^*)_w$	oil steady-state perturbation velocities in the x, y, and z directions, respectively, in the region where water is flowing, m/s [ft/sec]
v_{wfa}	actual velocity of a water finger, m/s [ft/sec]
v_{wx}, v_{wy}, v_{wz}	x, y, and z components in water superficial velocity vector, respectively, m/s [ft/sec]
V_w	volume of water finger, m ³ [ft ³]
v_{wa}	average rate at which water crosses the base of a water finger, m/s [ft/sec]
\vec{v}_w	water superficial velocity vector, m/s [ft/sec]
$(v_{wx}^*)_o, (v_{wy}^*)_o, (v_{wz}^*)_o$	water steady-state perturbation velocities in the x, y, and z directions, respectively, in the region where water is flowing, m/s [ft/sec]
x, y, z	components of rectangular coordinates, m [ft]
W	weight of the fluids produced at the outlet end, kg [lb]
X	distance travelled by a given saturation, m [ft]
X_o	location where fingering commenced, m [ft]
α	angle core makes with vertical, radians [degrees]

α_x, α_y	separation constants in x and y directions, respectively, m^{-1} [ft $^{-1}$]
α_{xw}, α_{yw}	separation constants in x direction for oil and water regions, respectively, m^{-1} [ft $^{-1}$]
β_w	constant of proportionality
γ	wave number of eigenvalue, m^{-1} [ft $^{-1}$]
γ_c	characteristic eigenvalue for which capillary and gravity forces exactly balance viscous forces, m^{-1} [ft $^{-1}$]
γ_m	eigenvalue for which new surface is being created at the greatest rate, m^{-1} [ft $^{-1}$]
γ_{mi}	eigenvalue for which new surface for an incipient finger is being created at the greatest rate, m^{-1} [ft $^{-1}$]
γ_o, γ_w	eigenvalues for oil and water regions, respectively, m^{-1} [ft $^{-1}$]
$(\eta_w)_o$	function for the surface of a water finger in the region where only water is flowing, as defined by Equation 46, m [ft]
ξ	displacement of any point on the surface of a finger, m [ft]
θ	contact angle, radians [degrees]
λ^{-1}	reciprocal mobility, Pa.s/m 2 [atm.sec/ft 2]
λ_2^{-1}	reciprocal mobility at the outlet end of the core; Pa.s/m 2 [atm.sec/ft 2]
$\bar{\lambda}_2^{-1}$	average reciprocal mobility at the outlet end of the core, Pa.s/m 2 [atm.sec/ft 2]
$\bar{\lambda}_{2m}^{-1}$	average reciprocal mobility at outlet end of the core at $t = t_m$, Pa.s/m 2 [atm.sec/ft 2]
ξ	function for the surface of a finger, m [ft]
$(\xi_o)_w$	function for the surface of an oil finger in the region where water is flowing, as defined by Equation 24, m [ft]
$(\xi_w)_o$	function for the surface of a water finger in the region where oil is flowing, as defined by Equation 23, m [ft]

μ_o, μ_w	oil and water viscosities, respectively, poise
ρ	density, kg/m^3 [g/cm^3]
ρ_o, ρ_w	oil and water densities, respectively, kg/m^3 [g/cm^3]
σ	interfacial tension, mN/m [dyne/cm]
σ_e	pseudointerfacial tension, mN/m [dyne/cm]
τ	dimensionless time, defined as $\tau = \frac{q t}{A \phi L (1 - S_{wi} - S_{or})}$
ϕ	porosity, fraction
Φ	force potential, N.m/kg [lbf-ft/lbm]
Φ_c	capillary potential for water, N.m/kg [lbf-ft/lbm]
Φ_o, Φ_w	force potentials for oil and water, respectively, N.m/kg [lbf-ft/lbm]
$(\Phi_{cw})_o$	capillary potential for water in the region where only oil is flowing, N.m/kg [lbf-ft/lbm]
$(\Phi_{co})_w$	capillary potential for oil in the region where only water is flowing, N.m/kg [lbf-ft/lbm]
$(\Phi_o)_o$	oil force potential in region where only oil is flowing, N.m/kg [lbf-ft/lbm]
Φ_{oi}	initial value of the potential in oil on the oil side of the surface, N.m/kg [lbf-ft/lbm]
$(\Phi_o)_w$	oil force potential in region where only water is flowing, N.m/kg [lbf-ft/lbm]
$(\Phi_w)_o$	water force potential in region where only oil is flowing, N.m/kg [lbf-ft/lbm]
$(\Phi_w)_w$	water force potential in region where only water is flowing, N.m/kg [lbf-ft/lbm]
$(\Phi_w^*)_w$	perturbation potential for water in region where only water is flowing, N.m/kg [lbf-ft/lbm]

$(\Phi_w)_o$

perturbation potential for water in region where only oil is flowing.

N.m/kg [lbf-ft/lbm]

Φ_{wi}

initial value of the potential in water on the water side of the surface, N.m/kg [lbf-ft/lbm]

\rightarrow

vector notation

∇

gradient operator

1. INTRODUCTION

Despite the current crisis in the oil industry, which arose because of short term over-supply problems, most analysts believe that the crisis is temporary, and that oil prices will rise again. Also, most experts believe that a crude oil shortage will occur in the 1990s because most major oilfields have already reached their peak level of primary production, and because few new major discoveries have been reported in recent times. Therefore, they warn the oil-importing nations not to take comfort in their current lower energy bills because the crisis is temporary.

Notwithstanding current low oil prices and improved conservation measures, the amount of money Canada spends on imported oil is enormous. And unless new discoveries are found or production from existing fields is increased, Canada's oil import bill will become prodigious in the future, should oil prices rise again. Therefore, exploratory activities to discover new fields should be intensified even though such activities often involve high capital risk and uncertainties; and, even if successful, development of new fields may take an unusually long period to pay dividends. Meanwhile, parallel intensive efforts should be made towards improving recovery of oil from known fields as each one-percent cent increase in recovery from existing fields adds about four billion barrels of recoverable reserves. The strategy should be to intensify exploration activities by providing various tax incentives to the industry, and by maximizing the efficient recovery of existing reserves by adopting various research and development and cost saving measures. Thus, a generally expanded research effort in the area of enhanced oil recovery (EOR) processes may pay large dividends, and could push Canada closer to energy self-sufficiency.

However, the successful design and field implementation of any EOR technique involving the displacement of one fluid by another demands that we come to a better understanding of the displacement mechanisms involved within porous media. Two of the more important factors which determine the efficiency of any immiscible displacement process are the heterogeneity of the reservoir and the stability of the displacement process. While nature dictates the scale of the heterogeneities and the manner in which they are distributed

throughout the reservoir, man has some control over the parameters which dictate whether a displacement is stable or unstable. What type of displacement will take place in a porous medium is dictated by the balance existing among capillary, gravitational and viscous forces. If the combined forces of gravity and capillarity are greater than the viscous forces, the displacement will be stable, and if not, the displacement will be unstable. Thus, it is of interest to study the conditions under which a displacement becomes unstable.

Until recently it was generally believed that the most field displacements were stable. However, recent work carried out at the University of Alberta suggests that while most laboratory displacements are stable, most field displacements are not [1,2,3,4,5]. Thus, these studies at the University of Alberta bear special significance with respect to field applications, particularly to the displacement of heavy oils in Alberta. That is, because heavy oils are more viscous than the conventional oils, unstable displacements are much more likely in heavy oil reservoirs than in conventional oil reservoirs.

Because most field displacements are unstable, conventionally used displacement equations to describe such displacements are inappropriate and inadequate. In order to develop the necessary equations to describe unstable flow, Bear [6] recommends the use of macroscopic averaging of the appropriate conservation equations. As a consequence, detailed information at the pore level must be replaced by integrals which must be specified before the problem can be solved. For example, for immiscible displacements, these integrals would define the absolute permeability, relative permeabilities and capillary pressure. These integrals can be described in two ways: first, empirically, and second, by modelling through the introduction of an idealized structural model for the pore space bounded by the local averaging surface defined at each point within the porous medium. From a theoretical point of view, the latter approach is to be preferred, and this is the approach taken by Aleman-Gomez *et al.* [7]. However, from a practical standpoint, it will always be necessary to determine these integrals experimentally for real systems.

The importance of relative permeabilities and the capillary pressure curve in the displacement of one fluid by another is well recognized. But, currently available means of

determining relative permeabilities are limited to stable displacements. The same is true for the capillary pressure curve. That is, the equilibrium capillary pressure which is valid when the displacement is stable may be invalid when the displacement ceases to be stable.

Thus, to develop a better understanding of fluid-fluid displacement in porous media, one needs to develop a theory that describes stable, unstable and pseudostable displacements. Moreover, one must develop concepts of relative permeability and capillary pressure behaviour that are valid for unstable and pseudostable displacements. Hence, the overall objective of this study is to come to a better understanding of how one fluid displaces another in a porous medium with respect to the problems associated with the stability of displacements, and with respect to the proper definition of the concepts of relative permeability and capillary pressure associated with such displacements.

2. LITERATURE REVIEW

2.1 Stability Studies

Taylor[8] conducted a small perturbation analysis to investigate the stability of two superimposed fluids of different densities with the interface accelerated in a direction perpendicular to it. Effects of viscosity and interfacial tension were excluded from his investigations. Taylor suggested that a gravity-driven finger either grows or changes its shape but that it cannot decay. In a subsequent study, Lewis[9] confirmed this prediction through a series of experiments. In a later study, Bellman and Pennington[10] investigated the formation and the rate of growth of these instabilities by taking into account the effects of surface tension and viscosity.

Taylor and Saffman[11] studied the stability of flow of two immiscible fluids in a Hele-Shaw cell. Based on an analysis of small perturbations at the interface, they linearized perturbation equations to obtain a criterion for stability at the interface. They showed that the interface between the fluids became unstable when the displacing fluid was less viscous than the displaced fluid. Like Bellman and Pennington[10], they too showed that the surface tension had a stabilizing effect at the interface.

However, the term "viscous fingering" was coined by Engleberts and Klinkenberg[12] in 1951. They carried out a series of laboratory flood studies in homogeneous porous media and observed that the fluid recovery during a fluid-fluid displacement was a function of the viscosity ratio. Low recoveries were obtained when viscosity ratios were high. This prompted them to suggest that, when the viscosity ratio was high, viscous fingers might have formed, resulting in lower displacement efficiency. They also studied the effect of displacement rate on displacement efficiency and noted that higher displacement rates brought about lower recoveries. But Handy[13], who studied the effect of displacement rate on a consolidated sandstone model, reported that displacement rate had no effect on viscous fingering.

Van Meurs[14] studied the mechanisms of flow using a three-dimensional transparent model. He made several interesting observations during a displacement in a homogeneous

linear core and in a stratified formation using a 5-spot well pattern. Through a series of photographic snap shots taken at different stages of the displacement, he demonstrated that there was virtually no fingering effect at a viscosity ratio equal to one. But when the viscosity ratio was increased to 80, spectacular fingering phenomena were observed. In a subsequent study, van Meurs and van der Poel[15] argued that it was inappropriate to apply relative permeability concepts without taking into account viscous instabilities. These studies[11,13,14] were carried out in the absence of an initial connate water saturation.

In 1959, Chuoke *et al.*[16] put forward, in what is now regarded as a classic work, an analytical study based on a linear perturbation analysis of fingering phenomena for immiscible liquid-liquid displacement in porous media. They used a piston-like displacement model in which a solution to predict the dynamic response to a perturbation of the displacing fluid front was presented. They included in their treatment a perturbation analysis of the equations of motion and continuity in pressure across the interface in terms of an interfacial tension effect. By examining the sinusoidal frontal distortion of each wavelength, they found that a different (initial) growth rate occurred for each wavelength. Through a number of experimental runs, they arrived at relationships relating displacement rate to the wavelength of the fingers generated. While they reported excellent agreement between their theoretical predictions and experimental observations for their studies in a Hele-Shaw cell, they could not obtain similar agreement using van Meurs[14] data from bead-packed model studies.

In 1962, Outmans[17] advanced a non-linear theory for frontal stability and viscous fingering in porous media. Using the method of successive approximation, he was able to consider perturbations up to the fourth degree in his solutions to the perturbation equations. He suggested that the shape of fingers was a function of interfacial tension, displacement rate and gravity. Hence, he contended that interfacial tension could not be regarded simply as a positive proportionality constant in a linear relationship between pressure difference and curvature of the interface.

Benham and Olsen[18] carried out a number of elaborate experimental runs to identify the factors that affect viscous fingering. They used both a Hele-Shaw cell and bead-packed

models for their studies. A wide range of mobility ratios (1 to 90) and displacement rates (0.1 ft/day to 4.0 ft/day) were employed and they arrived at conclusions similar to those of van Meurs[14].

Rachford[19] was the first author to present a stability analysis on the basis of Buckley-Leverett theory. He argued that it was inappropriate to apply stability theory based on a parallel plate displacement model to immiscible displacement in a strongly water-wet system containing a connate water saturation. Because the displacement in a parallel plate model obeys Buckley-Leverett theory[20], its stability analysis should be based on the Buckley-Leverett equations. By basing his approach on Buckley-Leverett theory, he successfully derived the partial differential equations for a perturbation of the interface. To circumvent the problems arising out of non-linearity, he made two simplifying assumptions. First, the coefficients of the equations were held constant and, second, he considered only a few select initial perturbations for his numerical analysis. Notwithstanding the serious limitations introduced by these simplifying assumptions to his analysis, Rachford nevertheless made some interesting observations. In all the cases he studied, he observed no tendency towards instability in the presence of connate water saturation. However, a later study by Perkins and Johnston[21] contradicted Rachford's findings. They observed that the presence of connate water had a significant effect on viscous fingering patterns and behaviour. Experiments were carried out in both a Hele-Shaw cell and bead-packed models. In both types of model, no viscous fingering was observed at favourable viscosity ratios. In the case of the packed model with connate water saturation, numerous fingers developed early in the displacement process at the inlet end of the system. These fingers subsequently damped out to form a graded saturation distribution at the front. Such noticeable influence of the presence of connate water saturation on viscous fingering led Perkins and Johnston to conclude that, if a study of viscous fingering were to be pertinent to water-wet reservoirs, it should be carried out in a connate water bearing porous medium.

Hagoort[22] offered yet another theory on the basis of the Buckley-Leverett model[20]. He considered certain hitherto unanswered stability questions for a water-wet

medium containing a connate water saturation. The mobility ratio used by Hagoort was based on the so-called shock mobility ratio rather than on the end-point mobility ratio. Also, Hagoort assumed that capillary forces determined the wavelength of the instability and, hence, used energy arguments to justify his assumptions. Thus, his theory is devoid of the existence of a critical wavelength. Hagoort substantiated his claims through a series of displacement runs at several adverse viscosity ratios in the presence of connate water saturation. The major conclusion drawn from these displacements studies was that a decrease in breakthrough recovery occurred at high displacement rates due to instability.

Sarma[23] carried out a number of experimental runs in a transparent rectangular bead-packed model to study the effect of a number of parameters on viscous fingering and instability for both miscible and immiscible displacements. The parameters he considered were viscosity ratio, interfacial tension, direction of saturation change - imbibition and drainage, and displacement rate. Also studied was the miscible displacement of the non-wetting phase in the presence of a high wetting-phase saturation. As expected, he observed more severe viscous fingering in displacements in the drainage direction than in the imbibition direction. Drainage displacements at a high rate gave rise to a spectacular dendritic fingering pattern. It was also observed that a linear relationship existed between the finger-tip velocity and the displacement rate.

Sigmund *et al.*[24] demonstrated through a series of displacement runs in a system similar to the one used by Sarma[23] that viscous fingering depended upon flow rate. A spatial frequency domain analysis of finger growth at fixed time intervals indicated that the fluctuations comprising the fingered zone have a wave number corresponding to that for the maximum growth rate. These fluctuations decayed as their wave number increased beyond the maximum growth rate. The analysis further suggested that the amplitude of flow fluctuations in the spatial frequency domain could be characterized by a growth rate that was linear in time. They presented finite difference solutions to the two-dimensional equations of flow in porous media. These solutions exhibited similar frontal instability.

Peters and Flock[1] were, however, the first authors who sought to combine the various parametric variables which affect instability and viscous fingering in porous media into a dimensionless group which can then be used to quantify the stability criterion. They extended the analysis of Chuoke *et al.*[16] by imposing an additional condition at the walls of the porous medium. By imposing this boundary condition, all velocities normal to the core wall become zero. This enabled them to introduce the system dimensions into their analysis and combine the parametric variables into a dimensionless number, and as a consequence, they arrived at a stability criterion to predict the onset of instability. Two such numbers, one for cylindrical systems and another for rectangular systems, were suggested. Noteworthy in their analysis is the importance of the system dimensions which are raised to the power of two in the stability numbers, while all other terms are raised to the power of one. A later study by Jerauld *et al.*[25] also recognized the importance of the system dimensions on stability. Because Peters and Flock based their analysis on the velocity potential rather than on the force potential, they were unable to determine completely the effect of rock-fluid properties on the stability criterion.

In a more recent study, Bentsen[2] proposed a new approach to the study of instability. By basing his analysis on the concept of a force potential rather than that of a velocity potential, he was able to take proper account of the effect of rock and fluid properties on the stability problem. As a consequence, his instability number was proportional to that derived by Peters and Flock[1], the constant of proportionality being a function of mobility ratio.

All the terms in Bentsen's instability number, with the exception of the pseudointerfacial tension, are readily available. To overcome this problem, Bentsen[26] developed a defining equation for the pseudointerfacial tension associated with a pseudointerface located within a porous medium by implementing a coarser level (macroscopic) of averaging, and by employing the concept of force potential rather than that of work. Because the pseudointerfacial tension is defined in terms of the area under the capillary pressure versus saturation curve, he also suggested a parametric equation for

capillary pressure which can be used to estimate this area. Consequently, if the pseudointerfacial tension is to be estimated, one must establish a capillary-pressure versus water-saturation relationship through laboratory experiments for a particular rock-fluid system. Bentsen's theory[26] is based on the assumption that it is permissible to use the conventional (equilibrium) capillary pressure experiment as an experimentally realizable system for estimating pseudointerfacial tension. Assuming that the actual (dynamic) capillary pressure is proportional to its equilibrium value makes it possible to estimate the actual pressure drop across the interface, the size of the fingers, and the velocity at which they propagate.

A recent experimental study by Coskuner and Bentsen[3] has demonstrated that the non-linear time function used by Bentsen[2] in his stability analysis was inappropriate. This later study by Coskuner and Bentsen[3] demonstrated that the distance travelled by the tip of a finger, with respect to the moving boundary, was in fact a linear function of time. While the form of the time function used in developing the theory does not affect the stability boundary, the mode boundaries, the shape of the fingers, or their relative widths, it does affect the velocity at which the fingers propagate. Consequently, if breakthrough recoveries are to be predicted correctly, there is a need to incorporate a linear time function into the theory.

Yortsos and Huang[27] carried out a linear stability analysis of immiscible displacement which included the effects of continuous changing mobility and capillarity. They showed that the rates of growth of an unstable mode is a function of wavelength, and that capillarity exerts a strong stabilizing contribution to flow.

2 Stabilization

A stabilized displacement is one in which the average saturations at the displacement front remain invariant with time. The term "stabilized zone", first coined by Terwilliger *et al.*[28], refers to the region at the leading edge of the displacement process where saturations move with equal velocity. In a gas-oil gravity drainage study in a 13-ft vertical sandpack, they

observed that, above a certain liquid saturation, all saturation points moved downward at the same rate when the displacement rate is low. Only a short time interval was needed for stabilization to take place. Further, they observed that the saturation distribution curve retained the same shape until breakthrough of the displacing gas occurred at the other end. According to them, when the displacement rate was high, no such stabilized zone formed as the sandpack was not long enough to accommodate the entire length of the stabilized zone that would have formed at such a high displacement rate.

In a later study, Welge[29] demonstrated that the problem of triple values of saturation encountered by Buckley and Leverett[20] could be overcome by constructing a tangent to the fractional flow curve. The saturation at the point of tangency was defined as the saturation at the front, S_{wf} . According to Welge, the construction of this tangent indicated that there existed a lower limit of saturation below which the plot of fractional flow versus water saturation was not required. Therefore, Welge concluded that it was not necessary to obtain estimates of relative permeabilities of the fluids for saturations below the flood front saturation. Willhite[30] contends that Welge's technique to determine S_{wf} does not take into account the effects of the capillary pressure gradients on the fractional flow curve, and, therefore, it is doubtful whether the stabilized zone concept developed for mobile connate water saturation will still be applicable for all connate water saturations. Capillary pressure terms cannot and should not be dropped if the Buckley-Leverett theory is to be applied to analyse displacement data obtained using small cores of a few inches in length.

Owens *et al.*[31] referred to the stabilized zone as the position of the greatest capillary pressure gradient. They studied the effects of the stabilized zone on gas-drive type displacements, and noted that the effects could be quite serious. For example, they noted a shift towards the right in the k_g/k_o versus S_g curves at lower values of S_g when the pressure differentials were high.

Rapoport and Leas[32] were the first authors to make a comprehensive study of the stabilized zone. The frontal advance theory suggests that when a stabilized zone forms, the saturation at the breakthrough point and the recovery of the *in situ* fluid in the

post-breakthrough period should be independent of the core length and the displacement rate. But often that was not found to be the case with most laboratory tests. Furthermore, the presence of capillary end-effects complicated the analysis of data in some cases. Only with longer systems was the displacement behaviour observed to be independent of the length of the core and the displacement rate. To overcome such confusing situations which made many laboratory analyses questionable, Rapoport and Leas suggested a scaling criterion on the basis of dimensional analysis to determine whether or not a flood was stabilized. Based on theoretical and experimental considerations, they were able to show that displacement data for linear floods were independent of core length, displacement rate and viscosity of the displacing fluid (water), provided the scaling coefficient, $L\mu_w v$, exceeded a critical value. Rapoport and Leas reported that the critical value of the scaling coefficient ranged between 0.5 and 3.5 $\text{cm}^2\text{cp}/\text{min}$ for most laboratory core studies. It is, however, to be noted that these values of the scaling coefficient pertained to consolidated cores only.

Because the Buckley-Leverett solution describes immiscible displacements in a linear system where stabilized displacement occurs, it is imperative that one first determine whether the displacement is stabilized before employing frontal advance theory to analyse the displacement data. However, Rapoport and Leas reported that, for most field situations, the flooding behaviour usually was stabilized.

In a subsequent extension of the work by Rapoport and Leas, Jones-Parra and Calhoun[33] suggested a modified scaling coefficient, $L\mu_w v / [V(k\phi) \sigma \cos\theta]$, which included the absolute permeability (k) and porosity of the core (ϕ), interfacial tension (σ) between the displaced and displacing fluids, and the contact angle (θ).

Often the stabilized zone is neglected in linear-displacement calculations. Fortunately, in most cases, such neglect does not introduce serious errors into the calculations as the width of the stabilized zone is relatively small for most conventional flooding rates. Bail[34], who presented a detailed method of calculating the length of the stabilized zone for any flooding situation, also observed that the length of the stabilized zone could be neglected in most cases.

Parsons and Jones[35] employed a relaxed scaling technique, referred to as a "linear scaling technique", to study single-fluid and multi-fluid injection processes. According to them, a displacement process is linearly scalable for a given porous medium and fluid system if the fluid saturation at any point and time is a function only of the number of pore volumes of each fluid injected with respect to that point. Thus, by definition, a stabilized displacement has to be linearly scalable. Saturation profiles in such a displacement would be similar along the length of the core, differing from one another only by a linear magnification or reduction.

Based on an inspectional analysis of the immiscible displacement equation, Bentsen[36] suggested a capillary number which can be used as a criterion to determine whether or not a displacement process is stabilized. The advantage of using this capillary number is that it takes into account not only the fluid properties, but also the rock-fluid interactions and the pore-size distribution.

2.3 Relative Permeabilities

The importance of reliable relative permeability data in reservoir engineering studies is well recognized in the petroleum industry. In particular, when making a waterflood prediction, among the more important properties needed are the water-oil relative permeability characteristics of the reservoir rock. Such information may be obtained by either steady-state or unsteady-state methods for measuring effective permeability data. Unsteady-state methods are usually referred to as external-drive methods. While steady-state methods require approximately one day or more to acquire a complete set of effective permeability data, external-drive methods can acquire the same information in a few hours. Moreover, the external-drive methods are applicable to displacements where saturation gradients exist, while steady-state methods are not. Aleman-Gomez *et al.*[7] recently demonstrated that there could be considerable difference between steady-state and unsteady-state relative permeabilities if the dimensionless number as defined by Abrams[37] was large. This dimensional number is defined as $[(v\mu_w/\sigma_{ow})(\mu_w/\mu_o)^{0.4}]$ where v is the linear velocity, σ_{ow} is the interfacial tension between oil and water, μ_w is the viscosity of water and μ_o is the viscosity of oil.

2.3.1 Steady-State Method

Because the steady-state method uses the fewest assumptions in determining relative permeability curves, it has generally come to be regarded as a standard method. When compared with all other techniques are compared. However, steady-state methods may not be representative of field situations where saturation changes with respect to time and distance take place. Also, because most field displacements take place under dynamic conditions, the application of steady-state methods may be inappropriate and, at times, questionable. The work of Geffen *et al.*[38], Kimbler and Caudle[39], and Archer and Wong[40] also support this argument.

2.3.2 External-Drive Method

Use of external-drive methods is limited to displacements in which the assumptions underlying Buckley-Leverett theory[20] are met. This requires that the displacements used for measuring relative permeability curves be stabilized and one-dimensional (pressure and saturation uniform in any cross-section[41]). In addition, a Lagrangian formulation of the fluid displacement problem must be permissible. Thus, when using external-drive methods, it is important that the flow is neither unstabilized nor unstable, and that the saturation profiles are monotonic[42]. Based on the Buckley-Leverett frontal advance equation, Welge[29] developed a method to estimate the average saturation and the oil recovery. He showed that if the fractional recovery of one fluid phase was known, the ratio of the relative permeabilities might be obtained by using his method.

The external-drive method is not without problems. For example, this method uses the breakthrough point as a very important parameter. Consequently, the slightest delay in observing this point may cause erroneous results[40]. Moreover, because of discontinuities in saturation which may exist at the inlet and outlet ends of the core, the difference between the pressures measured externally at the inlet and outlet ends of the core may not be representative of the actual (internal) pressure drop across the core. Thus good experimental technique is required, if serious distortion of the effective permeability curves due to systematic experimental error is to be avoided. It is, therefore, suggested that an extrapolated

internal inlet pressure be used instead of the external inlet pressure[43].

Another limitation of the external-drive methods is that they require numerical or graphical differentiation of experimental data. Because inaccuracies in data measurement become amplified by the process of differentiation, there is a need to deal effectively with this problem. In this regard, two approaches may be taken, the implicit and the explicit.

If the displacement is unstabilized, or if the end-point mobility ratio is near one, resort must be had to implicit methods[40,44,45,46]. In this approach, a general model of the coreflood experiment, a reservoir simulator, for example, is used, and differentiation of measured data is not required. However, because such implicit approaches are iterative in nature, many runs may be required to obtain a good match. Archer and Wong[40] and Sigmund and McCaffery[44] used this approach to obtain relative permeability curves. Use of a reservoir simulator necessarily involves history matching of the observed production and pressure data. Because such history matching is non-unique, one must always use caution before accepting the relative permeability curves obtained by this technique as a true representation of the actual flow phenomena.

If the Buckley-Leverett[20] assumptions are met, it becomes possible to use the simpler, explicit approaches[47,48,49]. If these approaches are taken, the JBN method[47] or the Jones-Roselle method[48] are used to estimate the effective permeability values explicitly from the data collected during displacement experiments. Therefore, the procedures used to implement this process must be carefully selected, if the problems associated with differentiating experimental data are to be avoided[49].

One possible approach is to use linear regression analysis to construct approximating functions for each entire data set[49]. Then, the method of least-squares can be used to estimate the values of the coefficients of candidate regression equations. Finally, various statistical methods can be used to determine the "best" regression equation.

When undertaking this approach, it is generally not recognized that the functional forms used to fit cumulative oil and pressure drop histories must take proper account not only of the constants of integration for the two differential equations which describe the system,

but also the various physical conditions which may be imposed on the integrated forms of the equations used to model cumulative oil and pressure drop histories. The incorporation of such information into the regression equations is important because failure to do so may result in internal inconsistencies between the regression equations and those equations used to estimate the effective permeabilities.

2.3.3 Lagrangian Approach

External-drive methods, as currently employed, cannot be used to estimate effective permeabilities over the entire saturation range of interest. This limitation arises because of the difficulty of measuring both saturation and pressure accurately in the immediate vicinity of a displacement front [20,29]. This problem could be overcome if it were practicable to inject water at such a rate that a displacement front does not form. However, at such injection rates the displacement would be either unstable and/or unstabilized and, as a consequence, additional problems would arise. That is, because the flow is unstable and/or unstabilized, the usual external-drive equations used to estimate the saturation, S_w , and the reciprocal mobility, λ^{-1} , cannot be used. Moreover, use of the standard (Eulerian) methods for estimating the fraction of water (or oil) flowing at a particular location may not be able to be used either.

The problems with respect to the estimation of S_w and λ^{-1} can be eliminated, provided it is possible to measure saturation and pressure directly at a number of locations along the length of the core. However, because it is not possible to measure f_w directly, the problems associated with respect to the estimation of f_w at a number of locations along the core, when the displacement is unstable and/or unstabilized, are not so easily overcome. As it turns out, f_w as a function of saturation may be estimated at a specific time, say t^* , by focusing on a specific saturation profile rather than a specific location along the core. That is, a Lagrangian rather than an Eulerian approach must be taken.

2.3.4 Dynamic Method

If viscous forces dominate, even the unsteady-state methods are incapable of a true representation of actual flow phenomena because external-drive methods assume that pressure and saturation distributions remain uniform at all cross-sections of the linear pore body. Such an assumption is not valid if viscous fingers are present. Thus, according to Rose[50], a continuous observation of saturations during a displacement process as a function of time and length of the core is needed to understand the dynamic conditions during the displacement. He suggested simultaneous solution of the Buckley-Leverett equation and the capillary pressure equation of saturation to obtain dynamic relative permeabilities. But because Rose's solution is based on Buckley-Leverett theory, and because such solutions seem inappropriate in cases where the displacement is unstable, it becomes necessary to use directly the differential form of Darcy's equation for two-phase flow, if one wants to obtain relative permeabilities for an unstable displacement. In so doing, resort must be had to an averaged form of the fractional flow curve as determined from dynamic saturation profiles. Thus this method will require both saturation and pressure profiles during displacement with respect to time and space.

Using this technique, Islam and Bentsen[51] showed that, while the dynamic method gave relative permeabilities similar to those of the JBN method during stabilized and stable displacement, the discrepancy between relative permeabilities from these two methods was significant in cases of unstabilized and unstable displacement.

A more recent study by Peters and Khataniar[52] also reports experimental evidence similar to that reported by Islam and Bentsen[51]. But because Peters and Khataniar used the JBN method for their unstable displacements, it is doubtful whether their relative permeability curves represent the actual flow behaviour.

2.3.5 Effects of Capillary and Viscous Forces

Numerous studies have been reported in the literature pertaining to the effects of different parametric variables on relative permeabilities, such as the effect of gravity and capillary forces, the direction of saturation changes, wettability, pressure, displacement rate,

viscosity ratio and temperature. However, in view of the limited scope of the research objectives of this study, this review will be restricted to those studies which pertain to the study of the effects of gravity and capillary forces on relative permeabilities.

The effects of interfacial tension on relative permeabilities have been studied and investigated by several authors[53,54,55,56,57]. Most of these were studies aimed at studying the effect of interfacial tension on displacement recovery.

Amaefule and Handy[58] undertook a detailed investigation of the effect of interfacial tension on relative permeability. They reported that below an interfacial tension of 10^{-1} mN/m, relative permeability was a strong function of interfacial tension while at higher values of interfacial tension, relative permeability was not affected. Lefebvre du Prey[59] investigated the effects of capillary and viscous forces on liquid-liquid relative permeabilities. Based on dimensional analysis, he arrived at a dimensionless number which was the ratio of capillary to viscous forces, $(\sigma/v\mu)$, where v was the mean velocity, μ was the fluid viscosity, and σ was the interfacial tension between the fluids. Because this dimensionless number, also called the "capillary number", arose from dimensional analysis, it was capable only of describing flow displacements at the microscopic level. Lefebvre du Prey further demonstrated that for a contact angle in the range of 0° to 30° and a favourable viscosity ratio of one, relative permeabilities were strong functions of his capillary number. The relative permeability decreased as the value of this capillary number increased; or, more simply, if the capillary forces predominated.

The dimensionless number suggested by Abrams[37] in 1975 took into account the viscosity ratio in the case of water-oil systems. With the aid of his dimensionless number, he was able to show that the absence of capillary forces would allow viscous forces to cause a uniform distribution of each phase in every capillary in accordance with the saturation distributions of each phase. Thus, the absence of capillary forces will yield relative permeabilities having the form of two symmetrical diagonal lines, intersecting at 50% saturation, as reported by Bardon and Longeron[60]. Because viscous forces have a homogenizing effect, larger capillaries result in a more uniform saturation distribution.

It is more useful to obtain a capillary number that describes the macroscopic rather than microscopic behaviour of the fluid distribution and pertains to the particular rock-fluid system. Using inspectional analysis, Bentsen[36] obtained a capillary number, $(A_c k_{wor} / VL \mu_w)$, which takes into account the area under the capillary pressure versus saturation curve (A_c), effective permeability to water at irreducible water saturation (k_{wor}), the length of the system (L), the viscosity of displacing phase, say water (μ_w), and flow velocity (V). Because Bentsen's capillary number incorporates the area under the capillary pressure versus saturation curve and the effective permeability at the residual oil saturation, it takes into account the rock-fluid properties in addition to the flow properties. Theoretical considerations suggest that this capillary number should be less than 0.01, if the displacement is to be stabilized. However, practical considerations[42,51] suggest that a value of 0.01 may be too restrictive, and that a value of capillary number less than 0.1 may be more realistic.

Studies relating the effects of viscosity ratio on relative permeability are contradictory. While some authors[59,61,62,63] report that viscosity ratio does affect relative permeabilities, others[64,65,66,67] contend that it does not. Odeh[68] investigated the effect of viscosity ratio on relative permeabilities using steady-state methods. He concluded that the viscosity ratio had no effect on the wetting-phase relative permeability and also, on the non-wetting-phase relative permeability for samples with very high absolute permeability. However, studies conducted with low-permeability samples indicated that the non-wetting-phase relative permeability was directly proportional to the viscosity ratio. Furthermore, the effect of viscosity ratio was observed to be more pronounced at the lowest non-wetting-phase saturation. Odeh attributed this to the fact that a maximum capillary effect would arise at lower wetting-phase saturations.

It is interesting to note that a large number of experimental studies dealing with the effect of viscosity ratio on relative permeabilities are not only contradictory, but are also inconclusive. Maybe the argument put forward by Handy and Datta[69] can offer a possible explanation to these contradictions. They demonstrated that for consolidated porous media relative permeability depended on whether the method used incremental displacements leading

to small changes in saturations or macroscopic displacements resulting in large saturation changes.

In a later study, Slattery[70] demonstrated that such an incremental displacement would normally be a restricted imbibition displacement resulting in the entrapment of the non-wetting phase in the larger pores. On the other hand, a macroscopic displacement of the non-wetting phase would result in the entrapment of the non-wetting phase in the smaller pores.

Lin and Slattery[71] later showed that the fraction of the displaced phase trapped and stranded in pores depends on both the viscosity ratio between the displacing and displaced phases and the magnitude of the pressure gradient. Hence, relative permeabilities estimated using macroscopic displacements would exhibit dependence on both the viscosity ratio and the pressure gradient. However, in steady-state displacements, such dependence is not expected because the changes in saturation are very slow. Hence, this would result in a negligible effect of viscosity ratio and pressure gradient as compared to the effect of interfacial tension for steady-state displacements. That is, contradictions with respect to the exact nature of the effects of viscosity ratio on relative permeabilities are inevitable. This is not surprising because most of these authors tried to study the individual contribution of each parameter rather than the combined effects of the parameters making up a dimensionless group. In reality, the flow behaviour depends upon the simultaneous interaction of a number of forces.

Therefore, a judicious approach would be to utilize dimensionless groups, especially those which are the ratios of forces, to study the effects of viscous, capillary and gravitational forces on relative permeabilities. In this context, parameters such as Bentsen's capillary number[36] and instability number[2] could be very useful. The advantage in using these parameters is that these numbers incorporate most of the pertinent parameters. With the help of such numbers, Islam and Bentsen[51] reported that relative permeability was invariant only when the flow regime was stable and stabilized. In the case of unstable flow, effective permeability to oil varied not only with the flow rate but also with the distance along the length of the core, whereas the effective permeability to water remained invariant in all cases.

In this regard, it is to be noted that the displacements studied by Islam and Bentsen[51] were in the immediate vicinity of the stability boundary.

2.3.6 Relative Permeability Hysteresis

Hysteresis in capillary pressure is often observed when a change in the saturation direction takes place, i.e. when the displacement direction is changed from the drainage to the imbibition direction. By virtue of the fact that both capillary pressure and the relative permeability curves are functions of saturation, one would expect to find a similar hysteresis effect in the relative permeabilities, should a change in the direction of saturation take place. Most experimental studies[51,64,72] conducted to investigate this aspect report that because the wetting-phase relative permeability is a function of its own saturation, it was not likely to show any hysteresis effect. The non-wetting phase, however, is affected by the direction of the saturation change. During a displacement in the imbibition direction, lower relative permeabilities are obtained at any saturation. A possible explanation for this behaviour may be that during a displacement in the imbibition direction, more and more non-wetting phase becomes disconnected, and as a consequence, bypassing in the larger capillaries takes place[73]. In the displacement in the drainage direction, however, all the non-wetting phase remains continuous.

McCaffery and Bennion[74] observed no significant history dependence in relative permeability measurements under strongly wet conditions. However, when the contact angle was increased, a consistent shift in relative permeabilities to both phases was found for a porous medium containing an initial irreducible saturation of the displacing phase. In drainage experiments, they found that the relative permeability curves were little affected when the contact angle varied from 180 degrees to 90 degrees. They showed that the sensitivity of the relative permeability relations to contact angle changes was strongly affected by the saturation-history of the core. This agrees with an earlier study by Morrow *et al.*[75], wherein it was suggested that any small decrease in relative permeability because of an increase in the contact angle may be due to the curvature relaxation at the fluid-fluid interfaces. Such a

phenomenon, according to Morrow *et al.*[75], is saturation history dependent.

2.4 Capillary Pressure

According to Bass[76], capillary pressure can be regarded as a force per unit area resulting from the interaction of the surface forces and the geometry of the medium in which they exist. Capillary pressure, by definition, can be also regarded as a measure of the curvature between two fluid phases in a porous medium, and it depends upon several factors, notably: i) texture and wettability of the porous medium, ii) the interfacial tension between the fluids, iii) saturation distribution of the fluids, and iv) the manner in which the saturations were attained. Thus, for a given pair of immiscible fluids in a particular porous medium, capillary pressure is a unique function of fluid saturation.

Capillary pressure versus saturation curves are widely used in the petroleum industry to study fluid distributions in the formation, to estimate saturations, determine wettability, and to study the interconnectivity of the pores in the formation. These curves also represent an experimental correlation of the pressure difference between the two phases at equilibrium in a porous medium. Sneider *et al.*[77] observed that the shape of capillary pressure curves is a function of the rock type, with fine-grained rocks having higher capillary pressure at a particular saturation.

2.4.1 Laboratory Methods to Measure Capillary Pressure

Although one of the earliest capillary pressure experiments reported in the literature was carried out by Leverett[78] in 1941, his method did not gain wide acceptance because of several experimental constraints. Leverett used a long vertical unconsolidated sand pack for his experiments; but, core samples available for laboratory studies are usually small and can be only obtained in small sections. As a consequence, it would not be possible to carry out drainage experiments similar to those carried out by Leverett[78]. Therefore, several other methods have been proposed by various authors. These methods can be classified into the following five categories: i) restored-state method of Bruce and Welge[79], ii)

mercury-injection method proposed by Purcell[80], iii) centrifuge method developed by Slobod *et al.*[81], iv) dynamic capillary pressure method by Brown[82] and v) evaporation method proposed by Messer[83]. Among them, the evaporation method, which involves continuous monitoring of the decrease in the weight of the wetting-fluid content due to evaporation in a core initially saturated with 100% of the wetting fluid, has seldom been reported in literature. As a consequence, this method will not be discussed here.

All of the above methods were proposed before the early 1950s. Since then, numerous studies pertaining to the measurement of capillary pressures have been reported in the literature. In essence, the methods and techniques used in these later studies remain basically similar to those proposed by the pioneering authors; consequently, a detailed review of these studies will be avoided.

2.4.1.1 Restored-State Method

The restored-state method, also known as the desaturation or displacement and porous membrane method, was developed by Bruce and Welge[79] in 1951. The method uses a permeable membrane of uniform pore-size distribution such that the displacing fluid will not penetrate through the diaphragm until a certain threshold pressure is applied. The porous membrane they used had an average pore radius of one micron which was much smaller than the curvature of the oil-water interface required to penetrate the membrane. As a consequence, the capillary pressure required to penetrate the membrane was much higher than any pressure applied in their experiment. During the experiment, the applied pressure was increased in small increments and the system was then allowed to reach equilibrium before a reading of the corresponding saturation of the wetting phase was made. Because static equilibrium has to be attained before a reading at a particular pressure can be taken, this method is very time-consuming; often it takes several weeks to generate a single capillary pressure curve for a particular rock fluid system. Bruce and Welge measured the residual water precisely at the end of the experiment by distillation with toluene.

2.4.1.2 Mercury-Injection Method

The mercury-injection method to measure capillary pressure was proposed by Purcell[80] in 1949. In this technique, mercury, a non-wetting fluid, is injected under pressure into an evacuated core sample. The mercury vapor, together with any residual gas present, acts as the wetting fluid. Because this method does not need any membrane, much higher pressures can be applied. Furthermore, equilibrium in pressure is attained rapidly, thus enhancing the speed of the experiments. The method has, however, two serious limitations. First, because mercury is being used, it does not take into account the actual wetting characteristics of the fluids present in the formation. Appropriate conversion factors need to be applied to make use of the capillary pressure data obtained by this method in a particular rock-fluid system. The second limitation is that the rock sample used for the experiment cannot be reused to obtain reproducible results. Thus, the rock sample is permanently lost after a mercury-injection experiment.

2.4.1.3 Centrifuge Method

Although the centrifuge technique was used to study small-core plugs by McCullough *et al.*[84] and Hassler and Brunner[85], it was Slobod *et al.*[81] who were the first to conduct elaborate experimental studies to obtain capillary pressure data using this technique. They demonstrated that the centrifuge method had some definite advantages. They are: i) rapid establishment of equilibrium thereby cutting down experimental time significantly, ii) excellent precision yielding reproducible results, iii) availability of high pressure difference between the phases, iv) simple operational procedure and, v) ability to establish connate water saturation.

Slobod *et al.* compared their data with those obtained using the restored-state method, and obtained excellent agreement. Further, like the restored-state method, the centrifuge method also took into account actual wetting characteristics of the fluids. The main disadvantage of this method was that the centrifugal forces varied along the length of the sample, and this was not accounted for in the the

2.4.1.4 Dynamic Method of Capillary Pressure

Brown[82] was the first author to propose a method to measure dynamic capillary pressure in a steady-state flow experiment. The experimental technique he used was a modification of the technique developed by Hassler[86] to measure relative permeabilities. With the help of special wetted disks, he measured pressures in each phase, and then reported the difference between the pressures as the dynamic capillary pressure. Following each measurement of the capillary pressure, the saturation of the fluids was varied and another measurement was made. Thus, he obtained a capillary pressure curve over the entire range of saturations. He reported good agreement between the capillary pressure data obtained using the dynamic method and that obtained using the restored-state method. Based on such good agreement, Brown concluded that use of restored-state (i.e. static) capillary data was valid in dynamic situations of fluid flow.

No one, to the author's knowledge, has reported on the application of the dynamic capillary pressure method to unsteady-state laboratory experiments. In summary, it has been noted from studies in the literature that in spite of the long experimental time required, the restored-state method is considered a simple and yet reliable method to measure capillary pressure. Often this method is regarded as a standard method to which all other methods are compared.

2.4.2 Capillary Pressure Hysteresis

Capillary pressure curves exhibit hysteresis due to their dependency on the direction of saturation change in the porous medium – drainage or imbibition. Hysteresis in capillary pressure curves can be regarded as a measure of the shape of the fluid interfaces and the degree of interconnectedness along the direction of saturation change[87].

Because the direction of saturation change is dependent on the contact angle, capillary pressure can be regarded also as a function of the difference between the advancing and receding contact angles. During a drainage process (receding contact angle), displacement first

takes place in the larger pores, and then in the smaller pores. As a consequence, some non-wetting fluid remains trapped in smaller pores. This behaviour of capillary retention in the smaller pores illustrates why the capillary pressure corresponds to a higher saturation on the drainage curve. In the case of an imbibition process (advancing contact angle), fluid in the smaller pores gets displaced first. This leads to a lower capillary pressure for the corresponding saturation in an imbibition process. The drainage capillary pressure curve exists over a larger range of saturation than does the capillary pressure curve obtained during an imbibition process. In a more recent study, Morrow[88] reported that the pore geometry may also cause hysteresis in capillary pressure curves even when the contact angle is zero.

The most thorough study on this phenomenon has been reported by Killins *et al.*[89]. They carried out extensive capillary pressure studies using consolidated sandstone samples under both oil-wet and water-wet conditions. They observed that the slope of the capillary pressure curve was a function of the pore-size distribution in the rock sample. The rock samples with a more uniform pore size distribution yielded flatter capillary pressure curves.

2.5 Microwave Theory

A review of microwave theory is available in the literature[90,91,92,93,94].

Consequently, only a brief review of the subject is presented here. Microwaves are electromagnetic waves of smaller wavelengths (30cm to 1cm) in the frequency spectrum of 1 GHz to 30 GHz[92]. Owing to their small wavelengths, the phase varies with distance; as a consequence, it is necessary to analyse the circuit or the components in terms of electrical and magnetic fields associated with them. Compared to medium wave, short wave and VHF, microwaves have a much larger band width and, hence, need relatively smaller antenna sizes for a very sharp radiated beam. Microwave signals penetrate most non-conductors and, like light, propagate in a straight line. Because conductors are opaque to microwaves, they are used to contain and guide microwaves[94]. Insulators, on the other hand, reflect and transmit microwaves. Consequently they are regarded as being "transparent" to microwaves. Dielectrics are the other type of material which absorb microwaves and are characterized by their low

electrical conductivity in comparison to that of a metal.

2.5.1 Dielectric Behaviour

Dielectric permittivity is one of the principal factors which determine propagation of electromagnetic waves in materials, and it is proportional to the electric dipole moment per unit volume. An electric dipole is defined as a pair of electric charges, equal in size but opposite in sign, while the dipole moment is the product of one of the two charges and the distance between the charges. The dipole moment, in turn, is affected by electronic, ionic, interfacial and dipolar characteristics. The contribution due to electronic characteristics is basically in the form of electron clouds and it occurs at optical frequencies[91]. Ionic and interfacial contributions come from displacement and movement of ions and, therefore, are confined to low frequencies. The dipolar contribution is due to permanent electric dipoles which orient themselves in the direction of an applied field. Freedom of movement of a dipole is a very important factor in determining its contribution. For instance, in ice, the frequency due to the dipolar moment is of the order of a few kHz, while in water at room temperature it is of the order of 15-17 GHz. Water is one of the very few materials present abundantly in nature which has permanent electric dipoles.

The dielectric constant is defined as the ratio of the strength of an electrical field in a vacuum to that in the dielectric for the same distribution of charge. Thus, the dielectric constant or 'relative permittivity' as it is commonly called is a ratio (ϵ/ϵ_0 where ϵ_0 is the permittivity or the dielectric constant in free space i.e. vacuum). The relative dielectric constant in its dimensionless form is commonly used. The symbol is primed when variation of the dielectric constant may occur with frequency. However, the dielectric constant is usually expressed with reference to that of air which is equal to one, and a high dielectric constant is usually associated with polar compounds such as water.

Thus, it is evident from the preceding discussion that water, being a dipolar substance, strongly absorbs microwaves. A water molecule contains a positive and a negative charge. When an electric field is applied, molecules tend to align themselves in the direction of the

applied field. If the frequency of the applied field is high enough (1 GHz to 120 GHz) that the dipolar molecules are no longer able to keep pace with changes of the applied field, a lag between dipolar rotation and change in the applied field occurs. As a consequence, the microwaves are attenuated and the dielectric under the applied field is heated.

Microwaves respond differently to polar and non-polar substances. Consequently, they may be used to distinguish a polar substance such as water from a non-polar substance such as oil or gas. The effect of salinity is negligible at frequencies encountered in the microwave frequency spectrum. In this study a microwave frequency of 27 GHz in the Ka band (26.5-40 GHz) was chosen because maximum attenuation of the microwave signal by the water is achieved at this frequency.

3. STATEMENT OF THE PROBLEM AND OBJECTIVES

Two major observations can be made from the preceding discussion. First, it is evident from the literature that the immiscible displacement of one fluid by another in a porous medium is either stable or unstable, and that the nature of such displacement is dictated by the balance existing among viscous, capillary and gravitational forces. The foregoing discussion also points to the fact that most field displacements are unstable. This emphasizes the importance of instability analysis to determine whether a displacement process would be successful or not.

Although a large number of studies pertaining to instability analysis of displacement processes have been reported in the literature, only a few address the problem of instability of immiscible displacements with special reference to field situations. Noteworthy among them are the recent studies by Peters and Flock[1] and Bentsen[2] at the University of Alberta. Peters and Flock were the first authors to combine different parametric variables into a dimensionless group to predict the onset of instability, and to recognize the importance of the system dimensions with respect to the stability analysis. However, for reasons discussed earlier, their analysis is incapable of determining completely how the rock-fluid properties affect the stability criterion. Bentsen[2] overcame this limitation by using an analysis based on the concept of a force potential. However, it was demonstrated[3] that the non-linear time function used in his analysis was inappropriate.

The second major observation is that, because most field displacements are unstable, the conventional relationships for relative permeability and capillary pressure which are usually applied to stable displacements may not be applicable. Therefore, the steady-state and the unsteady-state or external-drive methods, which are valid in stable and stabilized displacements, may not be valid in unstable displacements. This can be attributed to two reasons: first, during an unstable displacement, viscous forces are quite large compared to capillary forces, and second, pressure and saturation distributions no longer remain uniform at all cross-sections in such a displacement. Hence, relative permeabilities estimated using an external-drive method will most likely fail to describe the actual flow phenomena taking place

in an unstable displacement.

The conventional equilibrium capillary pressure curve is applicable only when the displacement is stable. In an unstable displacement, in which viscous forces predominate over capillary forces, the distribution of non-wetting and wetting phases within the porous medium is significantly different than in a stable displacement. Therefore, one would expect that a capillary pressure curve obtained under equilibrium conditions may not be valid for an unstable displacement process. Bentsen[26] suggests that when the displacement is unstable, the capillary pressure is dictated by the macroscopic curvature of the viscous finger, and not by the local pore structure, as is the case in stable displacements. It is therefore necessary to experimentally verify this concept of non-equilibrium or dynamic capillary pressure under unstable flow conditions.

Thus, the objectives of this study were two-fold. The first objective was to modify the theory developed by Bentsen[2] so as to include a linear time function[4,95], and then to verify the modified theory experimentally in rectangular systems for stable displacements. The second objective was to validate the concepts of relative permeability and capillary pressure in unstable displacements. In order to meet this objective, it was necessary to develop a modified external-drive technique suitable for both unstabilized and unstable displacements. Moreover, it was necessary to develop appropriate functional forms to fit cumulative-oil and pressure-drop histories.

A further goal of this study was to develop a method to measure capillary pressure under dynamic conditions and validate it experimentally by comparing the dynamic capillary pressures with those using a standard (equilibrium) method.

Another goal of this study was to redesign the equipment, taking into account the shortcomings experienced by previous experimenters[42,51], and to develop a more efficient data acquisition system.

4. THEORY

4.1 Modification of Stability Theory

4.1.1 Introduction

Most secondary recovery schemes involve the displacement of one fluid by another. The success of such schemes may depend upon whether the displacement is stable or unstable. Thus, it is of interest to be able to predict the boundary which separates stable displacements from those which are unstable. While a theory has been developed for this purpose[2], the non-linear time function used in that theory is inappropriate[3]. The purpose of this section is to demonstrate how the theory developed in Reference 2 can be modified so as to include a linear time function.

To determine whether a perturbation of the interface separating water from oil will grow, one must be able to specify the potential on each side of the disturbed interface. Such potentials arise out of the contribution of three forces: gravitational, viscous and capillary. The contribution of gravitational and viscous forces is readily determined[2]. However, in order to determine the contribution of the capillary forces, one must be able to predict how the boundary which separates the water from the oil evolves over time. The approach taken here is to develop from first principles the differential equation which describes the evolution of such a surface. Then the solution to this differential equation is used to determine the contribution of the capillary forces to the potential. Because this enables specification of the force potential for the water on the oil side and on the water side of the interface, one can define the perturbation potential for the water as being the difference between these two potentials. This perturbation potential, when combined with the appropriate form of Darcy's law, gives the perturbation velocity for a water finger. A similar approach is taken to determine the perturbation velocity for an oil finger. The details of this approach, together with additional results obtained with this theory, are presented in the following sections.

4.1.2 Capillary Pressure Potential

To determine the capillary pressure potential, it is necessary to know how the boundary ξ , which separates the penetrating fluid from the displaced fluid, evolves as the amplitude of the surface increases in magnitude. The theoretical prediction of such a surface is not an easy task for two reasons. First, the surface separating the penetrating water from the displaced oil is not sharp. Rather, there is a transition zone (capillary fringe) separating the water from the oil. Second, the potential distributions on each side of the interface will, in general, change as the surface (transition zone) moves through the porous medium. If such is the case, the potential distributions must be determined simultaneously with ξ , an approach which poses great difficulties. Thus, in order to make the problem tractable, some simplifying assumptions are introduced.

When unstable displacements are conducted in the immediate vicinity of the stability boundary, only one or two water fingers propagate. Sectioning of the sandpack in which such displacements have been conducted reveals that the water fingers are usually almost circular, and that if only one finger is propagating, its diameter is about one-half of that of the sandpack[1,5]. Moreover, the transition zone (capillary fringe) separating the water from the oil is relatively small when compared to the diameter of the finger[96]. This suggests that it may be possible, without introducing significant error, to replace the transition zone by a sharp, macroscopic interface to which pressure discontinuities are assigned, and up to which the relatively uniform saturation and flow conditions prevailing outside the transition zone are extrapolated. Given the validity of introducing such a pseudosurface, the pseudointerfacial tension associated with the pseudosurface may be estimated using some recently developed theory[26].

To avoid the difficulty of solving simultaneously for ξ and the potential distribution on either side of the interface, it is assumed that the potentials may be specified a priori. Then the two-dimensional pseudosurface separating the two fluids may be determined by undertaking a summation of the normal forces acting on a differential element of the surface. If it is supposed that the force due to acceleration may be neglected, the appropriate

differential equation describing the evolution of the surface may be shown to be (see Appendix A)

$$\sigma_e \left[\frac{\partial^2 (\xi_w)_o}{\partial x^2} + \frac{\partial^2 (\xi_w)_o}{\partial y^2} \right] + (P_{cw}(x,y,z))_o = 0 \quad (1)$$

where $(\xi_w(x,y,z))_o$ gives the displacement of any point on the surface as a function of the amplitude of the surface, z , and where σ_e is the pseudointerfacial tension. The pressure difference across the surface, $(P_{cw}(x,y,z))_o$, may be viewed as a force function. Moreover, when divided by ρ_w , it is, by definition, the capillary pressure potential. Implicit in the writing of Equation 1 is the assumption that both $(\partial(\xi_w)_o/\partial x)$ and $(\partial(\xi_w)_o/\partial y)$ are much smaller than 1, and that σ_e is independent of location on the surface.

4.1.3 Macroscopic Capillary Pressure

In order to define the macroscopic capillary pressure, $(P_{cw})_o$, one must be able to specify the perturbation potential, $(\Phi_w^*)_o$. The perturbation potential of the water in the region where the oil is flowing is defined by[2]

$$(\Phi_w^*)_o = \frac{\Delta \rho}{\rho_w} g z \cos \alpha + \frac{\rho_o}{\rho_w} (\Phi_o)_o - (\Phi_w)_w + \frac{(P_{cw})_o}{\rho_w} + \frac{P_c(t)}{\rho_w} \quad (2)$$

where $(\Phi_w)_w$ and $(\Phi_o)_o$ are defined, respectively, by

$$\vec{v}_w = - \frac{k_{wor} \rho_w}{\mu_w} \nabla (\Phi_w)_w \quad (3)$$

and

$$\vec{v}_o = - \frac{k_{oiw} \rho_o}{\mu_o} \nabla (\Phi_o)_o \quad (4)$$

If it is assumed that, on the interface, $v_{wz} = v_{oz} = v$, and if it is supposed that k_{wor} and k_{oiw} are independent of z , and if the integration is carried out for fixed values of x and y , Equations 3 and 4 may be integrated with respect to z . By undertaking this integration, it may be shown that $(\Phi_w)_w$ and $(\Phi_o)_o$ may also be defined, respectively, by

$$(\Phi_w)_w = \Phi_{wi} - \frac{\mu_w v}{k_{wor} \rho_w} (\xi_w)_o \quad (5)$$

and

$$(\Phi_o)_o = \Phi_{oi} - \frac{\mu_o v}{k_{oiw} \rho_o} (\xi_w)_o \quad (6)$$

where $\Phi_{wi}(x,y)$ is the initial value of the potential in the water on the water side of the interface and $\Phi_{oi}(x,y)$ is the initial value of the potential in the oil on the oil side of the interface.

If Equations 5 and 6 are introduced into Equation 2, and if it is kept in mind that Equation 2 pertains to each point on the interface, it may be demonstrated, after some manipulation, that

$$(\Phi_w)_o = -\frac{1}{\rho_w} \left[\frac{\mu_w v}{k_{wor}} (M - 1 - N_g) (\xi_w)_o - (P_{cw})_o \right] + \frac{1}{\rho_w} (\rho_o \Phi_{oi} - \rho_w \Phi_{wi} + P_c(t)) \quad (7)$$

where

$$M = \frac{k_{wor} \mu_o}{\mu_w k_{oiw}} \quad (8)$$

and

$$N_g = \frac{\Delta \rho g k_{wor} \cos \alpha}{\mu_w v} \quad (9)$$

At zero displacement of the interface, the surface is plane. As a consequence, the pressure difference across it should be zero. Thus, if it is assumed that $(P_{cw})_0$ is zero at zero displacement of the interface, it follows that

$$(\Phi_w^*(z=0))_0 = \frac{1}{\rho_w} [\rho_o \Phi_{oi} - \rho_w \Phi_{wi} + P_c(t)] \quad (10)$$

Moreover, if the roots of the viscous fingers are to remain fixed in the surface which initially separates the oil from the water, it is necessary that $(\Phi_w^*(z=0))_0$ equal zero. Thus, if such is the case, $P_c(t)$ is defined by

$$P_c(t) = -(\rho_o \Phi_{oi} - \rho_w \Phi_{wi}) \quad (11)$$

That is to say, $P_c(t)$ may be interpreted, except for the negative sign, as being the pressure difference which existed across the pseudosurface, prior to its being perturbed. The negative sign enters the analysis because, for a water-wet porous medium, a reversal in sign of the radius of curvature takes place, once a viscous finger is initiated.

The number of viscous fingers propagating depends on the mode numbers m_1 and m_2 (see Equations 21 and 22). It sometimes happen that, during the course of a displacement, the number of fingers propagating decreases by one or more. That is, a change in mode takes place. When propagating viscous fingers shift from one mode to the next, the roots of the fingers no longer remain fixed in the surface which initially separated the oil from the water. In order to be able to discuss how such shifts in phase take place, at least qualitatively, it is supposed that, when a phase shift takes place, $P_c(t)$ is proportional to the initial difference in pressure across the interface; that is, that

$$P_c(t) = -C(\rho_o \Phi_{oi} - \rho_w \Phi_{wi}) \quad (12)$$

where C is the constant of proportionality. The introduction of Equation 12 into Equation 7

yields, for the perturbation potential of the water,

$$(\Phi_w^*)_o = -\frac{1}{\rho_w} \left[\frac{\mu_w v}{k_{wor}} (M - 1 - N_g) (\xi_w)_o - (P_{cw})_o \right] + \frac{1-C}{\rho_w} (\rho_o \Phi_{oi} - \rho_w \Phi_{wi}) \quad (13)$$

In order to develop the equation which defines the surface separating the water from the oil, it is necessary to assume that the roots of the viscous fingers remain fixed in the surface which initially separated the oil from the water. For the roots to remain fixed, it is necessary that the initial perturbation velocities in the x and y directions be zero. This can be achieved by setting C equal to one. Thus if the constant of proportionality, C, is assumed to be equal to one, Equation 13 may be revised to read

$$\rho_w (\Phi_w^*)_o = -\frac{\mu_w v}{k_{wor}} (M - 1 - N_g) (\xi_w)_o + (P_{cw})_o \quad (14)$$

Equation 14 defines the pressure difference across the pseudosurface which pertains at a given displacement of the surface, $(\xi_w)_o$. If the normal forces acting on the surface were in balance, the perturbation potential would be zero and, consequently, the equilibrium pressure difference across the interface would be defined by

$$(P_{cw})_{oe} = \frac{\mu_w v}{k_{wor}} (M - 1 - N_g) (\xi_w)_o \quad (15)$$

However, if a viscous finger is propagating, the forces acting on the surface will not be in balance. Rather, the pressure difference across the interface will be slightly smaller than the equilibrium macroscopic capillary pressure, $(P_{cw})_{oe}$. The actual relationship between the dynamic and the equilibrium capillary pressure is not known. However, assuming that the actual (dynamic) capillary pressure is proportional to its equilibrium value makes it possible to estimate the actual pressure drop across the interface, the size of the propagating fingers, and the velocity at which they propagate. Consequently, this approach is taken here. That is, it is assumed that the macroscopic capillary pressure is defined by

$$(P_{cw})_o = \frac{\beta_w(M) \mu_w v}{k_{wor}} (M - 1 - N_g) (\xi_w)_o \quad (16)$$

where $\beta(M)$ is the constant of proportionality. Note that assuming $(P_{cw})_o$ is proportional to $(P_{cw})_{oe}$ implicitly assumes that β is a function of M (see Equation 54).

4.1.4 Equation for Pseudosurface

If Equation 16 is assumed to define the macroscopic capillary pressure (force function), $(P_{cw}(x,y,z))_o$, Equation 1 may be written as

$$\frac{\partial^2 (\xi_w)_o}{\partial x^2} + \frac{\partial^2 (\xi_w)_o}{\partial y^2} + \frac{\beta_w(M) \mu_w v}{\sigma_e k_{wor}} (M - 1 - N_g) (\xi_w)_o = 0 \quad (17)$$

Then, if one defines

$$\gamma_w^2 = \frac{\beta_w(M) \mu_w v}{\sigma_e k_{wor}} (M - 1 - N_g) \quad (18)$$

it follows that

$$\frac{\partial^2 (\xi_w)_o}{\partial x^2} + \frac{\partial^2 (\xi_w)_o}{\partial y^2} + \gamma_w^2 (\xi_w)_o = 0 \quad (19)$$

Equation 19, which is known as the Helmholtz equation[97], is the defining equation for the surface $(\xi_w)_o$. It should be noted that the only requirement on $(\xi_w)_o$, if it is to be a solution to Equation 19, is that the surface be periodic in the x and y directions[98].

The solution to Equation 19 will take the form[1,2]

$$(\xi_w)_o = z_w \cos \alpha_{xw} x \cos \alpha_{yw} y \quad (20)$$

where

$$\alpha_{xw} = \frac{m_1 \pi}{2h} \frac{\gamma_w + \gamma_o}{\gamma_o} = \frac{\pi}{2h_w} \quad (21)$$

and

$$\alpha_{yw} = \frac{m_2 \pi}{2b} \frac{\gamma_w + \gamma_o}{\gamma_o} = \frac{\pi}{2b_w} \quad (22)$$

and where z_w , the amplitude of a water finger, is supposed to be a function of time.

4.1.5 Perturbation Velocities

Before deriving the equations for the perturbation velocities, it is necessary to revise the defining equations for macroscopic capillary pressure. Thus, if Equation 18 is introduced into Equation 16, it follows that macroscopic capillary pressure in the region where the oil is flowing may be defined by

$$(P_{cw})_o = \sigma_e \gamma_w^2 (\xi_w)_o \quad (23)$$

A similar approach may be taken to show that the macroscopic capillary pressure in the region where water is flowing may be defined by[2]

$$(P_{co})_w = \sigma_e \gamma_o^2 (\xi_o)_w \quad (24)$$

By combining Darcy's law with Equations 13 and 23, the perturbation velocities in the x, y and z directions in the region where the oil is flowing may be shown to be

$$(v_{wx}^*)_o = -(C_x - 1) [v(M - 1 - N_g) - \frac{k_{wor}}{\mu_w} \sigma_e \gamma_w^2] \frac{\partial (\xi_w)_o}{\partial x} \quad (25)$$

$$(v_{wy}^*)_o = -(C_y - 1) [v(M - 1 - N_g) - \frac{k_{wor}}{\mu_w} \sigma_e \gamma_w^2] \frac{\partial (\xi_w)_o}{\partial y} \quad (26)$$

and

$$(v_{wz})_o = [v(M - 1 - N_g) - \frac{k_{wor}}{\mu_w} \sigma_e \gamma_o^2] \frac{\partial(\xi_w)_o}{\partial z} \quad (27)$$

In deriving Equations 25 and 26, advantage was taken of the fact that both $(v_{wx})_o$ and $(v_{wy})_o$ must be identically equal to zero, if the root of a viscous finger is to remain fixed in the surface which initially separated the oil from the water. That is, if no phase shift is taking place, both C_x and C_y must be identically equal to one. If, however, a viscous finger begins to shift from one mode to the next, both C_x and C_y will differ from one. It is thought that if a finger is changing from one mode to the next, the magnitude of C_x and C_y will depend upon the nature of the perturbation which initiated the shift in phase.

By taking a similar approach, the perturbation velocities in the x, y and minus z directions, respectively, in the region where water is flowing may be shown to be

$$(v_{ox})_w = \frac{D_x - 1}{M} [v(M - 1 - N_g) - \frac{k_{wor}}{\mu_w} \sigma_e \gamma_o^2] \frac{\partial(\xi_o)_w}{\partial x} \quad (28)$$

$$(v_{oy})_w = \frac{D_y - 1}{M} [v(M - 1 - N_g) - \frac{k_{wor}}{\mu_w} \sigma_e \gamma_o^2] \frac{\partial(\xi_o)_w}{\partial y} \quad (29)$$

and

$$(v_{oz})_w = -\frac{1}{M} [v(M - 1 - N_g) - \frac{k_{wor}}{\mu_w} \sigma_e \gamma_o^2] \frac{\partial(\xi_o)_w}{\partial z} \quad (30)$$

4.1.6 Time Function

While Equation 20 indicates how $(\xi_w)_o$ depends on x, y and z_w , it does not show how z_w depends on t. To learn how z_w depends on t, it is supposed that $z_w = z$, and that the displacement of any point on the surface, ξ , depends on x, y and z (i.e. $\xi = \xi(x, y, z)$) and that x, y and z are functions of t. For such a situation, one may write

$$F(\xi, x, y, z) = 0 \quad (31)$$

for which the total derivative with respect to time is given by

$$\frac{dF}{dt} = \frac{\partial F}{\partial \xi} \frac{d\xi}{dt} + \frac{\partial F}{\partial x} \frac{dx}{dt} + \frac{\partial F}{\partial y} \frac{dy}{dt} + \frac{\partial F}{\partial z} \frac{dz}{dt} = 0 \quad (32)$$

The subsidiary system of ordinary differential equations for this quasi-linear, partial differential equation is [99]

$$\frac{d\xi}{d\xi/dt} = \frac{dx}{dx/dt} = \frac{dy}{dy/dt} = \frac{dz}{dz/dt} \quad (33)$$

or

$$\left. \frac{d\xi}{dt} \right|_{y,z} = \frac{d\xi}{dx} \bigg|_{y,z} \frac{dx}{dt} = \frac{\partial \xi}{\partial x} \frac{dx}{dt} \quad (34)$$

$$\left. \frac{d\xi}{dt} \right|_{x,z} = \frac{d\xi}{dy} \bigg|_{x,z} \frac{dy}{dt} = \frac{\partial \xi}{\partial y} \frac{dy}{dt} \quad (35)$$

and

$$\left. \frac{d\xi}{dt} \right|_{x,y} = \frac{d\xi}{dz} \bigg|_{x,y} \frac{dz}{dt} = \frac{\partial \xi}{\partial z} \frac{dz}{dt} \quad (36)$$

In view of Equations 25, 26 and 27, the solutions, for a water finger, to Equations 34, 35 and 36 are

$$(\dot{v}_{wx})_o = \frac{\partial(\xi_w)_o}{\partial x} \frac{dx}{dt} = - (C_x - 1) [v(M - 1 - N_g) - \frac{k_{wor}}{\mu_w} \sigma_e \gamma_w^2] \frac{\partial(\xi_w)_o}{\partial x} \quad (37)$$

$$(\dot{v}_{wy})_o = \frac{\partial(\xi_w)_o}{\partial y} \frac{dy}{dt} = - (C_y - 1) [v(M - 1 - N_g) - \frac{k_{wor}}{\mu_w} \sigma_e \gamma_w^2] \frac{\partial(\xi_w)_o}{\partial y} \quad (38)$$

and

$$(v_{wz})_0 = \frac{\partial(\xi_w)_0}{\partial z} \frac{dz}{dt} = [v(M-1-N_g) - \frac{k_{wor}}{\mu_w} \sigma_e \gamma_w^2] \frac{\partial(\xi_w)_0}{\partial z} \quad (39)$$

From Equations 37, 38 and 39, it can be seen that

$$\frac{dx_w}{dt} = -(C_x - 1) [v(M-1-N_g) - \frac{k_{wor}}{\mu_w} \sigma_e \gamma_w^2] \quad (40)$$

$$\frac{dy_w}{dt} = -(C_y - 1) [v(M-1-N_g) - \frac{k_{wor}}{\mu_w} \sigma_e \gamma_w^2] \quad (41)$$

and

$$\frac{dz_w}{dt} = [v(M-1-N_g) - \frac{k_{wor}}{\mu_w} \sigma_e \gamma_w^2] \quad (42)$$

Equations 40 and 41 define the rate at which the base of a water finger increases in the x and y directions, respectively. It should be noted that, because of the assumptions underlying Equation 19, the root of a water finger must remain fixed in the surface which initially separated the water from the oil. That is, both C_x and C_y must be identically equal to one. Consequently, both dx_w/dt and dy_w/dt become equal to zero. As noted earlier, the possibility of C_x and C_y differing from one has been included in the analysis in order to be able to discuss, at least qualitatively, how a shift from one mode to the next takes place.

Equation 42 defines the rate at which the amplitude of a water finger increases in the z direction. From this equation it can be seen that, for any given value of γ_w , the velocity of propagation of a water finger must be constant, provided v is constant. Thus, it may be supposed that

$$z_w = z = a_w + (v_{wm})_0 t \quad (43)$$

where $(v_{wm})_0$ is defined by Equation 42 and where a_w is the initial amplitude of the disturbance. A similar approach may be used to show that

$$z_0 = -z = -a_o - (v_{om})_w t \quad (44)$$

where a_o is the initial amplitude of an oil finger, and where $(v_{om})_w$ is defined by

$$(v_{om})_w = \frac{1}{M} [v(M-1-N_g) - \frac{k_{wor}}{\mu_w} \sigma_e \gamma_o^2] \quad (45)$$

Introducing Equation 43 into Equation 20 yields, for the displacement of any point on the initial interface as a function of time,

$$(\eta_w(x,y,t))_0 = \cos \alpha_{xw} x \cos \alpha_{yw} y (a_w + (v_{wm})_0 t) \quad (46)$$

Differentiating Equation 46 with respect to t gives, for the rate at which the amplitude of the surface is increasing,

$$\frac{\partial (\eta_w)_0}{\partial t} = (v_{wm})_0 \cos \alpha_{xw} x \cos \alpha_{yw} y \quad (47)$$

The velocity at which the tip of the finger is propagating may be found by setting $x=y=0$ in Equation 47. If this is done, it follows that $(v_{wm})_0$ is the velocity at which the tip of a water finger is propagating. A similar approach may be used to show that $(v_{om})_w$ is the velocity at which the tip of an oil finger is propagating.

4.1.7 Compatibility Conditions

Certain conditions must be met if the growth of two or more pairs of oppositely directed fingers is to be compatible. For this study, it is sufficient to impose conditions of symmetry, similarity and continuity. If the symmetry condition is to be met, the roots of

oppositely directed pairs of fingers must be located symmetrically within the rectangular interface that initially separated the oil from the water. This may be achieved by requiring that the integral values of m_1 and m_2 be the same for $(\eta_w)_o$ as for $(\eta_o)_w$ [2].

The second condition, that of similarity, requires that the shape of a given water finger be similar to that of the contiguous, oppositely directed oil finger over the entire time span of finger growth. Because the same functional form was assumed for both the oil and the water fingers, similarity can be assured by demanding that the capillary velocity vectors for the water fingers be colinear with those for the oil fingers at equivalent locations on the surface of each finger. Upon applying this condition, it may be shown that[2]

$$\gamma_o^3 = M \gamma_w^3 \quad (48)$$

which implies that the wavelength of a water finger is $M^{1/3}$ times that of an oil finger. The validity of this relationship has been confirmed experimentally in analogue models of porous media[3,100].

The final compatibility requirement is that of continuity. Continuity can be guaranteed by requiring that the volume of water contained within a water finger be the same as the volume of oil contained within the contiguous, oppositely directed oil finger.

Application of this condition leads to the requirement that

$$\frac{(v_{wm}^*)_o}{(v_{om}^*)_w} = \frac{z_w}{z_o} = \frac{a_w}{a_o} = \frac{\gamma_w^2}{\gamma_o^2} \quad (49)$$

Moreover, by combining Equations 43 and 44 with the appropriate form of Equation 20 and introducing the proper form of the resulting equations into Equations 27 and 30, it also follows, at equivalent locations on each finger, that

$$\frac{(v_{wz}^*)_o}{\gamma_w^2} = \frac{(v_{oz}^*)_w}{\gamma_o^2} \quad (50)$$

Equations 49 and 50 guarantee that continuity is met, provided that the roots of the oppositely directed fingers remain fixed in the surface which initially separated the water from the oil.

4.1.8 Velocity of Penetrating Fingers

Equations 27, 30, 48 and 50 comprise a system of four equations in the four unknowns: $(v_{wz}^*)_o$, $(v_{oz}^*)_w$, γ_w and γ_o . This system of equations may be solved to show that

$$(v_{wz}^*)_o = \frac{M^{2/3} - 1}{M^{5/3} + 1} \frac{k_{wor}\sigma_e}{\mu_w} \gamma_w^2 \cos\alpha \cos\alpha_{wy} \quad (51)$$

where

$$\gamma_w^2 = \frac{\mu_w v (M - 1 - N_g)}{k_{wor}\sigma_e} \frac{M^{5/3} + 1}{M^{2/3}(M + 1)} \quad (52)$$

defines the value of γ_w^2 that corresponds to a particular velocity, v . By setting $x=y=0$ and by introducing Equation 52 into Equation 51, the velocity at the tip of a propagating finger may be shown to be

$$(v_{wm}^*)_o = \frac{v(M - 1 - N_g)}{M + 1} \frac{M^{2/3} - 1}{M^{2/3}} \quad (53)$$

This result may be obtained also by introducing Equation 52 into Equation 42. Moreover, a comparison of Equation 52 with Equation 18 reveals that $\beta_w(M)$ is defined by

$$\beta_w(M) = \frac{M^{5/3} + 1}{M^{2/3}(M + 1)} \quad (54)$$

It should be noted that both $\beta(1)$ and $\beta(\infty)$ equal one, whereas, for values of M between one and infinity, $\beta_w(M)$ is somewhat less than one, the amount depending on the value of M .

4.1.9 Most Probable Finger Width

As noted in an earlier section, it seems likely that the dominant finger will be the one for which new surface is being created at the greatest rate. To investigate this possibility, it is necessary to ascertain the surface area to volume ratio for a finger. The surface area of a water finger is defined by [101]

$$A_{sw} = \iint_R \sqrt{\left(\frac{\partial(\xi_w)_0}{\partial x}\right)^2 + \left(\frac{\partial(\xi_w)_0}{\partial y}\right)^2} dx dy \quad (55)$$

By introducing Equation 20 into Equation 55, and by assuming (for purposes of simplification) that $\alpha_{xw} = \alpha_{yw}$ it may be shown that

$$A_{sw} = \iint_R \sqrt{[z_w^2 \gamma_w^2 \sin^2 \alpha_{xw} \cos^2 \alpha_{yw} + 1]} dx dy \quad (56)$$

Equation 56 cannot be integrated analytically. However, approximate integrals can be obtained for limiting cases. That is, an approximate value for the surface area of a water finger is given by

$$A_{sw} \approx \frac{z_w \gamma_w}{\alpha_{xw} \alpha_{yw}} \quad (57)$$

provided that z_w is much larger than one. Moreover, in view of Equation 20, the volume of the same finger may be demonstrated to be

$$V_w = \frac{z_w}{\alpha_{xw} \alpha_{yw}} \quad (58)$$

As a consequence, the surface area to volume ratio for a long water finger may be shown to be

$$\frac{A_{sw}}{V_w} = \gamma_w \quad (59)$$

Multiplying Equation 59 by the cross-sectional area of the base of a finger times the average velocity at which fluid is crossing the base of the finger gives, for the rate at which new surface is being created,

$$R_{sw} = \gamma_w v_{wa} b_w h_w \quad (60)$$

The maximum velocity of a water finger may be found by setting $x=y=0$ in Equation 51. Moreover, the average rate at which water is crossing the base of a water finger may be found by integrating the point velocity (defined by Equation 51) over the total area through which flow is occurring. If these steps are taken, it may be shown that the average rate at which water is crossing the base of a water finger is related to the maximum rate by

$$v_{wa} = \frac{4}{\pi^2} (v_{wm})_0 \quad (61)$$

Introducing Equations 61 and 42 into Equation 60 and dividing through by the area of the base of the finger yields

$$n_w = \frac{4}{\pi^2} \gamma_w \left[v(M-1-N_g) - \frac{k_{wor}}{\mu_w} \sigma_e \gamma_w^2 \right] \quad (62)$$

for the time constant of a water finger. By differentiating Equation 62 with respect to γ_w , and setting the resulting equation equal to zero, the most probable finger width may be shown to be defined by

$$\gamma_m^2 = \frac{1}{3} \gamma_c^2 \quad (63)$$

where

$$\gamma_c^2 = \frac{\mu_w v (M-1-N_g)}{\sigma_e k_{wor}} \quad (64)$$

Equation 63 is consistent with results obtained earlier[1,2,16]. However, it should be emphasized that this result is valid only for fingers for which $z_w \gamma_w \gg 1$.

For an incipient water finger ($z_w \gamma_w \ll 1$), the surface area of the finger is approximately equal to the area of its base. Thus, an estimate of the surface area to volume ratio is given by

$$\frac{A_{sw}}{V_w} = \frac{\pi^2}{4} \frac{1}{z_w} \quad (65)$$

Equation 65 cannot be used to determine the most probable finger width for an incipient finger because it does not contain the parameter γ_w . However, because there is enough energy available initially to drive the interface at the wavelength corresponding to the maximum mode, it is thought that every displacement should start at this mode[95]. Given the validity of this assumption, the most probable incipient finger width is defined by

$$\gamma_{m1} = \gamma_c \quad (66)$$

That is to say, when a finger first forms, its wavelength will be that dictated by the critical wavelength, γ_c . However, as the finger begins to grow, and as it is perturbed by variations in rock properties, the mode of the finger is likely to switch to the most probable mode because it takes less energy per unit volume of finger to create new surface for such a finger.

Moreover, the likelihood of the most probable mode propagating increases as the displacement becomes further removed from the stability boundary[2].

4.1.10 Stability Criterion

The type of displacement that takes place in a porous medium depends upon the balance existing among the capillary, gravitational and viscous forces. If the combined forces of gravity and capillarity are greater than the viscous forces, the displacement will be stable. If, however, the reverse is true, the displacement will be unstable. The characteristic value of

the superficial velocity that separates these flow regimes is defined by the instability number, $I_{sr}[2]$. Thus the displacement will be stable provided that

$$I_{sr} = \frac{\mu_w v (M - 1 - N_g)}{k_{wor} \sigma_e} \frac{M^{5/3} + 1}{(M + 1)(M^{1/3} + 1)^2} \frac{4h^2b^2}{h^2 + b^2} \leq \pi^2 \quad (67)$$

4.1.10.1 Pseudointerfacial Tension

In order to use Equation 67, one must be able to estimate the pseudointerfacial tension, σ_e . In this study, σ_e is estimated by making use of a recently developed mechanistic model[26] that requires the capillary pressure versus saturation curve. Given that such a curve is available, σ_e may be obtained from

$$\sigma_e = \frac{A_c \phi_r (1 - S_{wi} - S_{or})}{2/\bar{r}_m} \quad (68)$$

where, by definition[26], $2/\bar{r}_m$ equals a unit reciprocal length and where A_c is the area under the capillary pressure versus saturation curve.

4.1.11 Breakthrough Recovery

Because an equation for the perturbation velocity is available (Equation 53), it should be possible to estimate the breakthrough recovery. However, certain assumptions must be made before this can be done. Moreover, these assumptions differ somewhat dependent upon whether the displacement is stable or unstable.

4.1.11.1 Stable Displacements

The idealized displacement model which forms the basis for instability theory is based on the assumption that the displaced and displacing fluids will remain separated by a saturation discontinuity, if the displacement is stable. However, in a real porous medium such is not the case because a distribution of saturations will evolve to separate the two regions where only one fluid is flowing. To model this saturation distribution, it

is assumed that the superficial velocity is such that the stability boundary has just been crossed (i.e., that $m_1 = m_2 = 1$) and that, as a consequence, half of a water finger is propagating. The velocity of the tip of such a finger is given by Equation 53. If one adds the superficial velocity, v , to Equation 53 and then divides by the porosity times the change in saturation, the actual velocity of the tip of a finger may be shown to be

$$v_{wfa} = \frac{v}{\phi(1 - S_{wi} - S_{or})} \left[1 + \frac{M - 1 - N_g}{M + 1} \frac{M^{2/3} - 1}{M^{2/3}} \right] \quad (69)$$

It is to be noted that this equation differs slightly (a factor $\pi^3/16$ is missing) from an equation developed earlier[2]. This difference arises because, in Reference 2, the maximum perturbation velocity, $(v_{wmp})_0$, was incorrectly related to the average velocity of the propagating finger, rather than to the velocity at the tip of the finger, as is the case in this study. Knowing v_{wfa} enables the prediction of the time to breakthrough and the amount of oil produced at breakthrough. Consequently, the breakthrough recovery, as a fraction of the initial oil-in-place, may be shown to be

$$R_{bt} = \frac{1 - S_{wi} - S_{or}}{1 - S_{wi}} \left[\frac{X_o}{L} + \frac{1 - \frac{X_o}{L}}{1 + \frac{M - 1 - N_g}{M + 1} \frac{M^{2/3} - 1}{M^{2/3}}} \right] \quad (70)$$

where X_o is the location where fingering began.

4.1.11.2 Pseudostable Displacements

For values of I_{sr} (dimensionless velocity) at or near π^2 , only one finger width is possible. However, as the instability number is increased above π^2 , fingers with smaller and smaller wavelengths can be formed. Which wavelength will dominate the displacement depends upon the amount by which I_{sr} exceeds π^2 . Moreover, as the value of I_{sr} increases the likelihood that one wavelength, the most probable one, will dominate the displacement becomes much greater. When the value of I_{sr} is high enough that the most probable wavelength invariably dominates, the displacement is said to be

pseudostable[2,5]. If the displacement is pseudostable, the perturbation velocity of a finger is three times that of the critical perturbation velocity associated with the actual injection rate[2]. That is to say, the velocity of the tip of the most probable finger is given by

$$(v_{wm})_0 = \frac{3 v (M-1-N_g)}{(M+1)} \frac{(M^{2/3} - 1)}{M^{2/3}} \quad (71)$$

As a consequence, the breakthrough recovery equation for a pseudostable displacement becomes

$$R_{bt} = \frac{1-S_{wi}-S_{or}}{1-S_{wi}} \left[\frac{X_o}{L} + \frac{1 - \frac{X_o}{L}}{1 + 3 \frac{M-1-N_g}{M+1} \frac{M^{2/3} - 1}{M^{2/3}}} \right] \quad (72)$$

4.2 Stabilization

External-drive methods are valid only if the displacement is stabilized. To determine the degree of stabilization achieved in a given run, the capillary number, N_c , defined by[36]

$$N_c = \frac{A_c k_{wor}}{V L \mu_w} \quad (73)$$

was evaluated for each run. Here A_c is a lumped parameter which represents the area under the capillary pressure curve and, as such, includes the effects of wettability, interfacial tension, and pore-size distribution. Theoretical considerations[36] suggest that N_c should be less than 0.01, if the displacement is to be stabilized. However, practical considerations[42,51] suggest that a value of 0.01 for N_c may be too restrictive, and that a value of N_c less than 0.1 may be more realistic.

4.3 Estimation of Relative Permeabilities

4.3.1 Introduction

In this section it is demonstrated how improved functional forms for smoothing cumulative-oil and pressure-drop histories can be obtained by taking proper account of the constants of integration for the two differential equations describing the system, and by imposing various physical conditions on the integrated forms of the equations used to model cumulative-oil and pressure-drop histories. It is also shown that a further benefit of this approach is that the functional forms used to fit the data and those used to estimate the effective permeabilities are internally consistent.

The theory presented herein is based on Buckley-Leverett theory[20]. As a consequence, the practical application of the equations developed is limited to those displacements wherein the assumptions underlying Buckley-Leverett theory are met. The approach taken here is based on the equations derived by Jones and Roszelle[48].

4.3.2 Basic Equations

Given that gravity and capillary effects may be neglected, the water and oil relative permeabilities are defined by

$$k_{rw} = \frac{\mu_w f_{w2}}{k \lambda_2^{-1}} \quad (74)$$

and

$$k_{ro} = \frac{\mu_o f_{o2}}{k \lambda_1^{-1}} \quad (75)$$

To utilize these equations, the fractional flow of oil, f_{o2} , and the reciprocal mobility, λ_2^{-1} , evaluated at the outlet end of the core, must be determined as functions of time. Moreover, the saturation to water at the outlet end of the coreholder, S_{w2} , must be determined as a

function of time.

4.3.3 Estimation of Fractional Flow and Saturation

Jones and Roszelle[48] have demonstrated that

$$\bar{S}_w = S_{wi} + \frac{N_p}{V_p} \quad (76)$$

and

$$S_{w2} = \bar{S}_w - Q_1 \frac{d\bar{S}_w}{dQ_1} \quad (77)$$

If Equation 76 is introduced into Equation 77, and if the definition for Q_1 is introduced into the resulting expression, it follows that

$$S_{w2} - S_{wi} = \frac{N_p}{V_p} - \frac{t}{V_p} \frac{dN_p}{dt} \quad (78)$$

or, upon rearrangement, that

$$\frac{dN_p}{dt} - \frac{1}{t} N_p = -V_p \frac{(S_{w2} - S_{wi})}{t} \quad (79)$$

Equation 79 is a linear differential equation of the first order which possesses $1/t$ as an integrating factor[99]. Consequently, its integral can be shown to be

$$\frac{N_p}{t} = \frac{N_{pm}}{t_m} + V_p \int_t^{t_m} \frac{S_{w2} - S_{wi}}{\tau^2} d\tau \quad (80)$$

where N_{pm} is the maximum (total) amount of oil recoverable, and t_m is the time necessary to recover that oil. Given that N_{pm} is defined by

$$N_{pm} = V_p (1 - S_{wi} - S_{or}) \quad (81)$$

it follows that

$$N_p = \frac{V_p(1-S_{wi}-S_{or})t}{t_m} + V_p t \int_t^{t_m} \frac{S_{w2}}{\tau^2} d\tau \quad (82)$$

Because the constant of integration term is multiplied by t , the arbitrary regression equations used by other authors (see, for example, Reference 49) to fit cumulative oil production histories may not be consistent with Equation 82. It has been the author's experience that a lack of agreement between Equation 82 and the regression equation results in inconsistencies between the regression equation and the equation used to predict the fraction of oil flowing at the outlet end of the core as a function of time.

It is not possible to carry out the integration indicated in Equation 82 because the functional form for $S_{w2}(t)$ is unknown. However, this problem can be circumvented if one postulates a functional form for $S_{w2}(t)$. In choosing a functional form for this purpose, two points must be kept in mind. First, such functional forms are not necessarily unique, as several quite different forms may prove adequate from a fitting point of view. If several equations give essentially the same fit, the one with lowest number of parameters should be chosen [49]. Second, any form chosen must be such that S_{w2} asymptotically approaches $(1-S_{or})$ as t tends to t_m .

To illustrate the method being developed here, it is supposed that S_{w2} may be defined by

$$S_{w2} = \frac{3a_2}{t_m^2} - \frac{3a_2}{t^2} + \frac{2a_3}{t_m} - \frac{2a_3}{t} + a_4 \ln \frac{t}{t_m} - a_5 t + a_5 t_m + 1 - S_{or} \quad (83)$$

If Equation 83 is introduced into Equation 82, and the indicated integration is carried out, it can be shown that

$$N_p = V_p \left\{ \frac{3a_2}{t_m^2} - \frac{a_2}{t^2} + \frac{2a_3}{t_m} - \frac{a_3}{t} + a_4 \left(1 + \ln \frac{t}{t_m} \right) - \left(\frac{2a_2}{t_m^3} + \frac{a_3}{t_m^2} + \frac{a_4}{t_m} + a_5 \right) t \right. \\ \left. + a_5 \left(t_m + t \ln \frac{t}{t_m} \right) + (1 - S_{wi} - S_{or}) \right\} \quad (84)$$

Moreover, by differentiating Equation 84 with respect to t , and by noting that

$$f_{o2} = \frac{1}{q} \frac{dN_p}{dt} \quad (85)$$

it follows that

$$f_{o2} = \frac{V_p}{q} \left\{ \frac{2a_2}{t^3} + \frac{a_3}{t^2} + \frac{a_4}{t} - \frac{2a_2}{t_m^3} - \frac{a_3}{t_m^2} - \frac{a_4}{t_m} + a_5 \ln \frac{t}{t_m} \right\} \quad (86)$$

As can be seen from Equation 86, the fraction of oil flowing at the outlet end of the core becomes zero at $t = t_m$, as it should. Finally, it is to be noted that, if Equation 84 (or 86) is to be useful, cumulative oil production data must be available so that the values of the parameters which give the "best" fit to the experimental data can be estimated.

4.3.4 Reciprocal Mobility

In order to use Equations 74 and 75 to estimate the effective permeabilities as a function of saturation, it is necessary to predict how the reciprocal mobility, λ_2^{-1} , varies with time. To accomplish this, it is first necessary to determine how the average reciprocal mobility, $\bar{\lambda}_2^{-1}$, defined by

$$\bar{\lambda}_2^{-1} = \frac{A \Delta P}{q L} \quad (87)$$

varies with time. The functional relationship between λ_2^{-1} and $\bar{\lambda}_2^{-1}$, as determined by Jones and

Roselle[48], is given by

$$\lambda_2^{-1} = \bar{\lambda}_2^{-1} - t \frac{d\bar{\lambda}_2^{-1}}{dt} \quad (88)$$

Introducing the definition for Q_1 and rearranging, Equation 88 becomes

$$\frac{d\bar{\lambda}_2^{-1}}{dt} - \frac{1}{t} \bar{\lambda}_2^{-1} = - \frac{\bar{\lambda}_2^{-1}}{t} \quad (89)$$

Following the same procedure used to integrate Equation 80, it follows that

$$\frac{\bar{\lambda}_2^{-1}}{t} = \frac{\bar{\lambda}_{2m}^{-1}}{t_m} + \int_t^{t_m} \frac{\lambda_2^{-1}}{\tau^2} d\tau \quad (90)$$

where $\bar{\lambda}_{2m}^{-1}$ is the value of the reciprocal mobility at the outlet end of the core when $t = t_m$. At $t = t_m$, only one fluid, water, is flowing in the core. Consequently, $\bar{\lambda}_{2m}^{-1}$ is defined by

$$\bar{\lambda}_{2m}^{-1} = \frac{\mu_w}{k_{wor}} \quad (91)$$

Hence, Equation 90 may be written

$$\frac{\bar{\lambda}_2^{-1}}{t} = \frac{\mu_w}{k_{wor}} \frac{t}{t_m} + t \int_t^{t_m} \frac{\lambda_2^{-1}}{\tau^2} d\tau \quad (92)$$

As noted earlier, any regression equation used to fit the pressure history of the core must be consistent with Equation 92. Because the true functional form for $\lambda_2^{-1}(t)$ is unknown, it is again necessary to postulate a functional form. In choosing a particular form for $\lambda_2^{-1}(t)$, it is necessary to keep in mind that $\lambda_2^{-1}(t)$ asymptotically approaches μ_w/k_{wor} as t tends to t_m . Thus, by way of illustration, it is supposed that

$$\lambda_2^{-1}(t) = \frac{3b_2}{t^2} - \frac{3b_2}{t_m^2} + \frac{2b_3}{t} - \frac{2b_3}{t_m} - b_4 \ln \frac{t}{t_m} - b_5 t_m + b_5 t + \frac{\mu_w}{k_{wor}} \quad (93)$$

Introducing Equation 93 into Equation 92 and carrying out the indicated integration, it follows that

$$\bar{\lambda}_2(t) = \frac{b_2}{t^2} - \frac{3b_2}{t_m^2} + \frac{b_3}{t} - \frac{2b_3}{t_m} - b_4 \left(1 + \ln \frac{t}{t_m}\right) + \left(\frac{2b_2}{t_m^3} + \frac{b_3}{t_m^2} + \frac{b_4}{t_m} + b_5\right)t - b_5 \left(t_m + t \ln \frac{t}{t_m}\right) + \frac{\mu_w}{k_{wor}} \quad (94)$$

Note that $\bar{\lambda}_2(t_m) = \mu_w/k_{wor}$, as expected. Here again, it is necessary to determine the values of the parameters which give the "best" fit of the experimental data.

4.4 Cumulative Oil Recovery

By undertaking a material balance, it is possible to derive a relationship between cumulative oil produced and the total weight of the produced fluids at any given point in time. Thus, given that the fluids are incompressible and immiscible, it can be shown that

$$N_p = \frac{\rho_w q t - W}{\rho_w - \rho_o} \quad (95)$$

where W is the total weight of the produced fluids.

4.5 Time to Breakthrough

Prior to breakthrough, a plot of W versus t yields a straight line whose slope may be used to determine q . Subsequent to breakthrough, the plot of W versus t yields a second, essentially straight line of greater slope. The point of intersection of these two lines can be used to estimate the time to breakthrough.

It can be demonstrated that, for a horizontal system[102], the velocity at which the tip of a first mode finger propagates is defined by

$$v_{wfa} = \frac{v}{\phi(1-S_{wi}-S_{or})} E(M) \quad (96)$$

where

$$F(M) = \frac{M-1}{M+1} \frac{M^{2/3}-1}{M^{2/3}} \quad (97)$$

and

$$M = \frac{k_{wor}}{\mu_w} \frac{\mu_o}{k_{oiw}} \quad (98)$$

It is also demonstrated in Reference 102 that Equation 96 can be used to estimate the velocity at which the saturation discontinuity (shock) introduced in Buckley-Leverett theory[20] propagates through the system. Given the validity of this assumption, it follows that the time to breakthrough is defined by

$$t_{bt} = \frac{L}{v_{wfa}} = \frac{V_p(1 - S_{wi} - S_{or})}{q F(M)} \quad (99)$$

where

$$V_p = A \phi L \quad (100)$$

4.6 Maximum Time

According to Buckley-Leverett theory[20], the distance travelled by a given saturation is given by

$$X = \frac{qt}{A \phi} \frac{dF_w}{dS_w} \quad (101)$$

provided that the injection rate, q , is constant, the system is horizontal, and the saturation was everywhere equal to the irreducible saturation initially. Consequently, the time necessary for the saturation $S_w = 1 - S_{or}$ to reach the outlet-end of the system can be estimated using

$$t_m = \frac{A\phi L}{q(dF_w/dS_w)} \Big|_{1-S_{or}} \quad (102)$$

By taking limits, it can be shown that

$$\frac{dF_w}{dS_w} \Big|_{1-S_{or}} = - \frac{\mu_w}{\mu_o} \frac{k_o(1-S_{or})}{k_{wor}} \quad (103)$$

where $k_o(1-S_{or})$ is the slope of the effective permeability to oil curve evaluated at $S_w = 1-S_{or}$. Introducing Equation 103 into Equation 102 yields, as an estimate for the time needed to produce all of the displaceable oil,

$$t_m = - \frac{V_p \mu_o k_{wor}}{q \mu_w k_o(1-S_{or})} \quad (104)$$

4.7 Lagrangian Method for Estimating Relative Permeabilities

4.7.1 Introduction

The external-drive method developed in the preceding section cannot be used to estimate permeabilities over the entire saturation range of interest. This limitation can be removed, if data from an unstabilized displacement may be used. The purpose of this section is to demonstrate how a Lagrangian rather than an Eulerian approach may be used to develop a method for estimating relative permeabilities which makes use of unstabilized displacement data, and which enables the generation of effective permeability curves over the entire saturation range of interest.

The theory presented herein is based on one-dimensional displacement theory. As a consequence, the practical application of the equations developed below is limited to those displacements wherein the pressure and saturation are uniform at any cross-section. Moreover, a Lagrangian formulation of the fluid displacement problem must be permissible. That is to say, the saturation profiles must be monotonic. Finally, the porous medium in which the displacements are conducted must be homogeneous and isotropic.

4.7.2 Basic Equations

In the practical application of external-drive theory, it is usual to neglect the capillary pressure gradient, because of the difficulties normally encountered in measuring it[103]. As a consequence, estimation of effective permeability is restricted to saturations for which such neglect is permissible. Recently, it has become practicable to estimate the capillary pressure gradient[104,105]. If advantage is to be taken of this ability, it is necessary to modify the external-drive equations which are customarily used to estimate the effective permeabilities to water and oil.

For a horizontal, linear system, Leverett[78] has demonstrated that the fraction of water flowing, f_w , at a given cross-section in a homogeneous porous medium is defined by

$$f_w = \frac{k_w/\mu_w (1 + A/q k_o/\mu_o \partial P_c/\partial x)}{k_w/\mu_w + k_o/\mu_o} \quad (105)$$

Solving for k_w , the effective permeability to water, Equation 105 becomes

$$k_w = \frac{\mu_w f_w}{\lambda^{-1} (1 + A/q k_o/\mu_o \partial P_c/\partial x)} \quad (106)$$

where the reciprocal mobility, λ^{-1} , is defined by

$$\lambda^{-1} = \frac{1}{k_w/\mu_w + k_o/\mu_o} \quad (107)$$

By taking a similar approach, it may also be shown that

$$k_o = \frac{\mu_o f_o}{\lambda^{-1} (1 - A/q k_w/\mu_w \partial P_c/\partial x)} \quad (108)$$

It is to be noted that Equations 106 and 108 degenerate to the usual equations used in external-drive theory, provided the capillary-pressure gradient terms are small enough to be neglected, and provided that λ^{-1} is evaluated at the outlet end of the system.

To utilize Equations 106 and 108, it must be practicable to estimate f_w and λ^{-1} at a number of points along a particular saturation profile. Moreover, it must be possible to estimate S_w and $\partial P_c / \partial x$ at the same points.

4.7.3 Reciprocal Mobility

To arrive at a defining equation for reciprocal mobility, use is made of Darcy's law for each phase. Darcy's law for each phase is defined, for a horizontal, linear system, by

$$q_w = - \frac{k_w}{\mu_w} A \frac{\partial P_w}{\partial x} \quad (109)$$

and

$$q_o = - \frac{k_o}{\mu_o} A \frac{\partial P_o}{\partial x} \quad (110)$$

If use is made of the definition for capillary pressure ($P_c = P_o - P_w$), Equation 109 may be revised to read

$$q_w = - \frac{k_w}{\mu_w} A \left(\frac{\partial P_o}{\partial x} - \frac{\partial P_c}{\partial x} \right) \quad (111)$$

By adding Equations 110 and 111, and making use of the fact that, at any cross-section along the length of the core $q = q_o + q_w$, and rearranging, it may be shown that

$$\lambda^{-1} = \frac{1}{k_w/\mu_w + k_o/\mu_o} = - \frac{A}{q} \frac{\partial P_o}{\partial x} + \frac{A}{q} F_w \frac{\partial P_c}{\partial x} \quad (112)$$

where, by definition,

$$F_w = \frac{k_w/\mu_w}{k_w/\mu_w + k_o/\mu_o} \quad (113)$$

Note that, if use of Equation 112 is to be practicable, it must be possible to measure both P_w and P_o along the length of the core.

4.7.4 Fractional Flow

If a displacement is unstabilized, use can no longer be made of the standard (Eulerian) methods for estimating the fraction of water (or oil) flowing at a particular location in the core [104,105]. Rather, a Lagrangian approach must be taken. Buckley and Leverett [20] have shown that

$$\frac{\partial x}{\partial t}(S_w, t) = \frac{q}{A \phi} \frac{\partial f_w}{\partial S_w}(S_w, t) \quad (114)$$

For a specific saturation, say S_w^* , Equation 114 may be integrated to yield

$$x(S_w^*, t) = \frac{q}{A \phi} \int_0^t \frac{\partial f_w}{\partial S_w}(S_w^*, t) dt \quad (115)$$

where it has been assumed that $x(S_w^*, 0) = 0$. Because Equation 115 must hold for all possible values of S_w^* ($S_{wi} \leq S_w^* \leq 1 - S_{or}$), it may be written

$$x(S_w, t) = \frac{q}{A \phi} \int_0^t \frac{\partial f_w}{\partial S_w}(S_w, t) dt \quad (116)$$

If $x(S_w, t)$ is a single-valued function of S_w , both sides of Equation 116 may be integrated with respect to S_w to obtain

$$\int_{S_{wi}}^{S_w^*} x(S_w, t) dS_w = \int_{S_{wi}}^{S_w^*} \frac{q}{A \phi} \int_0^t \frac{\partial f_w}{\partial S_w}(S_w, t) dt dS_w \quad (117)$$

Moreover, if $f_w(S_w, t)$ is a well-behaved function, the order of integration may be changed and

$$\int_{S_{wi}}^{S_w^*} x(S_w, t) dS_w = \frac{q}{A \phi} \int_0^t \int_{S_{wi}}^{S_w^*} \frac{\partial f_w(S_w, t)}{\partial S_w} dS_w dt \quad (118)$$

or, upon carrying out the integration with respect to S_w ,

$$\int_{S_{wi}}^{S_w^*} x(S_w, t) dS_w = \frac{q}{A \phi} \int_0^t f_w(S_w^*, t) dt \quad (119)$$

where it has been assumed that $f_w(S_{wi}, t) = 0$. Finally, if $Q_w(S_w^*, t)$ is defined by

$$Q_w(S_w^*, t) = q \int_0^t f_w(S_w^*, t) dt = A \phi \int_{S_{wi}}^{S_w^*} x(S_w, t) dS_w \quad (120)$$

it follows, upon differentiating Q_w with respect to t , that

$$f_w(S_w^*, t) = \frac{1}{q} \frac{dQ_w(S_w^*, t)}{dt} = \frac{A \phi}{q} \int_{S_{wi}}^{S_w^*} x(S_w, t) dS_w \quad (121)$$

To estimate $f_w(S_w, t)$ for some specific saturation, say S_w^* , $Q_w(S_w^*, t)$ must be estimated at a number of different times. This can be done, with the aid of Equation 120, provided saturation profiles measured at a number of different times are available. Then, by using least-squares techniques to fit a model equation to these data, it becomes possible to differentiate analytically the model equation to obtain an estimate for $f_w(S_w^*, t)$ at the time of interest. Moreover, by undertaking this procedure for a number of different values of S_w^* , the f_w versus saturation curve which pertains to a specific point in time can be constructed.

4.3 Distance Travelled by a Particular Saturation

Because Equation 121 must hold for all values of S_w , it may be written for some specific point in time, say t^* ,

$$\int_0^{t^*} f_w(S_w, t) dt = \frac{1}{q} Q_w(S_w, t^*) \quad (122)$$

Taking the derivative of both sides of Equation 122 with respect to S_w , one obtains

$$\int_0^{t^*} \frac{\partial f_w(S_w, t)}{\partial S_w} dt = \frac{1}{q} \frac{dQ_w(S_w, t^*)}{dS_w} \quad (123)$$

Hence, by virtue of Equation 116, it may be shown that

$$x(S_w, t^*) = \frac{1}{A\phi} \frac{dQ_w(S_w, t^*)}{dS_w} \quad (124)$$

4.9 Estimation of Water Saturations During Waterflood

Over the years, a number of different methods has been proposed to measure saturation profiles in a porous medium. These include resistivity techniques[106], X-ray methods[107,108,109] and techniques based on the principle of microwave attenuation[35,42,51,90,110,111]. Because the quality of saturation profiles measured by the microwave attenuation technique was superior to the other methods, and also because it is a non-destructive method in that it does not interfere with the waterflood process, this method was chosen to measure saturation as a function of time and distance.

The amount of attenuation which takes place when a parallel beam of monochromatic radiation passes rectilinearly through a homogeneous medium of thickness, h , is dictated by Lambert's law[112]. Thus, if I_0 is the intensity (power) of the incident beam of radiation, and \bar{k} is the absorption coefficient of the medium, the intensity of the attenuated beam leaving the medium, I_x , is given by

$$I_x = I_0 \exp(-\bar{k}h) \quad (125)$$

If the absorbing medium is a substance in solution, the attenuation of radiation traversing a given path length depends, according to Beer's law[112], on the concentration of the solution. That is, if \bar{c} is the solution concentration,

$$\bar{k} = k \bar{c} \quad (126)$$

where,

$$k = \frac{4 \pi f k_e}{c} \quad (127)$$

Here f is the frequency of the microwave signal, c is the velocity of light, and k_e is the extinction coefficient. By combining Equations 125, 126 and 127, it may be shown that

$$I_x = I_o \exp\left(-\frac{4 \pi f h k_e \bar{c}}{c}\right) \quad (128)$$

In the context of the present study, the concentration of the absorptive substance through which microwaves must pass may be considered to be analogous to the fraction of water contained within a given cross-section of the core. Thus, one may write

$$\bar{c} = \phi S_w \quad (129)$$

The introduction of Equation 129 into Equation 128, taking the logarithm of both sides of the equation, and then converting to logarithms to the base ten, yields

$$\log_{10}\left(\frac{I_x}{I_o}\right) = -\frac{4 \pi f h k_e \phi S_w}{2.303 c} \quad (130)$$

The microwaves traversing the core encounter not only water, but also fibreglass, sand and oil. While the absorbance of these materials is small compared to that of water, it still must be taken into account. Because the total absorbance of materials other than water is small compared to water, it is assumed that the absorbance of these materials can be lumped together in one term. Given the validity of this assumption, one may write

$$A_T = A_w + A_{ls} \quad (131)$$

where A_T is the total absorbance, A_w is the absorbance due to water and A_{ls} is the absorbance of the fiberglass, sand and oil. If Equation 131 is introduced into Equation 130, it follows that

$$\log_{10}\left(\frac{I_x}{I_o}\right) = A_w + A_{ls} \quad (132)$$

where, in view of Equation 130, the absorbance due to water is defined by

$$A_w = -\frac{4 \pi f k_e h \phi S_w}{2.303 c} = B S_w \quad (133)$$

Now, all the constant terms in Equation 133 can be included in a lumped parameter, B .

To estimate the parameters B and A_{ls} , Equation 132 may be written for two different saturations, and the resulting equations solved simultaneously for the two parameters. For the case where the end-point saturations S_{wi} and $(1-S_{or})$ are used, the resulting defining equations for B and A_{ls} are

$$B = \frac{1}{1-S_{wi}-S_{or}} \log_{10}\left[\frac{I_x(1-S_{or})}{I_x(S_{wi})}\right] \quad (134)$$

and

$$A_{ls} = \log_{10}\left[\frac{I_x(S_{wi})}{I_o}\right] - B S_{wi} \quad (135)$$

Introducing Equation 133 into Equation 132 and rearranging, one obtains

$$S_w = (\log_{10}\frac{I_x}{I_o} - A_{ls})/B \quad (136)$$

5. EXPERIMENTAL EQUIPMENT, MATERIALS AND PROCEDURE

5.1 Equipment

Two separate experimental apparatuses were used, one to validate the modified stability theory, and the other to validate the concepts of relative permeability and capillary pressure in stable and unstable displacements.

5.1.1 Stability Experiments

A schematic diagram of the equipment used in experimental verification of the modified stability theory is shown in Figure 1. The equipment is similar to the equipment used in earlier studies[1,5]. However, the coreholders used in this study differ in two ways from those used earlier. First, the coreholders, which were made of aluminum, were rectangular in cross-section rather than being circular, as in the earlier studies. Second, the end-cap design was modified to include water-wet, fused glass-bead sections to distribute the water across the entire inlet and outlet face of the end-cap with the hope of reducing, as much as possible, inlet and outlet end effects. Three different coreholder lengths and three different aspect ratios were used in this study, in order to investigate the effect of geometry on the stability boundary. Details concerning the dimensions of various coreholders used are provided in Table 1.

5.1.2 Relative Permeability and Capillary Pressure Experiments

Presented in Figure 2 is a schematic diagram of the equipment used to estimate relative permeabilities and dynamic capillary pressures. The rectangular coreholder used in this study was constructed using insulating-type fibreglass, because this material readily transmits microwaves, has high strength, and is inexpensive. The coreholder had fourteen pressure-transducer taps, seven located on the top and seven located on the bottom of the coreholder. The placement of the transducers is depicted in Figure 2. Oil-wet fritted discs were mounted in the pressure-transducer taps located on the top of the coreholder, while

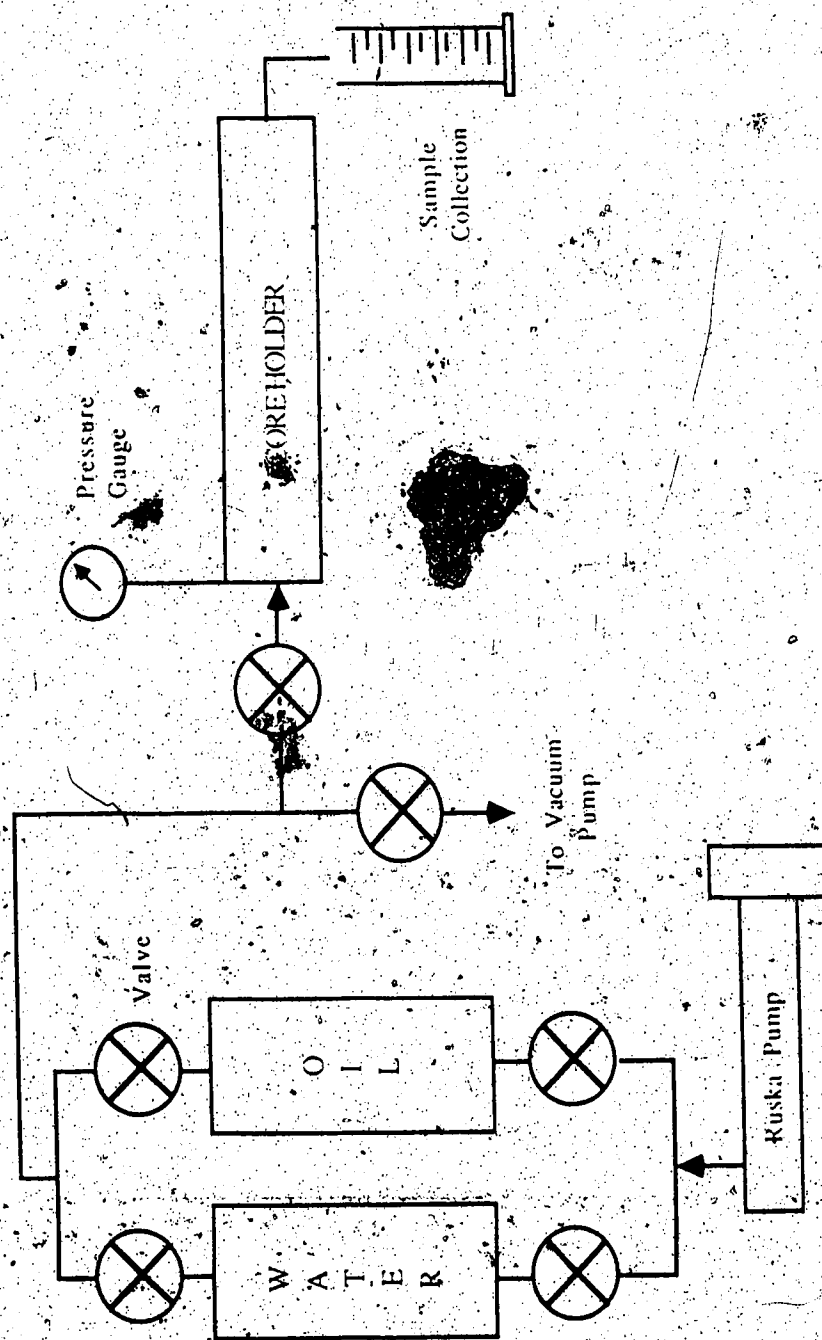


FIGURE 1: SCHEMATIC DIAGRAM OF EXPERIMENTAL EQUIPMENT
(STABILITY EXPERIMENTS)

Table 1: Physical Dimensions of Coreholders

Core	b (cm)	h (cm)	(b/h)	Section 1 Length (cm)	Section 2 Length (cm)	Section 1 Bulk Volume (cc)	Section 2 Bulk Volume (cc)	Total† Bulk Volume (cc)
1	5.08	5.08	1.0	30.5	61.0	787	1573	2360
2	7.62	3.49	2.2	30.5	61.0	811	1622	2433
3	10.16	2.54	4.0	30.5	61.0	787	1573	2360

† Sections 1 and 2 combined

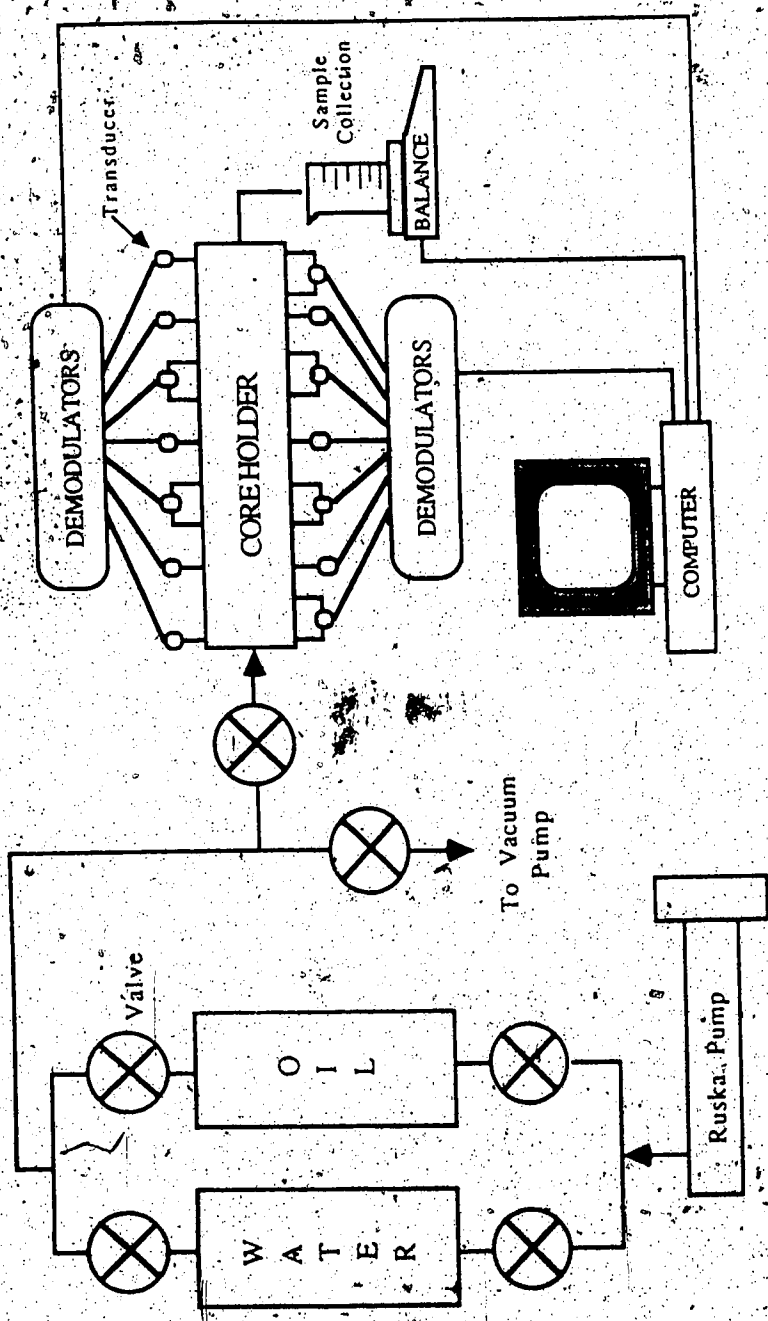


FIGURE 2: SCHEMATIC DIAGRAM OF EXPERIMENTAL EQUIPMENT
(RELATIVE PERMEABILITY AND CAPILLARY PRESSURE EXPERIMENTS)

water-wet fritted discs were mounted in those located on the bottom of the coreholder.

Consequently, it was possible to measure the pressure in both the water and the oil at a given position along the length of the core.

The inlet endcap to the coreholder was designed so that the injected water was distributed as evenly as possible across the entire inlet face of the core. This was accomplished in two ways. First, the inlet endcap was designed in the shape of a rectangular horn which was filled with large glass beads. Second, these glass beads were held in place by a water-wet, fritted glass plate made of fused glass beads. The outlet endcap, on the other hand, was somewhat simpler in design. It consisted of a fritted plate made of fused glass beads, followed by a single layer of large glass beads, all housed in a plexiglass end piece. The use of a single layer of glass beads behind the fritted plate, together with the transparent plexiglass end piece, enabled the visual detection of water breakthrough. As shown in the figure, an electronic balance was used to record, as a function of time, the total amount of fluid produced during the course of an experiment. Data from the electronic balance, as that from the fourteen transducers mounted on the coreholder, were recorded automatically, via an interface, by an HP-310 computer, which acted as the controller. Moreover, a comprehensive, interactive software routine was developed which enabled almost complete automation of the experimental runs and continuous data acquisition. The program code of the software developed is presented in Appendix C. The only unit not controlled by the computer was the Ruska Pump used to inject water at a constant rate.

5.1.2.1 Interface System

Central to the data acquisition designed for this study was the HP-IB interface system. The HP-IB interface system is comprised of a multiprogrammer, HP6940B, and a multiprogrammer interface, HP59500A. An interface system performs three basic functions: i) talk, ii) listen, and iii) service request and serial poll.

Multiprogrammer

The multiprogrammer, HP6940B, functioned as a multi-channel bi-directional interface between the controller (HP310 computer) and the "real world" environment to which command signals were sent, and from which status signals were received. Thus, it was regarded as the master control unit for bi-directional interfacing. Communications between the multiprogrammer and the external device were realized via plugged-in input/output cards in the multiprogrammer. While data transfers between the multiprogrammer mainframe and the I/O cards were digital i.e. twelve data bits, the transfers between the cards and the external devices were either digital or analog, i.e. in the form of voltages or currents.

Data transfers from the controller to the multiprogrammer took the form of a sixteen-bit output word; while, for transfers from the multiprogrammer to the controller, they took the form of a thirteen-bit (twelve data bits plus one status bit) word.

The following cards were installed in the mainframe of the multiprogrammer: i) standard input; ii) remote/local; iii) logic and timing; iv) a scanner card capable of scanning 16 single-ended or eight differential voltages from the pressure transducers at very high speed; v) a digital output card to provide logic-level outputs to reflect the status of 12 programmed bits; vi) a high speed analog-to-digital converter card to provide high conversion speed and excellent accuracy; vii) a digital input card to receive 12 separate digital logic-level inputs from an external device; viii) a timer/pacer card to pace multiprogrammer I/O operations, and to generate accurate one-shot pulses; ix) unit select cards; and x) a voltage regulator card to provide isolated sources of ± 15 -volt d.c. power which was required when the multiprogrammer used the high-speed A/D converter card. Specific addresses made to each of these cards were indicated in the software packages developed for this study (Appendix C).

Multiprogrammer Interface

Bi-directional operation of the multiprogrammer was achieved by the use of a multiprogrammer, HP59500A, which buffered and transmitted data and control signals between the HP-IB and the multiprogrammer. Thus, multiprogrammer operations was initiated only when the HP59500A was listening. It converted the serial ASCII characters, both alpha and numeric, from the controller into a 16-bit word format required by the multiprogrammer. When the HP59500A talk address was received, the encoder translated the 15th bit into an octal digit and bits 11-0 to four octal digits.

The service request line was used by HP59500A to indicate that the multiprogrammer requires service. This service line was enabled whenever the multiprogrammer was operating in the timing mode. As a consequence, it was set when the multiprogrammer completed an operation or requested an interruption of the current programming sequence. Control signals from the multiprogrammer, HP6940B, to HP59500A implemented the service request function.

Serial poll was a method used by the controller to determine which bus device had requested service. Thus, essentially, it consisted of interrogating bus devices in sequence, and then reading back a status byte from each device which was used to identify the devices requesting service. When addressed to talk in serial poll mode, the multiprogrammer interface, HP59500A, returned a status byte of 64 if it was requesting a service; if not, a status byte of zero was returned.

5.1.2.2 Microwave Instrumentation

To facilitate use of the microwave technique to estimate the dynamic water saturation during a waterflood, a microwave instrumentation package was assembled as shown in Figure 3. The microwave instrumentation unit consisted of following units and instruments:

1. a Klystron and Power Supply Unit to supply very stable single-phase.

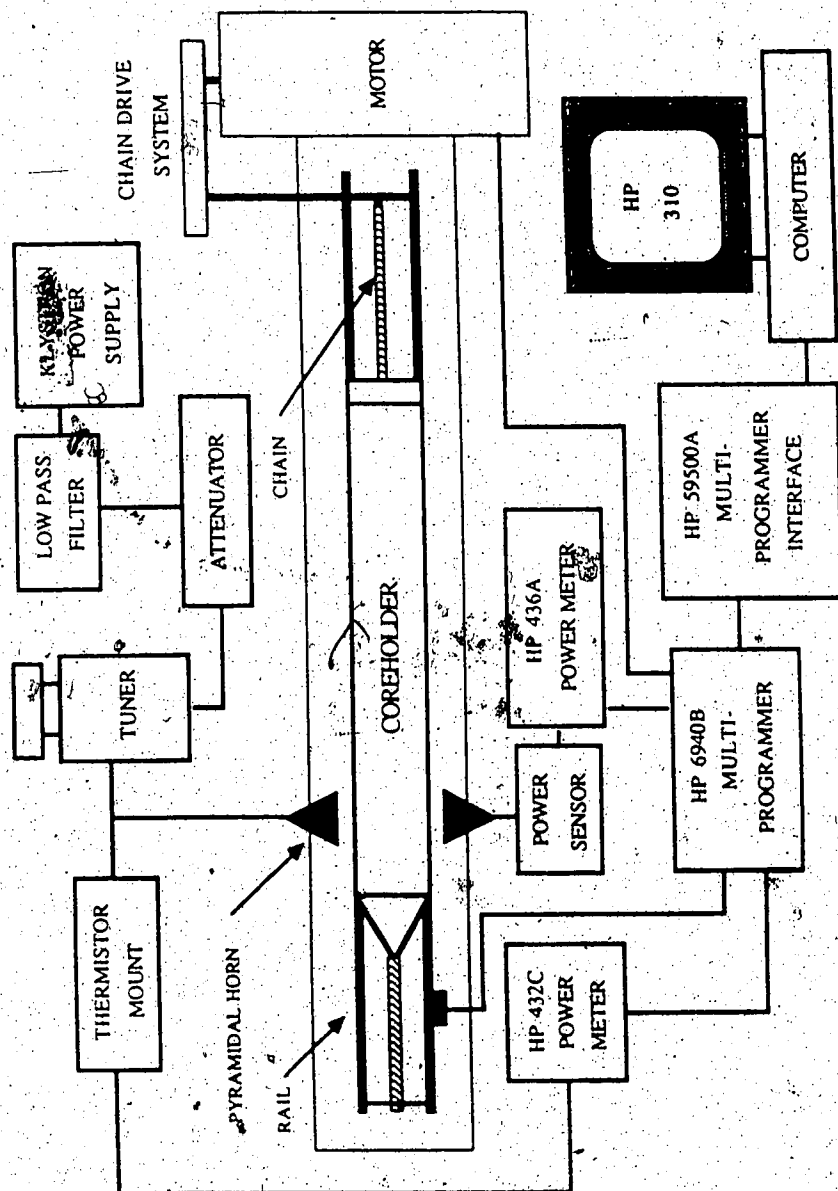


FIGURE 3: SCHEMATIC DIAGRAM OF MICROWAVE INSTRUMENTATION

single-frequency microwave signals.

2. an attenuator to regulate the microwave signal to the desired level.
3. a tuner to fine-tune the microwave frequency.
4. pyramidal horns with lens antennas on both sides of the core to facilitate transmitting and receiving of the microwave signals. Directional couplers were used along with the waveguides, which acted as a "conduit" for microwave transmission, to attain proper alignment between the horns.
5. two power meters, one on each side of the coreholder, to measure microwave signals via power sensors. The power meter on the input side was an HP432C Power Meter and was used for input reference power. The power meter on the output side was a digital power meter, HP436A, which received microwave signals via an HP8486A Power Sensor. With the aid of an HP-Option 022 Kit installed in the power meter, the analogue microwave data were fed readily to the computer via the HP-IB. While interfacing the power meter with the interface, the meter response time to read data had to be taken into account. This was done by incorporating in the software a time interval such that readings were taken at a fixed interval of length along the core. Transmitted microwave signals at the other side of the core were "sensed" by a sophisticated power sensor, HP-R8486A. This sensor is capable of measuring power in the range of 1 micro-watt to 100 milli-watt (i.e. -30 dBm to +20 dBm) in the frequency range 26.5 GHz - 40 GHz. The operating principle of the power sensor is fairly simple. It contains two thermocouples. When the resistor at the hot junction converts the applied microwave energy to heat, the temperature difference between the hot and cold junctions generates a d.c. voltage, called a thermoelectric electromotive force, which is proportional to the temperature difference between the junctions and, thus, is a function of the power from the microwave source.

5.2 Materials

For all runs, the unconsolidated porous media were prepared by wet-packing coreholders with Ottawa silica sand (80-120 mesh) and vibrating for eight hours to obtain as uniform a sandpack as possible. For each run the sandpack was dried, evacuated and then resaturated with distilled water in order to be able to measure the porosity and absolute permeability of the sandpack. Average porosities and permeabilities of the sandpacks obtained by using this method of packing are presented in Table 2.

Distilled water was used to create an irreducible water saturation, while distilled water doped with sodium fluorescein was used as the displacing fluid. Use of sodium fluorescein in distilled water obtained a better contrast between the displaced and displacing fluids. In the runs pertaining to the verification of the modified stability theory, the displaced fluids used were refined oils, namely, MCT-5, Light Atmospheric Gas Oil (LAGO), MCT-10, and a 50%-by-volume mixture of MCT-5 and LAGO. However, for runs pertaining to the estimation of relative permeabilities, LAGO, MCT-5 and MCT-10 were used as the displacing fluids. The relevant properties of these fluids are provided in Table 3.

5.3 Experimental Procedure

5.3.1 Stability Experiments

The following procedure, using the experimental apparatus depicted in Figure 1, was used in each of the runs pertaining to the experimental verification of the modified stability theory. First, the resident (pure, distilled) water was displaced, in order to establish an irreducible water saturation, by injecting the appropriate refined oil until such time as the incremental recovery of water became essentially zero. This usually required the injection of three to four pore volumes of oil. Once the irreducible water saturation had been established, the effective oil permeability of the sandpack was determined. Next, a waterflood was conducted using distilled water doped with sodium fluorescein as the injection fluid. The sodium fluorescein was used to achieve a better colour contrast between the injected water and

Table 2: Porosities and Absolute Permeabilities of Sandpacks

Runs	Porosity (fraction)	Absolute Permeability(d)
1 - 61†	0.30 ± 0.04 ‡	16.8 ± 1 ‡
62	0.334	20.46
63	0.362	20.46
64	0.378	17.40
65	0.359	20.46
66	0.365	21.50
67	0.365	20.80
68	0.309	20.40

† average values; ‡ one standard deviation

Table 3: Fluid Properties @ 21°C

Fluid System	Density (gm/cc)	Viscosity (cp)	Interfacial Tension (dyne/cm)	γ_c (dyne/cm ²)
1. Distilled Water	0.9982	1.0		
2. MCT-5	0.8123	34.2	33.08	16342
3. LAGO	0.7963	4.7	36.72	13566
4. MCT-5+LAGO	0.8043	11.1	29.30	14185
5. MCT-10	0.8576	60.0	34.20	13573
6. LAGO + 2% v/v Surfactant	0.7963	4.7	31.85	10330
7. MCT-5 + 2% v/v Surfactant	0.8123	34.2	31.00	13970
8. MCT-5 + LAGO + 2% v/v Surfactant	0.8043	11.1	24.80	12911

the displaced oil. The waterflood was continued until oil production ceased (usually three to four pore volumes of water injected); at which time the effective water permeability of the sandpack was determined. During the waterflood, the fractional recovery of the displaced and displacing fluids, together with the total pressure drop across the core, were recorded as functions of pore volumes of displacing fluid injected. This procedure, which was carried out for each of the different runs conducted in this study, yielded sandpacks having an average irreducible water saturation of 0.11 ± 0.01 and an average residual oil saturation of 0.22 ± 0.015 . In addition, a capillary pressure curve was determined for each of the fluid pairs used, so as to be able to estimate A_c , the area under a capillary pressure curve. The values of A_c estimated for each of the capillary pressure curves determined using the restored-state method are reported in Table 3.

5.3.2 Relative Permeability and Capillary Pressure Experiments

For the set of runs pertaining to the estimation of relative permeabilities and dynamic capillary pressures, the following procedure was used in each of the runs. First, the resident water was displaced, in order to establish an irreducible water saturation, by injecting mineral oil until such time as the incremental recovery of water becomes essentially zero. This usually required the injection of three to four pore volumes of oil. During this part of the procedure, the pressure transducer taps were fitted with dummy plugs. Once the irreducible saturation to water had been established, the effective oil permeability of the sand pack was determined. This was accomplished by replacing two of the dummy plugs, one at the inlet end and one at the outlet end, with pressure transducers, so that the total pressure drop across the core could be determined. Next, the remaining dummy plugs were removed so that water-wet (or oil-wet) fritted discs and pressure transducers could be installed in the remaining taps. To avoid entrapment of air during the mounting of the transducers, oil was circulated at a very slow rate while the transducers were being installed. Finally, a waterflood, at a fixed rate of injection, was begun. The injection rate used was selected to conform to the desired stabilization and stability criteria (for stabilized displacement: $N_c \leq 0.1$ and for stable

displacement: $I_{sr} \leq \pi^2$). The data needed to estimate the effective permeability curves were automatically recorded for later processing by the interactive software package developed for this purpose.

During a waterflood, the core was periodically scanned with microwaves to determine how water and oil were distributed along the core. The interval between scans was preselected on the basis of the displacement rate at the beginning of the run. This facilitated the taking of scan profiles at a regular time interval. During scanning, an interrupter box, controlled by the digital output card in the HP-IB, activated the piston of the air actuator valve, causing the piston to lock onto a chain driven at a constant rate by an electric motor. Because this air actuator valve was fitted to the clamp holding the coreholder, it enabled movement of the core on the rails between the two microwave antennas. Once the coreholder was scanned over its entire length and hit the interrupter switch fitted in the rails, the piston of the air actuator valve was unlocked from the moving chain. The deadweight attached at the output-end side of the coreholder helped it roll back to its initial position. In order to prohibit a fast and "violent" rollback, the deadweight was allowed to slide into a column of water. The water acted as a cushion and helps the coreholder roll back gently and slowly.

6. EXPERIMENTAL RESULTS

6.1 Validation of the Modified Stability Theory

6.1.1 Introduction

The immiscible displacements conducted in this study were carried out in sandpacks which were water-wet. In carrying out these displacements, the length, aspect ratio, superficial velocity, mobility ratio and interfacial tension were varied in order to validate experimentally not only the stability boundary, but also the equation used to estimate the pseudointerfacial tension. The data taken also enabled the experimental validation of the equations used to estimate the breakthrough recovery for displacements which were stable and for those which were pseudostable. Because several different fluids were used, the displacement data are tabulated according to the mobility ratio of the fluid pairs used.

The breakthrough recoveries predicted by Equation 70 (stable displacement) and Equation 72 (pseudostable displacement) for the four average mobility ratios used in this study are reported (assuming $X_o=0$) in Table 4. The displacing fluid in each series of runs was distilled water doped with sodium fluorescein. The displacement data for the LAGO displacements ($M=2.53$) are reported in Table 5, for the MCT-5 plus LAGO displacements ($M=4.06$) in Table 6, for the MCT-5 displacements ($M=8.13$) in Table 7, and for the MCT-10 displacements ($M=29.72$) in Table 8. The breakthrough recovery as a fraction of the original oil in place is plotted versus the instability number, I_{st} , in Figure 4. Also plotted on Figure 4 are the theoretical breakthrough recoveries (assuming $X_o=0$) for each mobility ratio for stable displacements. The solid lines plotted to the left of the stability boundary, $I_{st}=\pi^2$, pertain to stable displacements, while the solid lines plotted to the right of the pseudostable boundary, $I_{st}=900$, pertain to pseudostable displacements. The boundary for pseudostable displacement was established experimentally by Demetre *et al.*[5].

Table 4: Predicted Breakthrough Recoveries (R_{bt}) as Fractions of Initial Oil-in-Place

Mobility Ratio	R_{bt}	R_{bt}
	Stable	Pseudostable
$2.53 \pm 0.1^*$	0.625	0.469
4.06 ± 0.1	0.553	0.360
8.13 ± 0.2	0.472	0.271
29.72 ± 0.24	0.324	0.169

* One standard deviation

Table 5: Displacement Data For LAGO Displacements (M = 2.53)

Run	Fluid System	L (cm)	(b/h)	Q (cc/hr)	kwor (d)	PseudolIFT (dyne/cm)	Isr	Rbt (%OIP)
1	3	61.0	4.0	145	4.54	3035	1.23	61.0
2	3	30.5	4.0	145	4.54	3749	0.98	64.0
3	3	91.4	4.0	145	4.53	2836	1.32	62.0
4	3	61.0	1.0	575	4.53	3506	9.00	62.0
5	6	91.4	2.18	575	4.54	1964	12.16	58.0

Table 6: Displacement Data For MCT-5 + LAGO Displacements (M=4.06)

Run	Fluid System	L (cm)	(b/h)	Q (cc/hr)	kwor (d)	PseudolFT (dyne/cm)	Isr	Rbt (%OIP)
6	4	30.5	1.0	10	2.303	2715	1.06	54.0
7	4	61.0	2.18	10	2.03	2576	0.80	55.0
8	4	91.4	4.0	10	2.03	2575	0.50	55.0
9	4	91.4	1.0	50	2.04	2621	5.29	56.0
10	4	30.5	2.18	50	2.04	2575	4.00	56.0
11	4	30.5	4.0	50	2.05	2575	2.49	55.0
12	4	61.0	1.0	100	2.04	2621	10.57	55.5
13	4	61.0	2.18	100	2.05	2603	8.01	6.5
14	4	61.0	4.0	100	2.03	2528	4.98	56.5
15	4	91.4	1.0	120	2.02	2621	12.69	53.0
16	4	30.5	2.18	120	2.03	2603	9.61	55.5
17	8	61.0	4.0	120	2.035	2621	5.97	55.5
18	8	30.5	1.0	160	2.04	2621	16.92	47.0
19	8	30.5	2.18	160	2.03	2621	12.82	52.0
20	4	91.4	4.0	160	2.04	2575	7.96	55.5
21	4	61.0	1.0	200	2.03	2621	21.15	42.0
22	4	30.5	2.18	200	2.04	2603	16.02	48.5
23	4	91.4	4.0	200	3.95	2621	9.95	56.0
24	4	30.5	1.0	10	2.303	2650	1.06	51.0
25	4	61.0	2.18	10	2.03	2621	0.80	51.5
26	4	91.4	4.0	10	2.03	2621	0.50	50.5
40	8	61.0	1.0	200	3.92	2660	13.17	50.0

Table 7: Displacement Data For MCT-5 Displacements ($M_p = 8.13$)

Run	Fluid System	L (cm)	(b/h)	Q (cc/hr)	kwor (d)	PseudoIFT (dyne/cm)	Isr	Rbt (%OIP)
27	7	91.4	1.0	500	2.60	2622	120.95	35.0
28	7	91.4	2.18	500	2.58	2790	86.12	38.0
29	6	91.4	4.0	2215	2.6	2812	235.10	31.0
30	7	61.0	2.18	500	2.6	2620	91.68	37.0
31	2	30.5	2.18	125	2.59	3602	16.68	42.0
32	2	30.5	4.0	500	2.6	3904	38.23	37.0
33	7	61.0	1.0	145	2.6	2976	30.91	3.0
34	2	61.0	1.0	575	2.59	3232	112.85	34.0
35	2	61.0	1.0	1280	2.59	3375	240.58	31.0
36	2	30.5	4.0	641	2.59	3452	55.43	38.0
37	2	30.5	2.18	335	2.58	3290	48.92	35.0
38	2	30.5	1.0	335	2.6	3118	68.14	34.0
39	2	30.5	2.18	418	2.59	3001	66.92	38.0
42	7	91.4	4.0	500	2.61	2974	13.85	42.0
43	7	61.0	4.0	10	2.6	2659	1.12	47.0
44	7	30.5	2.18	10	2.58	2659	1.81	48.0
45	7	91.4	1.0	10	2.59	2659	2.39	47.0
46	7	61.0	4.0	50	2.59	2659	5.61	46.0
47	7	61.0	2.18	50	2.58	2659	9.04	47.0
48	7	61.0	1.0	50	2.6	2659	11.93	45.0

Table 8: Displacement Data For MCT-10 Displacements (M = 29.72)

Run	Fluid System	L (cm)	(b/h)	Q (cc/hr)	K _{hor} (d)	PseudoIFT (dyne/cm)	I _{sr}	R _{bt} (%OIP)
49	S	30.5	4.0	200	12.78	1433	46.01	23.0
50	S	91.4	4.0	167	12.73	1433	38.42	25.0
51	S	30.5	2.18	200	12.76	1451	74.07	20.0
52	S	61.0	2.18	335	12.77	1421	124.07	18.0
53	S	30.5	1.0	500	12.78	1445	244.45	16.0
54	S	61.0	1.0	641	12.78	1433	313.39	16.0
55	S	91.4	1.0	1280	12.77	1433	625.80	16.0
56	S	61.0	4.0	50	12.78	1463	11.50	32.0
57	S	61.0	4.0	100	12.77	1451	23.00	25.0
58	S	30.5	4.0	10	12.78	1451	2.30	33.0
59	S	91.4	1.0	2500	12.78	1433	1222.30	16.0
60	S	91.4	2.18	2500	12.78	1439	925.90	16.0
61	S	61.0	4.0	2500	12.78	1445	575.18	17.5

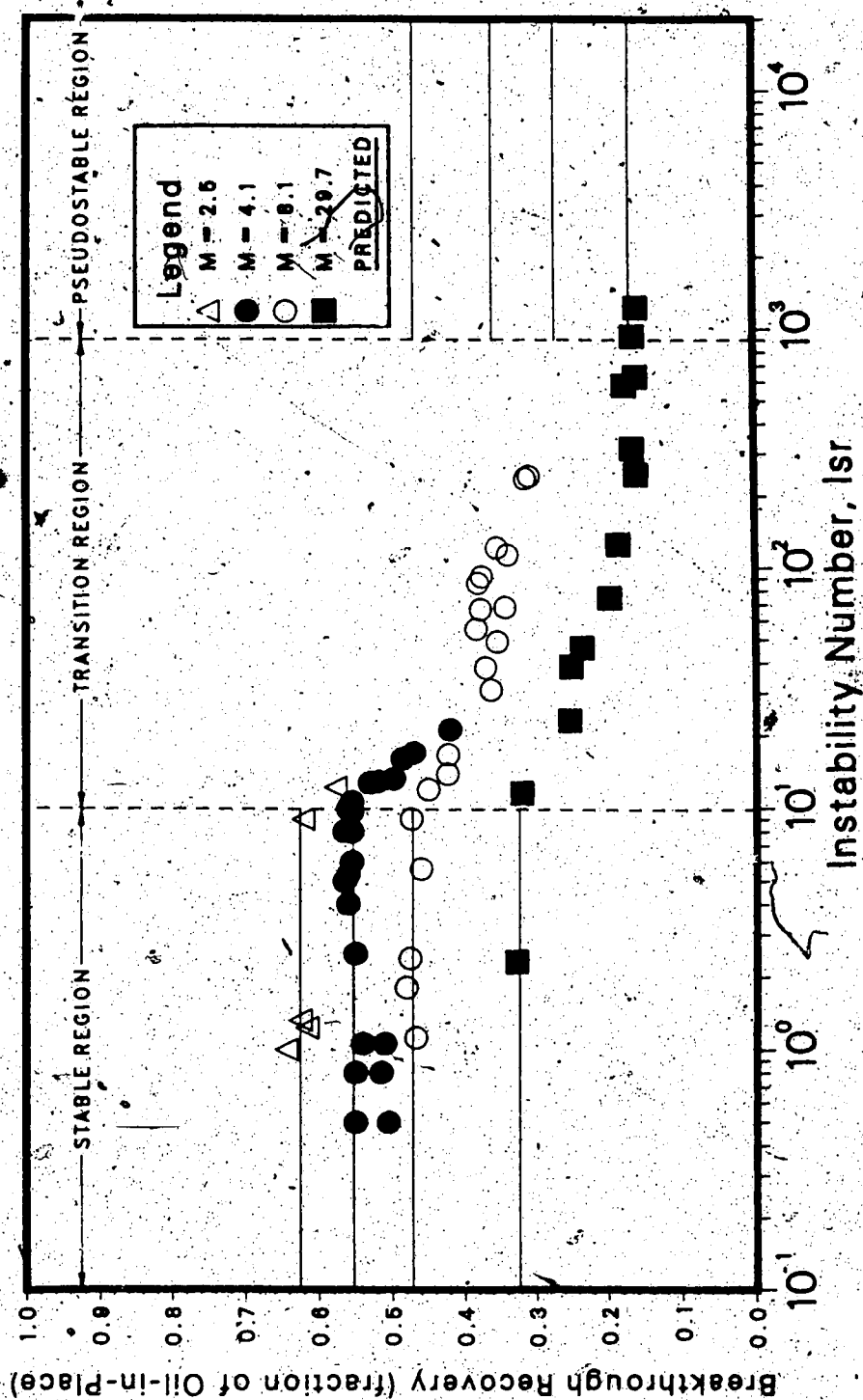


FIGURE 4: BREAKTHROUGH RECOVERY AS A FUNCTION OF INSTABILITY NUMBER

6.1.2 Results

The theory presented herein is based on the assumption that it is permissible to replace the transition zone (capillary fringe) separating the fluid within a viscous finger from the fluid through which the finger is propagating by a sharp macroscopic interface to which a pseudointerfacial tension can be assigned. Moreover, in order to derive a differential equation capable of describing the evolution of the two-dimensional surface separating the two fluids, it was assumed that the potential in the displacing fluid on each side of the pseudosurface could be specified *a priori*. In addition, it was necessary to assume that the root of a finger remained fixed in the surface which initially separated the displacing fluid from the displaced fluid. The introduction of these assumptions enabled the derivation of two sets of equations: one for a water finger and one for an oppositely directed, contiguous oil finger. Finally, these two sets of equations were combined by imposing a number of compatibility conditions to obtain a complete description of the viscous fingering problem. Despite the need to introduce these simplifying assumptions, it would appear, as can be seen from the discussion of results which follows, that the theory adequately describes the viscous fingering problem, provided the underlying assumptions are not seriously violated.

6.1.2.1 Stability Boundary

The stability of a displacement, as can be seen from Equation 67, depends upon the aspect ratio of the coreholder, and upon the mobility ratio, superficial velocity and pseudointerfacial tension of the fluids used in the displacement. The pseudointerfacial tension, in turn, depends upon (see Equation 68) the porosity, irreducible water saturation, residual oil saturation, and the area under the capillary pressure curve. The area under the capillary pressure curve depends upon the wettability of the porous medium, the properties of the sandpack, and the interfacial tension between the displaced and displacing fluid. All of these parameters were varied, to a greater or lesser extent, in this study. In addition, the length of the coreholder was varied because end effects might have affected the breakthrough recoveries.

As can be seen from Figure 4, good agreement between the theoretically predicted value for the stability boundary and that determined experimentally was obtained for each of the four mobility ratios used in this study. This suggests that Equation 67 properly accounts for the effect that aspect ratio, mobility ratio, superficial velocity, and pseudointerfacial tension have on the stability of the displacement. Moreover, such a conclusion is consistent with the results presented in earlier studies[1,5] for systems with higher mobility ratios which were conducted in cylindrical coreholders.

Because the stability boundary was correctly predicted for each of the mobility ratios used in this study, it may be inferred also that Equation 68 correctly predicts the pseudointerfacial tension for a displacement. This supports a similar conclusion drawn in an earlier study[51]. It should be noted that only minor variations in porosity, irreducible water saturation, residual oil saturation and interfacial tension occurred from run to run in this study. As a consequence, Equation 68 should be used with care, if the properties of the fluids or the porous medium differ significantly from those which pertained for this study.

6.1.2.2 Breakthrough Recovery

The theory developed in this study is based on the assumption that the boundary curve (root) of the pseudosurface which separates the oil from the water remains fixed in the $x-y$ plane. This assumption is valid in two situations. First, if I_{sr} is only slightly greater than π^2 , the only wavelength possible is that associated with the critical eigenvalue, γ_c . Given that such is the case, Equation 70 may be used to predict the breakthrough recovery. Second, if the magnitude of I_{sr} is such that the displacement is pseudostable ($I_{sr} \geq 900$), the likelihood is large that the wavelength associated with the most probable eigenvalue, γ_m , is the one which is propagating[2,5]. Under these circumstances, Equation 72 may be used to predict the breakthrough recovery. It should be noted that, because it was impossible to determine where a finger was initiated, it was assumed that X_o was zero in both Equations 70 and 72.

As can be seen from Figure 4, it would appear that the predicted values for breakthrough recovery of a stable displacement are in good agreement with the values determined experimentally for each of the four average mobility ratios used in this study. In this regard, it is to be noted that (see Table 6) Runs 24, 25 and 26 ($M=4.06$) were replicate runs for Runs 6, 7 and 8, respectively. Why consistently lower recoveries were obtained in the latter three runs, as compared to the former three, is not well understood. However, a routine packing procedure had yet to be developed when Runs 6, 7 and 8 were undertaken. Consequently, the packing procedure used for Runs 24, 25 and 26 differed slightly from that used for the earlier runs. As it is known that differences in packing, particularly at low displacement rates[1,5], can result in fairly large variations in breakthrough recovery, it is thought that this might provide a possible explanation for the difference in recovery between the two sets of runs.

The variation in breakthrough recovery, which can be seen in Figure 4, for displacements which were stable comes about for two reasons. First, the end-point mobility ratio varied slightly from run to run whereas the theoretically predicted value for breakthrough recovery was estimated using an average value for the mobility ratio. Second, as was demonstrated in earlier studies[1,5], minor variations in packing can, and often do, result in variations in breakthrough recovery.

Because of equipment limitations (high displacement rates and small pore volumes of the sandpacks), it was not feasible to conduct displacements for high values of the instability number in those runs for which the mobility ratio was small. As a consequence, it was possible only to conduct displacements which were pseudostable for the highest mobility ratio ($M=29.7$) used. Moreover, as can be seen from Figure 4, only two such displacements were possible. However, based on this limited amount of experimental data, it would appear that Equation 72 yields a reasonable estimate of the breakthrough recovery to be expected when the displacement is pseudostable.

As has been mentioned earlier, Bentsen's instability number[2] is proportional to the one derived by Peters and Flock[1]. The constant of proportionality

$$C(M) = \frac{4(M^{5/3} + 1)}{(M + 1)(M^{1/3} + 1)} \quad (137)$$

is a function of the mobility ratio. Thus, if $C(M)$ is taken into consideration when determining the onset of the pseudostable region, one would expect an instability number differing from that reported by Peters and Flock by the factor, $C(M)$. Peters and Flock suggested that the pseudostable region begins when $I_{sr} = 1000$. If, however, the constant of proportionality is taken into account for $M \approx 29.7$, the instability number at which the onset of the pseudostable region occurs becomes $(1000/2.22) = 450$. This seems to agree with the experimental evidence obtained in this study. For example, Runs 55 ($I_{sr} = 625.8$) and 61 ($I_{sr} = 575.18$) appear to be in pseudostable region (see Figure 4).

Three different coreholder lengths were used to see if length had any effect on the breakthrough recovery. Runs 43, 44 and 45 (see Table 7), which were all stable displacements, were conducted in coreholders having lengths of 61 cm, 30.5 cm and 91.4 cm, respectively. Because only minor variations in breakthrough recovery were recorded in these runs, it may be inferred that the effect of length on the breakthrough recovery of a stable displacement must be small because it appears to be completely masked by small variations in breakthrough recovery brought about by small changes in mobility ratio and packing.

Similar comments can be made with respect to the unstable displacements. For example, Runs 29 and 35 (see Table 7) have similar instability numbers, different lengths, and the same breakthrough recovery, whereas Runs 38 and 39 have the same length, similar instability numbers and breakthrough recoveries which differ by 4 per cent. Thus length effects, if such exist for unstable displacements, are also masked by variations in breakthrough recovery due to small variations in packing and mobility ratio. Because similar comments can be made with respect to runs conducted at the other mobility ratios used in this study, it is concluded that length effects, if such exist, do not have a significant effect on breakthrough recovery.

It is not possible to make a theoretical estimate of breakthrough recovery in the transition region ($\pi^2 \leq I_{sf} \leq 900$) for two reasons. First, there exists the possibility that a propagating finger might change mode in this region and, if such is the case, one of the assumptions underlying the theory used to develop the breakthrough recovery equations is seriously violated. Moreover, when such mode changes take place, the velocity of the propagating finger also changes, at least in analogue models of porous media[3]. Second, at low values of I_{sf} , the time constant, n_w , as a function of wavelength, possesses a very broad maximum. As a consequence, it is unlikely that the wavelength of maximum instability will distinguish itself during the course of the experiment[2]. That is, it is possible in replicate experiments that fingers with quite different wavelengths (and different perturbation velocities) might dominate the displacement, if the displacement takes place in the transition region. Thus, because neither the width nor the velocity of a propagating finger is known with any certainty in the transition region, it is not possible to make a theoretical estimate of breakthrough recovery in this region. This also provides a possible explanation for the increased scatter in the data, which is particularly noticeable in the MCT-5 displacements ($M=8.1$) in Figure 4, in the transition region[2].

The breakthrough recovery equations developed in this study are based on the assumption that the distance traveled by the tip of a viscous finger is a linear function of time. Because there is good agreement between the theoretically predicted breakthrough recoveries and those determined experimentally, it would appear that the use of a linear time function is acceptable, at least in the displacements conducted in this study. This is consistent with the results obtained in an earlier study[3].

6.2 Estimation of Relative Permeabilities Using the External-Drive Technique

6.2.1 Introduction

As has been noted in the development of the theory, use of the external-drive technique to estimate relative permeabilities is valid provided the displacement is both stable ($I_{sr} \leq \pi^2$) and stabilized ($N_c \leq 0.1$). Moreover, it is important that the functional forms used to describe the cumulative oil production and pressure-drop histories are internally consistent and monotonic, and that they are consistent with the various physical conditions which can be imposed on the system.

6.2.2 Data Analysis

To undertake a least-squares analysis, it is necessary to specify a number of different functions which can be used as "predictor" variables. The predictor variables used in this study included $\ln t$, $t/\ln t$, and t^j for $j = -3, -2, -1, 1, 2, 3$. Once a specific set of predictor variables had been chosen, they were modified, as illustrated in the section on theory, so as to be consistent with Equation 84 for the cumulative oil production data, and with Equation 94 for the pressure data. Then the method of least-squares was used to estimate the values of the coefficients of the regression equation selected. This was repeated for a number of different regression equations which were selected by setting some of the a_i or b_i equal to zero. Then various statistical methods provided within the BMDP program[113], a non-linear regression analysis package available on the MTS at the University of Alberta, were used to select the "best" regression equation. Typical curve matches are shown in Figure 5 for Run 62. The estimated mean-square error for the recovery data in this plot is 0.095 while that for the pressure history data is 6.9×10^{-5} . Similar matches were achieved for other runs.

Once the best regression equation had been determined, a number of tests were undertaken to make sure that the data and estimated parameters were consistent. Of particular importance in this regard is the time to breakthrough. Because rapid changes in both saturation and flowing volume fractions occur at water breakthrough, the time to

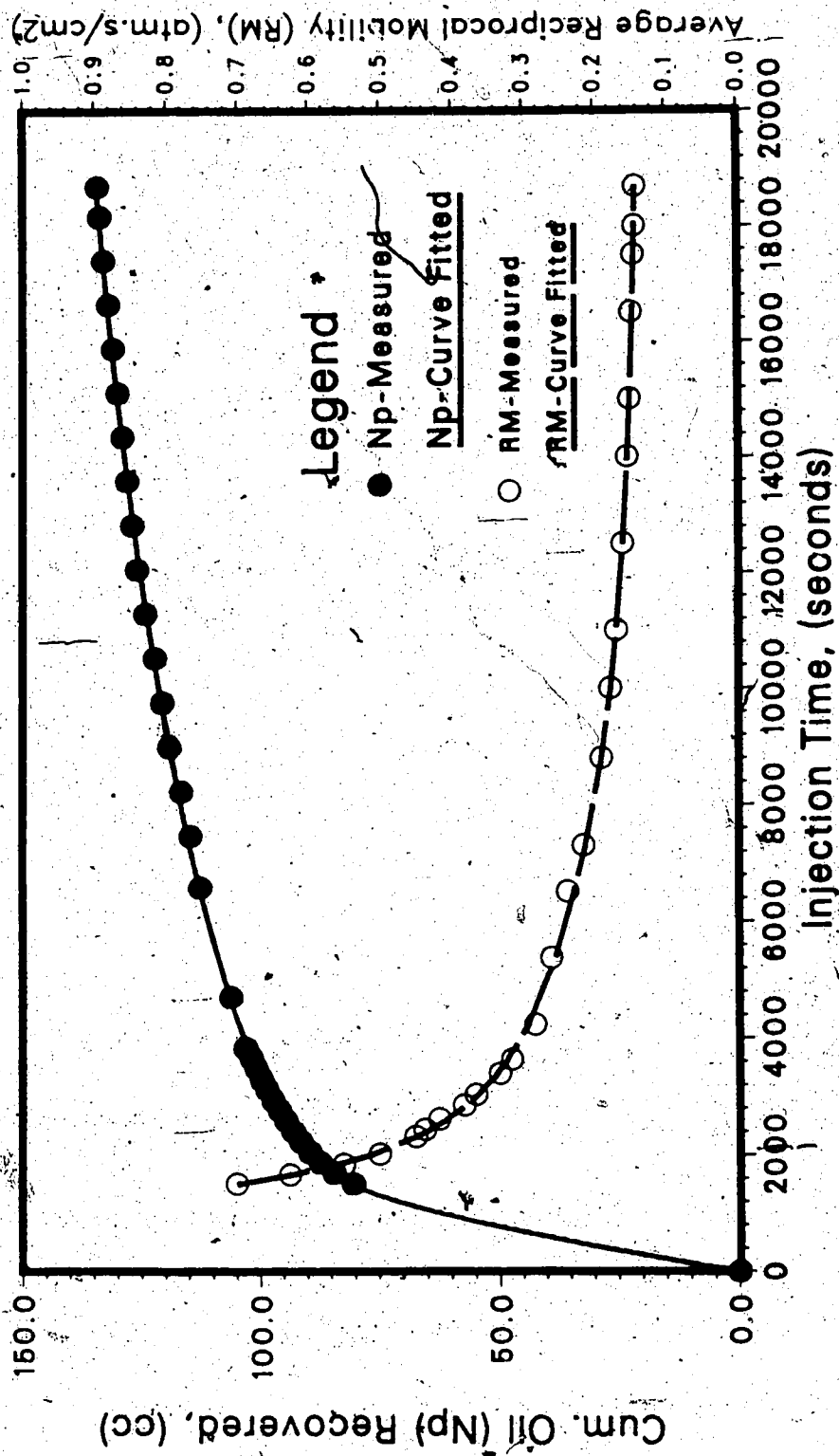


FIGURE 5: CUMULATIVE-OIL HISTORY AND RECIPROCAL MOBILITIES (RUN 62)

breakthrough, and experimental data at or near breakthrough, may be suspect [40,114,115]. Problems may also arise if the Buckley-Leverett [20] assumptions are violated. That is, if the displacement is not stabilized, or if the displacement is unstable, the saturation front will not be as "sharp" as assumed in Buckley-Leverett displacement theory.

In this study, the time to breakthrough was established in three ways: visually, from the total weight of the fluids produced versus time plot, and by means of Equation 95. A typical weight versus time plot is shown in Figure 6. It was usually found that there was good agreement between the three estimates. If the visually observed time to breakthrough was significantly smaller than that predicted using Equation 95, this was taken as an indication that the displacement was either unstabilized or unstable. Moreover, any data points in the immediate vicinity of the breakthrough point which were obviously erroneous were excluded from the analysis.

The parameter t_m can be estimated from both the pressure drop and the cumulative oil production histories. Because both N_p and $\bar{\lambda}_2^{-1}$ approach their limiting values asymptotically, it is very difficult to estimate t_m accurately. Consequently, the value of t_m estimated using Equation 84 can be quite different from that obtained using Equation 94. To help select the most appropriate value for t_m , Equation 104 was also used to estimate t_m . In evaluating Equation 104, the value of k_{wor} was estimated by extrapolating a trial effective permeability-to-water curve to $S_w = 1 - S_{or}$. Moreover, in estimating the slope of a trial effective permeability to oil curve, use was made of the fact that the permeability to oil must be zero at $S_w = 1 - S_{or}$. The parameters k_{wor} and S_{or} can also be estimated using the regression equations. That is k_{wor} can be estimated from μ_w/k_{wor} , a parameter in Equation 94, while S_{or} can be estimated from $(1 - S_{wi} - S_{or})$, a parameter in Equation 84. When, for a particular value of t_m , the values of k_{wor} and S_{or} estimated from the effective permeability curves were consistent with those estimated using the regression equations, the value of t_m was deemed to be acceptable.

When polynomials are used to construct an approximating function, oscillations of the approximating functions may prove troublesome. In order to lessen the severity of the

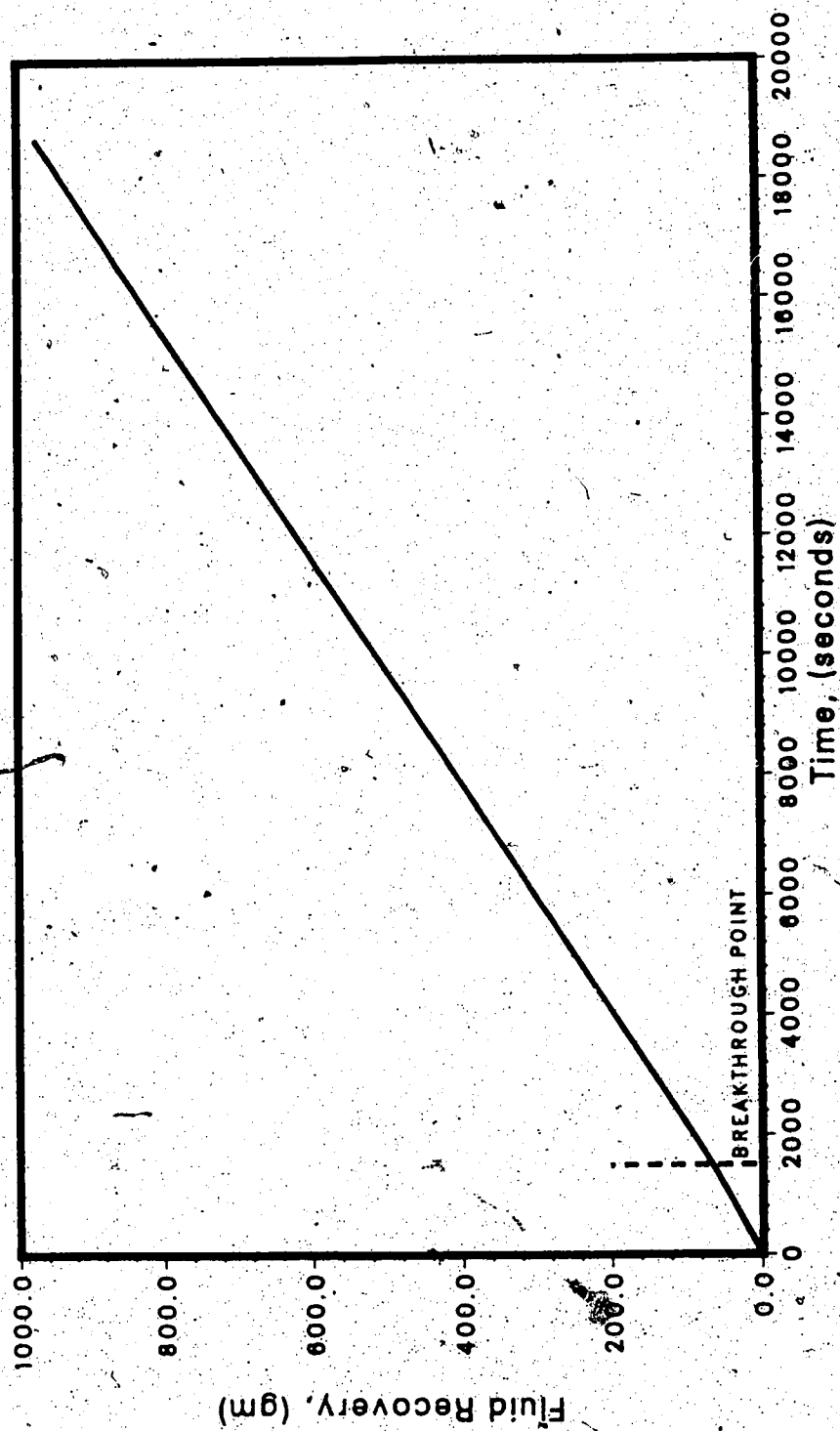


FIGURE 6: ESTIMATION OF BREAKTHROUGH POINT
FROM FLUID RECOVERY DATA (RUN 62)

problem, only polynomials of relatively low degree were used in the regression function. Moreover, to ensure that the equations used were smooth and monotonic, the second derivative with respect to time for both $\bar{\lambda}_2^{-1}$ and N_p was calculated. Thus, if $d^2\bar{\lambda}_2^{-1}/dt^2$ was positive over the interval $t_{bt} \leq t \leq t_m$, and if it decreased monotonically, the function used to model $\bar{\lambda}_2^{-1}(t)$ was deemed acceptable. Similarly, if d^2N_p/dt^2 was negative over the same range, and if it increased monotonically, the function used to model $N_p(t)$ was deemed acceptable.

Finally, when regression equations with internally consistent parameters had been obtained, Equations 86 and 93, together with Equations 74 and 75 were used to generate the final relative permeability versus saturation curves.

6.2.3 Results

In order to evaluate the approach suggested in this study three sets of data were utilized, one from Run 62, and two from the literature[48,113,114]. A summary of the core data for each of the displacements studied is provided in Table 9. It should be noted that the values of S_{or} reported in this table are based on the average saturation existing in the core at the termination of the experiment. Consequently, if all of the displaceable oil had not been displaced at this time, the true value of S_{or} may be somewhat smaller.

The values of the parameters obtained from fitting the cumulative oil recovery data are reported in Table 10. Also reported in this table are the residual sum of squares and the estimated mean square error for each of the runs. The analogous data for the pressure histories are reported in Table 11.

A comparison of the end-point effective permeabilities for water, breakthrough times, and residual oil saturations are presented in Table 12. Because it was not possible to estimate N_c for two of the displacements, another scaling parameter, $L\mu_{wv}$ [32], which is also presented in Table 12, was used to assess the stabilization of the displacements. Also reported in Table 12 are the estimated values of $k_o(1-S_{or})$. The observed values of k_{wo} reported in the table correspond to the values determined experimentally, while the calculated values of k_{wor} are those estimated during the fitting of Equation 94. The observed values of t_{bt} reported in the

Table 9: Summary of Core Data

Experimental Data	Jones-Roselle	Miller	Run 62
Length of Core (cm)	12.70	51.47	100.00
Diameter of Core (cm)	3.81	5.04	-
Cross-sectional Area (cm ²)	11.4	19.98	5.58
Porosity (fraction)	0.215	0.380	0.334
Pore Volume (cm ³)	31.13	391.20	186.37
Displacement Rate (cm ³ /s)	0.02722	0.384	0.05361
Swi (fraction)	0.350	0.073	0.075
Sor (fraction)	0.313	0.186	0.203
Oil Viscosity (cp)	10.45	28.37	34.2
Water Viscosity (cp)	0.97	0.953	1.0
Absolute Permeability (d)	0.0354	7.06	20.46
k _{oiw} (d)	0.0274	4.80	18.66

Table 10: Parameters Obtained From Fitting of Cumulative Oil Recovery Data

Parameters	Jones-Roselle	Miller	Run 62
1-S _{wi} -S _{or}	0.33088	0.7541	0.7657
t _m	13369.5	16686.3	36573.4
a ₂	-4837.893533	32024.349359	151680.958225
a ₃	53.072793	-91.148191	-2.2620
a ₄	-0.019394	0.128903	-0.0142791
a ₅	-4.0301E-6	-8.5114E-7	-7.68657E-6
Residual Sum of Squares	0.00186894	3.46579	2.56869
Estimated Mean-Square Error	0.00062298	0.2310526	0.095137

Table 11: Parameters Obtained From Fitting of Pressure Function

Parameters	Jones-Roszelles	Miller	Run 62
μ_w/kw	179.888339	0.400722	0.137543
t_m	13369.5	16686.3	36573.4
b_2	-1352539.35584	803612.593732	1244835.63536
b_3	11755.156221	-2864.096802	-848.969234
b_4	18.016794	2.345720	0.368628
b_5	-1.3480E-3	1.7736E-4	9.9999E-6
Residual Sum of Squares	3.98486	0.00302155	0.006199
Estimated Mean-Square Error	0.9962	0.00023343	0.000069

Table 12: Comparison of Observed and Calculated Breakthrough Time (t_{bt}), k_{wor} and S_{or}

Data	Estimated k_o (1-Sor)	$L\mu_w v$ (cm ² cp/s)	Observed tbt (s)	Predicted tbt (s)	Observed k_{wor} (d)	Predicted k_{wor} (d)	Observed Sor	Predicted Sor
Jones- Roszelle Miller Run 62†	0.00608 4.32 23.63	0.024 0.943 0.961	315 444 1502	434 441 1559	0.00566 2.189 7.0	0.00539 2.38 7.27	0.313 0.186 0.203	0.319 0.173 0.159

• based on pore volumes injected at termination of experiment. † $N_c = 0.091$; $Isr = 9.99$.

calculated values were obtained using Equation 99. The observed values of S_{or} are based on the average saturation values which pertained at the termination of the displacement experiment, while the calculated values are those estimated from the parameters obtained in the fit of Equation 84. Note that, when the displacement was stopped before all the displaceable oil was produced, there is a significant difference between the observed and calculated values of both k_{wor} and S_{or} .

The relative permeability curves for these three displacements are shown in Figures 7, 8 and 9. Note that values of permeability estimated by Jones and Roszelle[48] and Miller[115] are reported as symbols, while the curves estimated using the method developed in this section are reported as solid lines.

6.2.4. Discussion of Results

As has been noted earlier, the method proposed in this study was evaluated using data from three different displacements. Two of the displacements utilized unconsolidated cores while the third utilized a consolidated core. Moreover, the length of the coreholder, properties of the fluids and the core properties varied significantly from displacement to displacement.

6.2.4.1 Jones-Roszelle Data

Jones and Roszelle used a consolidated core in their displacement tests[48]. As can be seen from Table 9, their core had the shortest length, the smallest pore volume, and the lowest permeability of the three displacement systems being considered.

Moreover, the viscosity of the oil used was the lowest of the three displacements. A comparison of the values of k_{wor} , t_{bt} and S_{or} estimated by Jones and Roszelle and by the method used in this study is presented in Table 12. The time to breakthrough value reported by Jones and Roszelle[48] is significantly smaller than that estimated using Equation 99. Because the value of the scaling parameter[32], $L\mu_w v$, is significantly smaller for this run (see Table 12) as compared to the others, it is thought that a possible explanation for this discrepancy is that the displacement is unstabilized. That

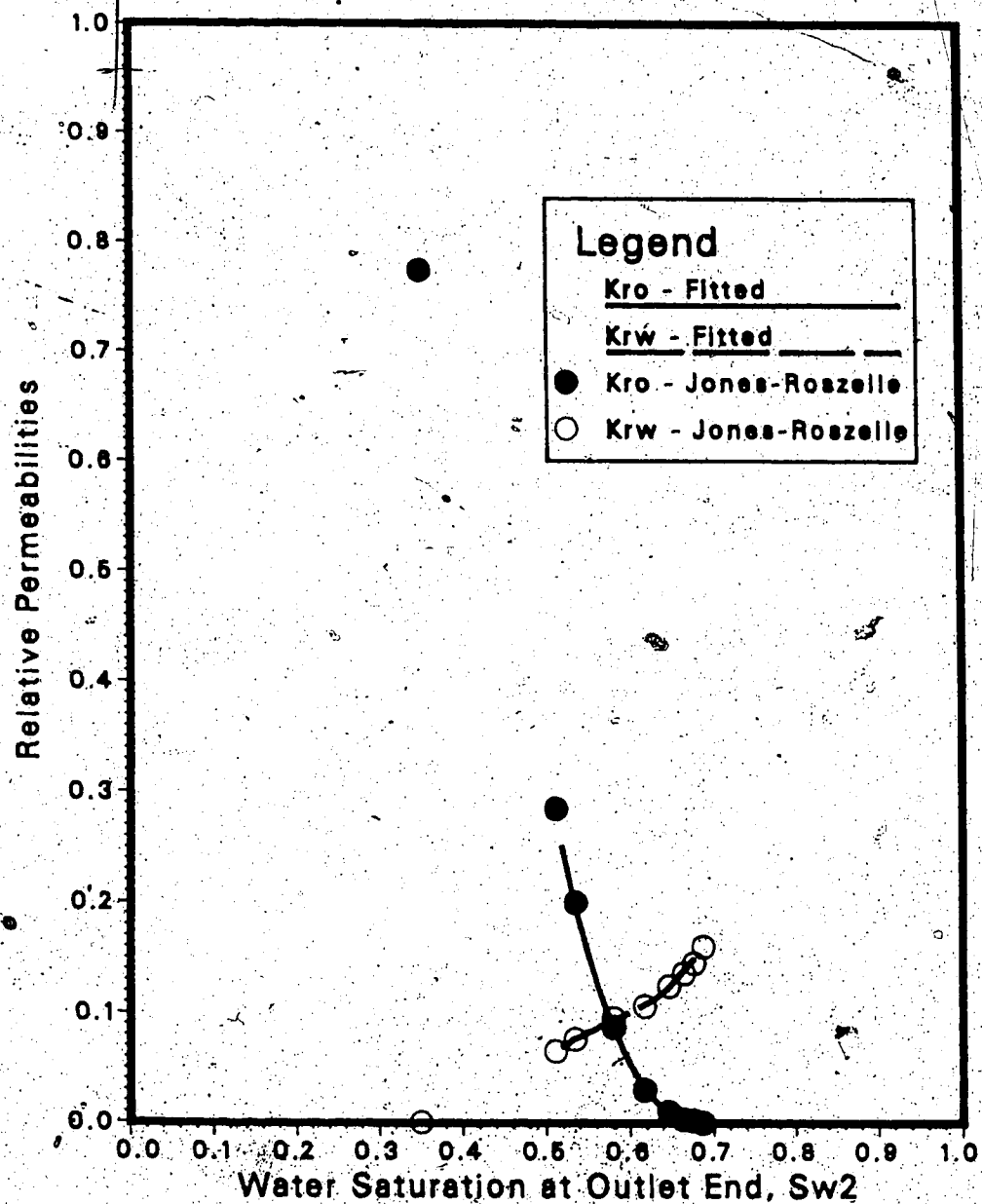


FIGURE 7: RELATIVE PERMEABILITY CURVES FOR OIL AND WATER (JONES-ROSZELLE DATA)

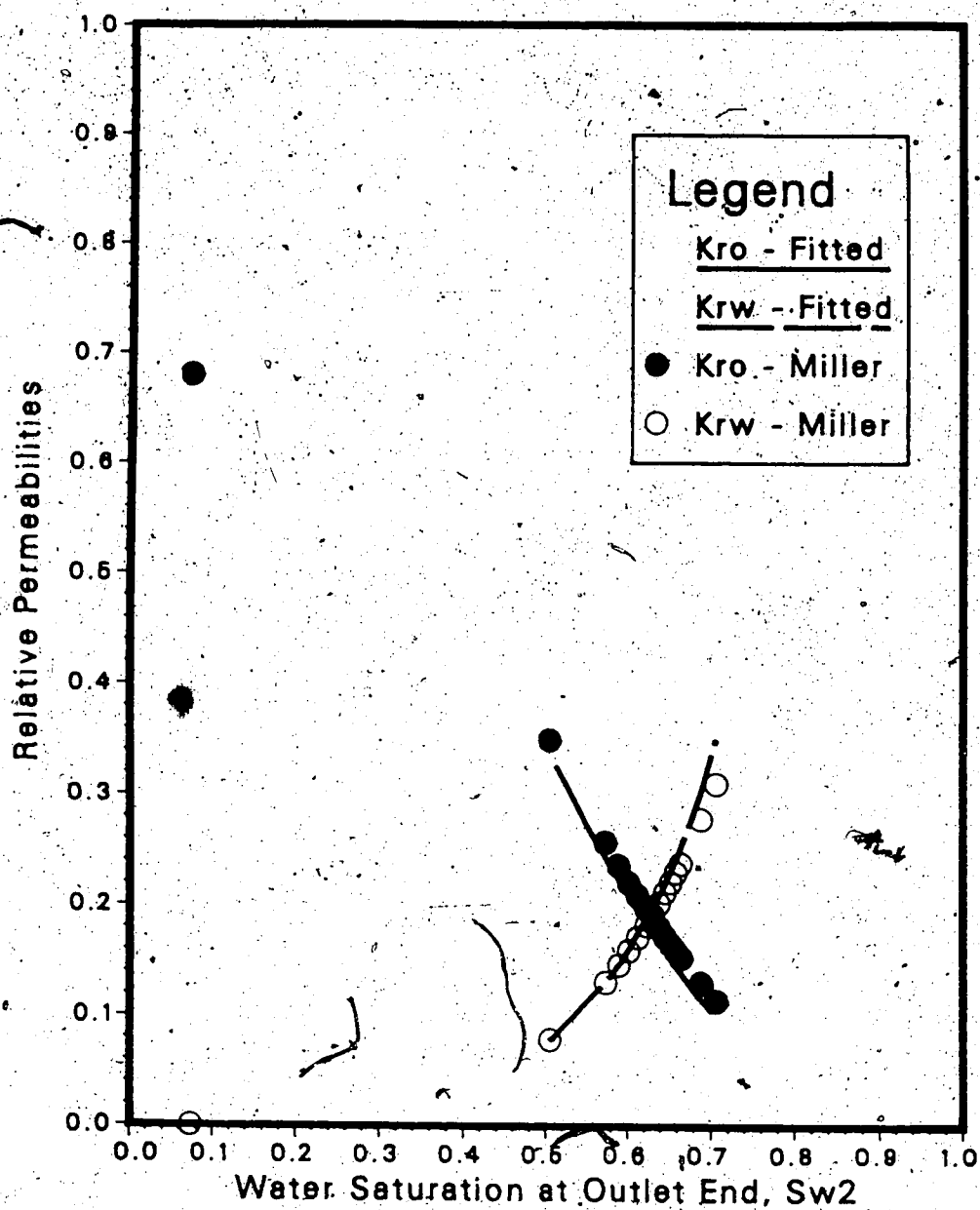


FIGURE 8: RELATIVE PERMEABILITY CURVES FOR OIL AND WATER (MILLER DATA)

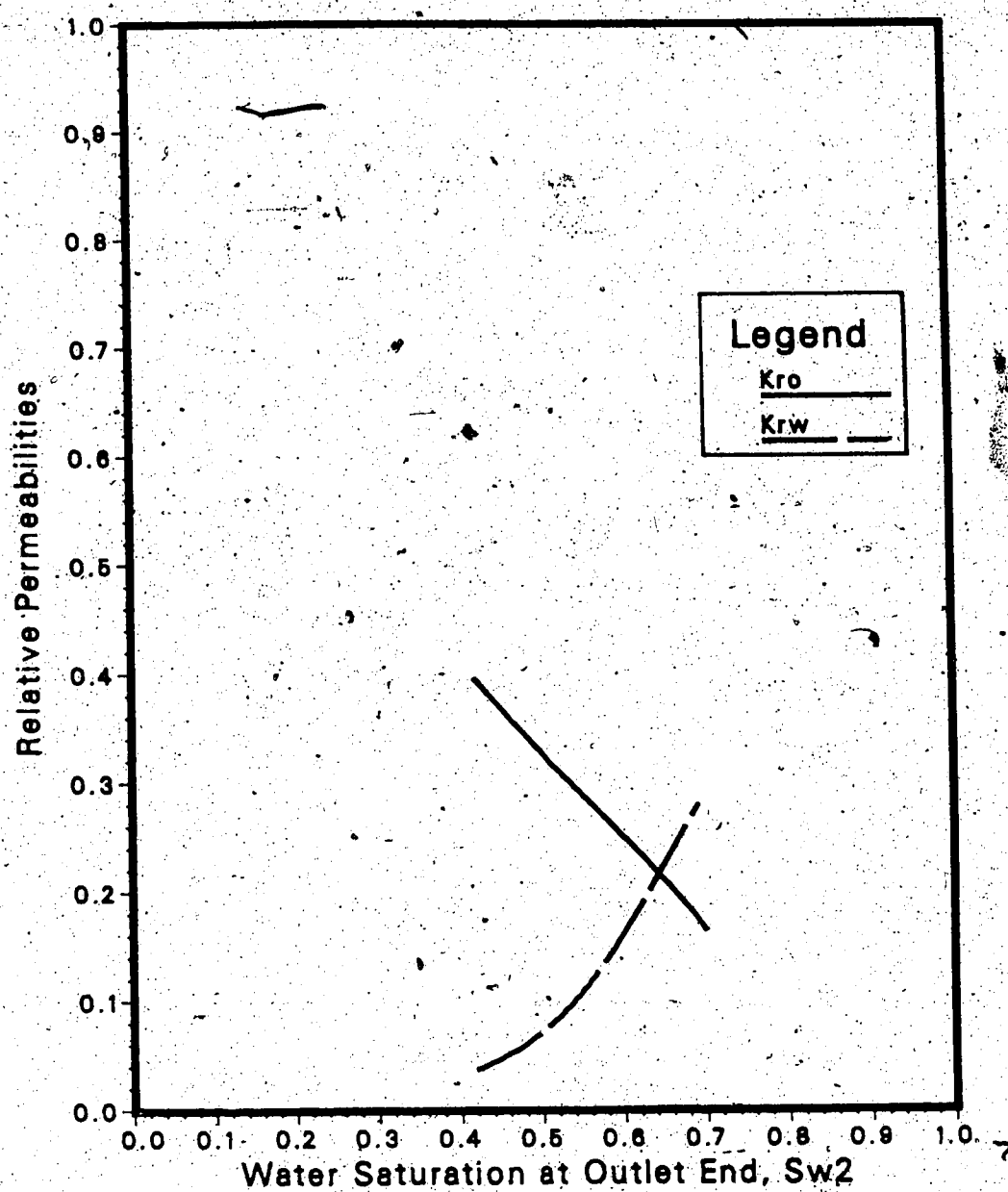


FIGURE 9: RELATIVE PERMEABILITY CURVES
FOR OIL AND WATER (RUN 62)

is, if the saturation front is not as "sharp" as assumed in Buckley-Leverett [20] displacement theory, it is to be expected that the breakthrough point will not be representative. In this regard, it is to be noted that Miller and Ramey [114] have also observed that the actual (true) breakthrough point was usually before the inferred breakthrough point on their recovery versus pore-volumes injected plots.

Because Jones and Roszelle injected a substantial number of pore volumes (10), there is good agreement between their observed value for S_{or} and that estimated parametrically. However, the agreement between their value for k_{wor} and that obtained by using Equation 94 to fit the pressure history data is not as good. The reason for this is that the author's approach taken in this study suggests that only 9.54 pore volumes ($t = 13,369.5$ seconds) are needed to produce all the displaceable oil while Jones and Roszelle [48] suggest that an infinite number of pore volumes is required. Despite these differences, the overall agreement, as can be seen from Figure 7, is quite good between the relative permeability curves obtained using the Jones and Roszelle method [48] and that used herein.

6.2.4.2 Miller Data

Miller used an unconsolidated core in his studies [115]. The viscosity of the oil, the length of the core and its permeability were intermediate, as compared to those of the other two displacements. The pore volume of the core was the largest of the three cores considered. Moreover, because Miller used an "inferred" value for t_{bt} , there is good agreement between his estimate and that calculated using Equation 99 (see Table 12). Because Miller did not inject sufficient pore volumes to produce all of the displaceable oil, there are uncertainties associated with the values estimated for both k_{wor} and S_{or} . The observed value reported for k_{wor} , as estimated by Miller, is the last value reported by him in his thesis [115]. Because the value of S_{w2} for which this value of permeability corresponds is too low, the observed value for k_{wor} is too low, while that for S_{or} is too high. The value for k_{wor} estimated in this study is about 8 per cent higher than that reported by Miller [115], while that for S_{or} is about 7.5 per cent lower.

Because the value of t_m was adjusted in such a way that the values of S_{or} and k_{wor} (see Data Analysis Section) estimated from the effective permeability curves were in good agreement with those obtained from Equations 84 and 94, respectively, it is thought that the latter values are to be preferred. However, it should be kept in mind that both N_p and λ_2^{-1} asymptotically approach their limiting values. Consequently, it is very difficult to estimate accurately the limiting values of these curves. Hence, the application of additional consistency tests need not necessarily improve the accuracy of the estimated values of k_{wor} and S_{or} . This points to the need to continue to inject water until such time as most of the displaceable oil has been produced, if accurate estimates of S_{or} and k_{wor} are to be achieved.

A comparison of the relative permeability curves obtained by Miller and by the method developed in this study is shown in Figure 8. As can be seen from the figure, there is reasonably good agreement between the two sets of curves. With respect to the relative permeability to water curves, the agreement worsens as the saturation to water increases. This comes about because the parametric estimate for k_{wor} is somewhat higher than that estimated by Miller. Because of the consistency tests which are incorporated into the method suggested in this study, it is thought, as noted earlier, that their method is likely to be somewhat more accurate.

Overall, the agreement between the two oil relative permeability curves is not quite as good. There are two reasons for this. First, both $\lambda_2^{-1}(t)$ and $f_{o2}(t)$ are concave downward, while $f_{w2}(t)$ is concave upward. Consequently, small errors in the magnitude and the slope of $\lambda_2^{-1}(t)$ and $f_{o2}(t)$ can result in larger errors in the estimated value of k_o (see Equation 75) than is the case for k_w (see Equation 74). Second, because f_{w2} is multiplied by μ_w while f_{o2} is multiplied by μ_o , any such errors are magnified to a greater extent in the case of the oil curve.

6.2.4.3 Run 62

The core utilized in Run 62 was unconsolidated. It has the longest length, an intermediate pore volume, and the highest permeability. Moreover, the viscosity of the

oil was the highest of the three runs. Because the capillary number, N_c , is less than 0.1, it is thought that the displacement was stabilized. However, because I_{sr} is slightly greater than π^2 , there exists the possibility that the displacement may be unstable. As a consequence, the observed breakthrough time might be smaller than it should be for a stable displacement. Despite this there is reasonably good agreement between the visually observed breakthrough time and that estimated using Equation 99.

Because Run 62 was stopped before all the displaceable oil had been produced, the observed value of k_{wor} is lower than its true value, while that of S_{or} is higher. While the consistency tests discussed in the Data Analysis Section were employed to obtain the estimated (calculated) values reported in Table 12, these values are not necessarily accurate for two reasons. First, because the Ruska pump used was capable of pumping only a limited volume of the displacing fluid, Run 62 was stopped at a point where the amount of oil still to be displaced was fairly large. Second, the accurate estimation of parameters which approach their limiting values asymptotically is very difficult. The relative permeability curves for this displacement are presented in Figure 9.

6.3 Further Validation of the External-Drive Technique

6.3.1 Introduction

In order to gain complete confidence in the external-drive technique developed in this study, it was necessary to validate the technique by carrying out some additional consistency checks. This was accomplished by measuring the saturation and the pressure gradient at the outlet end of the core and comparing these values with those estimated using the external-drive theory. Run 63 was carried out to meet this objective. A summary of the basic experimental data appears in Table 13.

Table 13: Summary of Experimental Data (Run 63)

Displaced Fluid	MCT-5
Viscosity of Displaced Fluid (cp)	34.2
Length of Core (cm)	100.5
Thickness of Core (cm)	1.1
Height of Core (cm)	5.65
Pore Volume (cm ³)	230.0
Displacement Rate (cm ³ /s)	0.0536
Porosity (fraction)	0.368
S _{wi} (fraction)	0.07
S _{or} (fraction)	0.073
Absolute Permeability (darcy)	20.46
Effective Permeability to Oil @S _{wi} (darcy)	19.0
Effective Permeability to Water @S _{or} (darcy)	3.96
Mobility Ratio	7.1
Time to Breakthrough - Measured (s)	2361
Time to Breakthrough - Predicted (s)	2372
Maximum Time - Estimated by Curve Fitting (s)	24426
Maximum Time - Estimated by Equation 32 (s)	44459
Stability Number	4.82
Stability	stable
Capillary Number	0.0737
Stabilization	stabilized

6.3.2 Data Analysis

The cumulative oil produced was estimated in two ways. First, the total quantity of fluids produced was weighed and then Equation 95 was used to calculate the amount of oil produced at a given point in time. Second, the cumulative oil produced was estimated by determining the area under a saturation profile measured at the same time and multiplying this area by the bulk volume times porosity. In both cases, these data were smoothed by using least-squares to determine the coefficients of Equation 84.

Because it was possible to measure the pressure in both the oil and the water, it was possible to estimate the total pressure drop across the core in both phases. Least-squares theory, in conjunction with Equations 87 and 94, was used to fit the total pressure drop histories for both the oil and the water.

Once acceptable fits to the data had been achieved, Equation 86 was used to estimate f_{o2} , while Equation 93 was used to estimate λ_2^{-1} . Then Equations 119 and 120 were used to estimate k_{rw} and k_{ro} , respectively. Equation 99 for t_{bt} and Equation 104 for t_m were used to apply the consistency checks.

An error analysis was undertaken for each of the experimentally determined variables (S_{w2} , λ_2^{-1} , N_p) used in this study. This was accomplished by estimating the standard error for each of the independent variables in Equations 118, 87, and 95. Then an overall error analysis of each of the equations was undertaken [116] to estimate the standard error associated with each dependent variable. The relative standard error for saturation ranged between 0.8% at $S_{w2} = S_{wi}$ and 0.2% at $S_{w2} = 1 - S_{or}$; for λ_2^{-1} it remained approximately constant at about 0.5% over the entire range of measurements; and for N_p it ranged between 0.15% at $t = t_{bt}$ and 1.3% at $t = t_m$.

6.3.3 Results

An immiscible displacement run, Run 63, was carried out using a water-wet, unconsolidated sand pack. Typical saturation profiles measured during the course of the displacement are shown in Figure 10. Because it was possible to measure the saturation at the

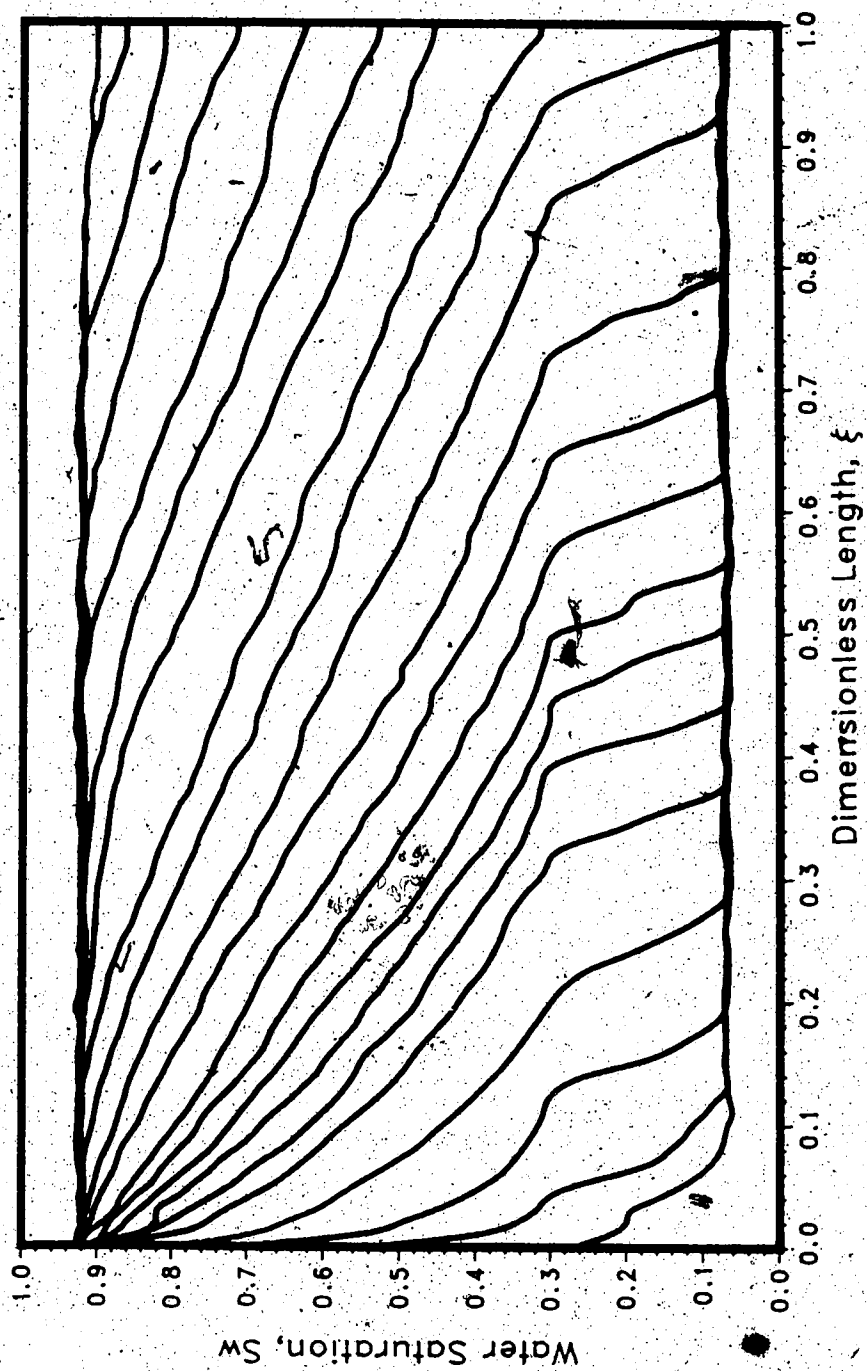


FIGURE 10: DYNAMIC SATURATION PROFILES DURING A STABLE DISPLACEMENT (RUN 63)

outlet end of the system, S_{w2} , it was practicable to compare this value with that estimated using Equation 78 developed by Welge[29]. Such a comparison is depicted in Figure 11. Also, the area under the saturation profiles may be used to estimate the amount of oil produced at the point in time the microwave scan was undertaken. The cumulative production estimated in this way is compared with that estimated by weighing the total production (Equation 95) in Figure 12.

Because of the use of fritted discs wetted with both oil and water it was possible to measure the pressure in both phases. Moreover, because saturations were also available, it was practicable to measure the dynamic capillary pressure as a function of saturation at the midpoint and outlet end of the core. A comparison of the dynamic capillary pressures measured at these two locations with the measured equilibrium capillary pressures is shown in Figure 13.

Normally, in this study, Equation 94 was used to smooth the average reciprocal mobility data, and then Equation 88 was used to estimate the reciprocal mobility at the outlet end of the system. However, because it was possible to measure the pressure gradient at the outlet end of the core, it was practicable also to estimate directly the reciprocal mobility, λ_2^{-1} , at this point. A comparison of λ_2^{-1} estimated in this way with that obtained using Equation 88 is presented in Figure 14 where the values of λ_2^{-1} estimated directly are represented by symbols and those estimated using Equation 93 by the solid line.

One of the assumptions underlying Buckley-Leverett theory[20] is that it is permissible to neglect the capillary pressure gradient. Consequently, it is usual to use the total pressure drop history for only one of the phases (water), when estimating the relative permeability curves using the external-drive techniques. Relative permeability curves obtained using this approach are depicted in Figure 15. Also shown in the figure is the relative permeability to oil curve obtained when the total pressure drop history for the oil phase, rather than that for the water phase, is used to estimate k_{ro} .

For Buckley-Leverett theory to be applicable, the displacement must be stabilized. That is, the shape of the frontal region must be invariant with time, if the theory is to be

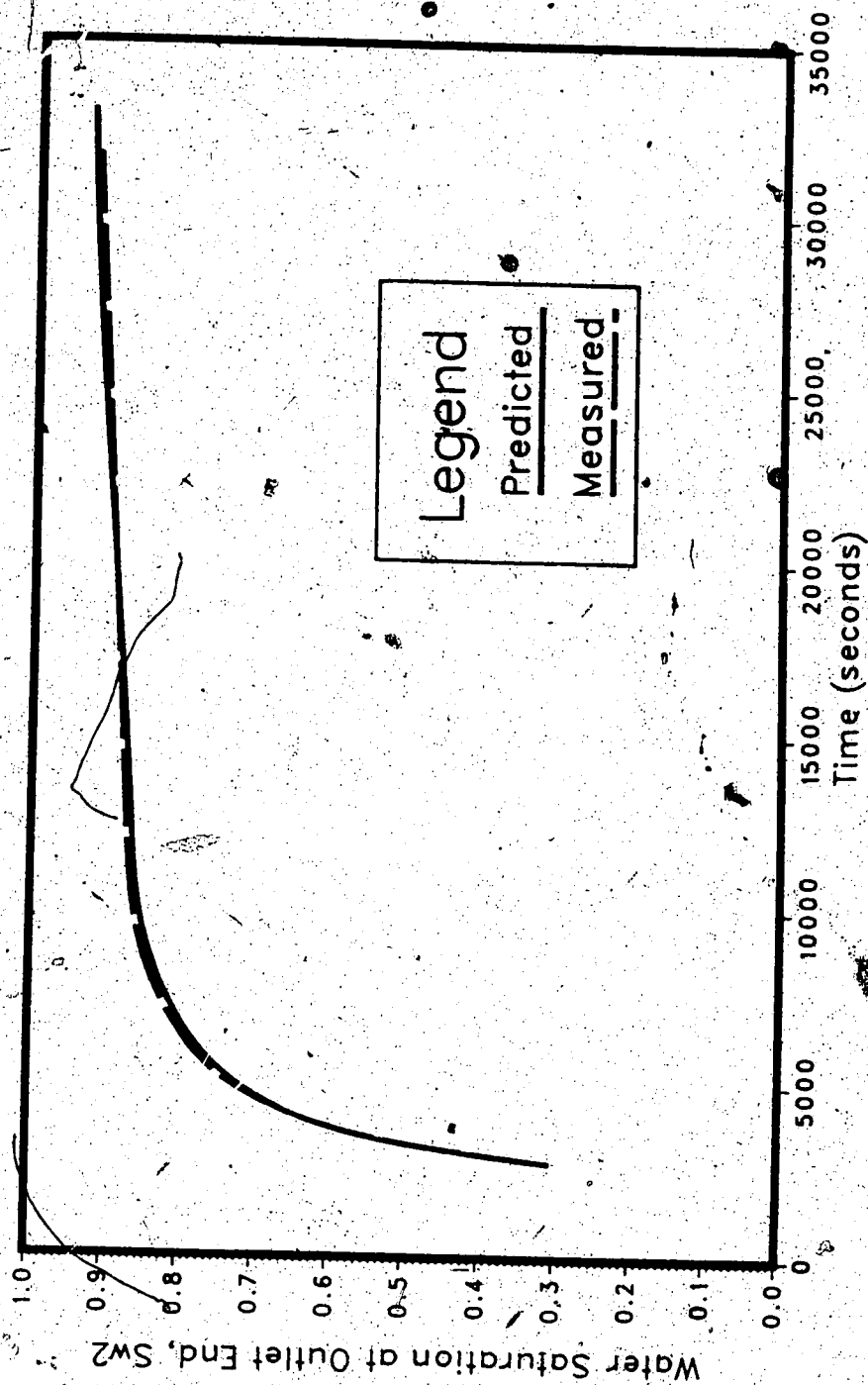


FIGURE 11: COMPARISON OF MEASURED AND PREDICTED SW2 (RUN 63)

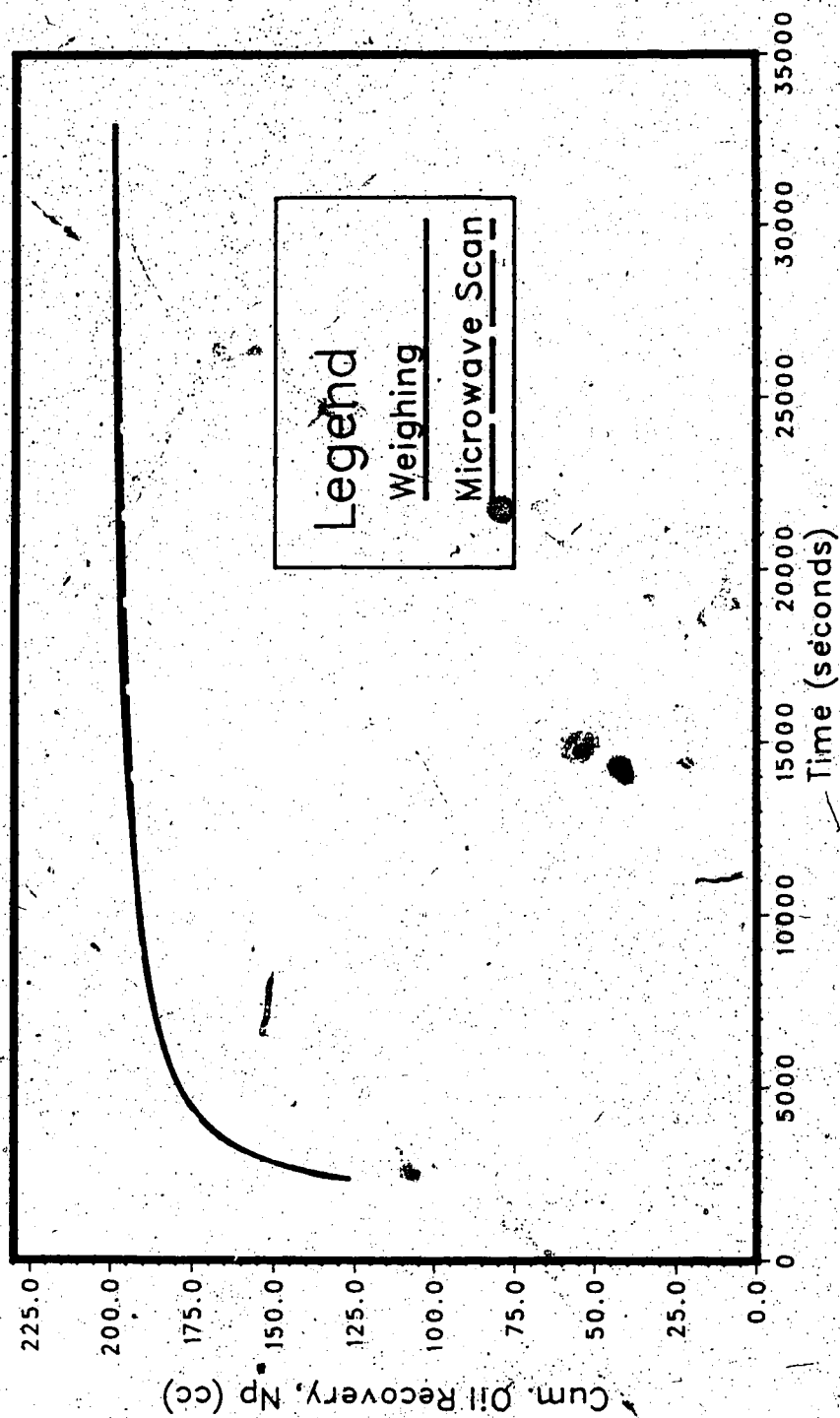


FIGURE 12: COMPARISON OF Np DETERMINED FROM WEIGHING AND MICROWAVE SCAN

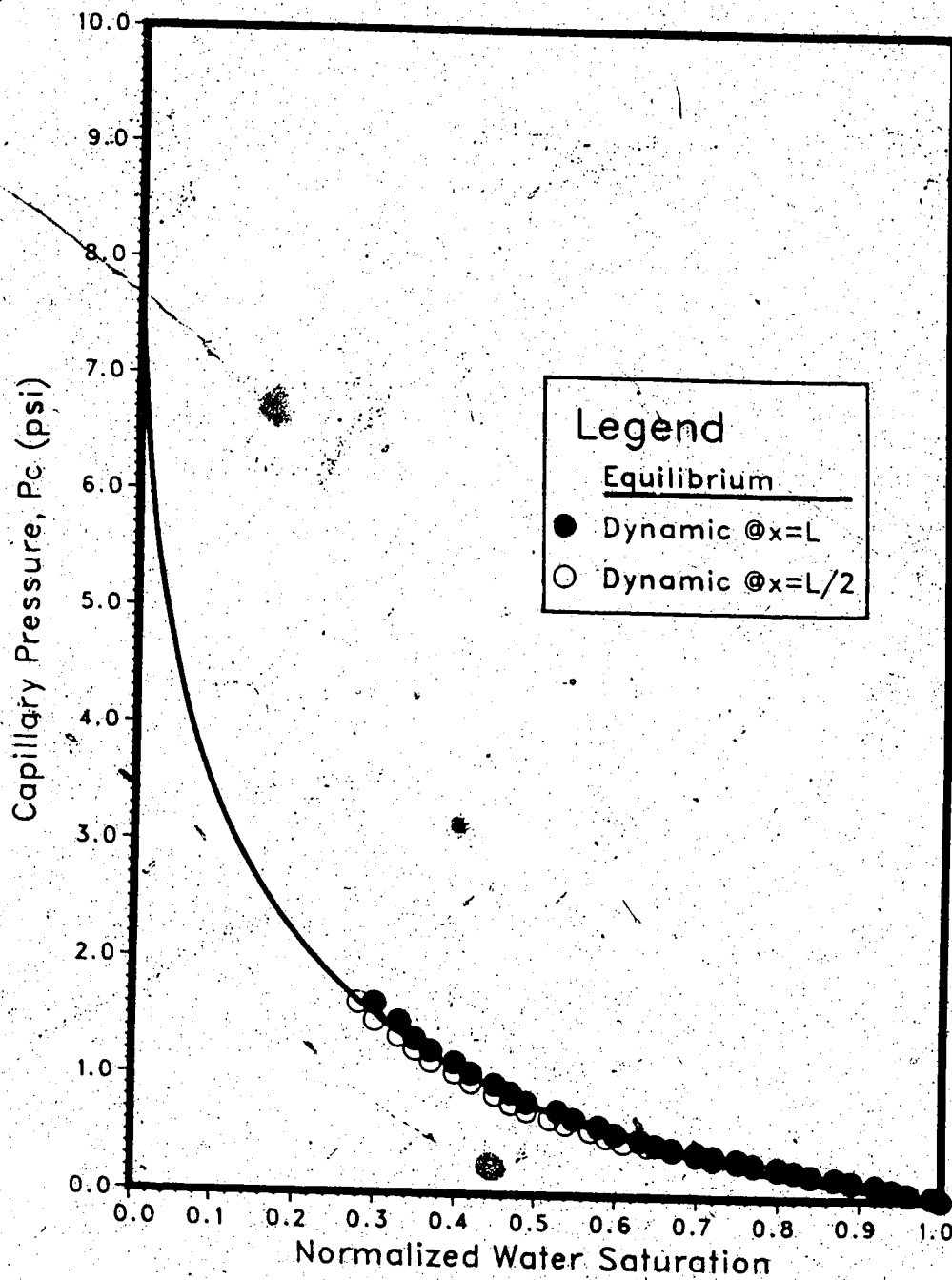


FIGURE 13: CAPILLARY PRESSURE-SATURATION CURVE (RUN 63)

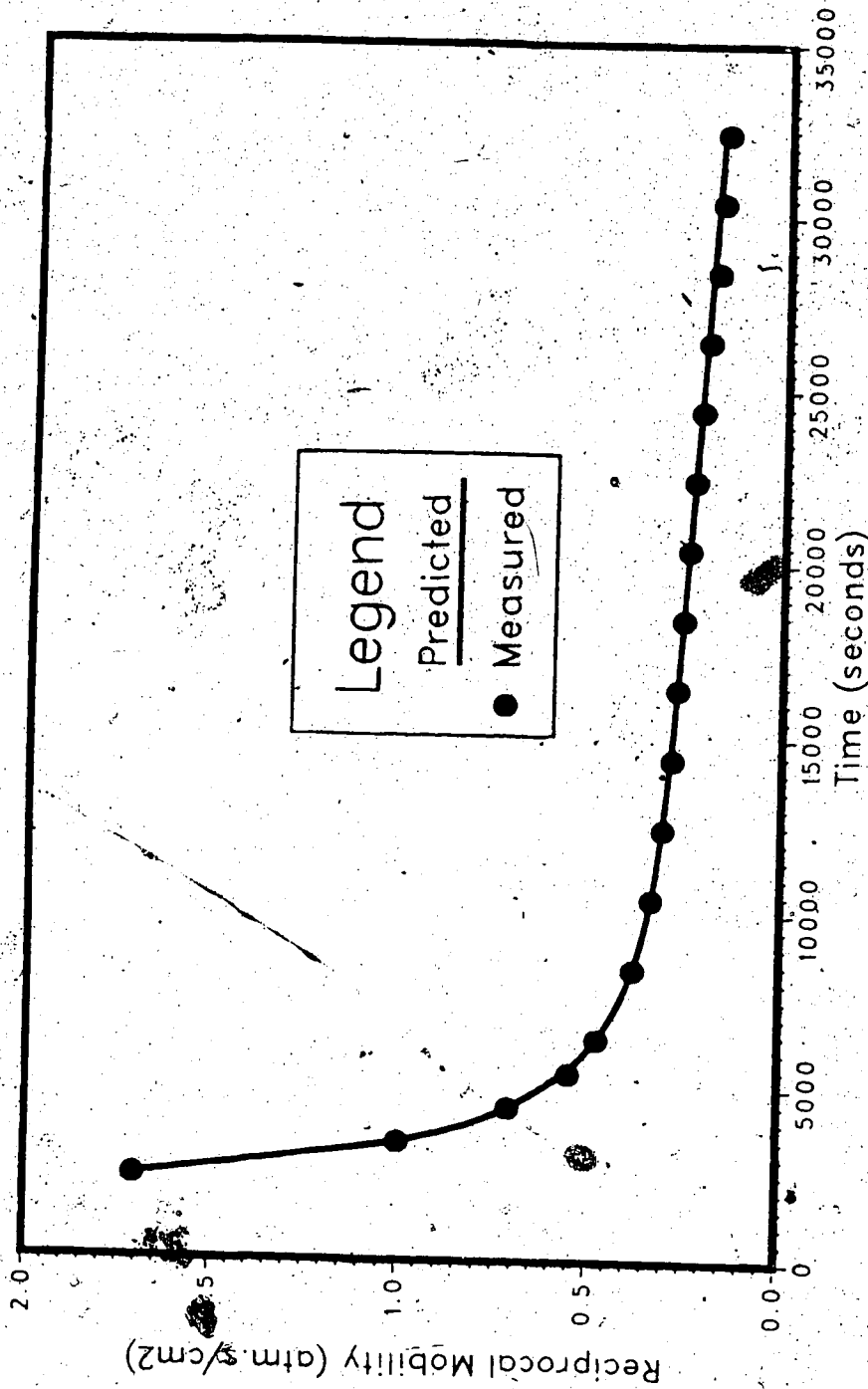


FIGURE 14. COMPARISON OF MEASURED AND PREDICTED
RECIPROCAL MOBILITY AT THE OUTLET END (RUN 63)

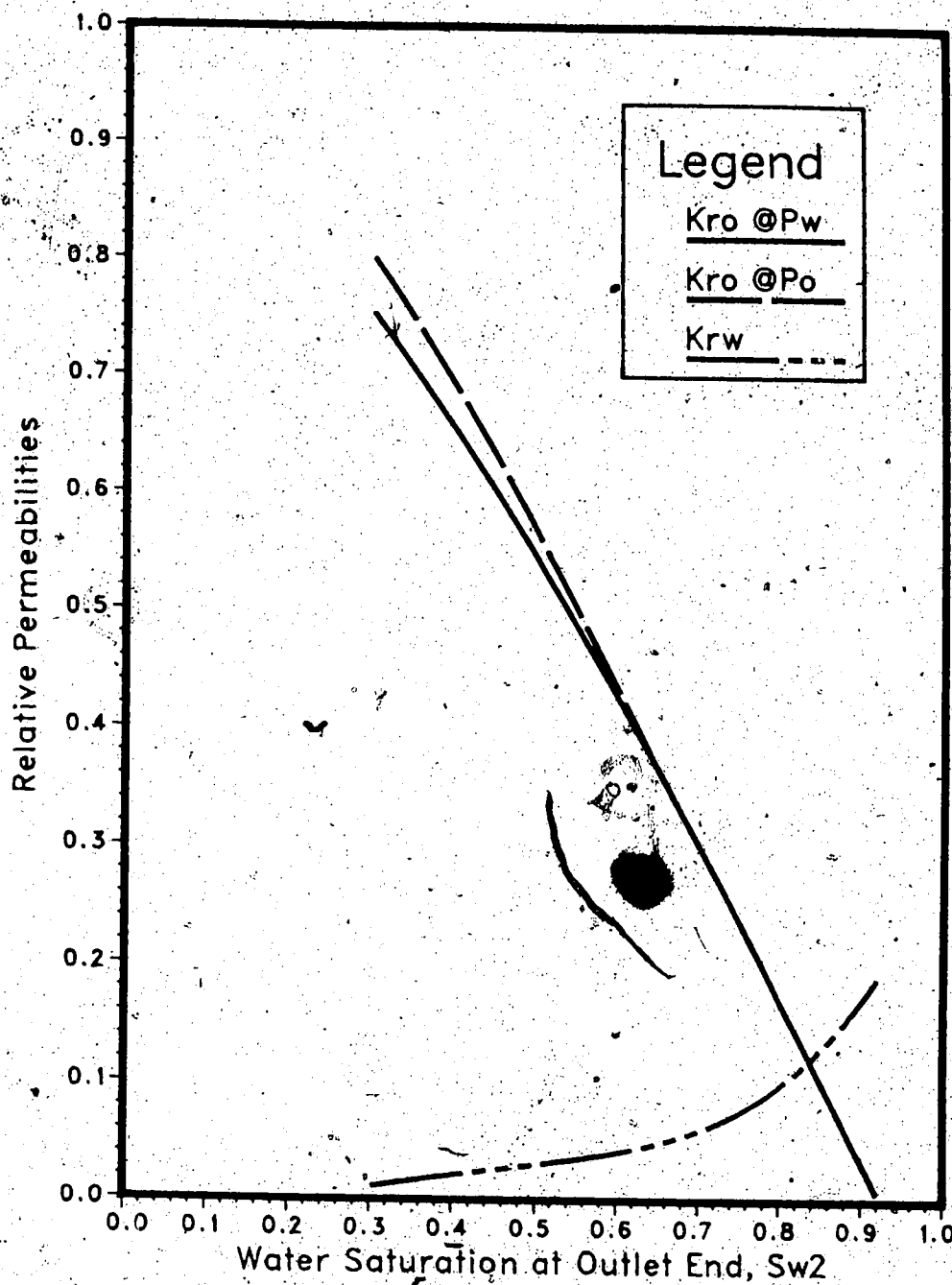


FIGURE 15: COMPARISON OF RELATIVE PERMEABILITIES USING P_o AND P_w (RUN 63)

valid. To illustrate this point, the actual profiles are compared with the Buckley-Leverett profiles in Figure 16.

6.3.4 Discussion of Results

6.3.4.1 Saturation Profiles

Saturation profiles for Run 63 are shown in Figure 10. Because the capillary number is less than 0.1 ($N_c = 0.074$), and because the instability number is less than π^2 ($I_{sr} = 4.82$), the displacement is stable and stabilized. Note, however, that the degree of stabilization increases as the saturation profiles progress along the length of the core. That is, for the first few profiles, the saturation at the inlet end of the system is less than $S_{wm} = 1 - S_{or}$ and increases with time. Moreover, the floodfront saturation, and the steepness of the frontal region have yet to reach their maximum values. As the profiles progress through the system, the floodfront saturation and the shape of the frontal region gradually change until relatively constant values are achieved. When the frontal saturation, the slope of the frontal region, and the shape of the frontal region become invariant with time, the displacement is said to be fully stabilized, and application of the external-drive theory is permissible. Note that, because of local heterogeneities, minor variations in the shape of the frontal region, from profile to profile, are apparent. Because the displacement is stable, such perturbations do not grow, and consequently they do not pose any problems. It is important to note also that had the core been only half as long, the profiles would not have been fully stabilized at the time they reached the outlet end of the system, and the application of external-drive theory would not have been warranted.

6.3.4.2 Saturations at Outlet End

Conventional external-drive theory uses Equation 78, a modified version of the equation suggested by Welge[29], to estimate S_{w2} , the saturation at the outlet end of the system. In this study, least-squares theory was used to fit Equation 84 to the

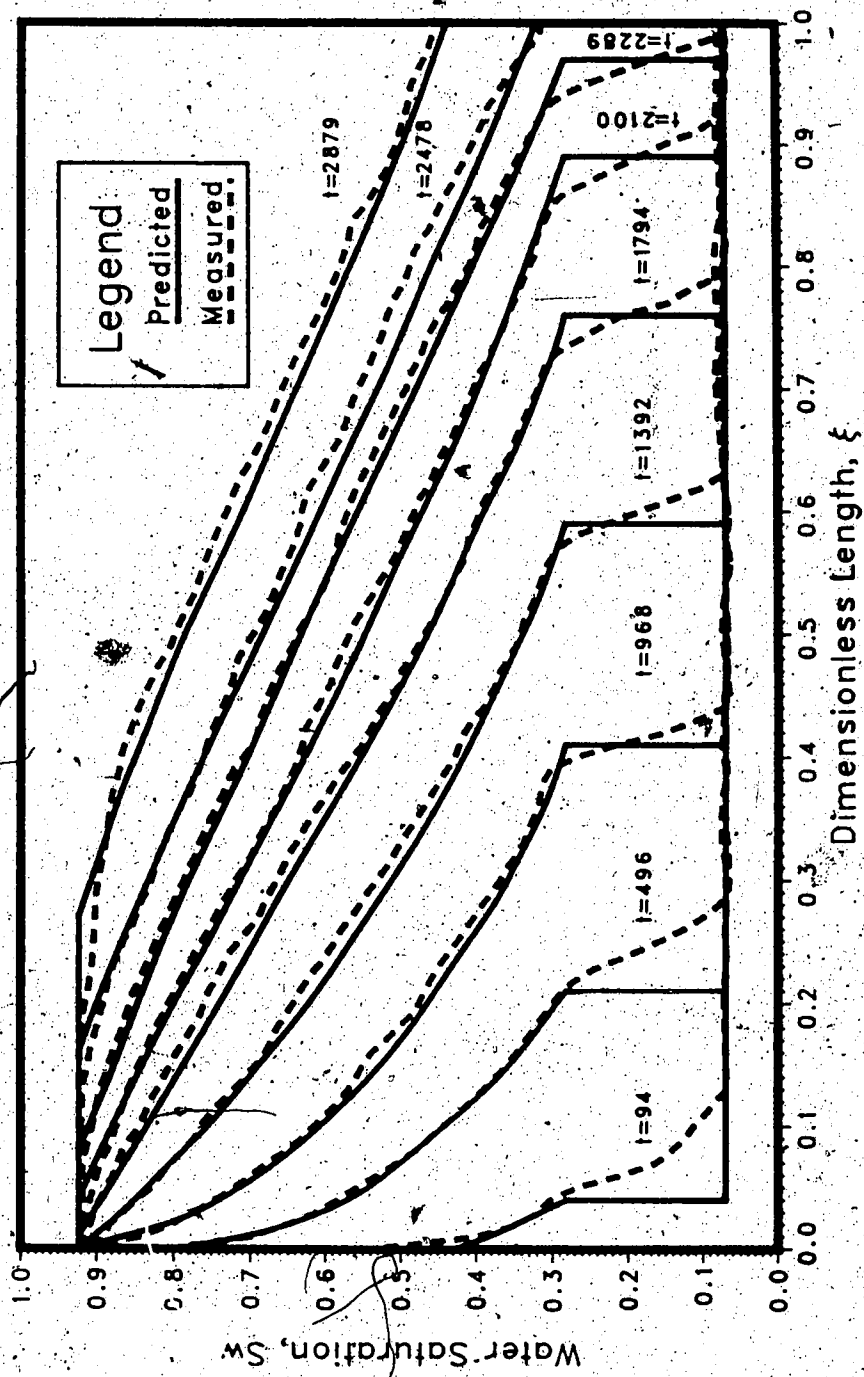


FIGURE 16: COMPARISON OF MEASURED AND PREDICTED SATURATION PROFILES (RUN 63)

cumulative oil production data. Then Equation 83, together with the "best-fit" parameters, was used to estimate S_{w2} . This is equivalent to using Equation 78 to estimate S_{w2} . The solid curve presented in Figure 11 was obtained in this way. Because of the availability of the microwave equipment, it was possible to measure directly the saturation at the outlet end of the core. Equation 83 was used to smooth these data, and the resulting curve is presented as a dashed line in Figure 11. As can be seen from the figure, reasonably good agreement was obtained between the directly measured value of S_{w2} and that estimated using Equation 78. The maximum difference between the two curves is less than one saturation per cent. Because there seems to be a systematic difference between the two curves, attempts were made to improve the agreement by using various weighting schemes when undertaking the least-squares fit. However, this approach did not result in improved agreement between the two curves. While the discrepancy between the two curves might be due to outlet end effects, this is not thought to be the case, because such effects were not observed in the experiments.

A more plausible explanation is that, because of local heterogeneities along the length of the core, the stabilization assumption underlying Equation 78 was not well met. Stabilization implies that the displacement is linearly scalable. That is to say, if the displacement is stabilized, all the saturation profiles along the length of the core should be similar - different by only a linear magnification or reduction[35]. As can be seen from Figure 10, the shape of the saturation profiles varies slightly as they progress along the length of the core. This is more apparent in Figure 16 where the actual profiles are compared with those predicted by Buckley-Leverett theory[20]. The consequence of this variation in the shape of the saturation profiles is that the value of S_{w2} predicted using Equation 78 differs slightly from that actually measured. Because the discrepancy is small (<1%), it is thought that the problem is not serious, at least in this experiment.

6.3.4.3 Material Balance

The area under the saturation profiles can be related to the cumulative oil produced. Consequently, as a material balance check, a program was written to integrate numerically the area under the saturation profiles. When the cumulative oil production estimated in this way was compared with that estimated using Equation 95, it was found that there was a systematic difference between the two curves. However, when data obtained by integrating the area under the saturation profiles were weighted according to the standard error estimates for S_{w2} , the agreement between the two curves improved. A comparison between the cumulative oil-production history obtained in this way with that obtained using Equation 95 is presented in Figure 12 where the solid line represents the cumulative oil-production history obtained by weighing and the dotted line the cumulative oil-production history obtained from the microwave scan. As can be seen from the figure, the agreement is good, with no systematic difference between the two curves. The maximal difference between the two curves is about 0.8 cc.

6.3.4.4 Capillary Pressure Data

In reservoir simulation, it is usual to assume that equilibrium capillary pressure curve can be used to estimate the pressure difference between the water and oil in a dynamic displacement. Because of the use of both water-wet and oil-wet fritted discs, it was possible to estimate how the pressure between the two phases varies as the saturation changes at two locations, during the course of a displacement experiment. A dynamic capillary pressure curve obtained in this way is presented in Figure 13 as a dashed line with symbols. Because of the rapid changes in saturation in the vicinity of the displacement front, it was not possible to measure saturation accurately in this region. As a consequence, the dynamic capillary pressure curve is defined only for saturations between the floodfront saturation and the maximal saturation, $S_{wm} = 1 - S_{or}$. Also shown in the figure is an equilibrium capillary pressure curve (solid line) obtained for the same sand-fluid system. Note that, within experimental error, the dynamic capillary pressures measured at the midpoint of the core are the same as those measured

at the outlet end for a given saturation. As can be seen from Table 14, the parameter A_c is almost equal in all three cases. This comes about because the small coreholder used in the equilibrium capillary pressure experiment could not be packed in the same way as the large coreholder used in the displacement experiments. As a consequence, there were minor differences in porosity and residual oil saturations in the two experiments. This in turn (see Equation 68) led to differences in the area under the equilibrium and dynamic capillary pressure curves. It also provides an explanation as to why the capillary pressure curves differ slightly. Given that the curves pertain to slightly different porous media, the curves are quite similar.

6.3.4.5 Reciprocal Mobility

Conventional external-drive theory is based on the assumptions that the displacement is stabilized, and that it is permissible to neglect the capillary-pressure gradient. Given that these assumptions are met, Equation 88, a modified version of an equation proposed by Jones and Roszelle[48], may be used to predict the reciprocal mobility, λ_2^{-1} , at the outlet end of the system. The solid curve presented in Figure 14 was estimated in this way. If an estimate of the pressure gradient at the outlet end of the coreholder is available, and if the capillary-pressure gradient may be neglected, it becomes practicable to estimate directly λ_2^{-1} . Values of λ_2^{-1} estimated directly are presented as symbols in Figure 14. As can be seen from the figure, the agreement between the two approaches is good, except for the second- and third-last data points where the relative error with respect to the smoothed data (solid line) is about 6.5 per cent. The reasons underlying the large relative error for these two points are unknown. However, it is speculated that because essentially only water was flowing at this point in the displacement history, the pressure transducers sensing pressure at the oil-wet fritted discs may not have been able to do so accurately. To investigate this possibility, the relative error with respect to the smoothed pressures in the water was estimated also for the same two data points. In this case, the relative error was found to be 2.8%, which supports the hypothesis that there were accuracy problems with respect to the pressures

Table 14: Fluid Properties @21°C

Fluid	Density (gm/cc)	Viscosity (cp)	IFT (dyne/cm)	Ac(Equilibrium) (dyne/cm ²)	Ac(Dynamic) @x = L/2 (dyne/cm ²)	Ac(Dynamic) @x = L (dyne/cm ²)
Distilled Water	0.9982	1.0	—	—	—	—
MCT-5	0.8123	34.2	33.08	16342	16341	16339

measured in the oil. However, because the relative error for the water-pressure gradient was much larger for these two points than for the other points, there is likely some other, unexplained phenomenon contributing to the problem.

6.3.4.6 Relative Permeability Curves

When estimating the relative permeability curves, it is usual to use the total pressure history for only one of the phases (water) in calculating $\bar{\lambda}_2^{-1}$. Implicit in this approach is the assumption that the capillary pressure gradient may be neglected. Relative permeability curves obtained under this assumption are presented in Figure 15, where the oil relative permeability curve is depicted by a solid line. Because of the use of oil-wet fritted discs, it was also possible to estimate the total pressure drop history for the oil phase. If this total pressure drop history is used to estimate $\bar{\lambda}_2^{-1}$, the oil relative permeability curve presented as a dashed line is obtained. As can be seen from the figure, neglect of the capillary pressure gradient is not serious, provided the water saturation is high. However, as the floodfront saturation is approached, the error becomes significant, the relative error being approximately six per cent at the floodfront saturation.

6.3.4.7 Buckley-Leverett Saturation Profiles

Buckley-Leverett profiles were estimated using the relative permeability curves depicted in Figure 16. The oil curve based on pressures measured in the oil was used for this purpose. In this regard it is to be noted that whether the relative permeability curve to oil is based on pressures in the oil or on pressures in the water made only a slight difference (0.001 saturation %) in the predicted value for the flood front saturation. A comparison of the Buckley-Leverett profiles with those measured using the microwave equipment is presented in Figure 16. From the figure, it can be seen that there is a significant difference, in the frontal region, between the first measured profile and the Buckley-Leverett profile. This is because the displacement is not yet stabilized at this point. As time goes on, the agreement in the frontal region improves. At the time

corresponding to the third-last profile prior to the front's reaching the outlet, the displacement is essentially stabilized. This can be inferred because the "triangular" areas on either side of the Buckley-Leverett front are essentially equal.

Saturations in the "trailing" zone are more susceptible to perturbations caused by local heterogeneities than are those located in the frontal region. This is because the magnitude of the capillary pressure gradient, which provides the driving force to damp out the perturbations, is less in the trailing zone. Because the magnitude of the capillary pressure gradient decreases with increasing saturation, it is to be expected that problems with perturbations would be greater for the higher saturations. An inspection of Figure 16 reveals this to be the case. Given that Buckley-Leverett theory is based on the assumption of a homogeneous porous medium, while the porous medium used in this study only approximates this assumption, there is reasonably good agreement between the measured profiles and those predicted using Buckley-Leverett theory.

6.4 Lagrangian Method for Estimating Relative Permeabilities

6.4.1 Introduction

Standard external-drive techniques for estimating f_w as a function of saturation are based on the assumption that the displacement is stable and stabilized. As a consequence, they may not be used when the displacement is unstabilized [117] and/or unstable. To utilize unstabilized and/or unstable displacement data to estimate f_w , it is necessary to undertake the analysis at a specific point in time rather than at specific location along the length of the core. That is to say, the analysis must be carried out from the Lagrangian rather than the Eulerian point of view.

6.4.2 Data Analysis

In this study, f_w as a function of S_w , for a specific time, was estimated as follows. First, a specific saturation profile (measured at time t^*) was chosen as the basis for the

analysis. Then the volume Q_w , defined by the integral in Equation 120, was evaluated at a specific value of S_w , say S_w^* . Next the volume $Q_w(S_w^*, t)$ was evaluated for a sufficient number of saturation profiles (measured at times both before and after t^*) to enable the least-squares methods discussed in References 69 and 98 to be used to fit the $Q_w(S_w^*)$ versus time data. Then the model equation used to fit the data was differentiated with respect to t (see Equation 121) and evaluated at t^* to obtain an estimate of $f_w(S_w^*, t^*)$. Finally, this process was repeated for a sufficient number of different values of S_w^* to define $f_w(S_w, t^*)$.

Because of local heterogeneities in porosity and permeability, the measured saturation profiles were not smooth. In order to smooth the saturation profiles, a model equation was fitted to the $Q_w(S_w, t^*)$ data. Next the model equation was differentiated to obtain an equation for $f_w(S_w, t^*)$. Then smoothed saturation profiles were constructed with the aid of Equation 124.

If estimates of the effective permeabilities to oil and water (see Equations 106 and 108) and reciprocal mobility (see Equation 112) are to be obtained, one must have at hand estimates of the pressure gradients in the oil and water as well as the capillary pressure gradient along the length of the core. To obtain such estimates, pressures were measured in both the oil and the water at various locations along the length of the core (see Figure 1). Then model equations were fitted to these data. Hence, by differentiating the model equations with respect to x , it became possible to obtain smoothed estimates of the various pressure gradients at any point of interest along the core.

The effective permeabilities for a specific saturation, say S_w^* , were estimated as follows. First, the model equation for f_w was used to obtain a smoothed estimate of $f_w(S_w^*, t^*)$. Then the distance travelled by S_w^* was estimated using the model equation representation of Equation 124. Next the model equations for the various pressure gradients were used to estimate the value of $\partial P_o / \partial x$, $\partial P_w / \partial x$ and $\partial P_c / \partial x$ which pertained for this value of x . This enabled the use of Equation 112 to estimate $\lambda^{-1}(S_w^*)$. Note that, because F_w appears in the second term on the right-hand side of Equation 112, a trial-and-error

procedure is necessary. Finally, Equations 106 and 108 were used to estimate $k_w(S_w^*)$ and $k_o(S_w^*)$, respectively. Again note that, because k_o appears on the right-hand side of Equation 106 and k_w on the right-hand side of Equation 108, a trial-and-error procedure is necessary. The method of successive substitution was used for this purpose[118].

An error analysis was undertaken for $k_{rw}(S_w)$, $k_{ro}(S_w)$ and $Q_w(S_w, t)$. This was accomplished by estimating the standard error for each of the independent variables in Equations 106, 108 and 120. Then an overall error analysis[116] of each of the equations was undertaken to estimate the standard error associated with each dependent variable. The relative standard error for k_{rw} varied between 1.13% at $S_w = S_{wi}$ and 1.6% at $S_w = 1 - S_{or}$; for k_{ro} it ranged between 0.58% at $S_w = S_{wi}$ and 0.97% at $S_w = 1 - S_{or}$. The relative standard error for Q_w ranged between 0.8% at $S_w = S_{wi}$ and 0.4% at $S_w = 1 - S_{or}$. The relative standard error for saturation and pressure was similar to that reported in Section 6.3.

6.4.3 Results

Immiscible displacement runs were carried out using water-wet, unconsolidated sand packs. Among them, Run 64 was stable but unstabilized, while Runs 65, 66 and 67 were stabilized but unstable. Because of experimental limitations with respect to the pressure rating of the coreholder, runs at a higher stability number were not possible.

In the following section, a typical analysis, using the Lagrangian approach developed in this study, is presented for Run 64, and basic experimental data for this run are summarized in Table 15. The application of this approach to analyse data from Runs 65, 66 and 67 is similar to that of Run 64. As a consequence, analyses for the other runs will not be discussed in detail.

Typical saturation profiles measured during the course of the unstabilized displacement, Run 64, are shown in Figure 17. Because it was possible to measure the saturation at the midpoint of the system, it was practicable to compare this value with that estimated using the equation developed by Welge[29]. Such a comparison is depicted in Figure 18.

Table 15: Summary of Experimental Data (Run 64)

Displaced Fluid	LAGO
Viscosity of Displaced Fluid (cp)	4.7
Length of Core (cm)	98.5
Thickness of Core (cm)	1.1
Height of Core (cm)	5.0
Pore Volume (cm ³)	175.0
Displacement Rate (cm ³ /s)	0.0667
Porosity (fraction)	0.318
S _{wi} (fraction)	0.07
S _{or} (fraction)	0.10
Absolute Permeability (darcy)	17.4
Effective Permeability to Oil @S _{wi} (darcy)	13.1
Effective Permeability to Water @S _{or} (darcy)	10.5
Mobility Ratio	3.767
Time of Arrival @x = L/2 - Measured (s)	590
Time of Arrival @x = L/2 - Predicted (s)	810
Time to (1-S _{or}) @x = L/2 - Predicted (s)	1831
Time to (1-S _{or}) @x = L/2 - Measured (s)	1840
Stability Number	1.07
Stability	stable
Capillary Number	0.24
Stabilization	unstabilized

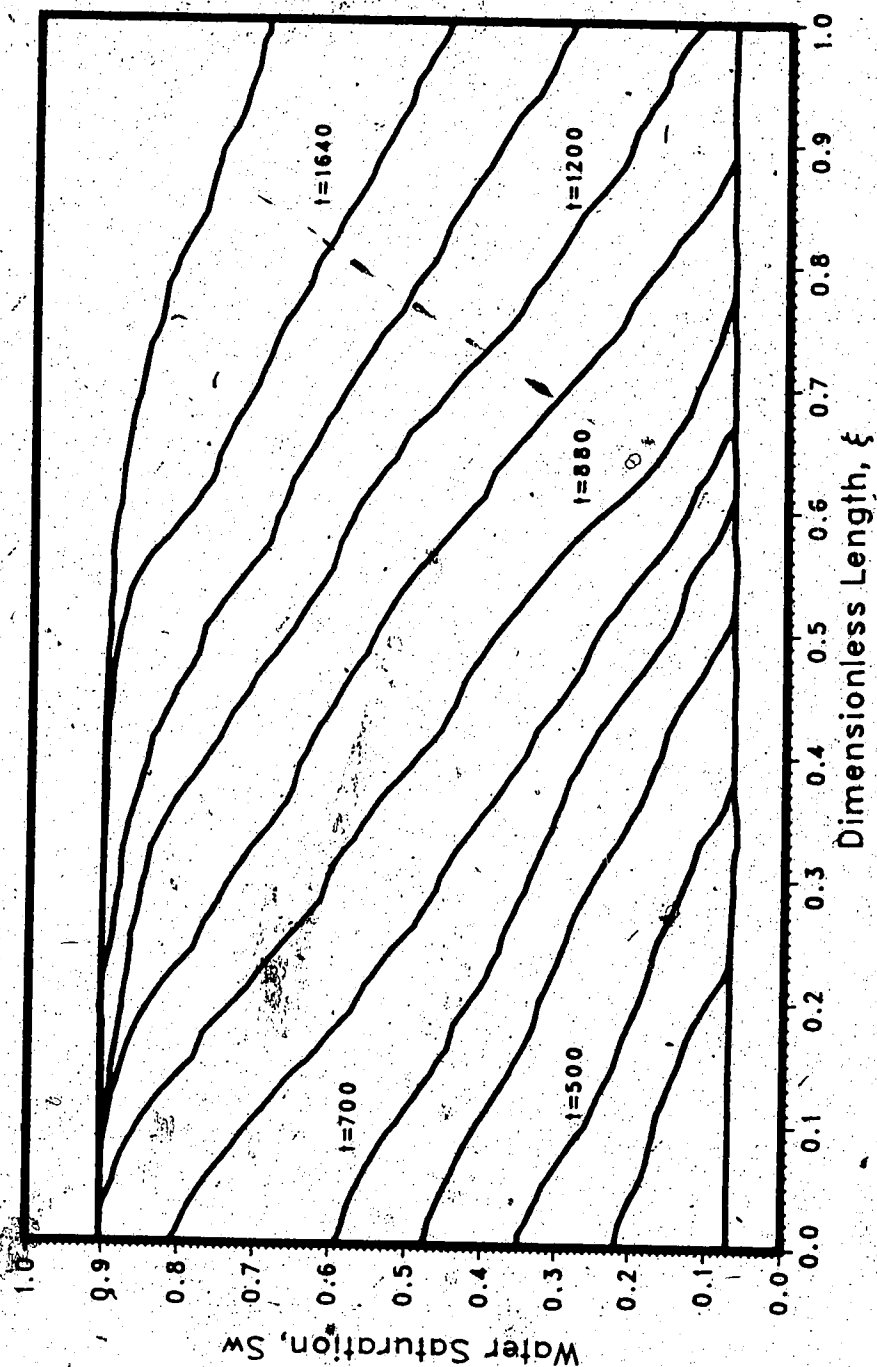


FIGURE 17: DYNAMIC SATURATION PROFILES DURING AN UNSTABILIZED WATERFLOOD (RUN 64)

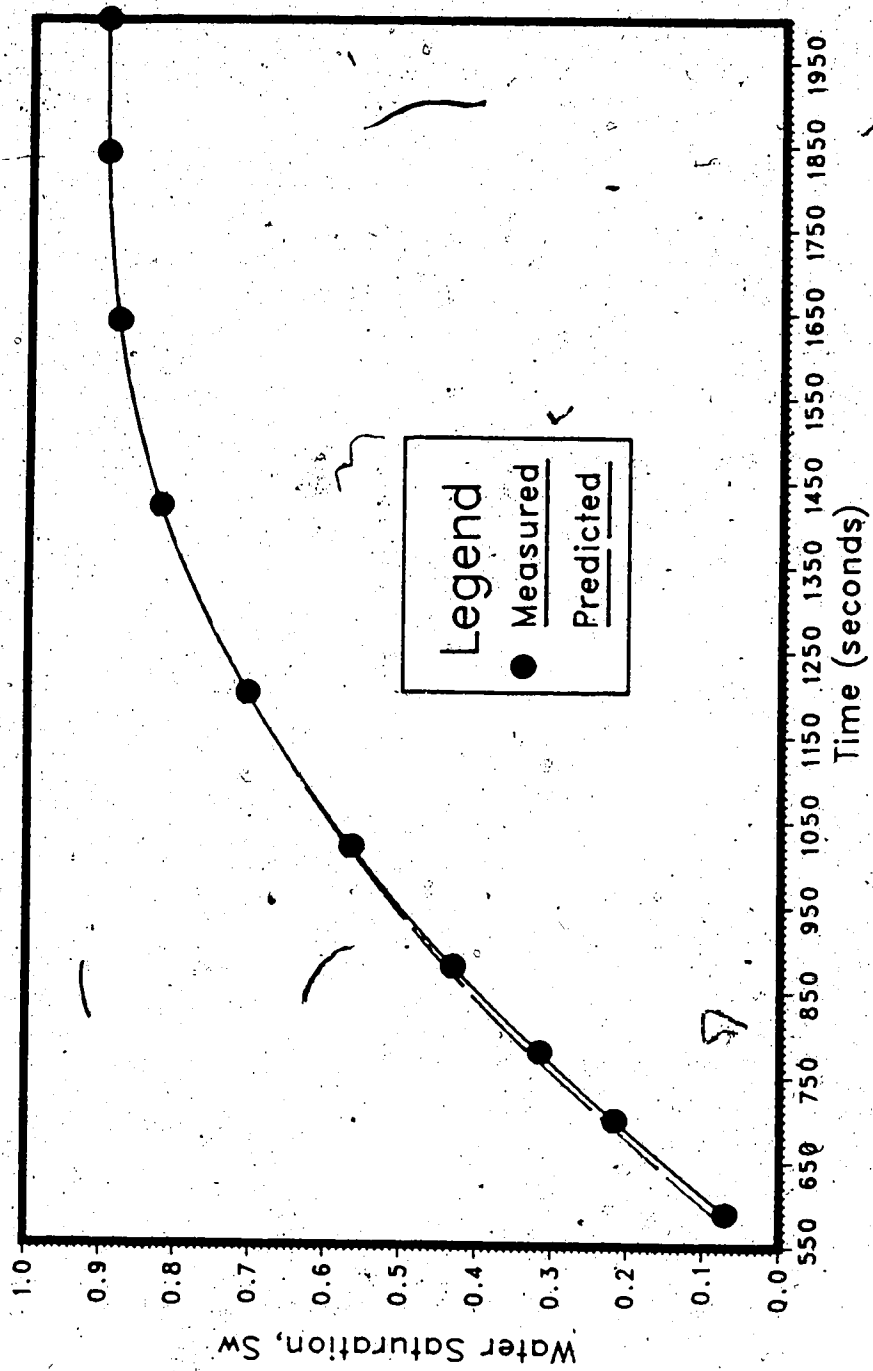


FIGURE 18: WATER SATURATION VERSUS TIME AT THE MIDPOINT
OF THE CORE (RUN 64)

Because of the use of fritted discs wetted with both oil and water, it was possible to measure the pressure in both phases. Moreover, because saturations were also available along the length of the core, it was practicable to measure the dynamic capillary pressure as a function of saturation at several locations along the core. In Figure 19, dynamic capillary pressures measured in this way at the midpoint and the outlet end of the core are compared with equilibrium capillary pressures measured in section 6.1 for the same sand-fluid system.

The pressure gradient in both phases is needed to estimate the reciprocal mobility, λ^{-1} . Errors in estimating these pressure gradients could arise if the absolute permeability varies significantly along the length of the core. To investigate this possibility, model equations were fitted to the pressure versus length data. Then these model equations were differentiated with respect to x to obtain smoothed estimates of the pressure gradient along the core. Because certain pressure transducers were differential pressure transducers (see Figure 2), it was possible also to measure directly the pressure gradient in both the oil and the water at various locations along the core. A comparison of the smoothed pressure gradient in the oil and the water (lines) with the directly measured values of the pressure gradient (symbols) is depicted in Figure 20.

Conventional external-drive theory uses the average pressure gradient ($\Delta P/L$) to estimate the reciprocal mobility, λ^{-1} , at a particular location [104,105]. Because it was possible to measure both $\partial P_o/\partial x$ and $\partial P_w/\partial x$ directly, it was practicable to use Equation 112 to estimate λ^{-1} at the midpoint of the core. A comparison of λ^{-1} estimated in this way with that estimated using conventional external-drive theory is presented in Figure 21.

In order to estimate $f_w(S_w^*, t)$, one has to know how $Q_w(S_w^*)$ varied with time. Because of minor perturbations on the saturation profiles, it was necessary to smooth such data. This was accomplished by fitting a model equation to the $Q_w(S_w^*, t)$ data. Typical $Q_w(S_w^*, t)$ plots are shown in Figure 22. The fraction of water flowing as a function of saturation at a specific point of time, say t^* , was needed also. Again, because of the perturbations in the saturation profiles, the data had to be smoothed. This was achieved by fitting a model equation to the $f_w(S_w, t^*)$ data. Plots of $f_w(S_w, t)$ at two different times, 880

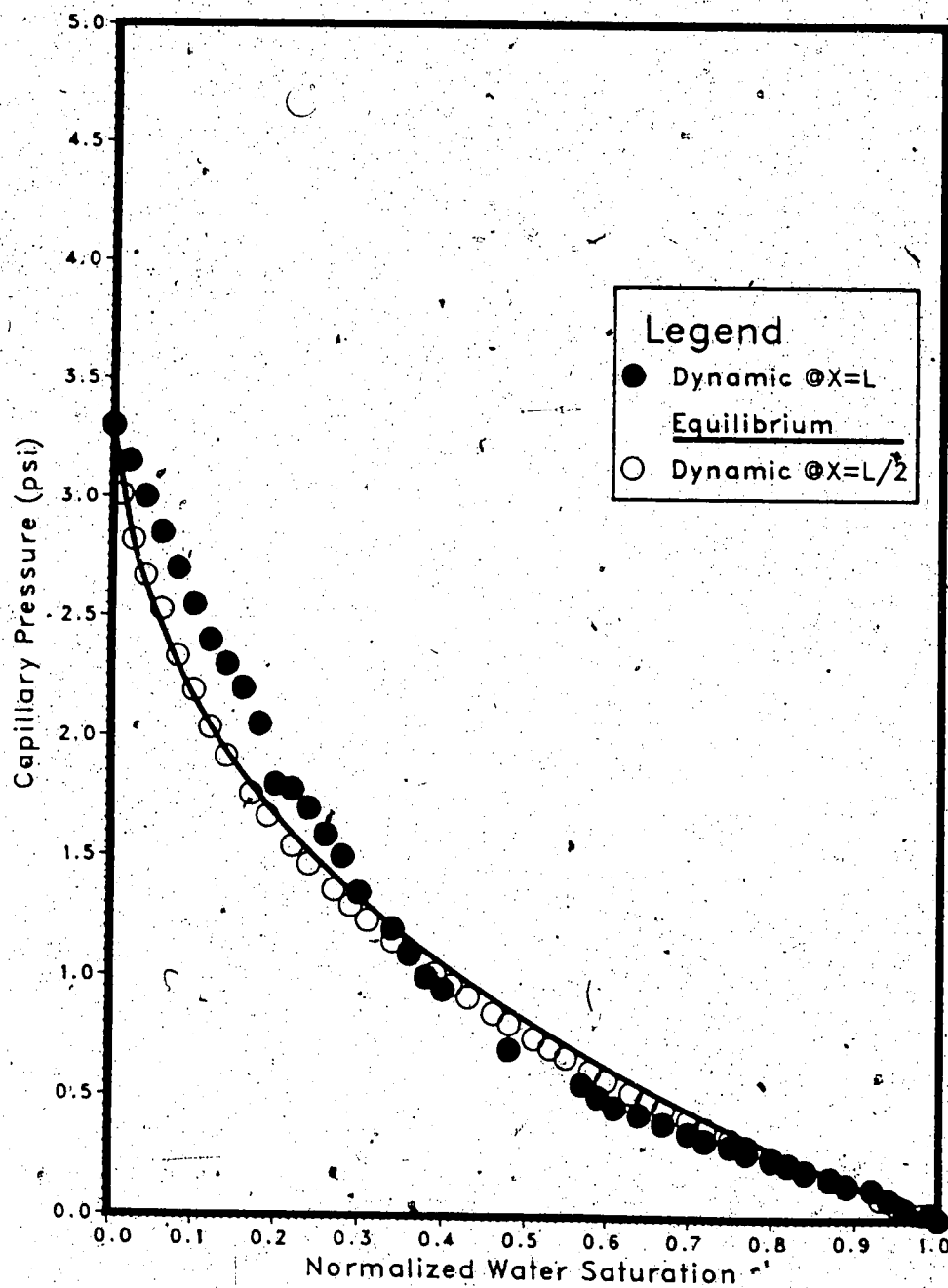


FIGURE 19: CAPILLARY PRESSURE-SATURATION CURVE FOR AN UNSTABILIZED RUN (RUN 64)

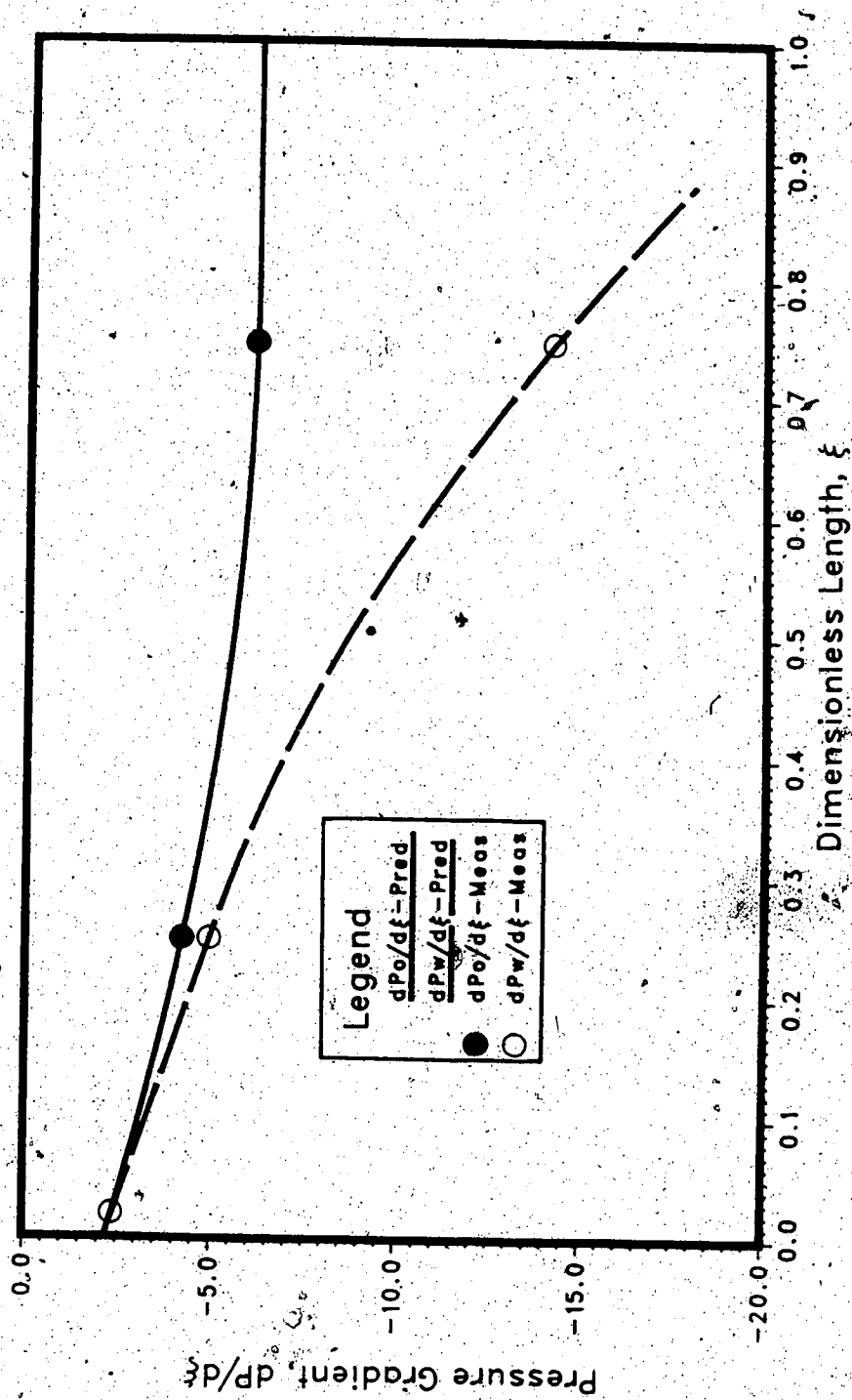


FIGURE 20: PRESSURE GRADIENT ALONG THE CORE AT
TIME = 1020 SECONDS (RUN 64)

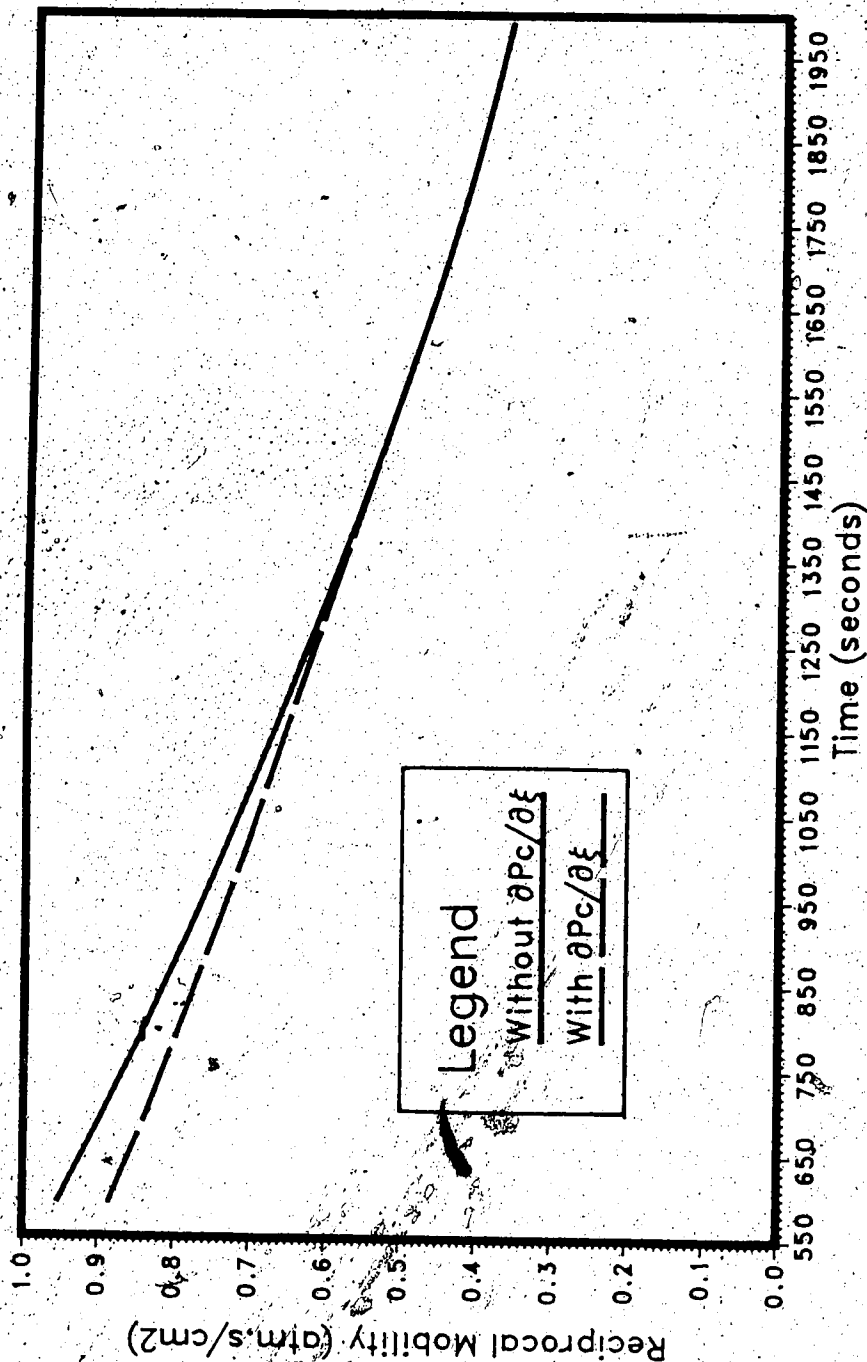


FIGURE 21: RECIPROCAL MOBILITY VERSUS DISPLACEMENT TIME
AT THE MIDPOINT OF THE CORE (RUN 64)

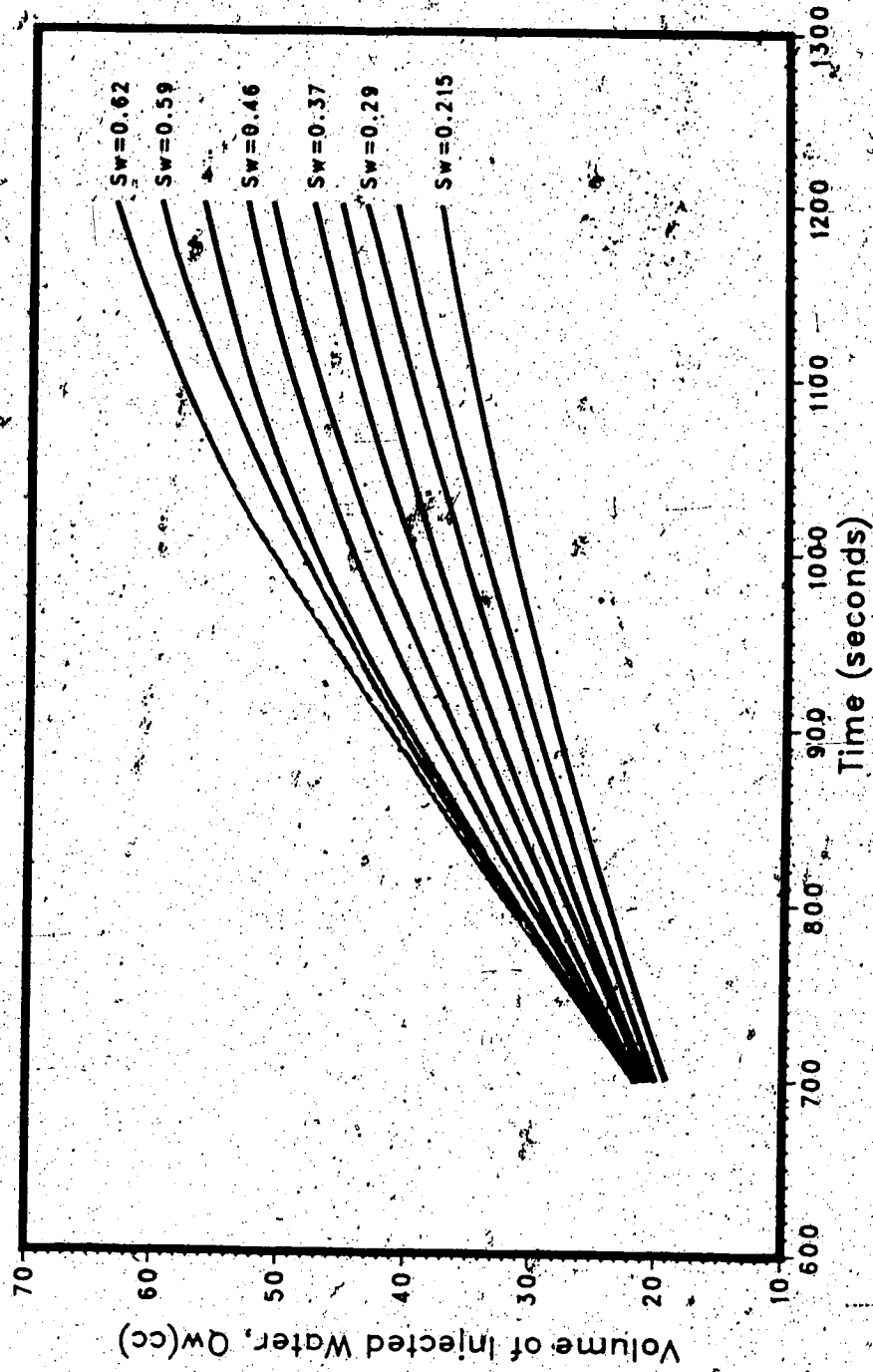


FIGURE 22: VOLUME OF INJECTED WATER, $Q_w(S_w)$, VERSUS TIME FOR VARIOUS VALUES OF S_w (RUN 64)

and 1020 seconds, are shown in Figure 23. Also shown in Figure 23 is a plot of F_w versus S_w .

Conventional external-drive methods for estimating f_w are based on an Eulerian approach to the problem. That is, the variation of f_w with S_w is determined at a specific point, usually at the outlet end, along the length of the core. Moreover, by necessity, $f_w(S_w, L)$ is evaluated at the different points in time. This is in contrast to the Lagrangian approach used in this study wherein $f_w(x(S_w), t^*)$ is evaluated at one specific point in time at a number of different locations along the core. A comparison of f_w estimated using the Lagrangian approach, $f_w(S_w, t^*)$, with f_w estimated at the midpoint of the core using the Eulerian approach, $f_w(S_w, L/2)$, is presented in Figure 24.

In unstabilized displacements, local variations in porosity and permeability give rise to small perturbations on the saturation profiles. To smooth out these perturbations, Equation 124 was used to determine the distance travelled by a number of different saturations. Then a model equation was fitted to the distance versus saturation data. A comparison of a smoothed profile obtained in this way with an actual profile ($t=1020$ seconds) is shown in Figure 25.

The relative permeability curves obtained using the Lagrangian approach described in this section are depicted in Figure 26. Also shown, for comparison, are the relative permeability curves obtained when conventional (Eulerian) external-drive theory is utilized to estimate f_w , S_w , and λ^{-1} at the midpoint of the core.

6.4.4 Discussion of Results

6.4.4.1 Saturation Profiles

Typical saturation profiles for a displacement in which water was injected at such a rate that a displacement front did not form are shown in Figure 17. Because the capillary number is greater than 0.1 ($N_c=0.24$), and because the instability number is less than π^2 ($I_{st}=1.07$), the displacement is stable but unstabilized. Note that the saturation does not rise immediately to $1-S_{or}$ at the inlet end of the core, and that the steepness of the saturation profiles increases as the saturation profiles advance toward the end of the core. That is, the degree of stabilization increases as the saturation

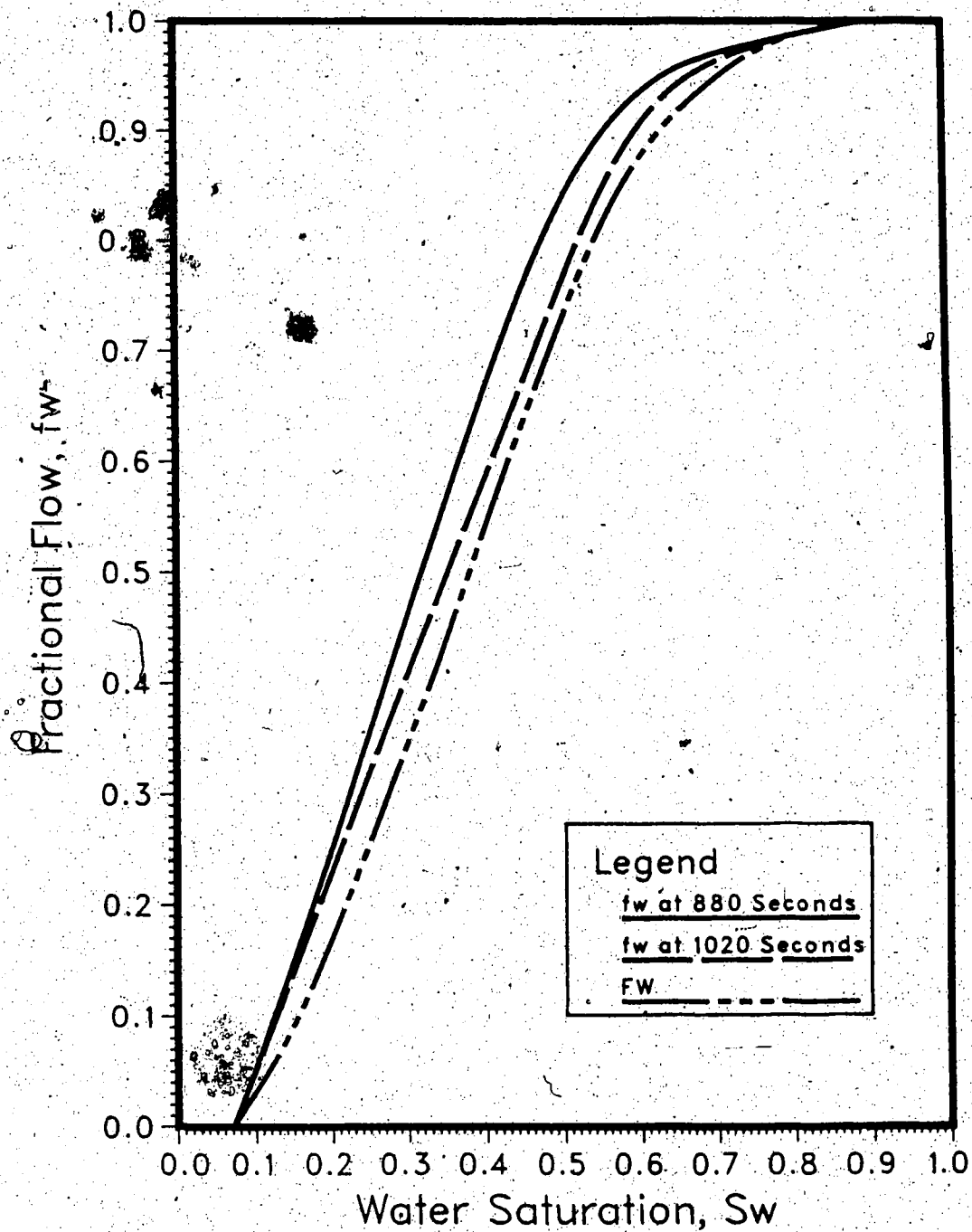


FIGURE 23: f_w VERSUS S_w DURING AN UNSTABILIZED WATERFLOOD @880 AND 1020 SECONDS (RUN 64)

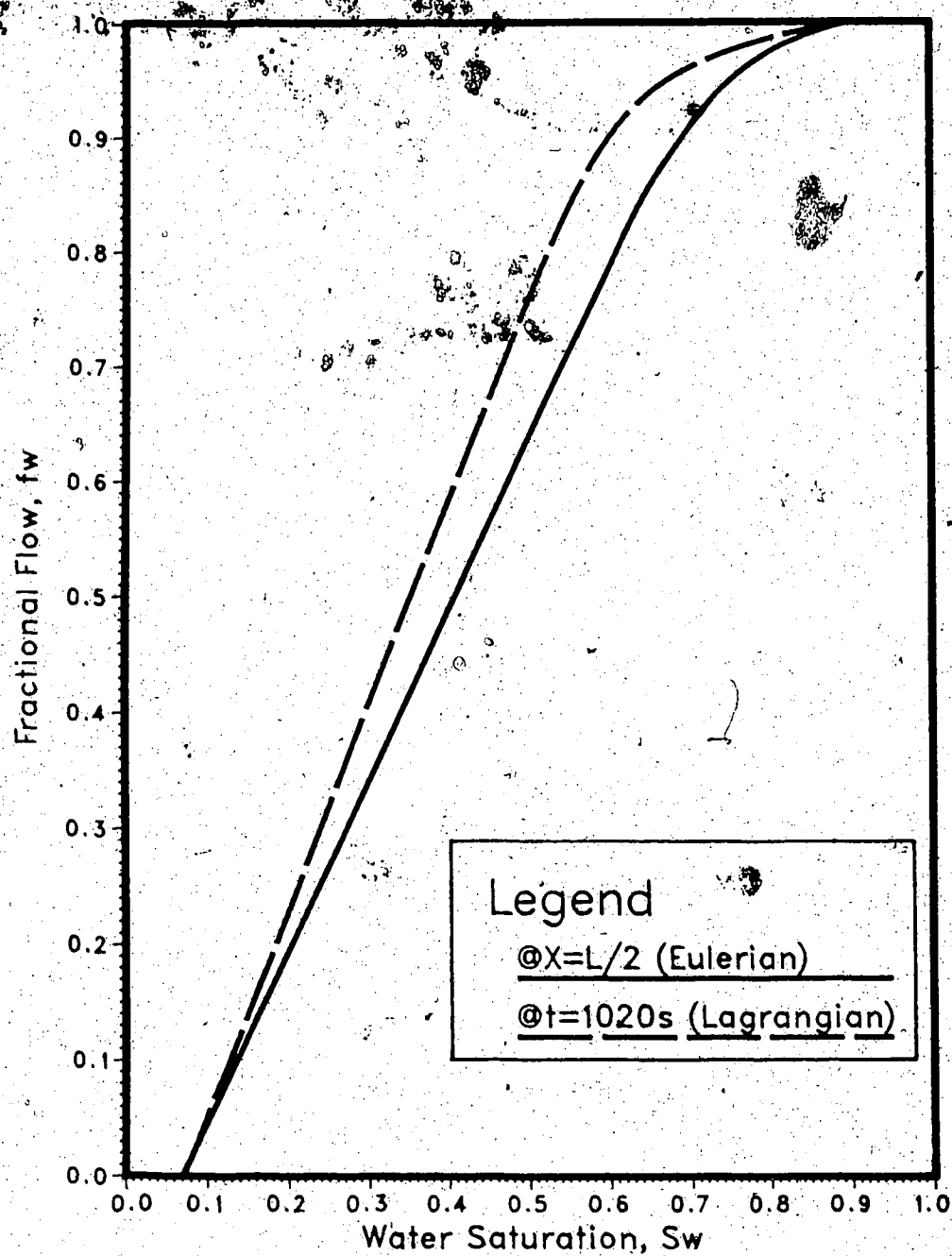


FIGURE 24: COMPARISON OF FW VERSUS SW CURVES OBTAINED USING THE LAGRANGIAN AND THE EULERIAN APPROACH (RUN 64)

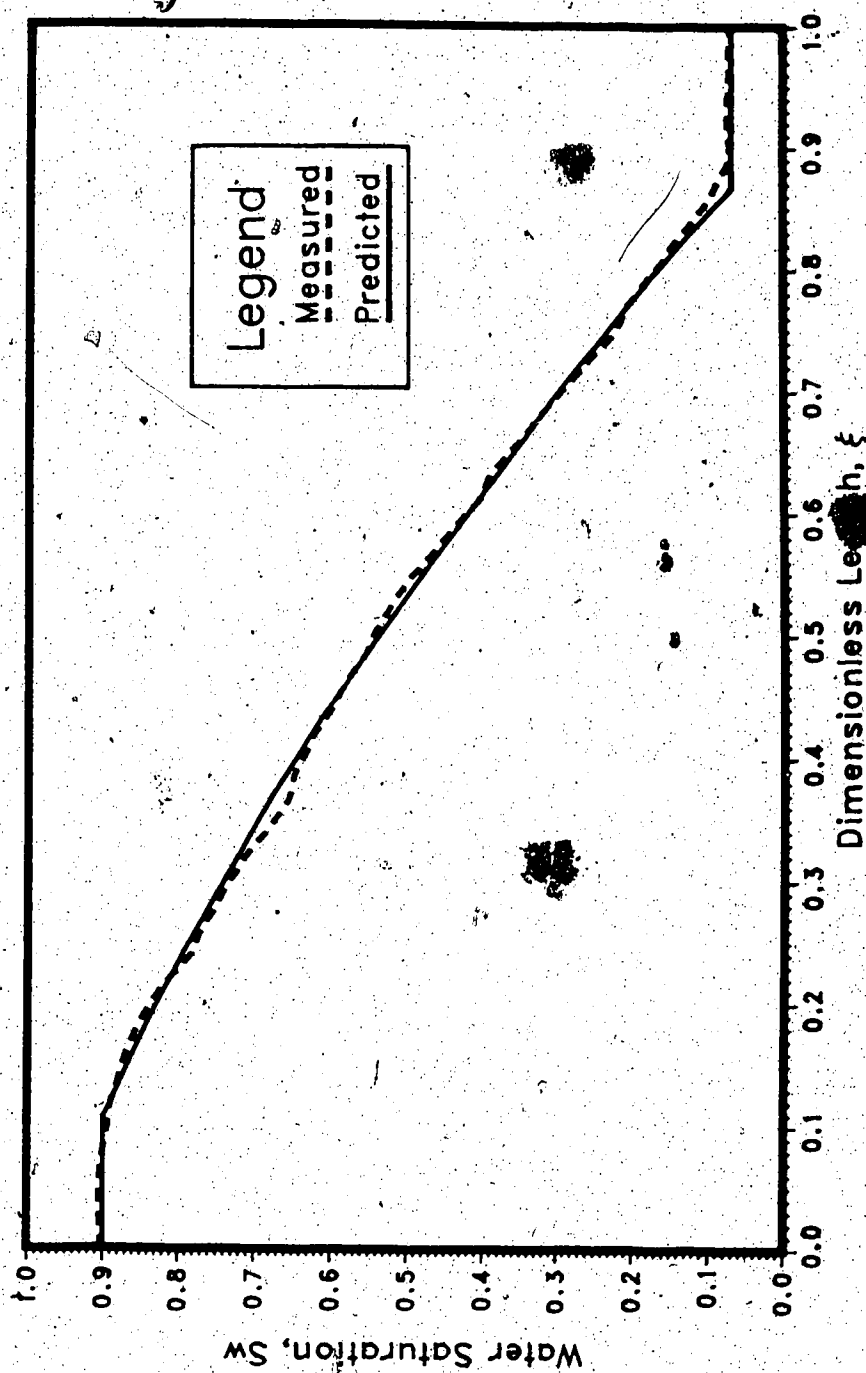


FIGURE 25: COMPARISON OF MEASURED AND PREDICTED SATURATION PROFILES AT TIME=1020 SECONDS FOR AN UNSTABILIZED DISPLACEMENT (RUN 64)

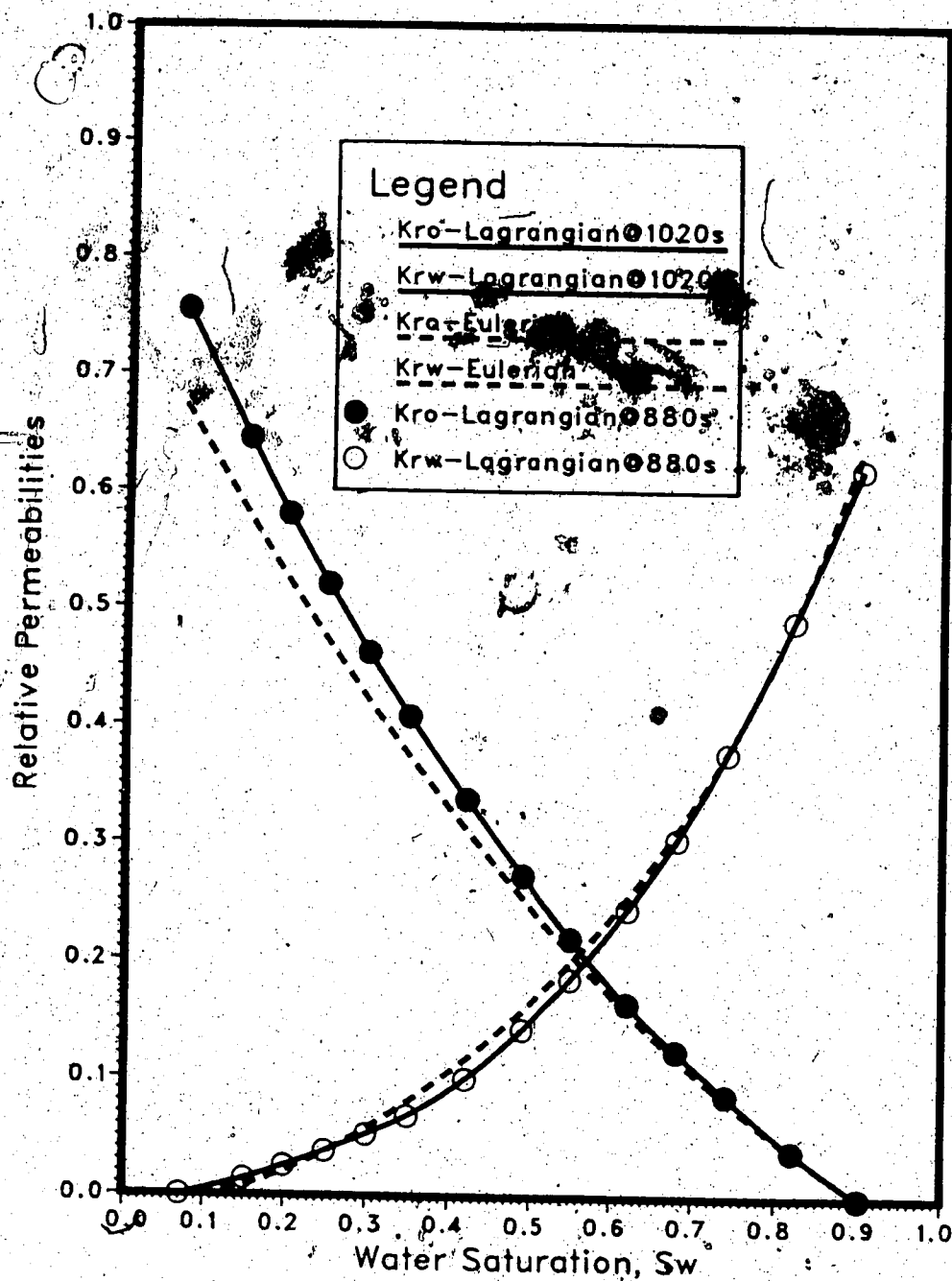


FIGURE 26: RELATIVE PERMEABILITY CURVES USING LAGRANGIAN AND EULERIAN APPROACHES (RUN 64)

profiles progress along the core. The minor perturbations of the saturation profiles, which are caused by local heterogeneities in porosity and/or permeability, are damped out as the saturation profiles move forward through the core. This is typical of a stable displacement. The magnitude of the perturbations on a typical saturation profile can be seen in Figure 25 where a smoothed saturation profile (solid line) is compared with the actual saturation profile measured at 1020 seconds.

6.4.4.2 Capillary Pressure Data

In reservoir simulation, it is usual to assume that the equilibrium capillary pressure may be used to predict the pressure difference between the water and oil in a dynamic displacement. In this study, because of the use of both water-wet and oil-wet fritted discs, it was practicable to measure directly how the dynamic capillary pressure varied at various locations along the core as the saturation changed during the course of a displacement experiment. Moreover, because the displacement was not stabilized (no region of steep saturation gradients), it was possible to measure saturations and pressures accurately over the entire range of interest. In Figure 19, dynamic capillary pressure curves measured in this way at the midpoint (open circles) and outlet end (solid circles) of the core are compared with an equilibrium capillary pressure curve (solid line) obtained for the same sand-fluid system used in section 6.1.

In Figure 19 it can be seen that, while there is good agreement between the equilibrium curve and the dynamic capillary pressures measured at the midpoint of the core, the agreement between the equilibrium curve and the dynamic capillary pressures measured near the outlet end is poor. Moreover, the agreement between the latter two curves appears to worsen as the normalized water saturation decreases. Because the outlet-end pressure transducers were located only one centimetre from the end of the core, it is thought that outlet end-effects disturbed the pressure measurements in the water and the oil. This hypothesis appears to be consistent with the improvement in agreement between the dynamic and equilibrium capillary pressure curves which takes place as the normalized water saturation increases. That is, the magnitude of the change

in saturation and, consequently, the magnitude of the perturbation in the immediate vicinity of the outlet face of the core should decrease as the saturation at the outlet face of the core increases. Such large disturbances of the dynamic capillary pressures measured near the outlet end of the core were not observed in section 6.3 in which the injection rate was high enough for the displacement to be stabilized. This points out the importance of carrying out displacements at sufficiently high rates to ensure full stabilization when conventional external-drive methods are employed to predict the reciprocal mobility at the outlet end of the core.

The size of the coreholder used in the equilibrium experiments was much smaller than the one used in the displacement experiments. As a consequence, the method used to pack the two coreholders differed considerably. This led to minor differences in porosity and residual oil saturation in the two types of cores. Thus, given that the equilibrium and dynamic capillary curves pertain to slightly different porous media, and given that different methods for measuring saturation and pressure were used in the two types of experiments, the agreement between the equilibrium curve and the dynamic curve measured at the midpoint of the core is quite good. Consequently, it would appear that the use of equilibrium capillary pressure data to predict the pressure difference between the water and oil in a dynamic displacement is acceptable.

6.4.4.3 Pressure Gradients

Accurate estimates of pressure gradients in both phases are needed to apply the theory developed in this study. Such estimates may be obtained by using a model equation to smooth the pressure versus distance data. In undertaking such smoothing, several pitfalls must be avoided, however[43]. For example, because of the saturation discontinuities which exist across the inlet and outlet faces of the core (see Figure 2), the inlet and outlet pressures measured internally need not be consistent with those measured externally. Moreover, if proper care is not taken when packing the core, the absolute permeability may vary along the core. Consequently, there is a need to verify the accuracy of the estimates of the pressure gradients.

In this study, only internally measured pressures were used. Pressures in the oil at the inlet and outlet faces of the core were obtained by linearly extrapolating internally measured pressure data. In undertaking this extrapolation, data from the differential pressure transducers located next to the inlet and the outlet end of the core (see Figure 2) were used to estimate the slope of the extrapolating equation. Once the inlet and outlet pressures in the oil phase had been obtained, a model equation was fitted to the pressure versus distance data.

Because only three measured pressures in the water phase were available, and because of the increased curvature of the water pressure versus distance curve, it was necessary to supplement the water pressure versus distance data. This was accomplished by using the model equation for $x(S_w, t^*)$ to predict the distance travelled by a particular saturation, say S_w^* . Then the model equation for $P_o(x)$, together with the model equation for $P_c(S_w^*)$, was used to estimate the value of $P_w(x)$ which pertained for $x(S_w^*)$. Finally, a model equation was fitted to the augmented water pressure versus distance data.

Once the model equations for $P_o(x)$ and $P_w(x)$ were obtained, they were differentiated with respect to x to obtain smoothed estimates of $\partial P_o / \partial x$ and $\partial P_w / \partial x$ along the core. Because certain pairs of fritted discs were used in conjunction with a differential pressure transducer (see Figure 2), it was possible also to measure directly the pressure gradient in the oil and the water at various locations along the core. A comparison of the smoothed pressure gradients in both the oil and the water (lines) with the directly measured values of the pressure gradients (symbols) is depicted in Figure 20. Note that, because of uncertainties with respect to the measurement of water pressure in the region where only oil is flowing, $\partial P_w / \partial x$ is not plotted beyond the flood front ($x_f \approx 0.8$). The good agreement between the predicted and observed pressure gradients suggests that the pressure data are consistent and that the absolute permeability does not vary significantly along the core.

6.4.4.4 Stabilization

Conventional external-drive theory is based on the assumption that the displacement is stabilized. Stabilization implies that the displacement is linearly scalable. That is to say, if the displacement is stabilized, all saturation profiles along the length of the core should be similar, differing by only a linear magnification or reduction [35].

If a displacement is stabilized, the average saturation up to a given point can be used to estimate the saturation at that point. To investigate the magnitude of the error introduced when the stabilization assumption is not well met, conventional external-drive theory was used to predict how the saturation at the midpoint of the core varied with time. The midpoint, rather than the outlet end of the core, was chosen for this purpose to avoid the large disturbances of the pressures measured near the outlet end of the core. Because of the availability of the microwave equipment, it was possible also to measure directly the saturation at the midpoint of the core. A model equation (see section 6.2) was used to smooth both the predicted and the measured data, and the resulting curves are presented in Figure 18.

As can be seen from Figure 18, the largest difference (1.5%) between the measured and predicted values of S_w occurred at the time (590 seconds) the foot of the saturation profile arrived at the midpoint of the core. This is to be expected because, as time goes on, the degree of stabilization increases and the error introduced because of violating the stabilization assumption decreases. At $t=940$ seconds, the saturation at the midpoint of the core had reached the floodfront saturation ($S_{wf}=0.497\%$) and the difference between the two curves had decreased to 0.8 saturation per cent (see Appendix D for the program code to estimate S_{wf}). That is, the difference between the observed and predicted values of S_w was about the same as the maximum difference (less than one saturation per cent) reported in section 6.3 in which the displacement was fully stabilized. Thus, it would appear that, for saturations greater than the floodfront saturation, the error introduced (because of lack of stabilization) into the external-drive estimate of the saturation at the midpoint of the core is not serious, at

least in this experiment. Moreover, as can be seen from Figure 18, the magnitude of this error decreases as time increases beyond 940 seconds.

The conventional external-drive theory used to estimate the reciprocal mobility at a particular point along the core is also based on the assumption that the displacement is stabilized. In this study, because it was possible to measure pressures in both phases along the core, it was possible also to use Equation 112 to estimate directly the reciprocal mobility at a particular location along the core. A comparison between the direct estimate of the reciprocal mobility at the midpoint of the core (dashed line) and that estimated using conventional external-drive theory (solid line) is presented in Figure 21.

Two factors contribute to the difference between the two curves in Figure 21: lack of stabilization and neglect of the capillary pressure gradient term in Equation 112. The largest difference (relative error = 7.2%) between the two curves occurs at the time of arrival, t_a , of the floodfront at the midpoint of the core. This is to be expected because the capillary pressure gradient, which is proportional to dP_c/dS_w , is largest when the "toe" of the saturation profile (where $S_w = S_{wi}$) reaches the mid-point of the core. As time goes on, the degree of stabilization increases as does the saturation at the midpoint of the core. This has two effects. First, the error introduced into the conventional external-drive method because the displacement is not stabilized decreases. Second, the magnitude of the correction term involving $\partial P_c / \partial x$ (see Equation 112) decreases because dP_c/dS_w decreases as S_w increases (see Figure 21). In this regard, note that the saturation gradient at the midpoint of the core remains approximately constant, or increases slightly, as time goes on (see Figure 18). Note also that the relative error is still fairly large (4.1%) at the time (940 secs) the saturation at the midpoint of the core reaches the flood front saturation ($S_{wf} = 0.497$) obtained from the tangent construction suggested by Welge[29]. For times larger than about 1250 seconds, there is good agreement between the two methods (relative error less than 1%) for estimating λ^{-1} . As the degree of stabilization of the displacement increases, the time at which acceptable

agreement between the two methods is obtained should decrease. Consequently, it is thought that in fully stabilized displacements acceptable agreement between the two methods should be obtained for times greater than the time to breakthrough. This is consistent with currently accepted practice.

When a displacement is unstabilized, the fraction of water flowing at a particular cross-section of the core is a function of both time and saturation. This can be seen by referring to Figure 23 where f_w is plotted versus S_w for two different times, 880 and 1020 seconds. The non-capillary fractional flow function, F_w , is also plotted versus saturation in the same figure. Note that, as time increases, the $f_w(S_w, t)$ curve shifts to the right. For sufficiently large injection times, $f_w(S_w, t)$ may be approximated by $F_w(S_w)$ for saturations above the floodfront saturation, and by a tangent to the $F_w(S_w)$ curve for saturations below the floodfront saturation[36]. For times large enough for this approximation to be valid, the fraction of water flowing at a particular cross-section of the core is a function of saturation only, and the displacement is said to be stabilized. Moreover, for times greater than the time to stabilization, the displacement will be linearly scalable.

When conventional external-drive techniques are used to estimate f_o (or f_w), the cumulative oil production versus time curve is differentiated with respect to time. The value of f_o so obtained pertains to the saturation which exists at the outlet end of the system at the time for which the derivative is evaluated. If the displacement is unstabilized, different $f_w(S_w, t)$ curves pertain for different points in time (see Figure 23). Consequently, if conventional external-drive methods are employed to estimate $f_w(S_w, L)$ when a displacement is unstabilized, serious error can be introduced into the analysis. The magnitude of such errors can be seen by referring to Figure 24 where a Lagrangian fractional flow curve measured at 1020 seconds is compared to the Eulerian fractional flow curve determined at the midpoint of the core. As can be seen from Figure 24, the difference between $f_w(S_w, 1020)$ and $f_w(S_w, L/2)$ is quite large. That is to say, if Eulerian methods are employed, it is important that the injection rate is such

that stabilization is achieved prior to breakthrough, if the introduction of large errors into the estimate of $f_w(S_w, L)$ is to be avoided.

If conventional external-drive methods are to be used to estimate k_{rw} and k_{ro} , it is important that one be able to estimate accurately the degree of stabilization achieved in a given displacement. In this study, the capillary number, N_c , was used for this purpose. Also useful in this regard is the time of arrival of the foot of the saturation profile at the point of interest along the length of the core. For example, the predicted time of arrival of the foot of the saturation profile at the midpoint of the core was 810 seconds (see Table 15) while the actual (measured) time of arrival was 590 seconds. That is, because the displacement was unstabilized, a displacement front did not form and, consequently, the actual time of arrival was much earlier than the theory developed in Reference 69 would predict. When this theory was used to predict the time to breakthrough in a stabilized displacement [104, 105], there was good agreement between the predicted and actual time to breakthrough.

The scaling coefficient, $L\mu_w v$, suggested by Rapoport and Leas can be used also to predict whether a displacement is stabilized [32]. In this study, this coefficient, evaluated at the midpoint of the core, was found to equal $35.3 \text{ cm}^2\text{cp/min}$. Rapoport and Leas reported that, for most of the materials tested, the critical value of their scaling coefficient fell between 0.5 and $3.5 \text{ cm}^2\text{cp/min}$. That is to say, because an $L\mu_w v$ value of $35.3 \text{ cm}^2\text{cp/min}$ is an order of magnitude greater than their critical value, the displacement should be stabilized. However, such was not the case. In this regard, it should be noted that the materials tested by Rapoport and Leas were consolidated (sandstones, limestones and alundum) having permeabilities ranging from 0.2 to 1.863 darcies while the porous medium used in this study was unconsolidated with a permeability of 17.4 darcies. Moreover, the materials used by Rapoport and Leas had wetting characteristics which varied from neutral to oil-wet while the porous medium used in this study was water-wet. Thus, as noted by Rapoport and Leas, it would appear that the critical value of $L\mu_w v$ depends strongly upon the porous medium used

and the fluids contained therein.

6.4.4.5 Relative Permeability Curves

A comparison of the relative permeability curves obtained using the fractional flow curve measured at 1020 seconds (solid lines) and the one measured at 880 seconds (circles) is presented in Figure 26. As might be expected, there is quite good agreement between the two sets of curves.

Also shown (dashed lines) for comparison are the relative permeability curves obtained using conventional external-drive theory. Note that, except for intermediate saturations, there is quite good agreement between the water relative permeability curves obtained using the two methods. However, the difference between the two oil curves is significant, particularly at lower values of saturation. A partial explanation for this difference can be seen by referring to Equations 106 and 108. In Equation 106, the capillary pressure gradient term is divided by μ_o while in Equation 108 it is divided by μ_w . That is to say, because μ_o is much larger than μ_w , neglect of the capillary pressure gradient term is expected to have a much larger influence on the estimated value of k_o than is the case for k_w . However, other factors have a role to play as well. For example, the degree of stabilization increases as the saturation increases, which would also be expected to affect the difference between the Lagrangian and Eulerian estimates of λ^{-1} , S_w , and f_w . Because of the large differences between the Lagrangian and Eulerian estimates, particularly in the cases of f_w (see Figure 24) and λ^{-1} (see Figure 23), it is surprising that the agreement between the two types of curves is as good as it is. In the case of the water curves, it would appear that the errors compensate, because of the relatively good agreement between the two estimates of $k_{rw}(S_w)$. However, the same degree of compensation does not appear to take place with respect to $k_{ro}(S_w)$, because the magnitude of the discrepancy between the two curves increases as S_w decreases. At the floodfront saturation ($S_{wf}=0.497$), the relative error in the Eulerian estimate of $k_{ro}(S_w)$ is 7.92 per cent while the relative error in the Eulerian estimate of $k_{rw}(S_w)$ is -9.33 per cent. Thus it would appear that a displacement must be fully

stabilized, if accurate estimates of k_{rw} and k_{ro} are to be obtained when using conventional external-drive techniques to estimate these functions.

When conventional external-drive theory is to be utilized, it is necessary to inject water until such time as the average saturation in the core approaches $1 - S_{or}$. If the mobility ratio is adverse, this may take a substantial period of time. However, if the method proposed in this section is used, it is necessary to inject water only until breakthrough is achieved. As a consequence, the time necessary to obtain the data needed to determine the relative permeability curves using the new method is substantially less than that required for the conventional external-drive method.

6.5 Unstable Displacements

6.5.1 Introduction

Earlier studies[51,52] have suggested that flow regime has an impact on relative permeability. To investigate this possibility further, and to investigate the impact of instability on capillary pressure, a series of unstable runs was conducted.

6.5.2 Results

To investigate the impact of instability on the displacement process, three runs (Runs 65, 66, and 67) were carried out. A summary of the experimental data for these runs is given in Table 16. It is to be noted that runs at an instability number higher than 36 were not possible, because of equipment limitations.

The saturation profiles versus dimensionless distance plots for Runs 65, 66 and 67 are depicted in Figures 27, 28 and 29, respectively. It should be noted that the character and shape of the saturation profiles in Runs 65, 66 and 67 (unstable displacements) are quite similar to those shown in Figure 17 for Run 64 (unstabilized displacement).

The fact that the saturation profiles for unstabilized and unstable displacements are similar suggests that it might be possible to correlate the shape of the saturation profiles with

Table 16: Summary of Experimental Data (Runs 65 - 67)

Parameters	Run 65	Run 66	Run 67
Displaced Fluid	MCT-5	MCT-10	MCT-10
Viscosity of Displaced Fluid (cp)	60.0	60.0	60.0
Length of Core (cm)	100.5	100.5	100.5
Thickness of Core (cm)	1.1	1.1	1.1
Height of Core (cm)	5.65	5.65	5.65
Pore Volume (cm ³)	224.4	228.17	228.17
Displacement Rate (cm ³ /s)	0.1167	0.1333	0.0667
Porosity (fraction)	0.359	0.365	0.365
S _{wi} (fraction)	0.07	0.07	0.07
S _{or} (fraction)	0.16	0.15	0.13
Absolute Permeability (darcy)	20.5	21.5	20.8
Effective Permeability to Oil @S _{wi} (darcy)	18.0	17.3	17.0
Effective Permeability to Water @S _{or} (darcy)	5.1	5.4	5.2
Mobility Ratio	9.69	18.64	18.36
Time of Arrival @x=L/2 - Measured (s)	420	360	728
Time of Arrival @x=L/2 - Predicted (s)	453	380	779
Recovery @Breakthrough - Measured (cc)	99.5	97.2	98.1
Recovery @Breakthrough - Predicted (cc)	105.6	101.1	103.8
Stability Number	14.4	35.8	17.7
Stability	unstable	unstable	unstable
Capillary Number	0.0436	0.0406	0.078
Stabilization	stabilized	stabilized	stabilized

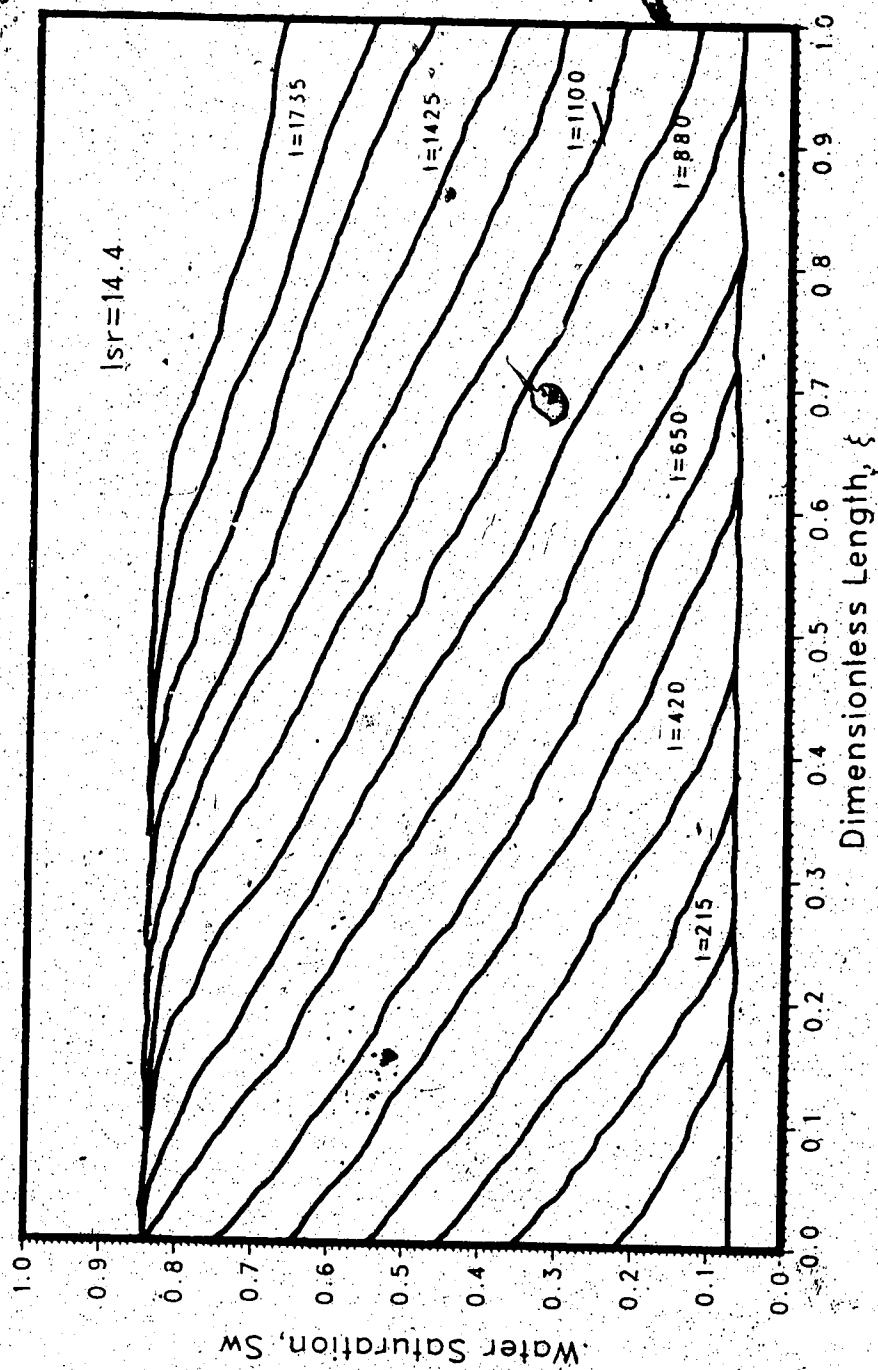


FIGURE 27: DYNAMIC SATURATION PROFILES DURING AN UNSTABLE DISPLACEMENT (RUN 65)

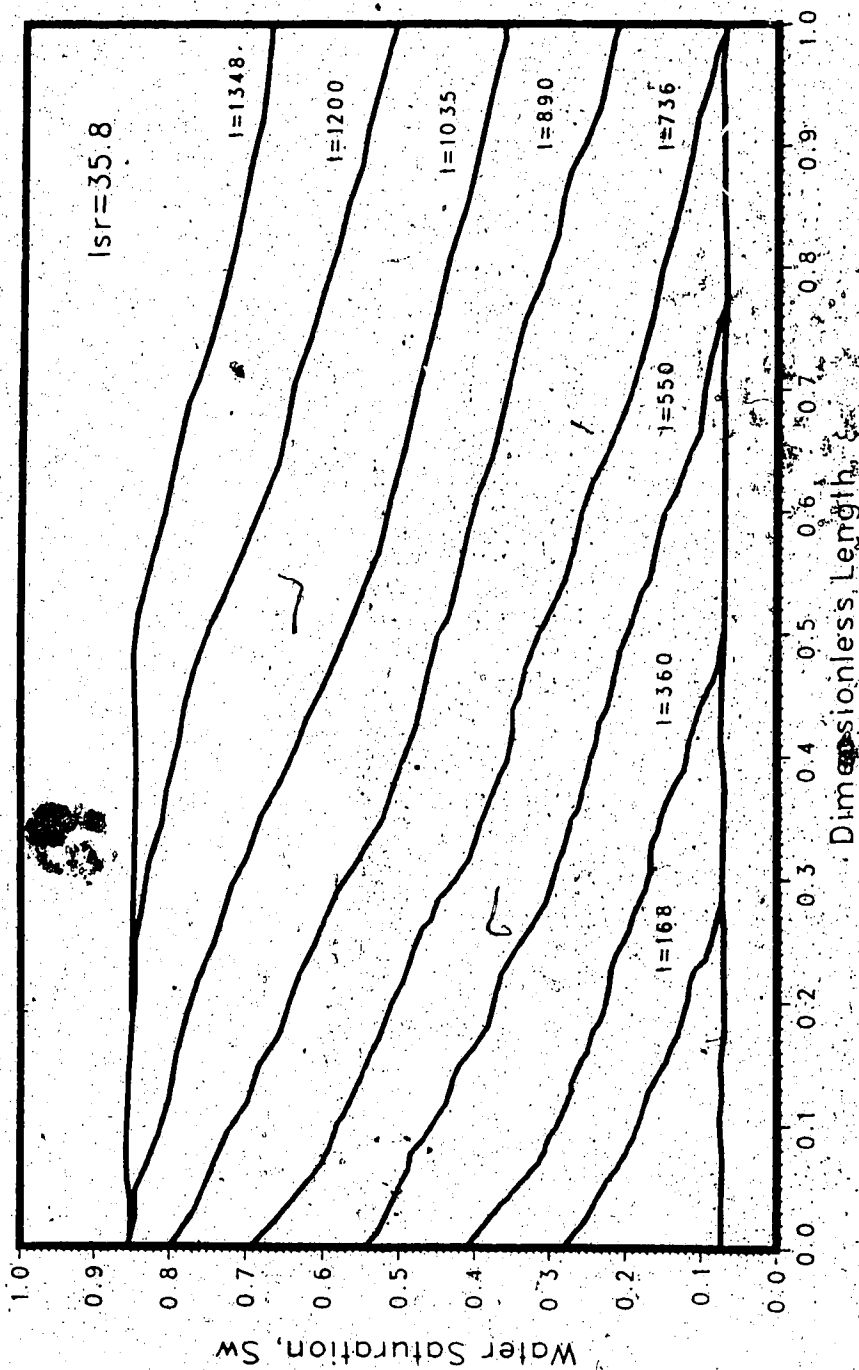


FIGURE 28. DYNAMIC SATURATION PROFILES DURING AN UNSTABLE DISPLACEMENT (RUN 66)

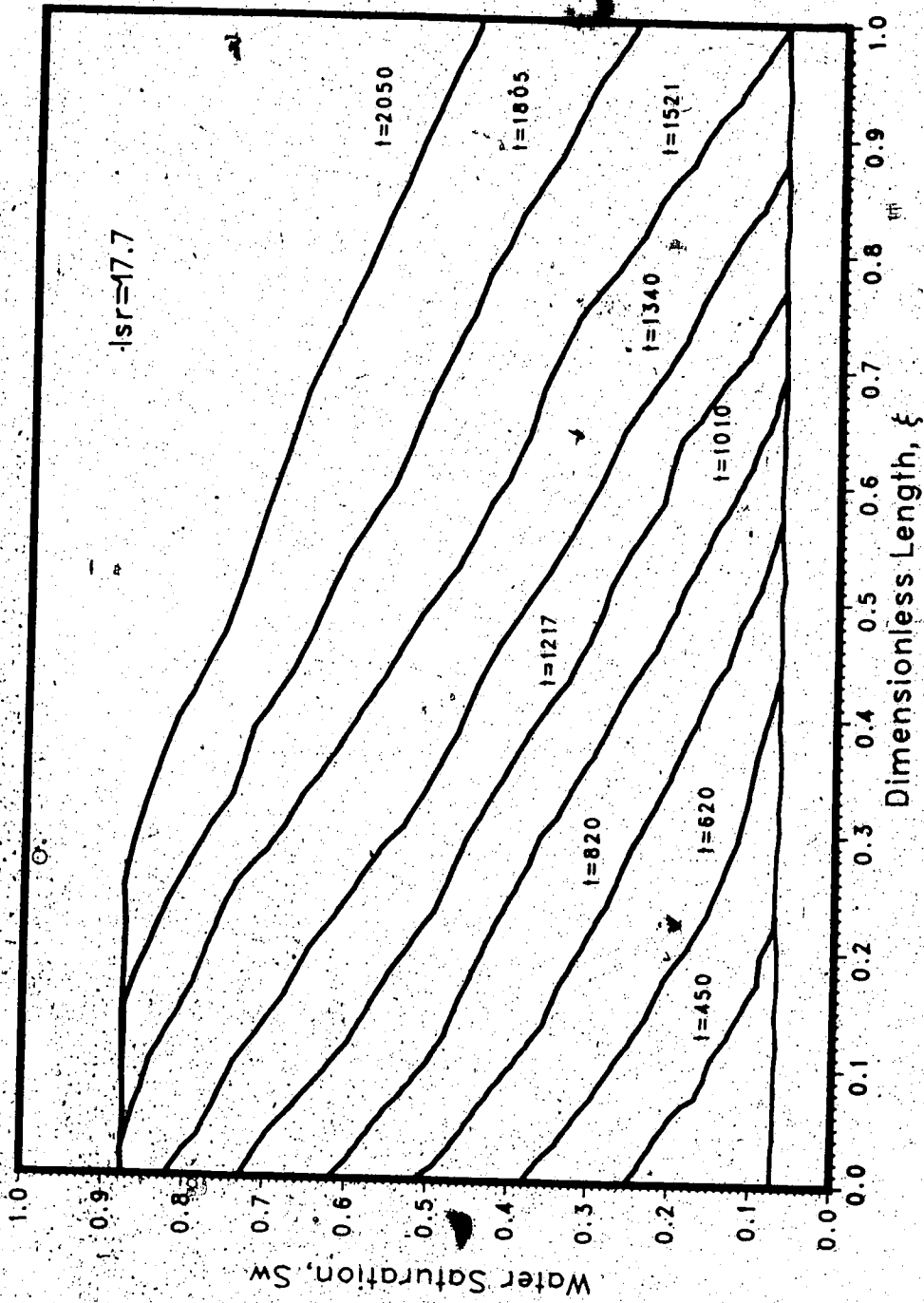


FIGURE 29: DYNAMIC SATURATION PROFILES DURING AN UNSTABLE DISPLACEMENT (RUN 67)

various dimensionless groups. In this regard, immiscible displacement theory[36] suggests that the saturation gradient, for a particular saturation, should be proportional to the ratio, M/N_c . A plot of the saturation gradient evaluated at the initial water saturation, S_{wi} , versus M/N_c is shown in Figure 30. Note that the saturation gradient for each run was evaluated at the same dimensionless time, $\tau=0.27$. Because the slope of the saturation profiles appeared to increase with increasing instability, this possibility was investigated also. A plot of the saturation gradient, evaluated at S_{wi} , versus the instability number, I_{sr} , is depicted in Figure 31.

It is also apparent from Figures 27, 28 and 29 that residual oil saturation, S_{or} , decreases with the increasing velocity. Several authors, such as Moore and Slobod[119], Melrose and Brandner[120], Abrams[37], Taber[121] and Taber *et al.*[122], have demonstrated that the residual oil saturation is a function of capillary and viscous forces. Usually the residual oil saturation is correlated with a microscopic capillary number[123], such as the one suggested by Lefebvre du Prey[59]. However, because macroscopic capillary numbers take into account the rock-fluid properties as well as the flow properties, it was decided to investigate whether a correlation between S_{or} and $1/N_c$ existed. Such a correlation is presented in Figure 32.

If a displacement is unstable, it might be expected that the fraction of water flowing at a given saturation is higher than is the case for a stable, stabilized displacement. To investigate this possibility, the fractional flow versus saturation plot for Run 63 (stable, $I_{sr}=4.8$) is compared to that for Run 65 (unstable, $I_{sr}=14.4$) in Figure 33. In addition, the fraction of water flowing at a given saturation might depend on the degree of stability. Consequently, the fractional flow curve for Run 66 ($I_{sr}=35.8$) is compared to that for Run 67 ($I_{sr}=17.7$) in Figure 34.

It is possible that the capillary pressure curves might depend on the flow regime. To see if such is the case the dynamic capillary pressure curves for an unstabilized displacement, a stable, stabilized displacement, and an unstable displacement are shown in Figure 35 for the water-MCT-5 system. Also shown, for the sake of comparison, is the equilibrium curve for the same sand-fluid system. Moreover, the dynamic curves for Run 66 ($I_{sr}=35.8$) and for

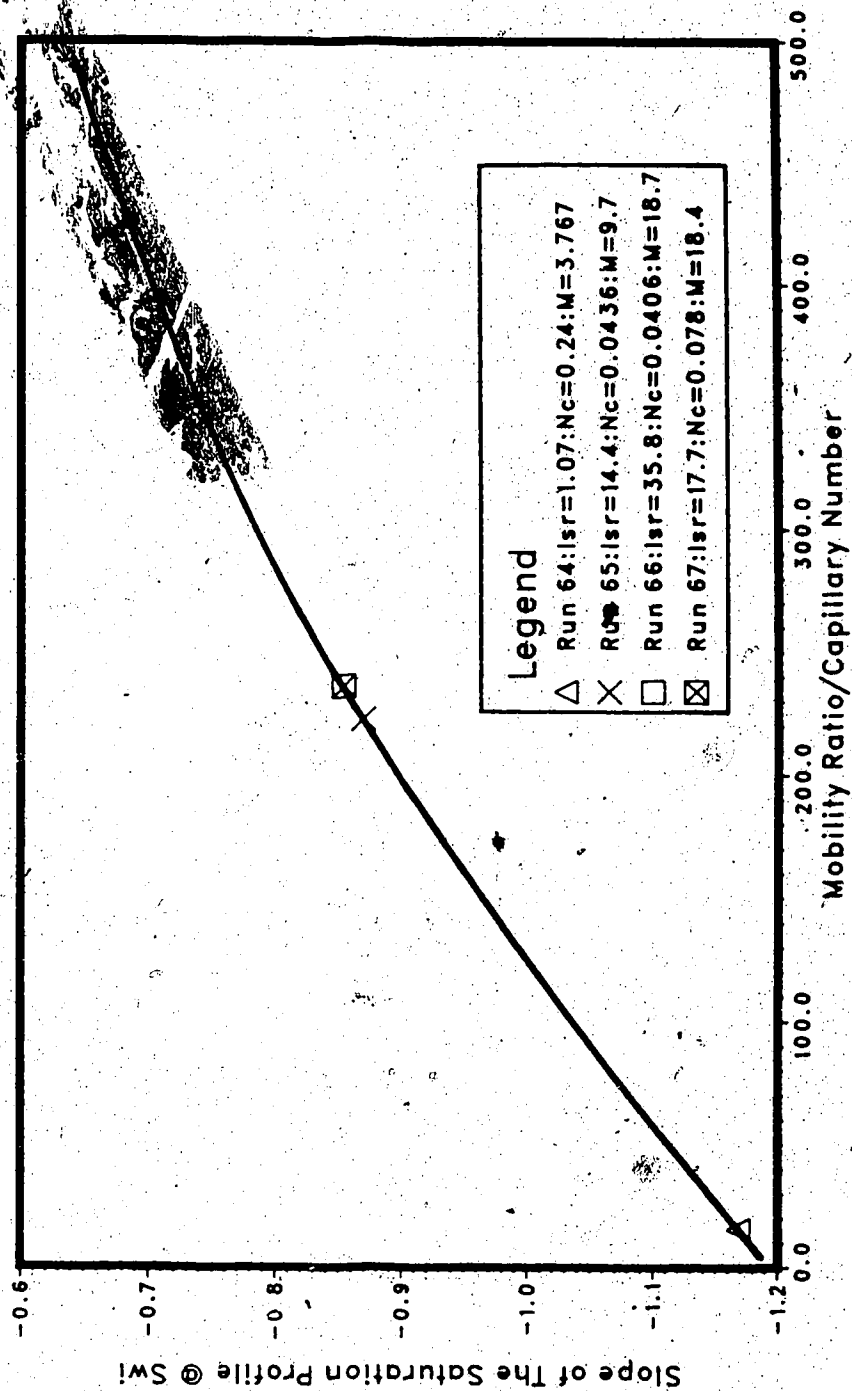


FIGURE 30: SLOPE OF THE SATURATION PROFILE @ Swi AS A FUNCTION
RATIO OF CAPILLARY NUMBER TO MOBILITY RATIO

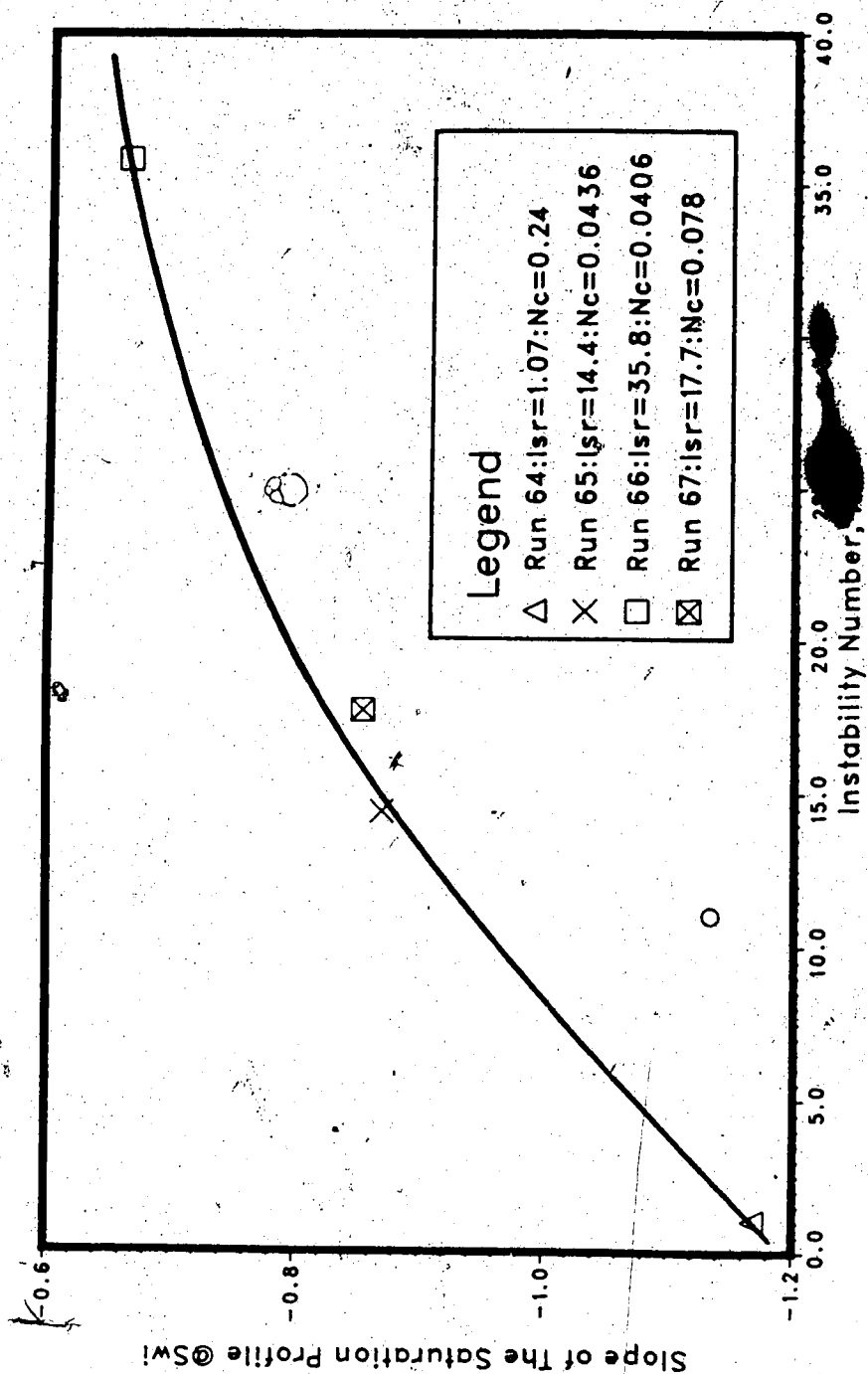


FIGURE 31: SLOPE OF THE SATURATION PROFILE @Swi AS
A FUNCTION OF THE INSTABILITY NUMBER

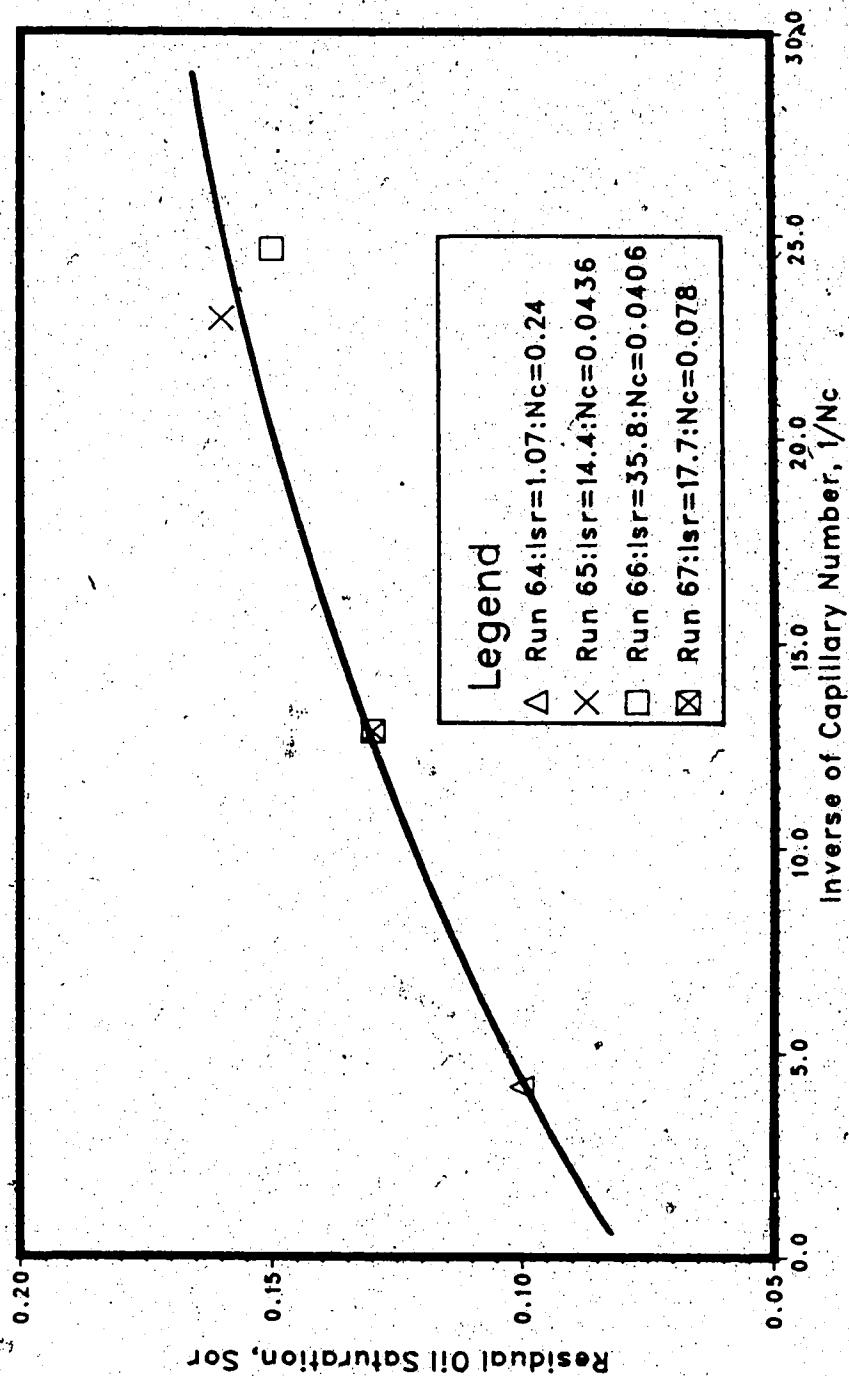


FIGURE 32: RESIDUAL OIL SATURATION AS A FUNCTION OF THE RECIPROCAL CAPILLARY NUMBER

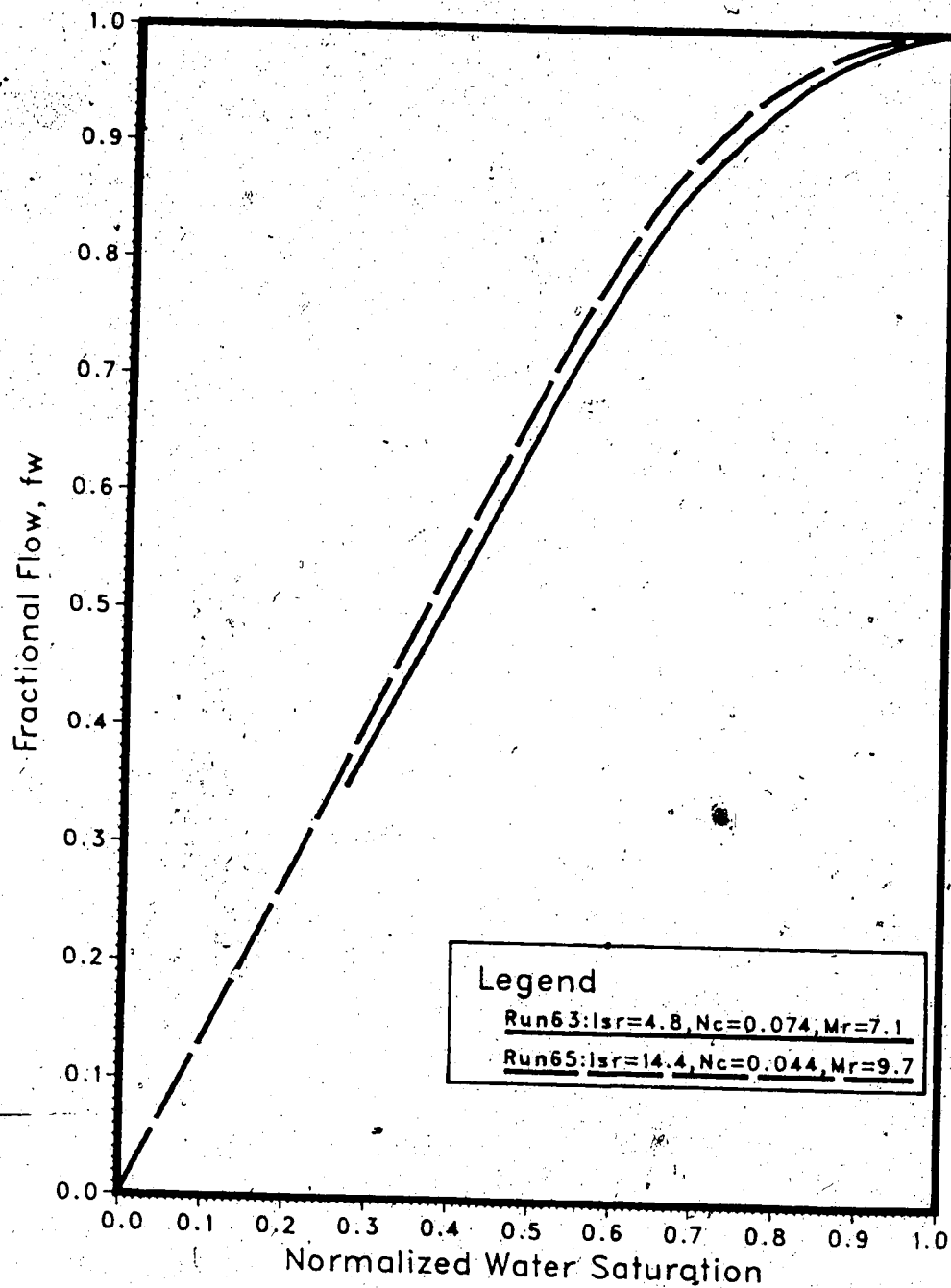


FIGURE 33: FRACTIONAL FLOW CURVES FOR RUNS 63 AND 65 USING WATER-MCT5 SYSTEM

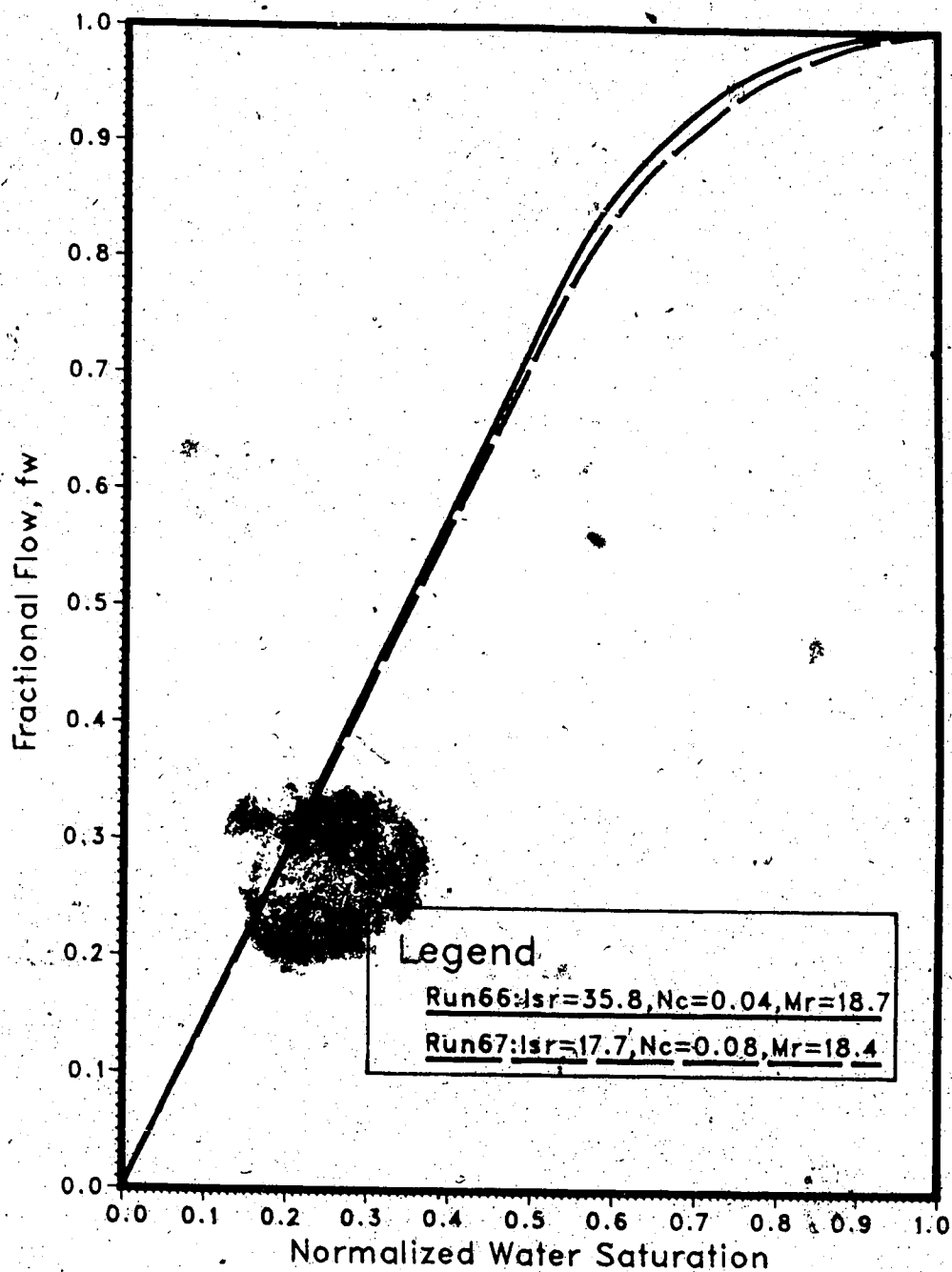


FIGURE 34: FRACTIONAL FLOW CURVES FOR RUNS 66 AND 67 USING WATER-MCT10 SYSTEM

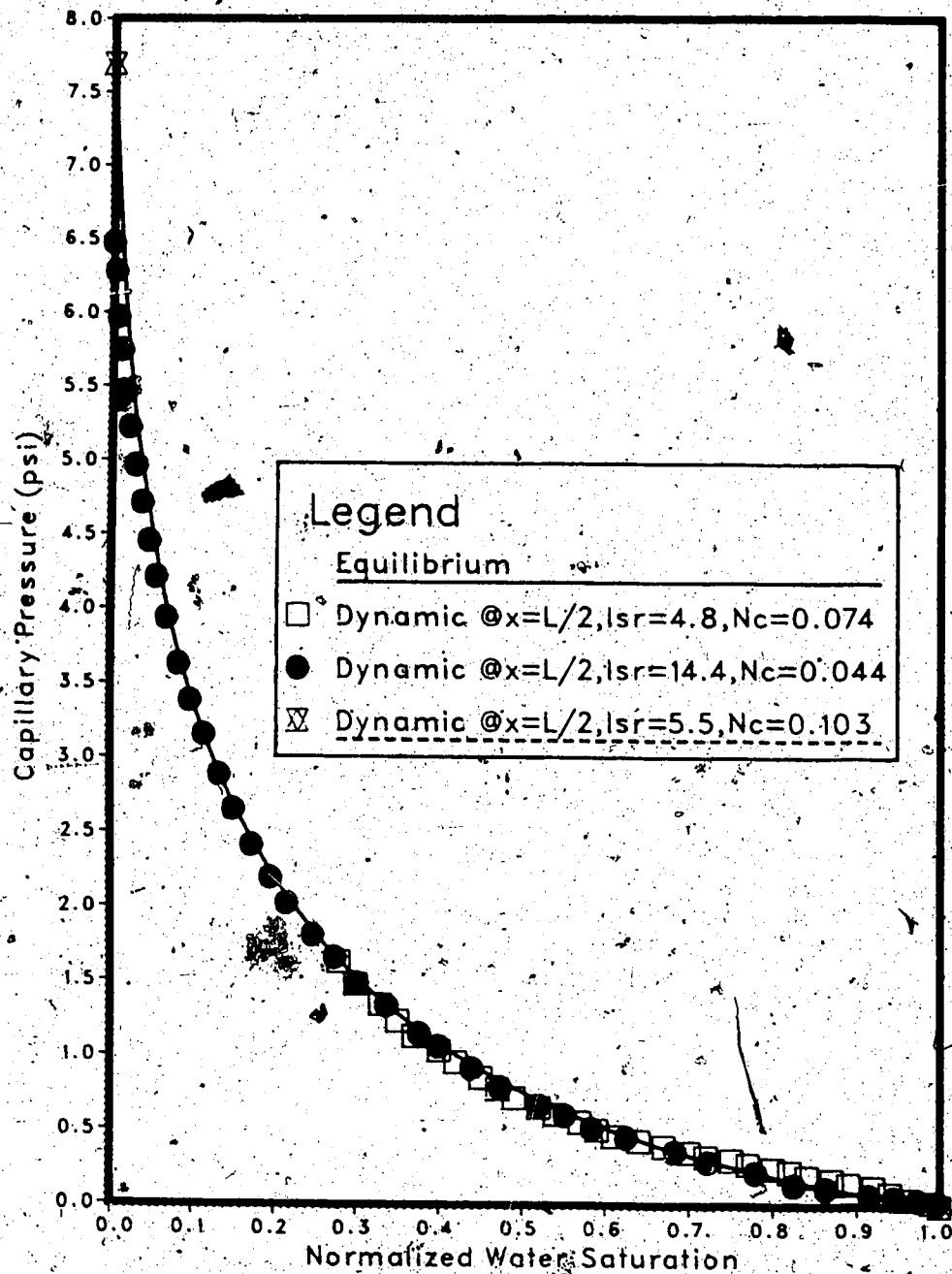


FIGURE 35: CAPILLARY PRESSURE-SATURATION CURVES FOR WATER-MCT5 SYSTEM

Run 67 ($I_{sr}=17.7$) are compared to the equilibrium curve for the water-MCT-10 system in Figure 36.

It has been suggested that relative permeabilities might depend on the flow regime. To investigate if such is the case, relative permeability curves for a stable, stabilized displacement (Run 63) and an unstable displacement (Run 65) for the water-MCT-5 system are compared in Figure 37. Figure 38 compares the relative permeability curves for Run 66 ($I_{sr}=35.8$) and Run 67 ($I_{sr}=17.7$) for the water-MCT-10 system. Note that, because of differences in S_{or} for each of the runs, the relative permeabilities are plotted versus normalized water saturation in both Figures 37 and 38.

Presented in Figure 39 is a comparison of relative permeabilities obtained by using the Lagrangian method with those obtained by using the Eulerian method for an unstable run (Run 66). In using the Eulerian method, two cases were considered; in case one, the conventional approach was taken and the correction terms for the capillary pressure gradient were neglected. In the second case, the Eulerian method was modified so as to incorporate the appropriate capillary pressure gradient terms.

6.5.3 Discussion of Results

6.5.3.1 Saturation Profiles

The saturation profiles presented in Figures 27, 28 and 29 pertain to the unstable displacements carried out in Runs 65, 66 and 67, respectively. The time in seconds is indicated for some of the saturation profiles, and the instability number for each case has been indicated on each figure. It is to be noted that the shape of the saturation profiles in these displacements is quite similar to that observed in Run 64, an unstabilized displacement. Moreover, the amount of "noise" on the profiles does not appear to increase as the instability of the displacement increases, nor does it seem to be much different from that seen on the unstabilized displacement profiles for Run 64 (Figure 17). Consequently, it is quite difficult to discern, at a glance, whether a given set of saturation profiles belongs to an unstabilized displacement, or to an unstable

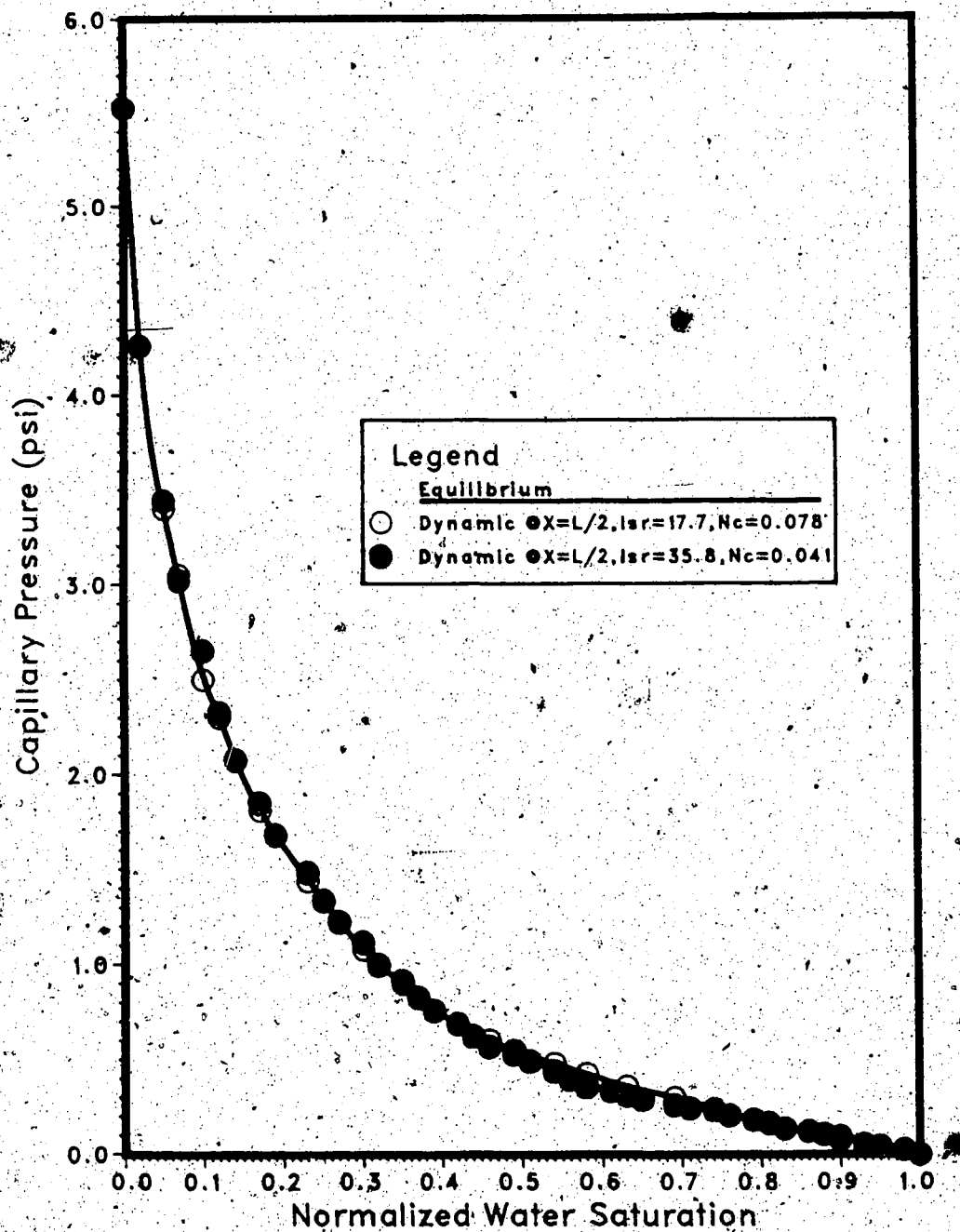


FIGURE 36: CAPILLARY PRESSURE-SATURATION CURVES FOR WATER-MCT10 SYSTEM

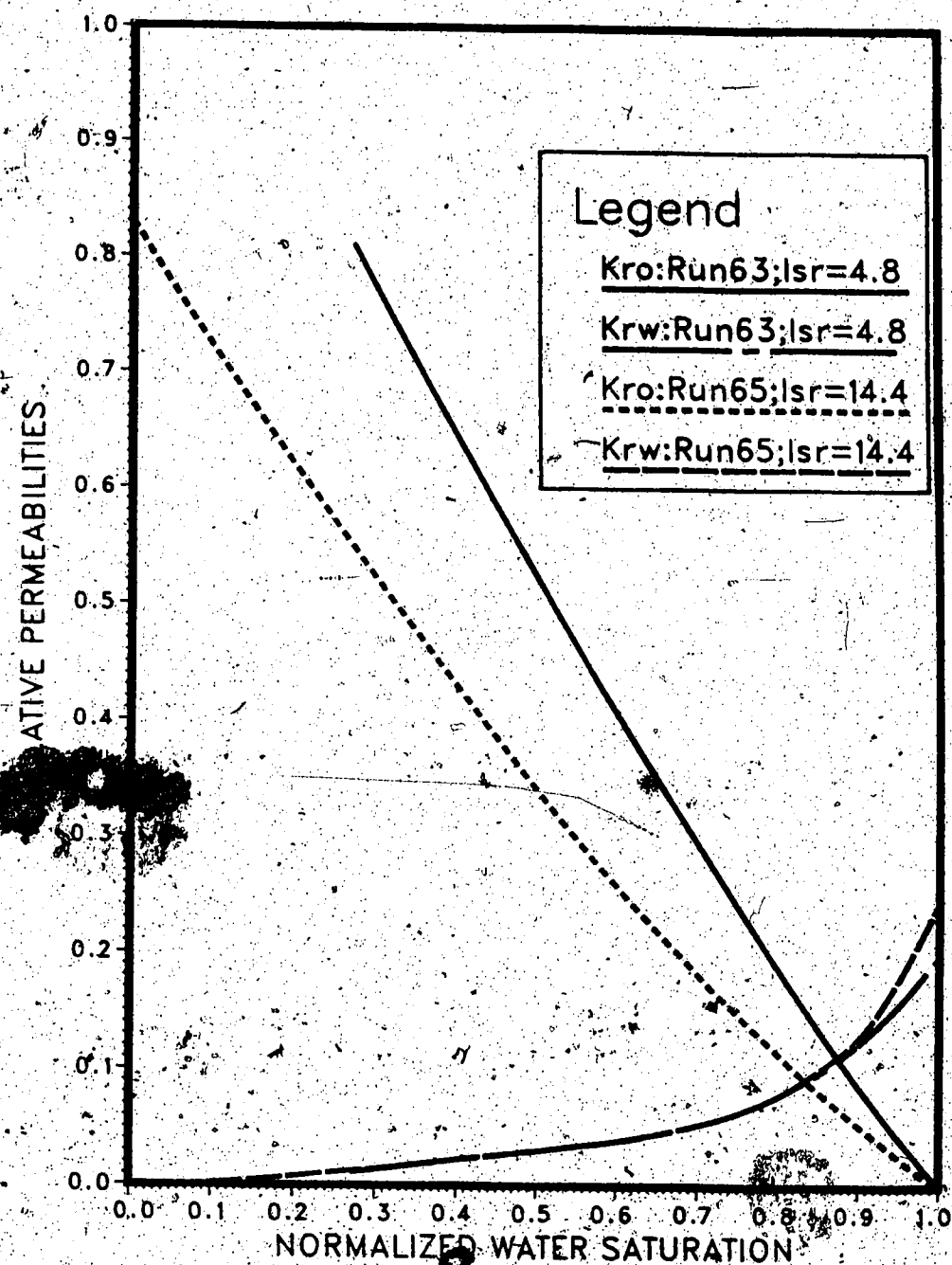


FIGURE 37: RELATIVE PERMEABILITY CURVES USING WATER-MCT5 SYSTEM (RUNS 63 AND 65)

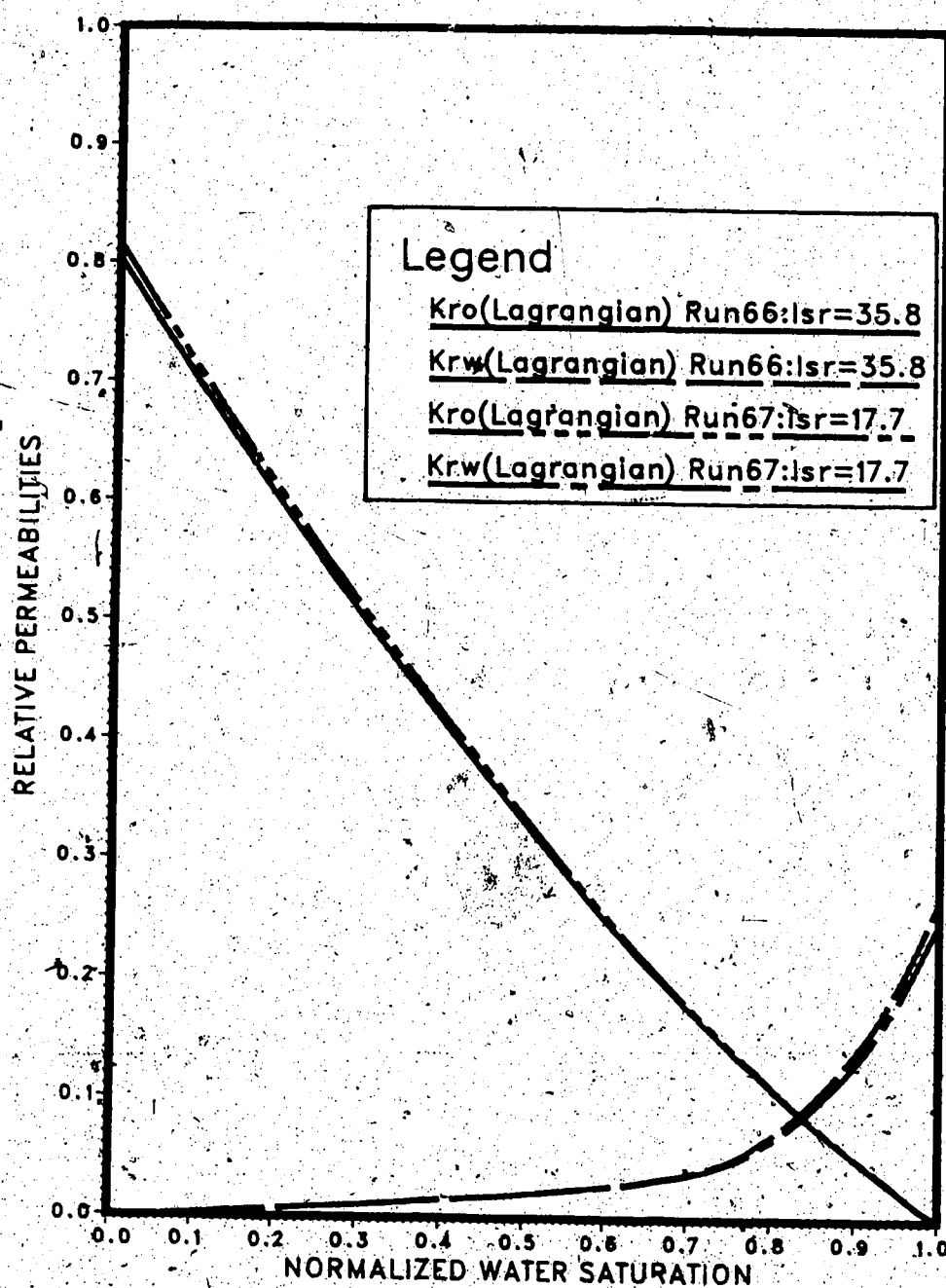


FIGURE 38: RELATIVE PERMEABILITY CURVES FOR UNSTABLE DISPLACEMENTS USING WATER-MCT10 SYSTEM

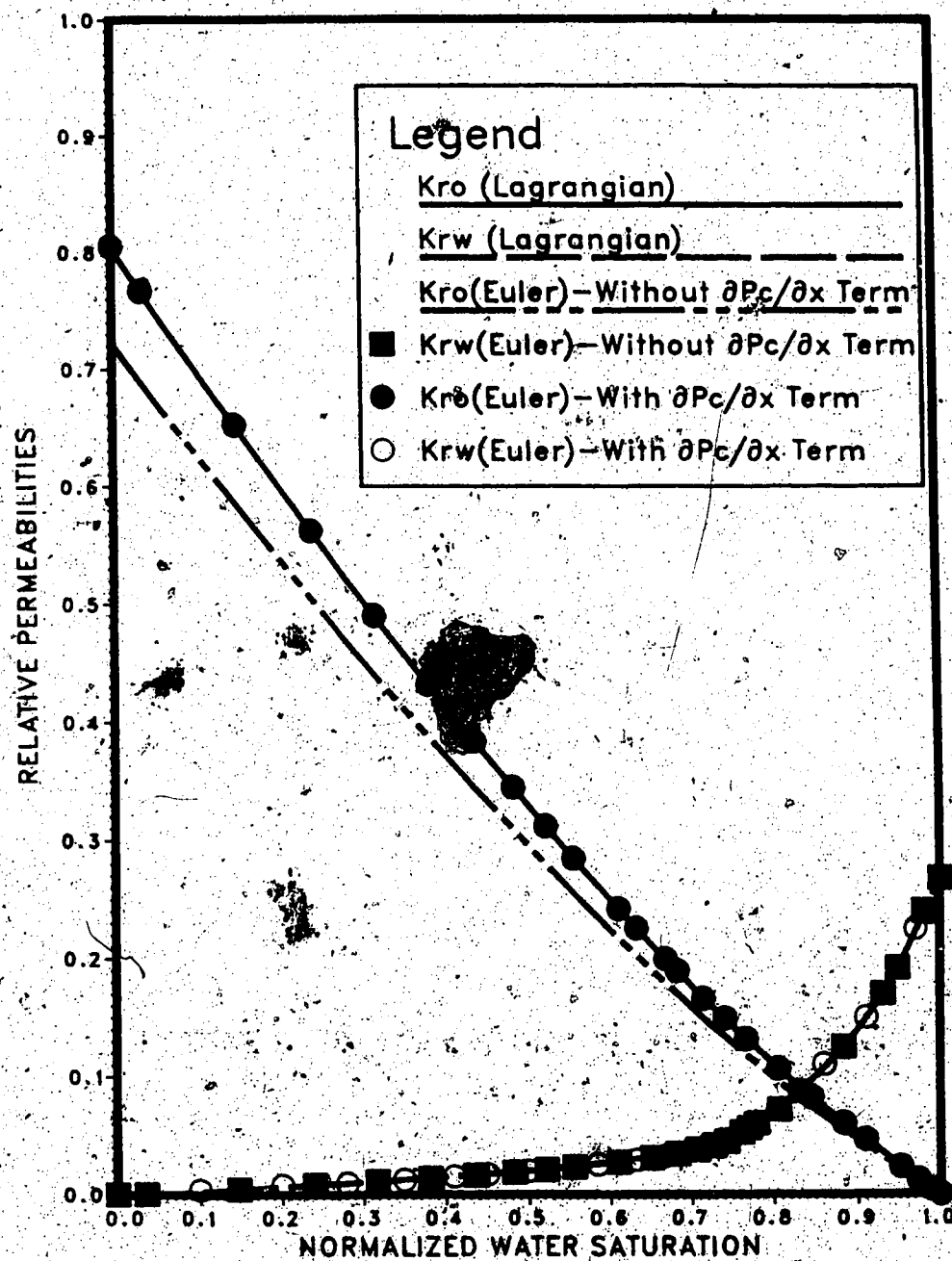


FIGURE 39: COMPARISON OF RELATIVE PERMEABILITIES
OBTAINED BY USING LAGRANGIAN AND
EULERIAN METHODS (RUN 66)

displacement. It is to be noted that all of the unstable displacements were carried out in the immediate vicinity of the stability boundary.

Immiscible displacement theory[36] suggests that the slope of a saturation profile, at a given saturation, should be proportional to M/N_c . As can be seen from Figure 30, such is indeed the case. Because the unstabilized displacement (Run 64) was carried out at much lower velocity than was the case for the unstable displacements, it is to be expected that the unstabilized displacement should have the largest (negative) slope, and, as can be seen from Figure 31, this was the case. Consequently, it can be argued that unstabilized displacements should have steeper slopes than is the case for unstable displacements.

Presented in Table 15 are the times of arrival of the "foot" of the saturation profile at the mid-point of the core. In each case, it is to be noted that the measured time of arrival of the foot of the saturation profile is less than the predicted time of arrival. This is also true for the unstabilized runs (see Table 15). Note that the relative error decreases as the instability number increases. That is, the relative error was -7.85% for Run 65 ($I_{sf}=14.4$), -7.0% for Run 67 ($I_{sf}=17.7$), and -5.5% for Run 66 ($I_{sf}=35.8$). For Run 64 ($I_{sf}=1.07$), the unstabilized displacement, the relative error was much higher, -37.3%. The effect of stabilization is to steepen the saturation profiles (or the front) while that of instability is to flatten the profiles (see Figure 31). Moreover, the relative error should decrease as the profiles steepen. Because the relative error decreases as I_{sf} increases, it is thought that the effect of stabilization is more important than the effect of instability, at least in the immediate vicinity of the stability boundary.

For all the runs, the irreducible water saturation was established prior to the start to the waterflood by using the procedure outlined in the preceding chapter. As a consequence, the value of S_{wi} obtained for each run was 0.07. However, such was not the case for S_{or} which varied from one run to the next. That is, as can be seen from Figure 32, the value of S_{or} increased as $1/N_c$ increased.

The microscopic capillary number ($N_{cm} = V\mu/\sigma$) varies from 3.14×10^{-6} (Run 67) to 6.27×10^{-6} (Run 66) for unstable displacements, while its value is 3.3×10^{-6} for the unstabilized displacement (Run 64). Over this range of values of N_{cm} , one might expect to see a slight decrease in S_{or} as the value of N_{cm} increases [123]. However, as can be seen from Figure 32 ($1/N_c$ equals approximately $4.0 \times 10^{-6} N_{cm}$ for the unstable displacements), the residual saturation to oil increases as $1/N_c$ (or N_{cm}) increases. Consequently, it would appear that the correlation of S_{or} with $1/N_c$ (or N_{cm}) behaves quite differently, depending upon whether the displacement is stable or unstable. That is, S_{or} increases as $1/N_c$ increases, if the displacement is unstable, while S_{or} decreases with increasing $1/N_c$ (or N_{cm}), if the displacement is stable [123, 124].

6.5.3.2. Fractional Flow Curves

A comparison of the fractional flow curves obtained for an unstable displacement (Run 65, $I_{sr} = 14.4$) and a stable displacement (Run 63, $I_{sr} = 4.8$) is presented in Figure 33. Notice that the mobility ratio for Run 63 is 7.1, while that for Run 65 it is 9.7. As can be seen from Figure 33, the fraction of water flowing at a given water saturation is higher in the case of the unstable displacement (Run 65) than it is for the stable displacement (Run 63). It must, however, be borne in mind that fractional flow of water is a function of mobility ratio, too. As a consequence, the difference between the mobility ratios contributed to the difference between the two fractional flow curves. That is, the fraction of water flowing at a given saturation for Run 65 is higher not only because the displacement is unstable, but also because the mobility ratio for the run is higher.

Presented in Figure 34 is a comparison between the fractional flow curves obtained for two unstable displacements, Run 66 ($I_{sr} = 35.8$) and Run 67 ($I_{sr} = 17.7$), both of which utilized a distilled water-MCT-10 system. Note that there is very little difference between the mobility ratio for these two runs. Consequently, the major reason that the fraction of water flowing, at a given saturation, is higher for Run 66 ($I_{sr} = 35.8$) than it is for Run 67 ($I_{sr} = 17.7$), is that Run 66 is more unstable. This is

consistent with the results reported by Peters and Khataniar[52].

6.5.3.3 Capillary Pressure Curves

As has been mentioned earlier, it was practicable to obtain dynamic pressures in the oil and water phase during the displacement process. Thus, it was also possible to obtain dynamic capillary pressures for each sand-fluid system. Presented in Figures 35 and 36 are dynamic capillary pressure data for the water-MCT-5 system and the water-MCT-10 system, respectively. As can be seen from Figures 35 and 36, dynamic capillary pressures are in good agreement with those obtained under equilibrium conditions for both sand-fluid systems. Such good agreement is quite remarkable and significant, particularly in view of the fact that these data were obtained over a wide range of instability numbers ($I_{sr}=4.8$ to $I_{sr}=14.4$ for the water-MCT-5 system and $I_{sr}=17.7$ to $I_{sr}=35.8$ for the water-MCT-10 system). Thus, for displacements which are moderately unstable, use of equilibrium capillary pressure data should not introduce any serious error into the analysis. However, whether such an agreement would hold at much higher instability number remains to be studied.

6.5.3.4 Relative Permeability Curves

In order to demonstrate that relative permeability curves may depend on the flow regime, a comparison of relative permeability curves obtained for an unstable displacement (Run 65) and a stable displacement (Run 63) has been made for the same sand-fluid system (distilled water-MCT-5 system). The relative permeability curves obtained for these two runs are presented in Figure 37. In order to make a more appropriate and meaningful comparison between the relative permeability curves for these two runs, a Lagrangian, rather than an Eulerian, method was used to obtain the relative permeabilities to oil and water for Run 63. However, because Run 63 was a stable, stabilized displacement, the analysis could be done only for saturations greater than S_{wr} . Note that there is significant difference between the stable and the unstable relative permeability curves. Moreover, this difference is larger for the oil curves than it

is for the water curves. In particular, the difference between the stable and unstable relative permeability curves for water becomes significant only for high values of the normalized water saturation. These results are consistent with those presented by Peters and Khataniar[52].

Presented in Figure 38 is a comparison of relative permeability curves for two unstable displacements, Runs 66 and 69, using the Lagrangian method developed in this study. In both of these runs, a distilled water-MCT-10 system was used. As is evident from Figures 37 and 38, relative permeabilities are affected by the type of flow regime. That is, as the displacement becomes more unstable, the relative permeability to oil decreases, while that to water increases. Peters and Khataniar[52] and Islam and Bentsen[51] also reported a similar impact of flow regime on relative permeability (at intermediate instability numbers).

The Eulerian method used by Peters and Khataniar makes use of Equations 74, 75 and 88. As a consequence, they neglected the correction terms involving the capillary pressure gradient, $\partial P_c / \partial x$. Thus, it would be of interest to see what effect, if any, neglect of the capillary pressure gradient term would have on relative permeabilities obtained by using the Eulerian method. To achieve this purpose, the Eulerian method was modified so as to include the capillary pressure terms. Equations 106 and 108 were used to obtain k_{rw} and k_{ro} by the method of successive substitution. The variable, λ^{-1} , was evaluated by using Equation 112 at $x=L$, i.e. at the outlet end of the core. In order to estimate $\partial P_c / \partial x$, $P_o(x)$ and $P_w(x)$ were first curve-fitted as a function of distance, x , using the functional equation, Equation B.2 (see Appendix B). Then the derivatives, $\partial P_o / \partial x$ and $\partial P_w / \partial x$, were obtained at $x=L$, the outlet end of the core. Having obtained these derivatives, $\partial P_c / \partial x$ was estimated for $x=L$.

The relative permeabilities to the oil and the water obtained by using the modified Eulerian method are shown in Figure 39. Note that the solid circles pertain to the oil relative permeability curve, while the open circles pertain to the water relative permeability curve. Also presented in the same figure, Figure 39, are the relative

permeability curves obtained by using the Lagrangian and the Eulerian methods without the capillary pressure term. As is evident from this figure, good agreement between relative permeabilities obtained by the Lagrangian method with those obtained by using the modified Eulerian method is obtained. However, comparison of the oil relative permeabilities obtained by the Eulerian method without the capillary pressure term with those obtained by using the Lagrangian method demonstrates that failure to include the capillary pressure term can introduce significant error into the oil curve. However, differences, for all cases, among the water relative permeability curves are negligible. An argument similar to the one made in section 6.4 may be appropriate in this context. That is, because the capillary pressure term appearing in Equation 106 is divided by μ_o , while that in Equation 108 is divided by μ_w , and because μ_o is 60 times larger than μ_w , neglect of the capillary pressure gradient term may have had a much more serious effect on the estimated values of k_{ro} than is the case for k_{rw} .

The preceding discussion suggests that the method used by Peters and Khataniar[52] introduces an error into the analysis because of neglect of the correction term involving the capillary pressure gradient term, and this error can become quite serious for the oil relative permeability curve. Because both the Lagrangian and the modified Eulerian methods are in good agreement, it might appear that either may be used. However, while the Lagrangian method is robust, it is more cumbersome to use and needs a more elaborate experimental design to obtain the dynamic saturation profiles and to record internal pressures along the length of the core. The modified Eulerian method, on the other hand, is simple to use and the experimental design needs are simpler.

6.5.3.5 Impact of Instability

When a displacement is unstable, the pressure and saturation are no longer uniform at all cross-sections. As a consequence, conventional displacement theory may no longer be applicable. That is, relative permeabilities estimated for a stable displacement using the external-drive theory may not be applicable to unstable

displacements. Moreover, the conventional equilibrium capillary pressure curve may not be applicable to unstable displacements.

In this study, the saturations measured were averaged over a volume of approximately 1 cm by 1 cm by 5 cm (height of the core). Moreover, the capillary pressure was averaged over a somewhat smaller volume. Consequently, even though the saturation and pressures may not have been uniform, because of viscous fingering, the effects of such non-uniformity seem to have been averaged out. This hypothesis is supported by the fact that saturation and pressure were distributed uniformly along the length of the core, even when the displacement was unstable.

As noted earlier, it was found that, in the immediate vicinity of the stability boundary, the relative permeability to oil at a particular saturation decreased with increasing instability, while the relative permeability to water increased. This is consistent with the results presented by Peters and Khataniar[52]. As a consequence, it would appear that different relative permeability curves apply to stable and unstable displacements.

Capillary pressures have been measured for two different water-oil systems, and for displacements which are unstable, as well as for those which are stable. Over the range of instability numbers utilized in this study, it was found that there was good agreement between the equilibrium and the dynamic capillary pressure curves. As a consequence, it would appear that equilibrium capillary pressure curves may be used to estimate the pressure difference between the oil and the water in an actual displacement, provided the instability number is not too far removed from the stability boundary.

Because capillary pressure was independent of I_{sr} , and because it was possible to measure relative permeability, and because pressure and saturation were distributed uniformly, it is thought that conventional displacement theory is applicable to unstable displacements, provided the porous medium is reasonably homogeneous, and provided the instability number is not too high. However, it must be kept in mind that relative permeability is dependent upon dimensionless velocity (I_{sr}), as is the residual oil

saturated, when a displacement is unstable.

7. SUMMARY AND CONCLUSIONS

As was specified at the outset, various broad objectives were set out for this study. As a consequence, the summary and conclusions for each of these objectives is discussed separately for the sake of clarity.

7.1 Modification of Stability Theory and Its Experimental Verification

The theory developed in an earlier paper[2] has been modified to take proper account of the fact that the distance travelled by a viscous finger is a linear function of time. This was accomplished by deriving from first principles the differential equation which describes how the two-dimensional surface of a viscous finger evolves as a function of time. The modified theory is validated by comparing theoretical results with those obtained experimentally. In particular, the modified theory correctly predicts the stability boundary for displacements carried out in rectangular coreholders packed with unconsolidated sand. Moreover, it is possible to use the modified theory to predict the breakthrough recovery for stable displacements and for those which are pseudostable.

Based on the experimental results presented herein, and keeping in mind that the modified theory may apply only to the particular geometry and sand-fluid system used in this study, the following conclusions may be drawn:

1. Equation 67 correctly predicts the boundary which separates stable displacements from those which are unstable in rectangular systems packed with unconsolidated sand. As a consequence, it may be inferred also that Equation 68 correctly predicts the pseudointerfacial tension for such displacements.
2. Equation 70 correctly predicts the breakthrough recovery for a stable displacement, provided it is assumed that the viscous fingers are initiated at the inlet end of the coreholder. Because Equation 70 is based on the assumption that the distance travelled by the tip of a finger is a linear function of time, it may be concluded also that the linear time function used in Equation 46 is acceptable.
3. Equation 72 correctly predicts the breakthrough recovery for a pseudostable

displacement provided it is assumed that viscous fingers are initiated at the inlet end of the coreholder. Moreover, because of the assumptions underlying Equation 72, it may be concluded that the perturbation velocity of a finger in a pseudostable displacement is three times that of the critical perturbation velocity associated with the actual injection rate. However, because of the scarcity of the data supporting these two conclusions, they should be considered as being tentative at present.

4. Over the range of lengths used in this study, the length of the coreholder used did not appear to have a significant effect on the breakthrough recovery of either stable or unstable displacements.
5. Equation 63, the defining equation for the eigenvalue which dictates the most probable finger width, is valid only for fully developed fingers ($z_w \gamma_w \gg 1$). For an incipient finger ($z_w \gamma_w \ll 1$), the most probable finger width is dictated by the smallest wavelength which can be formed at a given value of superficial velocity.
6. The replacement of the actual transition zone (capillary fringe) separating the displacing fluid from that which is being displaced by a macroscopic pseudosurface to which can be assigned a pseudointerfacial tension did not introduce any serious errors into the analysis, because good agreement between theoretical and experimental results was obtained.
7. Fixing the root of a finger in the surface which initially separated the displacing fluid from the displaced fluid did not introduce any serious errors into the analysis, provided the equations developed were restricted to situations where this assumption was not seriously violated.

7.2 Estimation of Relative Permeabilities Using the External-Drive Technique

Functional forms for smoothing cumulative oil and pressure-drop histories have been developed which incorporate not only the proper constants of integration for the two differential equations describing the system, but also the various physical conditions which can be imposed on the system. As a consequence, it is possible to utilize a number of

consistency tests when choosing the best parameters to model the system. While the imposition of such consistency tests increases the likelihood that the set of parameters chosen is the best possible for the situation at hand, it should be kept in mind that there is no sufficient condition that will guarantee that any set of parameters selected is correct. Consequently, the quality of the derived relative permeability curves depends upon the quantity and quality of the data, and on the experience of the analyst.

An apparatus for determining relative permeabilities to oil and water has been developed and tested. It has proven capable of determining accurately how saturation and pressure in both the water and oil phases are distributed along the length of the core. This has enabled direct verification of the external-drive theory.

Based on the experimental results presented herein, and keeping in mind that these results may apply only to the particular geometry and the sand-fluid system used in this study, the following conclusions may be drawn:

1. The method is simple, yet robust, in that it satisfies various physical conditions imposed, and it can withstand the various consistency checks placed upon it.
2. It does not involve any graphical differentiation of displacement data. Furthermore, use of displacement data in this method is direct and simple with no complex "pre-treatment".
3. Equation 78 correctly predicts the saturation at the outlet end of the core, provided the assumptions underlying external-drive theory are reasonably well met.
4. Equation 88 correctly predicts the reciprocal mobility at the outlet end of the system, provided the assumptions underlying external-drive theory are reasonably well met.
5. Use of the total pressure drop history for water rather than that for oil to estimate λ_2^{-1} introduces an error into the oil relative permeability curve. The magnitude of this error increases as the water saturation increases and reaches a maximum at the floodfront saturation.
6. Over the saturation range, $S_{wf} \leq S_w \leq (1 - S_{or})$, there is good agreement between the dynamic and the equilibrium capillary pressure curves.

7. There was good agreement between the measured saturation profiles and those predicted using Buckley-Leverett theory, provided the displacement was stabilized and stable.

7.3 Lagrangian Method for Estimating Relative Permeabilities

A method for estimating effective permeabilities to water and oil which makes use of unstable and unstabilized displacement data, and which enables the generation of effective permeability curves over the entire saturation range of interest has been developed and tested. While the method has proven to be expeditious and accurate, it must be kept in mind that it can be utilized only provided: (i) saturation profiles and pressure gradients in both phases can be measured directly, (ii) the external-drive theory is modified to account for the existence of capillary pressure gradients, and (iii) the analysis is carried out from a Lagrangian rather than an Eulerian point of view.

Based on the experimental results presented herein, and keeping in mind that these results may apply only to the particular geometry and the sand-fluid system used in this study, the following conclusions may be drawn:

1. It was possible to measure the pressure gradient in both the oil and water phases and, as a consequence, the capillary pressure gradient during the course of a displacement experiment.
2. Because it is possible to measure the capillary pressure gradient along the core, it is practicable to estimate the fractional flow curve $(f_w(x(\bar{S}_w), t^*))$ which pertains to a specific point in time. This enables the use of unstable and unstabilized displacement data to estimate the relative permeability curves.
3. The use of equilibrium capillary pressure data to predict the pressure difference between the water and oil in a dynamic displacement is acceptable, provided the displacement is stable.
4. If a displacement is unstable or unstabilized, pressures in the oil and water in the immediate vicinity of the outlet end of the coreholder may be disturbed by outlet end effects.

5. If a displacement is unstable or unstabilized, the saturation at the inlet end of the coreholder does not immediately rise to $1 - S_{or}$. Rather, a certain number of pore volumes of water must be injected before the saturation increases to this value.
6. If a displacement is unstable or unstabilized, the fraction of water flowing at a particular location along the core is a function of both time and saturation.
7. No displacement front develops during an unstable or unstabilized displacement. Qualitatively speaking, saturation profiles in both unstable and unstabilized displacements are similar in character. However, it was observed that the slope of the saturation profiles tend to decrease as the instability number for the displacement becomes higher.
8. Good agreement was obtained between relative permeabilities obtained by using the Lagrangian method with those obtained by using the modified Eulerian method, which takes into account the capillary pressure gradient term.

7.4 Validation of Concepts of Relative Permeability and Capillary Pressure for Unstable Displacements

The impact of instability on the relative permeability and capillary pressure curves was investigated for unstable displacements. Also investigated were the effects of instability on the saturation profiles, fractional flow curves and the residual oil saturation. Moreover, the effect of stabilization on the residual oil saturation was studied.

Furthermore, a comparison of relative permeabilities obtained by using the Lagrangian method with those obtained using the conventional (without capillary pressure term) and the modified (with the capillary pressure term) Eulerian methods was undertaken to demonstrate the effect of the neglect of the capillary pressure term on relative permeabilities.

Based on the experimental results presented herein, and keeping in mind that these results may apply only to the particular geometry and the sand-fluid system used in this study, the following conclusions were drawn:

1. The character and shape of the saturation profiles in unstable displacements are quite

similar to those in unstabilized displacements. However, it was noticed that the effect of stabilization was to steepen the saturation profiles, while the effect of instability was to flatten the profiles.

2. The residual oil saturation, S_{or} , is a function of the capillary number, N_c ; that is, S_{or} increases as $1/N_c$ increases, if the displacement is unstable.
3. The fraction of water flowing at a given saturation is a function of both the mobility ratio and the instability number. At a given saturation, the higher the instability number, the higher is the fraction of water flowing at that particular water saturation.
4. Within the range of instability numbers studied, there is a good agreement between the equilibrium and the dynamic capillary pressure curves.
5. Instability has a significant effect on the relative permeability curves. In the immediate vicinity of the stability boundary, the relative permeability to oil at a given saturation decreases with increasing instability, while the relative permeability to water increases.
6. Good agreement between relative permeabilities obtained by using the Lagrangian method and those obtained by the modified Eulerian method was obtained. Therefore, this suggests that the modified Eulerian method can be applied to unstable displacements without introducing any serious error; however, neglect of the capillary pressure term in the conventional Eulerian method to estimate relative permeabilities can introduce a serious error into the analysis.

7.5 Suggestions for Future Study

The theory developed in this study is inadequate to describe the displacement mechanisms within the transition region, i.e. for $\pi^2 \leq I_{sr} \leq 900$. It is recommended that future studies make an attempt to develop an appropriate theory to explain flow phenomena in this region, and validate it with experimental results.

Although the experimental equipment designed for this study is fairly accurate and reliable, there is some room for improvement in future studies. That is, in order to record microwave signals at a precise location in the coreholder, a stepper motor should be used and

this motor should be controlled directly by the controller, the HP310 System. Installation of such a motor will eliminate the delay in the power meter response time. Moreover, the ratio of the input microwave power to the output microwave power is the most important factor in obtaining an accurate estimation of S_w . In this study, two separate power meters were used to measure I_o and I_x . Even though utmost care was taken to measure the input and output microwave power simultaneously, some lag could not be avoided. To circumvent this problem, it is suggested that a dual sensor power meter, similar to the HP438A by Hewlett-Packard, be used to facilitate direct measurement of the ratio of the input to output power. Furthermore, the demodulators currently used to obtain the pressure-signals in volts should be replaced by a more reliable data acquisition system, such as the high speed data acquisition system developed by Validyne Engineering Corporation.

Because the inlet end-cap of the coreholder was made of plexi-glass material, it was not possible to conduct displacement experiments at higher inlet pressures. The objective of using the plexi-glass was to investigate visually whether the design of the inlet end-cap permitted uniform fluid injection across the entire cross-section of the core, rather than at a point. Now that this study has resolved that the design used was effective in obtaining uniform entry of the displacing phase across the entire cross-section of the core, it is recommended that the inlet end-cap used in future studies be made of a stronger material so that it can withstand higher inlet pressures. This will enable displacement studies at higher instability numbers.

REFERENCES

1. Peters, E.J. and Flock, D.L.: "The Onset of Instability During Two-Phase Immiscible Displacement in Porous Media", Soc. Pet. Eng. J. (April, 1981) 249.
2. Bentsen, R.G.: "A New Approach to Instability Theory in Porous Media", Soc. Pet. Eng. J. (October, 1985) 765.
3. Coskuner, G. and Bentsen, R.G.: "An Experimental Study of a New Approach to Instability Theory in Porous Media", Paper No. 85-36-3 Presented at the 36th Annual Tech. Meeting of the Petroleum Society of the CIM, Edmonton, June 2-5, 1985.
4. Coskuner, G. and Bentsen, R.G.: "A Modified Theory for Predicting Unstable Immiscible Displacement", AOSTRA J. of Res., (June, 1986), 155.
5. Demetre, G.P., Bentsen, R.G. and Flock, D.L.: "A Multi-Dimensional Approach to Scaled Immiscible Fluid Displacement", J. Can. Pet. Tech. (July-August, 1982), 49.
6. Bear, J.: *Dynamics of Fluid in Porous Media*, American Elsevier Publishing Company, Inc., New York (1972), 19.
7. Aleman-Gomez, M., Ramamohan, T.R. and Slattery, J.C.: "A Statistical Model for Unsteady-State Displacement in Porous Media", SPE Paper No. 13265 Presented at the 59th Annual Tech. Conf. of Soc. of Petr. Engr. of AIME, Houston, (1984).
8. Taylor, G.I.: "The Instability of Liquid Surfaces When Accelerated in a Direction Perpendicular to Their Planes", Proc. Roy. Soc. London, Ser. A, (1950) Vol. 201, 192.
9. Lewis, D.J.: "The Instability of Liquid Surfaces When Accelerated in a Direction Perpendicular to Their Planes II", Proc. Roy. Soc. London, Ser. A, (1950) Vol. 202, 81.
10. Saffman, P.G. and Taylor, G.I.: "The Penetration of a Fluid into a Porous Medium or Hele-Shaw Cell Containing a More Viscous Liquid", Proc. Roy. Soc. (1958) Vol. 245A, 312.
11. Bellman, R. and Pennington, R.H.: "Effects of Surface Tension and Viscosity on Taylor Instability", Quart. Appl. Math. (1954), Vol. 12, 151.
12. Engleberts, W.F. and Klinkenberg, L.J.: "Laboratory Experiments on the Displacements of Oil by Water from Rocks of Granular Materials", Proc., Third World Pet. Cong. (1957) Part II, 544.
13. Handy, L.L.: "An Evaluation of Diffusion Effects in Miscible Displacement", Trans. AIME, (1959), Vol. 216, 382.
14. Van Meurs, P.: "The Use of Transparent Three-Dimensional Models for Studying the Mechanism of Flow Processes in Oil Reservoirs", Trans. AIME, (1957), Vol. 210, 295.
15. Van Meurs, R. and van der Poel, C.: "A Theoretical Description of Water-Drive Processes Involving Viscous Fingering", Trans. AIME (1958) Vol. 213, 103.
16. Chuoke, R.L., van Meurs, R., and van der Poel, C.: "The Instability of Slow, Immiscible, Viscous Liquid-Liquid Displacements in Permeable Media", Trans. AIME (1959) Vol. 216, 188.

17. Outmans, H.D.: "Nonlinear Theory for Frontal Stability and Viscous Fingering in Porous Media", Soc. Pet. Eng. J., (June, 1962) 165; Trans., AIME, Vol. 225.
18. Benham, A.L. and Olsen, R.W.: "A Model Study of Viscous Fingering", Soc. Pet. Eng. J., (June, 1963), 138.
19. Rachford, H.H. Jr.: "Instability in Water Flooding Oil from Water-Wet Porous Media Containing Connate Water", Soc. Pet. Eng. J., (June, 1964) 133; Trans. AIME (1964) Vol. 231.
20. Buckley, S.E. and Leverett, M.C.: "Mechanism of Fluid Displacement in Sands", Trans. AIME (1942), Vol. 146, 107.
21. Perkins, T.K. and Johnston, O.C.: "A Study of Immiscible Fingering in Linear Models", Soc. Pet. Eng. J., (March, 1969), 39.
22. Hagoort, J.: "Displacement Stability of Water Drives in Water-Wet Connate-Water-Bearing Reservoirs", Soc. Pet. Eng. J. (February, 1974) 63; Trans., AIME, Vol. 257.
23. Sarma, H.K.: "Viscous Fingering: One of the Main Factors Behind Poor Flood Efficiencies in Petroleum Reservoirs", Powder Tech., (1986), Vol. 48, 39.
24. Sigmund, P.M., Sarma, H.K., Sheldon, D. and Aziz, K.: "Rate Dependence of Unstable Waterfloods", SPE Paper 14368 Presented at the 60th Annual Tech. Conf. of SPE, Las Vegas, Sept. 22-25, 1985.
25. Jerauld, G.R., Davis, H.T. and Scriven, L.E.: "Stability of Fronts of Permanent Form in Immiscible Displacement", SPE Paper No. 13164 Presented at the 59th Annual Tech. Conf. and Exhibition of SPE, Houston, Sept. 16-19, 1984.
26. Bentsen, R.G.: "Use of Capillary Pressure Data to Estimate the 'Pseudointerfacial Tension' for Analysis of Stability of Fluid Flow in Porous Media", AOSTRA J. of Res., (December, 1986), 213.
27. Yortsos, Y.C. and Huang, A.B.: "Linear Stability Analysis of Immiscible Displacement Including Continuous Changing Mobility and Capillary Effect: Part I - Simple Basic Flow Profiles", SPE Paper 12692 Presented at the SPE/DOE Fourth Symp. on EOR, Tulsa, April 15-18, 1984.
28. Terwilliger, P.L., Wilsey, L.E., Hall, H.N., Bridges, P.M. and Morse, R.A.: "An Experimental and Theoretical Investigation of Gravity Drainage Performance", Trans. AIME (1951), Vol. 192, 285.
29. Welge, H.J.: "A Simplified Method for Computing Oil Recovery by Gas or Water Drive", Trans. AIME, (1952), Vol. 195, 91.
30. Willhite, G.P.: *Waterflooding*, Society of Petroleum Engineers, Richardson, (1986), Chapters 3 and 5.
31. Owens, W.W., Parrish, D.R. and Lamoreaux, W.E.: "An Evaluation of a Gas Drive Method for Determining Relative Permeability Relationships", Trans. AIME (1956), Vol. 207, 275.
32. Rapoport, L.A. and Leas, W.J.: "Properties of Linear Waterfloods", Trans. AIME (1953), Vol. 198, 139.

33. Jones-Parra, J. and Calhoun, J.C.: "Computation of A Linear Flood by the Stabilized Zone Method", Trans. AIME(1953), Vol. 189, 335.
34. Bail, P.T.: "The Calculation of Water Flood Performance for the Bradford Third Sand from Relative Permeability and Capillary Pressure Data", Prod. Monthly, (July, 1956), Vol. 21, No. 7, 20.
35. Parsons, R.W. and Jones, S.C.: "Linear Scaling in Slug Type Processes - Application to Micellar Flooding", Soc. Pet. Eng. J., (February, 1977), 11.
36. Bentsen, R.G.: "Conditions Under Which the Capillary Term May be Neglected", J. Can. Pet. Tech. (October-December, 1978), 25.
37. Abrams, A.: "The Influence of Fluid Viscosity, Interfacial Tension, and Flow Velocity on Residual Oil Saturation Left by Waterflood", Soc. Pet. Eng. J., (December, 1975), 437.
38. Geffen, T.M., Owens, W.W., Parrish, D.R. and Morse, R.A.: "Experimental Investigation of Factors Affecting Laboratory Relative Permeability Measurements", Trans. AIME, Vol. 192, 99.
39. Kimbler, O.K. and Caudle, B.H.: "New Technique for Study of Fluid Flow and Phase Distribution in Porous Media", Oil & Gas J., (1957), Vol. 55, 85.
40. Archer, J.S. and Wong, S.W.: "Use of a Reservoir Simulator to Interpret Laboratory Waterflooding Data", Soc. Pet. Eng. J. (December, 1973), 343.
41. Collins, R.E.: *Flow of Fluids Through Porous Materials*, McGraw Hill Book Company, Inc., New York, (1961), 143.
42. Bentsen R.G. and Saeedi, J.: "Liquid-Liquid Immiscible Displacement in Unconsolidated Porous Media", J. Can. Pet. Tech (January-March, 1981), 93.
43. Islam, M.R.: *An Investigation on the Impact of Flow Regime on Effective Permeabilities*, M.Sc. Thesis, Univ. of Alberta, (1985), 99.
44. Sigmund, P.M. and McCaffery, F.G.: "An Improved Unsteady-State Procedure for Determining the Relative Permeability Characteristics of Heterogeneous Porous Media", Soc. Pet. Eng. J. (January, 1979), 15.
45. MacMillan, D.J.: "Automatic History Matching of Laboratory Corefloods to Obtain Relative-Permeability Curves", SPE Res. Eng. (February, 1987), 85.
46. Kerig, P.D. and Watson, A.T.: "A New Algorithm for Estimating Relative Permeabilities from Displacement Experiments", SPE. Res. Eng. (February, 1987), 103.
47. Johnson, E.F., Bossler, D.P. and Naumann, V.O.: "Calculation of Relative Permeability from Displacement Experiments", Trans., AIME (1959), Vol. 216, 370.
48. Jones, S.C. and Roszelle, W.O.: "Graphical Techniques for Determining Relative Permeability from Displacement Experiments", J. Pet. Tech. (May, 1978), 807.
49. Tao, T.M. and Watson, A.T.: "Accuracy of JBN Estimates of Relative Permeability: Part 2 - Algorithms", Soc. Pet. Eng. J. (April, 1984), 215.
50. Rose, W.: "Some Problems Connected with the Use of Classical Description of

- Fluid/Fluid Displacement Processes", Trans. Symp. on Fundamentals of Transport Phenomena in Porous Medium, Haifa, Israel, (1968), 229.
51. Islam, M.R. and Bentsen, R.G.: "A Dynamic Method of Measuring Relative Permeability", J. Can. Pet. Tech. (January-February, 1986), 39.
52. Peters, E.J. and Khataniar, S.: "The Effect of Instability on Relative Permeability Curves Obtained by Dynamic Displacement Method", SPE Form. Eval. (December, 1987), 469.
53. Moore, T.F. and Blum, H.A.: "Importance of Wettability in Surface-Active Agent Waterflooding", Oil & Gas J., (1952), Vol. 51, 108.
54. Warren, J.E. and Calhoun, J.C.: "A Study of Waterflood Efficiency in Oil-Wet Systems", Trans. AIME, (1955), vol. 204, 22.
55. [REDACTED], J., Reed, P. and Calhoun, J.C.: "Relationship Between Oil Recovery, Interfacial Tension, Pressure Gradient and Water-Wet Porous Media", Producers Monthly, (1955), Vol. 19, 34.
56. Mungan, N.: "Role of Wettability and Interfacial Tension in Waterflooding", Soc. Pet. Eng. J., (June, 1964), 115.
57. Wagner, R.O. and Leach R.O.: "Effect of Interfacial Tension on Displacement Efficiency", Soc. Pet. Eng. J., (December, 1966), 335.
58. Amaefule, J.O. and Handy, L.L.: "The Effect of Interfacial Tension on Relative Permeabilities of Consolidated Porous Media", Soc. Pet. Eng. J., (June, 1982), 371.
59. Lefebvre du Prey, E.J.: "Factors Affecting Liquid-Liquid Relative Permeability of a Consolidated Porous Medium", Soc. Pet. Eng. J., (February, 1973), 39.
60. Dardon, C. and Longeron, D.: "Influence of Very Low Interfacial Tension on Relative Permeability", Soc. Pet. Eng. J., (October, 1980), 391.
61. Scott, P.H. and Rose, W.: "An Explanation of the Yuster Effect", Trans. AIME, (1953), Vol. 198, 323.
62. Rose, W.: "Fluid Flow in Petroleum Reservoir III. Effect of Fluid-Fluid Interfacial Boundary Condition", Geol. Surv. Circ., (1960), Vol. 291, 18.
63. Singhal, A.K., Mukherjee, D.P. and Somerton, W.H.: "Effect of Heterogeneous Wettability on Flow of Fluids Through Porous Media", J. Can. Pet. Tech., (July-Sept., 1976), 63.
64. Schneider, F.N. and Owens, W.W.: "Steady-State Measurements of Relative Permeability for Polymer-Oil System", SPE Paper No. 9408 Presented at 55th Annual Tech. Conf. and Exhibition of SPE, Dallas, 1980.
65. Sandberg, C.R., Gournay, L.S., and Sippel, R.F.: "The Effect of Fluid-Flow Rate and Viscosity on Laboratory Determination of Oil-Water Relative Permeabilities", Trans. AIME, (1951), Vol. 192, 86.
66. Osoba, J.S., Richardson, J.G., Kerver, J.K., Hafford, J.A. and Blair, P.M.: "Laboratory Measurements of Relative Permeability", Trans. AIME, (1951), Vol. 192, 86.

67. Richardson, J.G., Perkins, Jr., F.M. and Osoba, J.S.: "Diffusion in Behaviour of Fresh and Aged East Texas Woodbine Cores", Trans. AIME, Vol. 205, 86.
68. Odeh, A.S.: "Effect of Viscosity Ratio on Relative Permeability" Trans. AIME, (1959), Vol. 216, 346.
69. Handy, L.L. and Datta, P.: "Fluid Distributions during Immiscible Displacements in Porous Media", Soc. Pet. Eng. J., (December, 1966), 261.
70. Slattery, J.C.: "Interfacial Effects in the Entrapment and Displacement of Residual Oil", AIChE J., (1974), Vol. 20, 1145.
71. Lin, C.Y. and Slattery, J.C.: "Three Dimensional Randomized Network Model for Two Phase Flow Through Porous Media", AIChE J., (1982), Vol. 28, 311.
72. Leverett, M.C. and Lewis, W.B.: "Steady Flow of Gas-Oil-Water Mixtures Through Unconsolidated Sands", Trans. AIME, (1942), Vol. 142, 107.
73. Melrose, J.C.: "Wettability as Related to Capillary Action in Porous Media", Soc. Pet. Eng. J., (September, 1965), 259.
74. McCaffery, F.G. and Bennion, D.W.: "The Effect of Wettability on Two-Phase Relative Permeabilities", J. Can. Pet. Tech., (October-December, 1974), 42.
75. Morrow, N.C., Cram, P.C. and McCaffery, F.G.: "Displacement Studies in Dolomite with Wettability Control by Octanoic Acid", Soc. Pet. Eng. J., (August, 1973), 221.
76. Bass, D.M., Jr.: *Petroleum Engineering Handbook*, Society of Petroleum Engineers, Richardson, Texas (1987), Chapt. 26.
77. Sneider, R.M., Richardson, F.H., Paynter, D.D., Eddy, R.E., and Wyant, I.A.: "Predicting Reservoir Rock Geometry and Continuity in Pennsylvanian Reservoir, Elk City Field, Oklahoma", J. Pet. Tech., (July, 1977), 851.
78. Leverett, M.C.: "Capillary Behavior in Porous Solids", Trans. AIME (1941), Vol. 142, 152.
79. Bruce, W.A. and Welge, H.J.: "The Restored-state Method for Determination of Oil in Place and Connate Water", Drill. and Prod. Prac., API, Dallas (1947), 166.
80. Purcell, W.R.: "Capillary Pressures - Their Measurement Using Mercury and the Calculation of Permeability Therefrom", Trans. AIME (1949), Vol. 186, 39.
81. Slobod, R.L., Chambers, A. and Prehn, W.L., Jr.: "Use of Centrifuge for Determining Connate Water, Residual Oil, and Capillary Pressure Curves of Small Core Samples", Trans. AIME (1951), Vol. 192, 127.
82. Brown, H.W.: "Capillary Pressure Investigations", Trans. AIME (1951), Vol. 192, 67.
83. Messer, E.S.: "Interstitial Water Determination By An Evaporation Method", Trans. AIME (1951), Vol. 192, 269.
84. McCullough, J.J., Albaugh, F.W. and Jones, P.H.: "Determination of Interstitial-Water Content of Oil and Gas Sand by Laboratory Tests of Core Samples", Drill. and Prod. Prac., API (1944), 180.

85. Hassler, G.L. and Brunner, E.: "Measurement of Capillary Pressures in Small Core Samples", Trans. AIME (1945), Vol. 160, 114.
86. Hassler, G.L.: *Method and Apparatus for Permeability Measurement*, U.S. Patent No. 2,345,935 (1944).
87. Willhite, G.P.: *Waterflooding*, Society of Petroleum Engineers, Richardson, Texas, (1986), Chapt. 3.
88. Morrow, N.R.: *Capillary Phenomena in Uniformly Wetted Porous Media*, Petroleum Recovery Institute, Research Report RR-23, (January, 1974), 2.
89. Killins, C.R., Nielsen, R.F. and Calhoun, J.C., Jr.: "Capillary Desaturation and Imbibition in Rocks", Prod. Monthly, (February, 1953), Vol. 18, No. 2, 30.
90. Parsons, R.W.: "Microwave Attenuation - A New Tool for Monitoring Saturations in Laboratory Flooding Experiments", Trans. AIME, (1975), Vol. 259, 302.
91. Baden Fuller, A.J.: *Microwaves: An Introduction to Microwave Theory and Techniques*, Pergamon Press, New York, Second Edition, (1979), 2.
92. Gupta, K.C.: *Microwaves*, Wiley Eastern Ltd., New Delhi (1979), 1.
93. Gandhi, O.P.: *Microwave Engineering and Applications*, Pergamon Press, New York, (1981), 2.
94. Musil, J. and Zacek, F.: *Microwave Measurements of Complex Permittivity by Free Space Methods and Their Applications*, Elsevier Science Publishers B.V., Amsterdam, (1986), Chapt. 2 and 7.
95. Coskuner, G. and Bentsen, R.G.: "On the Development of a Functional Form for the Surface of an Immiscible Viscous Finger and the Use of This Surface in Stability Theory", Chem. Engr. Res. and Design (January, 1987), 42.
96. Peters, E.J., Broman, J.A. and Broman, W.H., Jr.: "Computer Image Processing: A New Tool for Studying Viscous Fingering in Core Floods", SPE Paper 13668, Presented at the SPE California Regional Meeting, Bakersfield, California, March 27-29, 1985.
97. Sokolnikoff, I.S. and Redheffer, R.M.: *Mathematics of Physics and Modern Engineering* McGraw Hill Book Company, Inc., New York City, (1966), 499.
98. Yih, C.S.: *Stratified Flows*, Academic Press, London, (1980), 19.
99. Nelson, A.L., Folley, K.W. and Carol, M.: *Differential Equations*, Second Edition, D.C. Heath and Company, Boston, (1960), 99, 234.
100. Coskuner, G.: *An Experimental Study of a New Approach to Instability in Porous Media*, M.Sc. Thesis, U. of Alberta, Edmonton (1985).
101. Thomas, G.B., Jr.: *Calculus and Analytic Geometry*, Second Edition, Addison-Wesley Publishing Company, Inc., Cambridge, Mass., (1972), 552.
102. Sarma, H.K. and Bentsen, R.G.: "An Experimental Verification of a Modified Instability Theory for Immiscible Displacements in Porous Media", J. Can. Pet. Tech., (July-August, 1987), Vol. 26, 88.

103. Craig, F.F., Jr.: *The Reservoir Engineering Aspects of Waterflooding*, Monograph Volume 3, Henry L. Doherty Series, Society of Petroleum Engineers of AIME, New York (1971), 29.
104. Sarma, H.K. and Bentsen, R.G.: "An Improved Method of Estimation of Relative Permeabilities from Displacement Data", C.I.M. paper 87-38-51 presented at the 38th Annual Tech. Meeting of the Petroleum Society of the CIM, Calgary, June 7-10, 1987.
105. Sarma, H.K. and Bentsen, R.G.: "Further Experimental Validation of the External-Drive Technique", Paper No. 7, Presented at the First Annual Technical Meeting of the South Saskatchewan Section, the Petroleum Society of CIM, Regina, October 6-8, 1987.
106. Bail, P.T. and Marsden, S.S.: "Saturation Distribution in a Linear System During Oil Displacement", *Producers Monthly* (June, 1957), Vol. 21, No. 8, 22.
107. Laird, A.D.K. and Putman, J.A.: "Fluid Saturation in Porous Media by X-ray Technique", *Trans. AIME*, (1951), Vol. 192, 275.
108. Geffen, T.M. and Gladfelter, R.E.: "A Note on the X-ray Absorption Method of Determining Fluid Saturations in Cores", *Trans. AIME*, (1952), Vol. 195, 322.
109. Laird, A.D.K. and Putman, J.A.: "Three Component Saturation in Porous Media by X-ray Techniques", *Trans. AIME*, (1959), Vol. 216, 216.
110. Baker, P.E.: Discussion, *Trans. AIME*, (1975), Vol. 259, 309.
111. Sen, P.N. and Chew, W.C.: "The Frequency Dependent Dielectric and Conductivity Response of Sedimentary Rocks", *J. Microwave Power*, (1983), Vol. 18, No. 1, 95.
112. Harrison, G.R., Laird, R.C. and Loofbaurow, J.R.: *Practical Spectroscopy*, Prentice-Hall, Inc., Englewoods-Cliffs, N.J., (1948).
113. BMDP Statistical Software Manual, University of California Press, Berkeley, California (1985).
114. Miller, M.A. and Ramey, Jr., H.J.: "Effect of Oil/Water Relative Permeabilities of Unconsolidated and Consolidated Sands", *Soc. Pet. Eng. J.*, (December, 1985), 945.
115. Miller, M.A.: *Effect of Temperature on Oil-Water Relative Permeabilities of Unconsolidated Sands*, Ph.D. dissertation; Stanford University, (1983).
116. Hahn, G.J. and Shapiro, S.S.: *Statistical Models in Engineering*, John Wiley & Sons, Inc., New York (1967), 252.
117. Sarma, H.K. and Bentsen, R.G.: "A New Method for Estimating Relative Permeabilities from Unstabilized Displacement Data", C.I.M. paper 88-39-87 to be presented at the 39th Annual Technical Meeting of the Petroleum Society of C.I.M., Calgary, June 12-16, 1988.
118. McCormick, J.M. and Salvadori, M.G.: *Numerical Methods in FORTRAN*, Prentice-Hall (1964), Englewood Cliffs, N.J., 16.
119. Moore, T.F. and Slobod, R.L.: "The Effect of Viscosity and Capillarity on the Displacement of Oil by Water", *Producers Monthly*, (August, 1956), 20.

120. Melrose, J.C. and Brandner, C.F.: "Role of Capillary Forces in Determining Microscopic Displacement Efficiency for Oil Recovery by Waterflooding", J. Can. Pet. Tech., (October-December, 1974), 54.
121. Taber, J.J.: "Dynamic and Static Forces Required to Remove a Discontinuous Oil Phase from Porous Media Containing Both Oil and Water", Soc. Pet. Eng. J., (March, 1968), 3.
122. Taber, J.J., Kirby, J.C. and Schroeder, F.U.: "Studies on the Displacement of Residual Oil: Viscosity and Permeability Effects", Symp. Series, AIChE, New York City, (1973), Vol. 69, No. 127, 53.
123. Morrow, N.R. and Songkran, B.: "Effect of Viscous and Buoyancy Forces on Nonwetting Phase Trapping in Porous Media", *Proceedings of Symposium on Surface Phenomena in Enhanced Oil Recovery*, Stockholm, Sweden, August 20-25, 1979, 387.
124. Wardlaw, N.C.: "Effects of Capillary Number and its Component Variables on Waterflood Efficiency and Oil Mobilisation", AOSTRA J. of Res., (Winter, 1988), Vol. 4, 35.
125. Sokolnikoff, I.S. and Redheffer, R.M.: *Mathematics of Physics and Modern Engineering*, McGraw Hill Book Company, Inc., New York City, (1966), 474.

APPENDIX A: Derivation of Equation Describing the Pseudosurface Separating Oil From Water

Let a coordinate system be so chosen that the fixed, bounding curve of the pseudosurface which separates the oil from the water lies in the x - y plane. Moreover, let the vertical displacement of any point in the pseudosurface at a given amplitude, z , of the surface be denoted by $\xi = \xi(x, y, z)$, where z is supposed to be a function of time. To obtain a differential equation for the pseudosurface, let us consider a small, nearly square portion of the surface bounded by vertical planes through the points $(x, y, 0)$, $(x + \Delta x, y, 0)$, $(x, y + \Delta y, 0)$ and $(x + \Delta x, y + \Delta y, 0)$.

If the surface being considered were an elastic membrane having mass, it would be necessary to apply Newton's law (Force = mass \times acceleration) to the small portion of surface being studied[125]. However, in as much as the surface under consideration is that separating oil from water in a porous medium, it is assumed that the force due to acceleration may be neglected. As a consequence, if the pseudosurface is under uniform tension, T , the vertical component of the force in the x -direction, T_{1v} , is defined by

$$T_{1v} = \Delta y [(\sigma_e \sin \theta_1)_{x+\Delta x} - (\sigma_e \sin \theta_1)_x] \quad (A-1)$$

where σ_e is the pseudointerfacial tension of the surface separating the oil from the water, and where θ_1 is the angle between the tension vector, T_1 , and the x -axis. Similarly, the vertical component of the force in the y -direction, T_{2v} , is defined by

$$T_{2v} = \Delta x [(\sigma_e \sin \theta_2)_{y+\Delta y} - (\sigma_e \sin \theta_2)_y] \quad (A-2)$$

where θ_2 is the angle between the tension vector, T_2 , and the y -axis. In addition, there is a vertical force $P_c(x, y, z)\Delta x\Delta y$ due to the change in pressure across the pseudointerface. Taking

the algebraic sum of the vertical forces yields

$$\Delta y[(\sigma_e \sin \theta_1)_{x+\Delta x} - (\sigma_e \sin \theta_1)_x] + \Delta x[(\sigma_e \sin \theta_2)_{y+\Delta y} - (\sigma_e \sin \theta_2)_y] + P_c(x,y,z) \Delta x \Delta y = 0 \quad (A-3)$$

Upon dividing Equation (A-3) by $\Delta x \Delta y$ and letting $\Delta x \rightarrow 0$ and $\Delta y \rightarrow 0$, it follows that

$$\frac{\partial}{\partial x}(\sigma_e \sin \theta_1) + \frac{\partial}{\partial y}(\sigma_e \sin \theta_2) + P_c(x,y,z) = 0 \quad (A-4)$$

To obtain a simpler equation, it is noted that

$$\sin \theta_1 = \tan \theta_1 (1 + \tan^2 \theta_1)^{-1/2} = \frac{\partial \xi}{\partial x} (1 + (\frac{\partial \xi}{\partial x})^2)^{-1/2} \approx \frac{\partial \xi}{\partial x} \quad (A-5)$$

and

$$\sin \theta_2 = \tan \theta_2 (1 + \tan^2 \theta_2)^{-1/2} = \frac{\partial \xi}{\partial y} (1 + (\frac{\partial \xi}{\partial y})^2)^{-1/2} \approx \frac{\partial \xi}{\partial y} \quad (A-6)$$

provided $(\frac{\partial \xi}{\partial x})^2 \ll 1$ and $(\frac{\partial \xi}{\partial y})^2 \ll 1$. Moreover, if the displacement $\xi = \xi(x,y,z)$ is small, σ_e may be considered to be constant. Substituting these results into Equation (A-4) yields

$$\sigma_e \left[\frac{\partial^2 \xi}{\partial x^2} + \frac{\partial^2 \xi}{\partial y^2} \right] + P_c(x,y,z) = 0 \quad (A-7)$$

where $P_c(x,y,z)$, the pressure difference across the interface, may be viewed as a force function.

APPENDIX B: Functional Equations Used to Fit Data

Following functional equations were used to fit experimental data, using the BMDP statistical package[113] available on the MTS system of the University of Alberta. A typical routine needed for the use of the BMDP package is given in Appendix E.

B.1: Model Equation for Q_w as a Function of S_w

$$Q_w = V_p \left[\left(\frac{c_1}{S_w^2} - \frac{c_1}{S_{wi}^2} \right) + \left(\frac{c_2}{S_w} - \frac{c_2}{S_{wi}} \right) + c_3 \ln \frac{S_w}{S_{wi}} + \left(\frac{S_w - S_{wi}}{1 - S_{or} - S_{wi}} \right) (c_4(1 - S_{or}) + c_1 \left(\frac{1}{S_{wi}^2} - \frac{1}{(1 - S_{or})^2} \right)) + c_2 \left(\frac{1}{S_{wi}} - \frac{1}{1 - S_{or}} \right) c_3 \ln \frac{1 - S_{or}}{S_{wi}} \right] \quad (B.1)$$

B.2: Model Equation for Pressure Distribution Along the Core as a Function of the Core Length

$$P_o = d_1 - d_2x - d_3x^3 - d_4x^4 \quad (B.2)$$

B.3: Model Equation for f_w as a Function of S_w

$$f_w = \frac{S_w - S_{wi}}{S_{wm} - S_{wi} - g_1(S_{wm} - S_w) - g_2(S_{wm}^2 - S_w^2) - g_3(S_{wm}^3 - S_w^3) - g_4(S_{wm}^4 - S_w^4)} \quad (B.3)$$

B.4: Model Equation for k_{ro} as a Function of S_w

$$k_{ro} = h_1(S_{wm} - S_w) + h_2(S_{wm}^2 - S_w^2) + h_3(S_{wm}^3 - S_w^3) + h_4(S_{wm}^4 - S_w^4) \quad (B.4)$$

B.5: Model Equation for k_{rw} as a Function of S_w

$$k_{rw} = e_1(S_w - S_{wi}) + e_2(S_w^2 - S_{wi}^2) + e_3(S_w^3 - S_{wi}^3) + e_4(S_w^4 - S_{wi}^4) \quad (B.5)$$

Table B.1: Parameters for Q_w versus S_w Fit (Run 64)

c_1	- 0.004139
c_2	0.141969
c_3	0.697907
c_4	0.490472

Table B.2: Parameters for P_o versus x Fit (Run 64)

d_1	8.951583
d_2	2.191090
d_3	4.783354
d_4	- 1.950990

Table B.3: Parameters for f_W versus S_W Fit

Run	g_1	g_2	g_3	g_4
63	1.861575	- 5.75345	6.914168	- 2.562075
64	3.045151	- 10.159435	13.464184	- 5.718448
65	- 1.414947	2.829310	- 2.384128	1.165754
66	2.838331	- 9.700067	13.284559	- 5.809513
67	- 1.547248	2.202119	- 0.559711	- 0.019611

Table B.4: Parameters for k_{r0} versus S_w Fit

Run	h_1	h_2	h_3	h_4
63	2.754714	3.196859	3.42201	-1.487726
64	1.525025	-0.699644	0.038002	-0.037505
65	1.491391	-0.456247	0.158959	-0.187807
66	1.426591	-0.427593	0.142298	-0.170093
67	1.453078	-0.597808	0.439170	-0.321856

Table B.5: Parameters for k_{rw} versus S_w Fit

Run	e_1	e_2	e_3	e_4
63	-0.249220	1.469746	-2.651335	1.716503
64	0.265698	-0.398824	1.252327	-0.281678
65	-0.522336	3.111456	-6.241318	4.330461
66	-0.458679	2.827277	-6.020394	4.381274
67	-0.438147	2.605017	-5.370549	3.789289

APPENDIX C: Programs for Data Acquisition, Retrieval and Interpretation

C.1: Data Acquisition

```
10000 REM PROGRAM FOR INSTRUMENT CONTROL AND DATA ACQUISITION;
10010 REM STORES DATA INTO VARIOUS FILES.
10020 REM AUTHOR: HEMANTA KUMAR SARMA
10030 REM DEPT. OF MINING, METALLURGICAL AND PETROLEUM
ENGINEERING
10040 REM UNIVERSITY OF ALBERTA, EDMONTON, CANADA, T6G 2G6
10050 REM LANGUAGE USED: BASIC 4.0 VERSION
10060 REM THIS PROGRAM HAS BEEN WRITTEN AS USER FRIENDLY;
EXPERIMENTER
10070 REM MUST INTERACT AS AND WHEN ASKED TO DO SO.
10080 REM *****DEFINING THE INTEGERS*****
10090 OPTION BASE 1
10100 INTEGER I,J,K,N,M,L
10110 INTEGER II,III,Kk
10120 REM *****DIMENSIONING OF VARIABLES*****
10130 DIM A$(150)[17],Wt$(150)[17]
10140 DIM Ao$(60,100)[17]
10150 DIM Wgt(150),Tb(150),P(15)
10160 DIM Volt(150,14)
10170 DIM V(14),Delp(150),P1(150),P2(150)
10180 DIM T1(150),Tp(60),Tm(60)
10190 DIM T2(60)
10200 DIM Power(60,100),T7(10),Powin(60,100)
10210 DIM T3(10),Pk1(10),Pk2(10),Delpk(10)
10220 PRINTER IS 1
10230 PRINT "Today is :",DATE$(TIMEDATE)
10240 PRINT "Program Started @",TIME$(TIMEDATE)
10250 REM *****ASSIGNMENTS OF PERIPHERALS*****
10260 ASSIGN @Multi TO 723
10270 ASSIGN @Meter TO 713
10280 Sc=9
10290 CONTROL Sc,4;2+0+8+0
10300 CONTROL Sc,5;3
10310 CONTROL Sc,3;300
10320 REM *****ALLOCATE BYTES FOR STORAGE*****
10330 Msus$="":CS80,700,0"
10340 Pwr=101*8
10350 Pr=15*8
10360 REM *****ZEROING OF POWER METER*****
10370 OUTPUT @Multi USING "#.K";"O040TG17TO260T"
10380 REMOTE @Meter
10390 CALL Zero_meter(@Meter)
10400 BEEP
10410 DISP "COMPLETE MICROWAVE POWER AFTER ZERO, HIT CONTINUE"
10420 PAUSE
10430 REM **** ALLOCATE FILE NAMES FOR POWER & PRESSURE DATA ****
10440 INPUT "WATERFLOOD RUN No.?",Run$
10450 INPUT "FILENAME TO STORE MICROWAVE POWER DATA ?",Name$
```

```

10460 INPUT "DRIVE (ie : ,700,1) default current drive?",Msus$
10470 Size_records=Pwr
10480 No_records=60
10490 ON ERROR GOSUB Createfile
10500 ASSIGN @File3 TO Name$&Msus$
10510 OFF ERROR
10520 INPUT "FILENAME TO STORE INPUT POWER DATA ?",Name$
10530 INPUT "DRIVE (ie : ,700,1) default current drive?",Msus$
10540 Size_records=Pwr
10550 No_records=60
10560 ON ERROR GOSUB Createfile
10570 ASSIGN @File10 TO Name$&Msus$
10580 OFF ERROR
10590 INPUT "FILENAME TO STORE PRESSURE DATA ?",Name$
10600 INPUT "DRIVE (ie : ,700,1) default current drive?",Msus$
10610 Size_records=Pr
10620 No_records=150
10630 ON ERROR GOSUB Createfile
10640 ASSIGN @File4 TO Name$&Msus$
10650 OFF ERROR
10660 INPUT "IS BALANCE USED FOR RECOVERY DATA? 1= YES;0= NO",Ibal
10670 IF Ibal=0 THEN GOTO 10750
10680 INPUT "FILENAME FOR STORE BALANCE READINGS ?",Name$
10690 INPUT "DRIVE (ie : ,700,1) default current drive?",Msus$
10700 Size_records=3*8
10710 No_records=150
10720 ON ERROR GOSUB Createfile
10730 ASSIGN @File7 TO Name$&Msus$
10740 OFF ERROR
10750 OUTPUT @Multi USING. "#,K";"0040TG17T0260T"
10760 FOR H=1 TO 14
10770 OUTPUT @Multi USING. "#,K";"FT"
10780 ENTER @Multi;V(H)
10790 V(H)=V(H)-10000
10800 Octal$=VAL$(V(H))
10810 V(H)=DVAL(Octal$,8)
10820 IF V(H)>2047 THEN V(H)=V(H)-4096
10830 V(H)=.005*V(H)
10840 NEXT H
10850 PRINT V(*)
10860 PRINT "DO NOT START THE PUMP YETREMREMREM"
10870 INPUT "FILENAME FOR DATE AND TIME?",Name$
10880 INPUT "DRIVE (ie : ,700,1) default current drive?",Msus$
10890 Size_records=160
10900 No_records=1
10910 ON ERROR GOSUB Createfile
10920 ASSIGN @File5 TO Name$&Msus$
10930 OFF ERROR
10940 PRINTER IS 1
10950 Day$=DATE$(TIMEDATE)
10960 Tim$=TIME$(TIMEDATE)
10970 Tst1=TIMEDATE
10980 PRINT "PLEASE DO NOT HIT ANY KEY, PROGRAM FOR EXPT IS STILL
ACTIVE"
10990 PRINT "BEFORE YOU START WATERFLOOD, CHECK PUMP CONNECTIONS"
11000 BEEP 81.38,10

```

```

11010 PRINT "ADJUST RATE FOR THE TWO CYINDERS OF THE PUMP"
11020 PRINT "WATER CONNECTION IS TO BE CHECKED"
11030 INPUT "TOTAL VOLUME OF WATER TO BE PUMPED (IN CC)?",Tv
11040 INPUT "PUMP RATE SELECTED IN CC/HR?",R
11050 Et=(Tv/R)*3600.0
11060 INPUT "TIME INTERVAL FOR SAT. PROFILE IN SECONDS?",Insat
11070 Inprs=(Et-((Insat+10.81)*59.0))/91.0
11080 PRINT "SATURATION INTERVAL (seconds)",Insat
11090 PRINT "PRESSURE INETRVAL AFTER SCANNING PERIOD",Inprs
11100 BEEP
11110 PRINT "WHEN READY TO GO, HIT CONTINUE"
11120 PAUSE
11130 REM*****BEGINNING OF WATERFLOOD*****
11140 REM*****BALANCE DATA*****
11150 Tst=TIMEDATE
11160 FOR J=1 TO 59
11170 IF Ibal=0 THEN GOTO 11320
11180 Count=1
11190 A$(J)[Count]=" "
11200 REPEAT
11210 STATUS Sc,6;S
11220 UNTIL S=10
11230 REPEAT
11240 STATUS Sc,10;S
11250 IF BIT(S,0) THEN STATUS Sc,6;A
11260 IF BIT(S,0) THEN A$(J)[Count]=A$(J)[Count]&CHR$(A)
11270 IF BIT(S,0) THEN Count=Count+1
11280 IF (Count=2) AND (CHR$(A)<>" ") THEN GOTO 11180
11290 UNTIL Count=17
11300 Tb(J)=TIMEDATE-Tst
11310 DISP Tb(J),A$(J)[1:16]
11320 REM*****
11330 OUTPUT @Multi USING "#,K";"O040TG17TO260T"
11340 T1(J)=TIMEDATE-Tst
11350 FOR N=1 TO 14
11360 OUTPUT @Multi USING "#,K";"FT"
11370 ENTER @Multi;Volt(J,N)
11380 Volt(J,N)=Volt(J,N)/10000
11390 Octal$=VAL$(Volt(J,N))
11400 Volt(J,N)=DVAL(Octal$,8)
11410 IF Volt(J,N)>2047 THEN Volt(J,N)=Volt(J,N)-4096
11420 Volt(J,N)=.005*Volt(J,N)
11430 NEXT N
11440 REM*****MICROWAVE SCAN*****
11450 T2(J)=TIMEDATE-Tst
11460 OUTPUT @Multi;"O0140T@7775T"
11470 WAIT .01
11480 OUTPUT @Multi;"O0140T@7777T"
11490 T8=TIMEDATE
11500 FOR I=1 TO 100
11510 Timel=TIMEDATE
11520 OUTPUT @Multi USING "#,K";"O0240TKT"
11530 OUTPUT @Multi USING "#,K";"JT"
11540 ENTER @Multi;Ao$(J,I)
11550 OUTPUT @Meter;"3A+I"
11560 CALL Read_meter(@Meter,Power(J,I))

```

```

11570 DISP I,Power(J,I),Ao$(J,I)
11580 Time2=TIMEDATE
11590 Time3=.10-(Time2-Time1)
11600 WAIT Time3
11610 NEXT I
11620 T9=TIMEDATE-T8
11630 OUTPUT @Multi;"00140T@7776T"
11640 WAIT .01
11650 OUTPUT @Multi;"00140T@7777T"
11660 DISP J,T9
11670 WAIT Insat
11680 IF J>=59 THEN GOTO 11700
11690 NEXT J
11700 FOR J=60 TO 150
11710 PRINT "CURRENT READING IS",J
11720 REM *****READING THE BALANCE*****
11730 IF Ibal=0 THEN GOTO 11880
11740 Count=1
11750 A$(J)[Count]=" "
11760 REPEAT
11770 STATUS Sc,6;S
11780 UNTIL S=10
11790 REPEAT
11800 STATUS Sc,10;S
11810 IF BIT(S,0) THEN STATUS Sc,6;A
11820 IF BIT(S,0) THEN A$(J)[Count]=A$(J)[Count]&CHR$(A)
11830 IF BIT(S,0) THEN Count=Count+1
11840 IF (Count=2) AND (CHR$(A)<>" "+"") THEN GOTO 11740
11850 UNTIL Count=17
11860 Tb(J)=TIMEDATE-Tst
11870 DISP J,Tb(J),A$(J)[1;16]
11880 OUTPUT @Multi USING "#,K";"0040TG17TO260T"
11890 T1(J)=TIMEDATE-Tst
11900 FOR N=1 TO 14
11910 OUTPUT @Multi USING "#,K";"FT"
11920 ENTER @Multi;Volt(J,N)
11930 Volt(J,N)=Volt(J,N)-10000
11940 Octal$=VAL$(Volt(J,N))
11950 Volt(J,N)=DVAL(Octal$,8)
11960 IF Volt(J,N)>2047 THEN Volt(J,N)=Volt(J,N)-4096
11970 Volt(J,N)=.005*Volt(J,N)
11980 NEXT N
11990 IF J=150 THEN GOTO 12030
12000 WAIT Inprs
12010 NEXT J
12020 REM*****Scan for Saturation Profile @Sor*****
12030 T2(60)=TIMEDATE-Tst
12040 OUTPUT @Multi;"00140T@7775T"
12050 WAIT .01
12060 OUTPUT @Multi;"00140T@7777T"
12070 T88=TIMEDATE
12080 FOR I=1 TO 100
12090 Tiel=TIMEDATE
12100 OUTPUT @Multi USING "#,K";"00240TKT"
12110 OUTPUT @Multi USING "#,K";"KT"
12120 ENTER @Multi;Ao$(60,I)

```

```

12130 OUTPUT @Meter;"3A+I"
12140 CALL Read_meter(@Meter;Power(60,I))
12150 DISP I,Power(60,I),Ao$(60,I)
12160 Tie2=TIMEDATE
12170 Tie3=.10-(Tie2-Tie1)
12180 WAIT Tie3
12190 NEXT I
12200 T99=TIMEDATE-T88
12210 OUTPUT @Multi;"00140T@7776T"
12220 WAIT .01
12230 OUTPUT @Multi;"00140T@7777T"
12240 DISP J;T99
12250 DISP "NOW DATA STORAGE BEGINS"
12260 REM BCD CONVERSION ROUTINE FOR POWER METER HP432C
12270 FOR J=1 TO 60
12280   FOR I=1 TO 100
12290     FOR Ik=1 TO 15
12300       P(Ik)=0
12310     NEXT Ik
12320     FOR K=1 TO 5
12330       C=VAL(Ao$(J,I)[K,K])
12340       IF C=0 THEN
12350         H1=0
12360         H2=0
12370         H3=0
12380       END IF
12390       IF C=1 THEN
12400         H1=0
12410         H2=0
12420         H3=1
12430       END IF
12440       IF C=2 THEN
12450         H1=0
12460         H2=1
12470         H3=0
12480       END IF
12490       IF C=3 THEN
12500         H1=0
12510         H2=1
12520         H3=1
12530       END IF
12540       IF C=4 THEN
12550         H1=1
12560         H2=0
12570         H3=0
12580       END IF
12590       IF C=5 THEN
12600         H1=1
12610         H2=0
12620         H3=1
12630       END IF
12640       IF C=6 THEN
12650         H1=1
12660         H2=1
12670         H3=0
12680       END IF

```



```

12690 IF C=7 THEN
12700   H1=1
12710   H2=1
12720   H3=1
12730 END IF
12740 IF K=1 THEN
12750   P(1)=H1
12760   P(2)=H2
12770   P(3)=H3
12780 END IF
12790 IF K=2 THEN
12800   P(4)=H1
12810   P(5)=H2
12820   P(6)=H3
12830 END IF
12840 IF K=3 THEN
12850   P(7)=H1
12860   P(8)=H2
12870   P(9)=H3
12880 END IF
12890 IF K=4 THEN
12900   P(10)=H1
12910   P(11)=H2
12920   P(12)=H3
12930 END IF
12940 IF K=5 THEN
12950   P(13)=H1
12960   P(14)=H2
12970   P(15)=H3
12980 END IF
12990 NEXT K
13000 Xa=0
13010 Ya=0
13020 Za=0
13030 Ra=0
13040 FOR K=3 TO 1 STEP -1
13050   Xa=Xa+P(K)*2^(3-K)
13060 NEXT K
13070 FOR K=7 TO 4 STEP -1
13080   Ya=Ya+P(K)*2^(7-K)
13090 NEXT K
13100 FOR K=11 TO 8 STEP -1
13110   Za=Za+P(K)*2^(11-K)
13120 NEXT K
13130 FOR K=15 TO 12 STEP -1
13140   Ra=Ra+P(K)*2^(15-K)
13150 NEXT K
13160 Tot=(Xa*1000+Ya*100+Za*10+Ra)/100
13170 IF Tot>12.0 THEN Tot=Tot-10.0
13180 Powin(J,I)=Tot
13190 Power(J,I)=ABS(Power(J,I))*1000.0
13200 NEXT I
13210 DISP J
13220 NEXT J
13230 OUTPUT @File3;T2(*),Power(*)
13240 OUTPUT @File10;T2(*),Powin(*)

```

```

13250 OUTPUT @File5:Day$,Tim$,Run$
13260 FOR J=1 TO 150
13270 REM ..... Conversion To Pressure from Volt.....
13280 Volt(J,1)=(Volt(J,1)-V(1))*7.5
13290 Volt(J,2)=(Volt(J,2)-V(2))*7.5
13300 Volt(J,3)=(Volt(J,3)-V(3))*5
13310 Volt(J,4)=(Volt(J,4)-V(4))*3.0
13320 Volt(J,5)=(Volt(J,5)-V(5))*5
13330 Volt(J,6)=(Volt(J,6)-V(6))*3.0
13340 Volt(J,7)=(Volt(J,7)-V(7))
13350 Volt(J,8)=(Volt(J,8)-V(8))*5
13360 Volt(J,9)=(Volt(J,9)-V(9))*7.5
13370 Volt(J,10)=(Volt(J,10)-V(10))*5
13380 Volt(J,11)=(Volt(J,11)-V(11))*3.0
13390 Volt(J,12)=(Volt(J,12)-V(12))*5
13400 Volt(J,13)=(Volt(J,13)-V(13))
13410 Volt(J,14)=(Volt(J,14)-V(14))*5
13420 NEXT J
13430 WAIT .1
13440 OUTPUT @File4:T1(*),Volt(*)
13450 IF Ibal=0 THEN GOTO 13630
13460 FOR J=1 TO 150
13470 Wt$(J)[1,10]=A$(J)[2,10]
13480 Wgt(J)=VAL(Wt$(J))
13490 NEXT J
13500 OUTPUT @File7:Tb(*),Wgt(*)
13510 INPUT "DATA STORED. TYPE 1 IF PRINTOUTS NEEDED",Ipr
13520 IF Ipr=1 THEN PRINTER IS 701
13530 IF Ipr=1 THEN OUTPUT 701;CHR$(27)&"&11L"
13540 Ru=VAL(Run$)
13550 PRINT USING "" "EXPERIMENT NUMBER : "" ,DDD";Ru
13560 PRINT "DATE OF EXPERIMENT : ",Day$
13570 PRINT "-----"
13580 PRINT " #      Time(sec)   Fluid Wt.(gm) "
13590 PRINT "-----"
13600 FOR J=1 TO 150
13610 PRINT USING "DDD,4X,7D.D,4X,4D.2D";J,Tb(J)-Tb(1),Wgt(J)-Wgt(1)
13620 NEXT J
13630 IF Ipr=1 THEN PRINT CHR$(12)
13640 PRINT USING "" "EXPERIMENT NUMBER : "" ,DDD";Ru
13650 PRINT "DATE OF EXPERIMENT : ",Day$
13660 PRINT "SUMMARY OF PRESSURE DISTRIBUTION DURING THE RUN"
13670 PRINT "NOTE: Last column indicates dP(psi) across the core"
13680 PRINT "-----"
13690 PRINT " "
13700 FOR K=1 TO 150
13710 P1(K)=Volt(K,1)+2.0*(Volt(K,1)-Volt(K,2))/11.0
13720 P2(K)=Volt(K,7)-2.0*(Volt(K,6)-Volt(K,7))/11.0
13730 DelP(K)=P1(K)-P2(K)
13740 PRINT USING "M4D.DD";Volt(K,1),Volt(K,2),Volt(K,3),Volt(K,4),
Volt(K,5),Volt(K,6),Volt(K,7),DelP(K)
13750 PRINT USING "M4D.DD";Volt(K,8),Volt(K,9),Volt(K,10),Volt(K,11),
Volt(K,12),Volt(K,13),Volt(K,14)
13760 NEXT K
13770 BEEP
13780 DISP "PUT PAPER FOR PLOT AND HIT CONTINUE"

```

```

13790 PAUSE
13800 INPUT "DO YOU WANT HARD COPY PLOT ? ANSWER 1=YES 0=NO",Ipl
13810 IF Ipl=1 THEN DISP "CHANGE PAPER ON PLOTTER AND HIT CONTINUE"
13820 IF Ipl=1 THEN PAUSE
13830 PEN 1
13840 GINIT
13850 IF Ipl<>1 THEN PLOTTER IS CRT,"INTERNAL"
13860 IF Ipl=1 THEN PLOTTER IS 705,"HPGL"
13870 GRAPHICS ON
13880 X_gdu_max=100*MAX(1,RATIO)
13890 Y_gdu_max=100*MAX(1,1/RATIO)
13900 LORG 6
13910 REM FOR I=-.3 TO .3 STEP .1
13920 MOVE X_gdu_max/2,Y_gdu_max
13930 LABEL "mW vs X as Function of t"
13940 REM NEXT I
13950 DEG
13960 LDIR 90
13970 CSIZE 3
13980 MOVE 0,Y_gdu_max/2
13990 LABEL "Power (mW)"
14000 LORG 4
14010 LDIR 0
14020 MOVE X_gdu_max/2,.07*Y_gdu_max
14030 LABEL "Length of Core"
14040 VIEWPORT .1*X_gdu_max,.99*X_gdu_max,.15*Y_gdu_max,.9*Y_gdu_max
14050 FRAME
14060 WINDOW 0,.100,0,.MAX(Power(*))
14070 AXES 5.0,.05,0,0,5,5,2
14080 CLIP OFF
14090 CSIZE 2.5,.5
14100 LORG 6
14110 FOR I=0 TO 100 STEP 10
14120 MOVE I,-.1
14130 LABEL USING "#,K";I
14140 NEXT I
14150 LORG 8
14160 FOR I=0 TO MAX(Power(*))
14170 MOVE -.2,I
14180 LABEL USING "#,D.5D";I
14190 NEXT I
14200 PENUP
14210 FOR K=1 TO 60
14220 FOR L=1 TO 100
14230 PLOT L,ABS(Power(K,L))
14240 NEXT L
14250 PENUP
14260 WAIT .1
14270 NEXT K
14280 GRAPHICS OFF
14290 PEN 0
14300 BEEP
14310 INPUT "WANT HARD COPY PLOT ? ANSWER 1=YES 0=NO",Ipl1
14320 IF Ipl1=1 THEN
14330 DISP "CHANGE PAPER FOR PRESSURE PLOT AND HIT CONTINUE"
14340 PAUSE

```

```
14350 END IF
14360 PEN 4
14370 GINIT
14380 IF Ipl1<>1 THEN PLOTTER IS CRT,"INTERNAL"
14390 IF Ipl1=1 THEN PLOTTER IS 705,"HPGL"
14400 GRAPHICS ON
14410 X_gdu_max=100*MAX(1,RATIO)
14420 Y_gdu_max=100*MAX(1,1/RATIO)
14430 LORG 6
14440 MOVE X_gdu_max/2,Y_gdu_max
14450 LABEL "Pressure Distribution Along X"
14460 DEG
14470 LDIR 90
14480 CSIZE 3,5
14490 MOVE 0,Y_gdu_max/2
14500 LABEL "Pressure (psi)"
14510 LORG 4
14520 LDIR 0
14530 MOVE X_gdu_max/2,.07*Y_gdu_max
14540 LABEL "X-differ Location in Core"
14550 VIEWPORT .1*X_gdu_max,.98*X_gdu_max,.15*Y_gdu_max,.9*Y_gdu_max
14560 FRAME
14570 WINDOW 1.,7,0.,MAX(Volt(*))
14580 AXES 1,0,5,0,0,1,5,5,2
14590 CLIP OFF
14600 CSIZE 2.5,.5
14610 LORG 6
14620 FOR I=1 TO 7
14630 MOVE I,-.1
14640 LABEL USING "#,K":I
14650 NEXT I
14660 LORG 8
14670 FOR I=0 TO MAX(Volt(*)) STEP 5
14680 MOVE -.1,I
14690 LABEL USING "#,DDD.DD":I
14700 NEXT I
14710 PENUP
14720 PEN 1
14730 FOR K=1 TO 60 STEP 5
14740 PLOT 1,Volt(K,1)
14750 PLOT 2,Volt(K,2)
14760 PLOT 4,Volt(K,4)
14770 PLOT 6,Volt(K,6)
14780 PLOT 7,Volt(K,7),2
14790 PENUP
14800 PEN,4
14810 WAIT 1
14820 PLOT 2,Volt(K,9)
14830 PLOT 4,Volt(K,11)
14840 PLOT 6,Volt(K,13),2
14850 WAIT .1
14860 PENUP
14870 NEXT K
14880 PEN 0
14890 GRAPHICS OFF
14900 BEEP
```

```

14910 INPUT "HARD COPY PLOT FOR dP? 1=Y 0=N ",Ip2
14920 IF Ip2=1 THEN DISP "CHANGE PAPER ON THE PLOTTER AND HIT
CONTINUE"
14930 IF Ip2=1 THEN PAUSE
14940 PEN 4
14950 GINIT
14960 IF Ip2<>1 THEN PLOTTER IS CRT,"INTERNAL"
14970 IF Ip2=1 THEN PLOTTER IS 705,"HPGL"
14980 GRAPHICS ON
14990 X_gdu_max=100*MAX(1,RATIO)
15000 Y_gdu_max=100*MAX(1,1/RATIO)
15010 LORG 6
15020 MOVE X_gdu_max/2,Y_gdu_max
15030 LABEL "DIFFERENTIAL PRESSURE = f(TIME)"
15040 DEG
15050 LDIR 90
15060 CSIZE 3.5
15070 MOVE 0,Y_gdu_max/2
15080 LABEL "Pressure (psi)"
15090 LORG 4
15100 LDIR 0
15110 MOVE X_gdu_max/2,.07*Y_gdu_max
15120 LABEL "Time (sec)"
15130 VIEWPORT .1*X_gdu_max,.98*X_gdu_max,.15*Y_gdu_max,.9*Y_gdu_max
15140 FRAME
15150 WINDOW 0.,MAX(T1(*)),0.,MAX(Volt(*))
15160 AXES 500.,5,0,0,0,5,5,2
15170 CLIP OFF
15180 CSIZE 2.5,.5
15190 LORG 6
15200 FOR I=0 TO MAX(T1(*)) STEP 2000
15210 MOVE I,-.2
15220 LABEL USING "#,K";I
15230 NEXT I
15240 LORG 8
15250 FOR I=0 TO MAX(Volt(*)) STEP 10
15260 MOVE -.2,I
15270 LABEL USING "#,DDD.D";I
15280 NEXT I
15290 PENUP
15300 PEN 4
15310 FOR K=1 TO 150
15320 PLOT T1(K),Delp(K)
15330 NEXT K
15340 PEN 0
15350 GRAPHICS OFF
15360 DISP "YOU ARE DONE WITH EXPT. GO HOME. "
15370 GOTO 15420
15380 REM*****Creating Storage Files*****
15390 Createfile:REM
15400 CREATE BDAT Name$&Msus$,Size_records,No_records
15410 RETURN
15420 END
15430 SUB Zero_meter(@Meter)
15440 Rezero:OUTPUT @Meter;"ZIT"
15450 ENTER @Meter;Power

```

```
15460 IF ABS(Power)>2 THEN Rezero
15470 Unzero:OUTPUT @Meter;"3 + A1"
15480 ENTER @Meter;Power
15490 IF Power>=84 THEN Unzero
15500 Preset:OUTPUT @Meter;"3A + I"
15510 SUBEND
15520 SUB Read_meter(@Meter,Power)
15530 ENTER @Meter;Power
15540 SUBEND
```

C.2: Data Retrieval and Interpretation

```

10000 REM PROGRAM FOR DATA RETRIEVAL AND ANALYSIS FOR WATER FLOOD
10010 REM EXPERIMENT. DATA FILES ARE RETIEVAL BY CALLING THEM BY
10020 REM THEIR APPRPRIATE NAMES. THE PROGRAM IS INTERACTIVE.
10030 REM SOME ANALYSES ARE OPTIONAL, AND CAN BE BY-PASSED.
10040 REM AUTHOR: HEMANTA KUMAR SARMA
10050 REM      DEPT. OF MINING, MET. AND PETROLEUM ENGINEERING
10060 REM      UNIVERSITY OF ALBERTA, EDMONTON, CANADA, T6G 2G6
10070 REM*****DIMENSIONALISING OF VARIABLES*****
10080 OPTION BASE 1
10090 INTEGER J,K,N,H,M,L
10100 INTEGER Npoint,Nend,Ipoint,Nbegin,Nhalf
10110 DIM Sw(60,100),Aaw(60,100),Ccc(100),Bomb(100)
10120 DIM AS(150)[17],Wt$(150)[17]
10130 DIM Wgt(150),Tb(150),Vol(150)
10140 DIM Tbb(151),Wgtt(151)
10150 DIM Volt(150,14),Akw(150),Ako(150)
10160 DIM Perm(150)
10170 DIM V(14),Delp(150),P1(150),P2(150)
10180 DIM Vol1(150),Vol2(150),Vol3(150)
10190 DIM T1(150),Tp(60),Tm(60),Powin(60,100)
10200 DIM T2(60)
10210 DIM Power(60,100),T7(10)
10220 DIM T3(10),Pko(10,14),Pk1(10),Pk2(10),Delpk(10),Perm1(10)
10230 INPUT "DO YOU WANT HARD COPY PRINTOUT ? ... 1=YES;0=NO",Ipr
10240 INPUT "DO YOU WANT HARD COPY PLOT ? ... 1=YES;0=NON",Ipl
10250 IF Ipr=1 THEN OUTPUT 701;CHR$(27)&"&11L"
10260 REM*****RETRIEVING DATA FROM THE
FILES*****
10270 REM
10280 INPUT "FILENAME FOR DATE AND TIME EXPT. STARTED",Name$
10290 ASSIGN @File5 TO Name$
10300 INPUT "ENTER FILENAME POWER METER DATA",Name$
10310 ASSIGN @File3 TO Name$
10320 INPUT "ENTER FILENAME FOR PRESSURE DATA",Name$
10330 ASSIGN @File4 TO Name$
10340 INPUT "ENTER FILENAME FOR PERMEABILITY DATA",Name$
10350 ASSIGN @File6 TO Name$
10360 INPUT "ENTER FILENAME FOR BALANCE WEIGHT DATA",Name$
10370 ASSIGN @File7 TO Name$
10380 ENTER @File7;Tb(*),Wgt(*)
10390 ENTER @File3;T2(*),Power(*)
10400 ENTER @File4;T1(*),Volt(*)
10410 ENTER @File5;Day$,Tim$,Run$
10420 ENTER @File6;T3(*),Pko(*)
10430 Ru=VAL(Run$)
10440 INPUT "ENTER FILENAME FOR INPUT POWER METER DATA",Name$
10450 ASSIGN @File10 TO Name$
10460 ENTER @File10;Powin(*)
10470 Time=T1(150)
10480 PRINTER IS 1
10490 INPUT "PUMP FLOWRATE in CC/HR?",Rate
10500 INPUT "OBSERVED BREAKTHROUGH TIME DURING EXPT.?",Bt

```

```

10510 INPUT "OBSERVED OIL RECOVERY @BREAKTHROUGH IN GMS ? ",Gram
10520 INPUT "DENSITY OF DISPLACING FLUID i.e. WATER? ",Rhow
10530 INPUT "OIL USED? 1=LAGO,2=MCT5,3=MCT5+LAGO,4=MCT10",Ioil
10540 IF Ioil=1 THEN
10550   Rhoo=.7963
10560   Ac=16342.0
10570   Visl=4.7
10580 END IF
10590 IF Ioil=2 THEN
10600   Rhoo=.8123
10610   Ac=13566.0
10620   Visl=34.2
10630 END IF
10640 IF Ioil=3 THEN
10650   Rhoo=.8043
10660   Ac=14185.0
10670   Visl=11.1
10680 END IF
10690 IF Ioil=4 THEN
10700   Rhoo=.8576
10710   Ac=13573.0
10720   Visl=60.0
10730 END IF
10740 Bulkvol=625.0
10750 INPUT "ENTER PORE VOLUME OF THE SANDPACK IN CC ? ",Pv
10760 Por=Pv/Bulkvol
10770 INPUT "ENTER IRREDUCIBLE WATER SATURATION",Swr
10780 INPUT "ENTER RESIDUAL OIL SATURATION",Sor
10790 REM EXTRAPOLATE INTERNAL PRESSURES AT OUTLET ENDS
10800 FOR K=1 TO 150
10810   P1(K)=ABS(Volt(K,1)+2.0*(Volt(K,1)-Volt(K,2))/11.0)
10820   P2(K)=ABS(Volt(K,7)-2.0*(Volt(K,6)-Volt(K,7))/11.0)
10830   Delp(K)=ABS(P1(K)-P2(K))
10840 NEXT K
10850 INPUT "ENTER THE LENGTH OF COREHOLDER IN CM",Al
10860 INPUT "ENTER THE CROSS-SECTIONAL ARE OF SANDPACK",A
10870 Porvol=Al*A*Por
10880 Rate=Rate/3600.0
10890 IF Ipr=1 THEN PRINTER IS 701
10900 IF Ibal=0 THEN GOTO 11280
10910 PRINT USING "" "EXPERIMENTAL RUN No. "" ".3D";Ru
10920 PRINT USING "" "Time @Breakthrough (sec) "" ".6D.2D";Bt
10930 PRINT USING "" "Cum. Oil Recovery @Breakthrough (gm) "" ".3D.2D";Gram
10940 PRINT " "
10950 PRINT " "
10960 PRINT " #    TIME(s)  OIL(cc)  OIL(pv)  Total(gm)  Sw"
10970 PRINT "-----"
10980 Vol1(1)=0.
10990 Vol2(1)=0.
11000 Wi=Wgt(1)
11010 Tbi=Tb(1)
11020 FOR K=1 TO 150
11030   IF Tb(K)<=Bt THEN Tbb(K)=Tb(K)
11040   IF Tb(K)<=Bt THEN Wgtt(K)=Wgt(K)
11050   IF Tb(K)>Bt THEN GOTO 11070
11060 NEXT K

```



```

11070 Kbt=K
11080 FOR I=K TO 150
11090 Tbb(I+1)=Tb(I)
11100 Wgtt(I+1)=Wgt(I)
11110 NEXT I
11120 Tbb(Kbt)=Bt
11130 Wgtt(Kbt)=Gram
11140 FOR K=2 TO 151
11150 IF Tbb(K) <= Bt THEN Vol1(K-1)=(Wgtt(K)-Wgtt(1))/Rho0
11160 IF Tbb(K) > Bt THEN GOTO 11180
11170 NEXT K
11180 FOR K=2 TO 151
11190 IF Tbb(K) > Bt THEN Vol2(K-1)=((Tbb(K)-Bt)*Rhow*Rate-
(Wgtt(K)-Gram))/(Rhow-Rho0)
11200 NEXT K
11210 PRINTER IS 1
11220 FOR K=1 TO 150
11230 Vol3(K)=Vol1(K)+Vol2(K)
11240 Oilpv=Vol3(K)/Pv
11250 Savg=Swr+Oilpv
11260 PRINT USING "3D,3X,7D.D,3X,4D,2D,3X,D,3D,3X,15D,2D,3X,D,DDD";
K,Tb(K),Vol3(K),Oilpv,Wgtt(K)-Wgtt(1),Savg
11270 NEXT K
11280 INPUT "ENTER VISCOSITY OF WATER IN CP",Vis
11290 FOR K=1 TO 10
11300 Pk1(K)=ABS(Pko(K,1)+2.0*(Pko(K,1)-Pko(K,2))/11.0)
11310 Pk2(K)=ABS(Pko(K,7)-2.0*(Pko(K,6)-Pko(K,7))/11.0)
11320 Delpk(K)=ABS(Pk1(K)-Pk2(K))
11330 Perml(K)=(Rate*Vis1*Al*14.696)/(A*Delpk(K))
11340 NEXT K
11350 S1=0
11360 FOR K=1 TO 10
11370 S1=S1+Perml(K)
11380 NEXT K
11390 St1=S1/10.0
11400 Sc1=St1*9.869233E-9
11410 S=0
11420 FOR K=141 TO 150
11430 Perm(K)=(Rate*Vis*Al*14.696)/(A*Delp(K))
11440 S=S+Perm(K)
11450 NEXT K
11460 St=S/10.0
11470 Sc=St*9.869233E-9
11480 DISP "SET PRINTER TO A NEW PAGE i.e. PRESS FF AND THEN HIT
CONTINUE"
11490 PAUSE
11500 IF Ipr=1 THEN PRINTER IS 701
11510 PRINT USING "" "EXPERIMENTAL RUN No. ",3A";Run$
11520 PRINT "DATE OF EXPERIMENT ",Day$
11530 PRINT "TIME EXPT. STARTED ",Tim$
11540 PRINT "-----"
11550 PRINT " "
11560 PRINT USING "" "VISCOSITY OF DISPLACED FLUID, CP ",3D.DD";Vis1
11570 PRINT USING "" "VISCOSITY OF DISPLACING FLUID, CP ",3D.DD";Vis
11580 PRINT USING "" "DENSITY OF DISPLACED FLUID, GM/CC ",D,4D";Rho0
11590 PRINT USING "" "VOLUMETRIC FLOWRATE, CC/SEC ",D,5D";Rate

```

```

11600 PRINT USING "" "LENGTH OF COREHOLDER, CM"
11610 PRINT USING "" "RECTANGULAR AREA OF PACK, CM**2"
11620 PRINT USING "" "AVG Kwor @ Sor (cm**2)"
11630 PRINT USING "" "AVG Koiv @ Swr (cm**2)"
11640 Amr = St*Vis1/(St1*Vis)
11650 R1 = (1.0-Swr-Sor)/(1.0-Swr)
11660 R2 = ((Amr-1.0)/(Amr+1.0))*((Amr^(2./3.)-1.0)/Amr^(2./3.))
11670 R2 = 1.0/(1.0+R2)
11680 Rbt1 = R1*R2
11690 R3 = 1.0/(1.0+3.0*R2)
11700 Rbt2 = R1*R3
11710 PRINT USING "" "Kwor (darcy)"
11720 PRINT USING "" "Koiv (darcy)"
11730 PRINT USING "" "MOBILITY RATIO"
11740 PRINT USING "" "Rbt IN STABLE DISPLACEMENT"
11750 PRINT USING "" "Rbt IN PSEUDO-STABLE DISPLACEMENT"
11760 PRINT USING "" "POROSITY"
11770 PRINT USING "" "SWR"
11780 PRINT USING "" "SOR"
11790 Sige = Ac*Por*(1.0-Sor-Swr)
11800 Grv = (Amr-1.0)/(Sc*Sige)*Vis/100.0
11810 Gr2 = (Amr^(5./3.)+1.)/((Amr+1.)*(Amr^(1./3.)+1.)^2)
11820 Vel = Rate/A
11830 Gr1 = (Vis/100*Vel*(Amr-1.0))/(Sc*Sige)
11840 IF Ru < 14 THEN Gr3 = 4.0*4.7861507^2/(4.7861507^2+1.0)
11850 IF Ru >= 14 THEN Gr3 = 4.0*5.58^2/(5.215^2+1.07^2)
11860 Stab = Gr1*Gr2*Gr3
11870 Vc = (3.141592653^2)/(Grv*Gr2*Gr3)
11880 Qc = Vc*A*3600.0
11890 Aisr = 3.141592653^2
11900 PRINT USING "" "CRITICAL VELOCITY (cm/sec)"
11910 PRINT USING "" "CRITICAL FLOWRATE (cc/hr)"
11920 PRINT USING "" "PUMP RATE USED (cc/hr)"
11930 PRINT USING "" "STABILITY No. OBTAINED, Isr"
11940 PRINT USING "" "CRITICAL STABILITY No., Isrc"
11950 DISP "Isr OBTAINED. HIT CONTINUE IF YOU PROCEED FURTHER"
11960 PAUSE
11970 PRINTER IS 1
11980 FOR J=1 TO 100
11990 Bomb(J) = 1./(1.-Sor-Swr)*LOG(Power(60,J)/Power(1,J))
12000 Ccc(J) = LOG(Power(1,J)/Ao) - Bomb(J)*Swr
12010 NEXT J
12020 FOR K=1 TO 60
12030 FOR J=1 TO 100
12040 Sw(K,J) = (LOG(Power(K,J)/Ao) - Ccc(J))/Bomb(J)
12050 IF Sw(K,J) > .9 THEN Sw(K,J) = .9
12060 PRINT K,J,Sw(K,J)
12070 NEXT J
12080 DISP K
12090 NEXT K
12100 PRINTER IS 1
12110 INPUT "WANT INTEGRATION OF SATURATION DATA, 1=YES 0=NO ?", Idsat
12120 IF Idsat=0 THEN GOTO 12710
12130 PRINT "INTEGRATION OF DIMENSIONLESS SATURATION ALONG LENGTH"
12140 PRINT "-----"
12150 PRINT "BOTH SIMPSON'S 1/3 AND 3/8 RULES APPLIED."

```

```

12160 PRINT "BOTH RULES REQUIRED FOR ODD No. OF INTERVALS."
12170 PRINT "IN CASE OF EVEN NUMBER: 1/3 RULE; IN CASE OF ODD"
12180 PRINT "INTERVALS: 3/8 RULE FOR FIRST 3 PANELS AND,"
12190 PRINT "1/3rd RULE FOR THE REST."
12200 REM INCREMENT IN DIMENSIONLESS DISTANCE
12210 REAL Hx,Sss(60)
12220 Hx=1
12230 INPUT "ENTER NUMBER OF DATA POINTS i.e. NPOINT",Npoint
12240 Xd=Hx*Npoint
12250 PRINT " "
12260 PRINT " "
12270 PRINT "EXPERIMENTAL RUN NUMBER",Run$
12280 PRINT "DATE OF EXPERIMENT",Day$
12290 PRINT "TIME EXPT STARTED",Tim$
12300 PRINT USING ""Qo in PV AT DIMENSIONLESS DISTANCE = ""3D.DD";Xd
12310 PRINT "-----"
12320 PRINT "TIME(sec)      Qo(py)"
12330 PRINT "-----"
12340 Ipoint=Npoint-1
12350 Nhalf=Ipoint/2
12360 FOR K=1 TO 60
12370   Nbegin=1
12380   Ssw=0.
12390   IF (Ipoint-(2*Nhalf))=0 THEN GOTO 12450
12400 REM IF No. OF PANELS ODD, USE 3/8 RULE ON FIRST 3 PANELS.
12410 REM 1/3 RULE ON REST OF THEM
12420   Ssw=3.*Hx/8.*(Sw(K,1)+3.0*Sw(K,2)+3.*Sw(K,3)+Sw(K,4))
12430   Nbegin=4
12440 REM NOW APPLY 1/3 RULE - ADD 1st, 2nd AND LAST VALUES
12450   Ssw=Ssw+Hx/3.*(Sw(K,Nbegin)+4.0*Sw(K,Nbegin+1)+Sw(K,Npoint))
12460   Nbegin=Nbegin+2
12470   IF Nbegin=Npoint THEN GOTO 12530
12480 REM PATTERN AFTER (Nbegin+2) IS REPETITIVE TILL NEND
12490   Nend=Npoint-2
12500   FOR J=Nbegin TO Nend STEP 2
12510     Ssw=Ssw+Hx/3.0*(2.*Sw(K,J)+4.0*Sw(K,J+1))
12520   NEXT J
12530 PRINT USING "5D.DD,5X,MDD.DDDE";T2(K),Ssw,
12540 T2(K)=Rate*T2(K)/(A*Al*Por*(1.0-Sor-Swr))
12550 Sss(K)=Ssw/100.0
12560 NEXT K
12570 PRINT "DERIVATIVE CUM OIL RECOVERY, W.R.T. DIMENSIONLESS TIME"
12580 REAL Df(60)
12590 K=60
12600 Kk1=K-1
12610 FOR Kk2=2 TO Kk1
12620   Df(Kk2)=(Sss(Kk2+1)-Sss(Kk2-1))/(2.0*(T2(Kk2+1)-T2(Kk2)))
12630 NEXT Kk2
12640 Df(1)=(2.*Sss(2)-1.5*Sss(1)-.5*Sss(3))/(T2(2)-T2(1))
12650 Df(K)=(1.5*Sss(K)-2.0*Sss(K-1)+.5*Sss(K-2))/(T2(K)-T2(K-1))
12660 Ttime=T2(60)
12670 FOR I=1 TO 60
12680 REM PRINT USING "3D,3X,2D.3D,3X,D.3D,3X,2D.3D";I,T2(I),Sss(I),Df(I)
12690 NEXT I
12700 REM DERIVATIVE OF PRESSURES AT A GIVEN DIMESIONLESS LENGTH
12710 PRINTER IS 1

```

```

12720 INPUT "WANT TO SMOOTHEN PRESSURE DATA, 1=Y 0=N?".Ipd
12730 IF Ipd=0 THEN GOTO 14300
12740 PRINT "SMOOTHENING OF PRESSURE DATA ALONG DIMNESIONLESS
LENGTH"
12750 PRINT "-----"
12760 PRINT " "
12770 PRINT " "
12780 REAL X(11),Psi(60,11)
12790 FOR I=1 TO 60
12800 Psi(I,1)=P1(I)
12810 Psi(I,2)=Volt(I,1)
12820 Psi(I,3)=Volt(I,2)
12830 Psi(I,4)=Volt(I,4)
12840 Psi(I,5)=Volt(I,6)
12850 Psi(I,6)=Volt(I,7)
12860 Psi(I,7)=P2(I)
12870 NEXT I
12880 GOTO 12960
12890 Psi(60,1)=P1(150)
12900 Psi(60,2)=Volt(150,1)
12910 Psi(60,3)=Volt(150,2)
12920 Psi(60,4)=Volt(150,4)
12930 Psi(60,5)=Volt(150,6)
12940 Psi(60,6)=Volt(150,7)
12950 Psi(60,7)=P2(150)
12960 X(1)=0.
12970 X(2)=.0102
12980 X(3)=.12245
12990 X(4)=.50
13000 X(5)=.87755
13010 X(6)=.98979
13020 X(7)=1.0
13030 Np=7
13040 REM SMOOTH UNEQUISPACED PRESSURE DATA - VARIABLE H
13050 REM NP=NO. OF DATA PAIRS
13060 REM MS, MF = RANGE OF DEGREE OF POLYNOMIALS, MAXM DEGREE=9
13070 REM AA=AUGMENTED ARRAY OF COEFFICIENT OF NORMAL EQNS
13080 REM CC=ARRAY OF COEFFS OF LEAST SQUARE POLYNOMIAL
13090 REAL Aa(8,9),Cc(10),Xn(11)
13100 INTEGER Mf,Ms,Mfp1,Mfp2,Msp1,Kk,Ii,J1,Iint,Jm1,Iml,Ipt
13110 INTEGER Icoef,Jcoef,Ia,Ic,I
13120 INPUT "SMALLEST DEGREE OF POLYNOMIAL",Ms
13130 INPUT "GREATEST DEGREE OF POLYNOMIAL",Mf
13140 IF Mf<=(Np-1) THEN GOTO 13170
13150 Mf=Np-1
13160 PRINT "DEGREE OF POLYNOMIAL TOO LARGE. REDUCED TO ",Mf
13170 Mfp1=Mf+1
13180 Mfp2=Mf+2
13190 Kk=1
13200 IF Kk>6 THEN GOTO 18004
13210 FOR Ia=1 TO Mfp1
13220 FOR I_=1 TO Mfp2
13230 Aa(Ia,I_)=0.
13240 NEXT I_
13250 NEXT Ia
13260 PRINT USING "" "SCAN"" ,2D",Kk

```

```

13270 FOR I=1 TO Np
13280  Xn(I)=1.0
13290 NEXT I
13300 FOR I=1 TO Mfp1
13310  Aa(I,1)=0.
13320  Aa(I,Mfp2)=0.
13330  FOR N=1 TO Np
13340    Aa(I,1)=Aa(I,1)+Xn(N)
13350    Aa(I,Mfp2)=Aa(I,Mfp2)+Psi(Kk,N)*Xn(N)
13360    Xn(N)=Xn(N)*X(N)
13370  NEXT N
13380 NEXT I
13390 FOR I=2 TO Mfp1
13400  Aa(Mfp1,I)=0.
13410  FOR J=1 TO Np
13420    Aa(Mfp1,I)=Aa(Mfp1,I)+Xn(J)
13430    Xn(J)=Xn(J)*X(J)
13440  NEXT J
13450 NEXT I
13460 FOR J=2 TO Mfp1
13470  FOR I=1 TO Mf
13480    Aa(I,J)=Aa(I+1,J-1)
13490  NEXT I
13500 NEXT J
13510 PRINT "THE MATRIX OF NORMAL EQUATIONS"
13520 PRINT "-----"
13530 PRINT " "
13540 PRINT " "
13550 FOR J1=1 TO Mfp1
13560  PRINT USING "SSD.4D";Aa(J1,1),Aa(J1,2),Aa(J1,3),Aa(J1,4),
Aa(J1,5),Aa(J1,6),Aa(J1,7),Aa(J1,8),Aa(J1,9)
13570 NEXT J1
13580 PRINT " "
13590 PRINT " "
13600 REM L-U DECOMPOSITION OF AA. FORMS L-U EQUIVALENT
13610 REM OF SQUARE COEFFICIENT MATRIX, AA.
13620 FOR I=1 TO Mfp1
13630  FOR J=2 TO Mfp1
13640    Sumbl=0.
13650    IF J>I THEN GOTO 13720
13660    Jml=J-1
13670    FOR K=1 TO Jml
13680      Sumbl=Sumbl+Aa(I,K)*Aa(K,J)
13690    NEXT K
13700    Aa(I,J)=Aa(I,J)-Sumbl
13710    GOTO 13790
13720    Im1=I-1
13730    IF Im1=0 THEN GOTO 13770
13740    FOR K=1 TO Im1
13750      Sumbl=Sumbl+Aa(I,K)*Aa(K,J)
13760    NEXT K
13770    IF ABS(Aa(I,I))<1.0E-10 THEN GOTO 13820
13780    Aa(I,J)=(Aa(I,J)-Sumbl)/Aa(I,I)
13790  NEXT J
13800 NEXT I
13810 GOTO 13830

```

```

13820 PRINT "REDUCTION INCOMPLETE DUE TO SMALL DIVISOR VALUE IN ROW
      I
13830 Msp1=Ms+1
13840 FOR Ii=Msp1 TO Mfp1
13850   FOR J=1 TO Ii
13860     Cc(J)=Aa(J,Mfp2)
13870   NEXT J
13880   Cc(1)=Cc(1)/Aa(1,1)
13890   FOR I=2 TO Ii
13900     Imp=I-1
13910     Sumb2=0.
13920     FOR K=1 TO Imp
13930       Sumb2=Sumb2+Aa(I,K)*Cc(K)
13940     NEXT K
13950     Cc(I)=(Cc(I)-Sumb2)/Aa(I,I)
13960   NEXT I
13970   FOR J=2 TO Ii
13980     Nmjp2=Ii-J+2
13990     Nmjpl=Ii-J+1
14000     Sumb2=0.
14010     FOR K=Nmjp2 TO Ii
14020       Sumb2=Sumb2+Aa(Nmjpl,K)*Cc(K)
14030     NEXT K
14040     Cc(Nmjpl)=Cc(Nmjpl)-Sumb2
14050   NEXT J
14060   Imt=Ii-1
14070   PRINT USING "" "COEFFICIENTS FOR DEGREE = "",DD";Imt
14080   FOR Ih=1 TO Ii
14090     PRINT USING "DD,3X,S6D.8D";Ih-1,Cc(Ih)
14100   NEXT Ih
14110   Beta=0.
14120   Sumb=0.
14130   FOR Ipt=1 TO Np
14140     FOR Icoef=2 TO Ii
14150       Jcoef=Ii-Icoef+2
14160       Sumb=(Sumb+Cc(Jcoef))*X(Ipt)
14170     NEXT Icoef
14180     Sumb=Sumb+Cc(1)
14190     Beta=(Psi(Kk,Ipt)-Sumb)^2
14200   NEXT Ipt
14210   Beta=Beta/(Np-Ii)
14220   PRINT "          STATISTICAL VARIANCE, BETA^2",Beta
14230   FOR Ic=1 TO Ii
14240     Cc(Ic)=0.
14250   NEXT Ic
14260 NEXT Ii
14270 PRINT "PICK THE COEFFICIENTS WITH LEAST BETA FOR CURVE FITTING"
14280 Kk=Kk+1
14290 GOTO 13300
14300 DISP "PLOT BEGINS, FIRST PLOT WILL BE CUM OIL RECOVERY VS. TIME"
14310 BEEP
14320 PAUSE
14330 PEN 4
14340 GINIT
14350 PEN 4
14360 IF Ipl=1 THEN PLOTTER IS 705,"HPGL"

```

```

14370 IF Ipl<>1 THEN PLOTTER IS CRT,"INTERNAL"
14380 GRAPHICS ON
14390 X_gdu_max=100*MAX(1,RATIO)
14400 Y_gdu_max=100*MAX(1,1/RATIO)
14410 LORG 6
14420 MOVE X_gdu_max/2,Y_gdu_max
14430 LABEL USING "" "CUM. OIL RECOVERY IN CC, RUN"" ,DDD";Ru
14440 DEG
14450 LDIR 90
14460 CSIZE 3.5
14470 MOVE 0,Y_gdu_max/2
14480 LABEL "OIL RECOVERY (CC)"
14490 LORG 4
14500 LDIR 0
14510 MOVE X_gdu_max/2,.07*Y_gdu_max
14520 LABEL USING "" "TIME (SEC), Tmax="" ,6D.D";MAX(Tb(*))
14530 VIEWPORT .1*X_gdu_max,.98*X_gdu_max,.15*Y_gdu_max,.9*Y_gdu_max
14540 FRAME
14550 WINDOW 0.,MAX(Tb(*)),0.,250.0
14560 AXES 2000,25.0;0,0,5,5,2
14570 CLIP OFF
14580 CSIZE 2.5,.5
14590 LORG 6
14600 FOR I=0 TO MAX(Tb(*)) STEP 2000
14610 MOVE I,-.2
14620 LABEL USING "#,K";I
14630 NEXT I
14640 LORG 8
14650 FOR I=0 TO 250 STEP 25
14660 MOVE -.2,I
14670 LABEL USING "#,DDDD.DD";I
14680 NEXT I
14690 PENUP
14700 PEN 4
14710 FOR K=1 TO 150
14720 PLOT Tb(K),Cumoil(K)
14730 NEXT K
14740 PEN 0
14750 GRAPHICS OFF
14760 BEEP
14770 DISP "NOW OBTAIN DIFFERENTIAL PRESSURE AS FUNCTION OF TIME
PLOT"
14780 PAUSE
14790 PEN 4
14800 GINIT
14810 PEN 4
14820 IF Ipl=1 THEN PLOTTER IS 705,"HPGL"
14830 IF Ipl<>1 THEN PLOTTER IS CRT,"INTERNAL"
14840 GRAPHICS ON
14850 X_gdu_max=100*MAX(1,RATIO)
14860 Y_gdu_max=100*MAX(1,1/RATIO)
14870 LORG 6
14880 MOVE X_gdu_max/2,Y_gdu_max
14890 LABEL USING "" "DIFF PRESSURE AS FUNCTION OF TIME, RUN"" ,3D";Ru
14900 DEG
14910 LDIR 90

```

```

14920 CSIZE 3.5
14930 MOVE 0,Y_gdu_max/2
14940 LABEL USING "" "PRESSURE (psi), dPmax = "" ,3D.2D";MAX(Delp(*))
14950 LORG 4
14960 LDIR 0
14970 MOVE X_gdu_max/2,.07*Y_gdu_max
14980 LABEL USING "" "TIME (SECONDS), Tmax = "" ,6D.D";MAX(T1(*))
14990 VIEWPORT .1*X_gdu_max,.98*X_gdu_max,.15*Y_gdu_max,.9*Y_gdu_max
15000 FRAME
15010 WINDOW 0,T1(150),0..MAX(Delp(*))
15020 AXES 2000.,10.0,0,0,5,5,2
15030 CLIP OFF
15040 CSIZE 2.5,.5
15050 LORG 6
15060 FOR I=0 TO T1(150)-STEP 2000
15070 MOVE I,-.2
15080 LABEL USING "#,K";I
15090 NEXT I
15100 LORG 8
15110 FOR I=0 TO MAX(Delp(*)) STEP 10
15120 MOVE -.2,I
15130 LABEL USING "#,DDD.DD";I
15140 NEXT I
15150 PENUP
15160 PEN 4
15170 FOR K=1 TO 150
15180 PLOT T1(K),Delp(K)
15190 NEXT K
15200 PEN 0
15210 GRAPHICS OFF
15220 BEEP
15230 PRINTER IS 1
15240 DISP "OBTAIN SATURATION PROFILES"
15250 BEEP
15260 PAUSE
15270 PEN 4
15280 GINIT
15290 PEN 4
15300 IF Ipl=1 THEN PLOTTER IS 705,"HPGL"
15310 IF Ipl<>1 THEN PLOTTER IS CRT,"INTERNAL"
15320 GRAPHICS ON
15330 X_gdu_max=100*MAX(1,RATIO)
15340 Y_gdu_max=100*MAX(1,1/RATIO)
15350 LORG 6
15360 REM FOR I=-.3 TO .3 STEP .1
15370 MOVE X_gdu_max/2,Y_gdu_max
15380 LABEL USING "" "Sw PROFILES VS. TIME, RUN "" ,DDD";Ru
15390 REM NEXT I
15400 DEG
15410 LDIR 90
15420 CSIZE 3
15430 MOVE 0,Y_gdu_max/2
15440 LABEL "Sw (fraction)"
15450 LORG 4
15460 LDIR 0
15470 MOVE X_gdu_max/2,.07*Y_gdu_max

```



```

15480 LABEL "CORE LENGTH"
15490 VIEWPORT .1*X_gdu_max,.99*X_gdu_max,.15*Y_gdu_max,.9*Y_gdu_max
15500 FRAME
15510 WINDOW 0,.100,0,.100.0
15520 AXES 10,10,0,0,5,5,2
15530 CLIP OFF
15540 CSIZE 2.5,.5
15550 LORG 6
15560 FOR I=0 TO 100 STEP 10
15570 MOVE I,-.2
15580 LABEL USING "#,K";I
15590 NEXT I
15600 LORG 8
15610 FOR I=0 TO 100 STEP 10
15620 MOVE -.2,I
15630 LABEL USING "#,DDD.D";I
15640 NEXT I
15650 PEN 1
15660 FOR K=1 TO 40 STEP 5
15670 FOR L=1 TO 100
15680 PLOT L,Sw(K,L)*100
15690 NEXT L
15700 PENUP
15710 NEXT K
15720 GRAPHICS OFF
15730 PEN 0
15740 BEEP
15750 DISP "OBTAIN SCAN PROFILES ALONG THE CORE"
15760 PAUSE
15770 PEN 1
15780 GINIT
15790 PEN 1
15800 IF Ipl=1 THEN PLOTTER IS 705,"HPGL"
15810 IF Ipl<>1 THEN PLOTTER IS CRT,"INTERNAL"
15820 GRAPHICS ON
15830 X_gdu_max=100*MAX(1,RATIO)
15840 Y_gdu_max=100*MAX(1,1/RATIO)
15850 LORG 6
15860 REM FOR I=-.3 TO .3 STEP .1
15870 MOVE X_gdu_max/2,Y_gdu_max/2
15880 LABEL USING "" "SCAN PROFILES DURING RUN, RUN"" ,DDD";Ru
15890 REM NEXT I
15900 DEG
15910 LDIR 90
15920 CSIZE 3
15930 MOVE 0,Y_gdu_max/2
15940 LABEL USING "" "Power (mW), Max. "" M2D.4D";MAX(Power(*))
15950 LORG 4
15960 LDIR 0
15970 MOVE X_gdu_max/2,.07*Y_gdu_max
15980 LABEL "Length of Core (X)"
15990 VIEWPORT .1*X_gdu_max,.99*X_gdu_max,.15*Y_gdu_max,.9*Y_gdu_max
16000 FRAME
16010 WINDOW 0,.100,0,.MAX(Power(*))
16020 AXES 5.0,.1,0,0,5,5,2
16030 CLIP OFF

```

```
16040 CSIZE 2.5,.5
16050 LORG 6
16060 FOR I=0 TO 100 STEP 10
16070  MOVE I,-.1
16080  LABEL USING "#,K";I
16090 NEXT I
16100 LORG 8
16110 FOR I=0 TO MAX(Power(*))
16120  MOVE -.2,I
16130  LABEL USING "#,DD.DD";I
16140 NEXT I
16150 PENUP
16160 FOR K=1 TO 40
16170  FOR L=1 TO 100
16180   PLOT L,Power(K,L)
16190  NEXT L
16200  PENUP
16210 NEXT K
16220 WAIT .1
16230 GRAPHICS OFF
16240 PEN 0
16250 BEEP
16260 STOP
16270 END
```

C.3: Graphical Estimation of the Breakthrough Point

```

10000 REM THIS PROGRAM ESTIMATES BREAKTHROUGH POINT GRAPHICALLY
FROM
10010 REM FLUID RECOVERY DATA.
10020 REM AUTHOR: HEMANTA KUMAR SARMA
10030 REM      DEPT. OF MINING, MET. AND PETROLEUM ENGINEERING
10040 REM      UNIVERSITY OF ALBERTA, EDMONTON, CANADA, T6G 2G6
10050 REM *****DIMENSIONALISING OF VARIABLES*****
10060 OPTION BASE 1
10070 INTEGER I,J,K,N,H,M,L
10080 DIM Wgt(150),Tb(150),Ddwt(150)
10090 REM *****RETRIEVING DATA FROM THE
FILES*****
10100 REM
10110 INPUT "WANT PLOT ON PAPER OR CRT ? ...1=PAPER ...0=CRT",Ipl
10120 INPUT "ENTER FILENAME FOR DATE AND TIME EXPT. STARTED",Name$
10130 ASSIGN @File5 TO Name$
10140 ENTER @File5;Day$,Tim$,Run$
10150 Ru=VAL(Run$)
10160 INPUT "ENTER FILENAME BALANCE DATA",Name$
10170 ASSIGN @File7 TO Name$
10180 ENTER @File7;Tb(*),Wgt(*)
10190 Wi=Wgt(1)
10200 Ti=Tb(1)
10210 REM PRINT "TB,WT,CALC TIME,PRED TIME FROM DATA"
10220 FOR K=1 TO 150
10230   Tb(K)=Tb(K)-Ti
10240   Wgt(K)=Wgt(K)-Wi
10250 NEXT K
10260 INPUT "NEED ONLY BLOWUP OF A SECTION OF GRAPH? 1=Y,0=N",Ib
10270 IF Ib=1 THEN GOTO 11370
10280 INPUT "GUESS A HIGHER BREAKTHROUGH TIME IN SECONDS",Bt
10290 Ttime=Bt
10300 Twt=MAX(Wgt(*))
10310 DIM Dwt(150)
10320 Dwt(1)=0.
10330 FOR K=2 TO 150
10340   Dwt(K)=(Wgt(K)-Wgt(K-1))/(Tb(K)-Tb(K-1))*100.0
10350 NEXT K
10360 IF Ttime>1500 THEN Ttic=20
10370 IF Ttime<=1500 THEN Ttic=10
10380 Gap=10.0*Ttic
10390 DISP "CHANGE PAPER FOR WEIGHT PLOT"
10400 PAUSE
10410 PEN 4
10420 GINIT
10430 PEN 4
10440 IF Ipl=0 THEN PLOTTER IS CRT,"INTERNAL"
10450 IF Ipl=1 THEN PLOTTER IS 705,"HPGL"
10460 GRAPHICS ON
10470 X_gdu_max=100*MAX(1,RATIO)
10480 Y_gdu_max=100*MAX(1,1/RATIO)
10490 LOG 6

```

```

11060 MOVE X_gdu_max/2,.07*Y_gdu_max
11070 LABEL USING ""Time (sec), Tmax= "",6D.D";Ttime
11080 VIEWPORT .1*X_gdu_max,.98*X_gdu_max,.15*Y_gdu_max,.9*Y_gdu_max
11090 FRAME
11100 WINDOW 0.,Ttime,0.,150
11110 AXES Ttic,1,0,0.5,5,3
11120 AXES Ttic,1,Ttime,150.0,5,5,3
11130 GRID Gap,10,0,0.1,1
11140 CLIP OFF
11150 CSIZE 2.5,.5
11160 LORG 6
11170 FOR I=0 TO Ttime STEP Gap
11180 MOVE I,-.1
11190 LABEL USING "#,K";I
11200 NEXT I
11210 LORG 8
11220 FOR I=0 TO 150 STEP 10
11230 MOVE -.2,I
11240 LABEL USING "#,DD.DD";I
11250 NEXT I
11260 PENUP
11270 PEN 4
11280 FOR K=1 TO 150
11290 IF Tb(K)>Ttime THEN GOTO 11320
11300 PLOT Tb(K),Wgt(K)
11310 NEXT K
11320 PEN 0
11330 GRAPHICS OFF
11340 BEEP
11350 INPUT "DO YOU WANT TO BLOWUP ANY INTERVAL ? ...1=Y ...0=N",Iblow
11360 IF Iblow=0 THEN GOTO 11920
11370 INPUT "IS IT A TRIAL ON CRT ? ...1=Y, ...0=N",Itry
11380 INPUT "BLOWUP ... FROM TIME",Tblo1
11390 INPUT "BLOWUP ... TO TIME",Tblo2
11400 INPUT "BLOWUP ... FROM WEIGHT",Wblo1
11410 INPUT "BLOWUP ... TO WEIGHT",Wblo2
11420 DISP "CHANGE PAPER FOR WEIGHT PLOT"
11430 PAUSE
11440 PEN 4
11450 GINIT
11460 PEN 4
11470 IF Itry=1 THEN PLOTTER IS CRT,"INTERNAL"
11480 IF Itry=0 THEN PLOTTER IS 705,"HPGL"
11490 GRAPHICS ON
11500 X_gdu_max=100*MAX(1,RATIO)
11510 Y_gdu_max=100*MAX(1,1/RATIO)
11520 LORG 6
11530 MOVE X_gdu_max/2.5,Y_gdu_max
11540 LABEL USING ""Estimation of BT; Run"" ,DDD";Ru
11550 DEG
11560 LDIR 90
11570 CSIZE 3.5
11580 MOVE 0,Y_gdu_max/2
11590 LABEL "Fluid Recovered (gm)"
11600 LORG 4
11610 LDIR 0

```

```
11620 MOVE X_gdu_max/2.5,.07*Y_gdu_max
11630 LABEL "Time (sec)"
11640 VIEWPORT .15*X_gdu_max,.70*X_gdu_max,.15*Y_gdu_max,.9*Y_gdu_max
11650 FRAME
11660 WINDOW Tblo1,Tblo2,Wblo1,Wblo2
11670 AXES 1,..25,Tblo1,Wblo1,5,4,2
11680 AXES 1,..25,Tblo2,Wblo2,5,4,3
11690 GRID 25,5,Tblo1,Wblo1,1,1
11700 CLIP OFF
11710 CSIZE 2.5,.5
11720 LORG 6
11730 FOR I=Tblo1 TO Tblo2 STEP 25
11740 MOVE I,Wblo1-.25
11750 LABEL USING "#,K":I
11760 NEXT I
11770 LORG 8
11780 FOR I=Wblo1 TO Wblo2 STEP 5
11790 MOVE Tblo1-.2,I
11800 LABEL USING "#,DDD.D":I
11810 NEXT I
11820 PENUP
11830 PEN 4
11840 FOR K=1 TO 150
11850 IF Tb(K)<Tblo1 THEN GOTO 11880
11860 IF Tb(K)>Tblo2 THEN GOTO 11890
11870 PLOT Tb(K),Wgt(K)
11880 NEXT K
11890 PEN 0
11900 GRAPHICS OFF
11910 BEEP
11920 STOP
11930 END
```

APPENDIX D: Program to Evaluate Saturation at the Front, S_{wf}

```

C THIS PROGRAM ESTIMATES THE SATURATION AT THE
C FRONT i.e.  $S_{wf}$ , FROM  $f_w$  VERSUS  $S_{w2}$  PLOT.
C IT EVALUATES THE POINT OF TANGENCY.
C .....
C DEFINITIONS:
C SW = WATER SATURATION
C SM = MAXIMUM WATER SATURATION
C SI = IRREDUCIBLE WATER SATURATION
C TOL = TOLERANCE SET AS CONVERGENCE CRITERION
C XM = VISCOSITY RATIO OF DISPLACED TO DISPLACING FLUID
C C1 =  $dK_{rw}/dS_w$  ... functional form
C C2 =  $dK_{ro}/dS_w$  ... functional form
C C3 =  $d^2K_{ro}/dS_w^2$  ... functional form
C C4 =  $K_{rw}$  i.e. Relative Permeability To water
C      in Functional Form
C AKRO = Relative Permeability to Oil in Functiona Form
C A1, A2, A3, A4 = PARAMETERS IN FUNCTIONAL EQUATION FOR  $K_{ro}$ 
C B1, B2, B3, B4 = PARAMETERS IN FUNCTIONAL EQUATION FOR  $K_{rw}$ 
C .....
C IMPLICIT REAL*8(A-H,O-Z)
C LOGICAL FREE(1)/'.'/
C READ(5, FREE) XM, TOL
C READ(5, FREE) SI, SM
C READ(5, FREE) A1, A2, A3, A4
C READ(5, FREE) B1, B2, B3, B4
C SW = SM
C AKRO = A1*(SM-SW) + A2*(SM**2-SW**2)
C      + A3*(SM**3-SW**3)
C      + A4*(SM**4-SW**4)
C C1 = B1 + SW*(2.0*B2 + SW*(3.0*B3 + 4.0*B4*SW))
C C2 = -A1-SW*(2.0*A2 + SW*(3.0*A3 + 4.0*A4*SW))
C C3 = -2.*A2-SW*(6.*A3 + 12.*A4*SW)
C C4 = B1*(SW-SI) + B2*(SW**2-SI**2)
C      + B3*(SW**3-SI**3)
C      + B4*(SW**4-SI**4)
C DBETA = B2 + B3*(2.*SW + SI) +
C      + B4*(3.*SW**2 + 2.*SW*SI + SI**2)
C C5 = C2/C4
C GA1 = -C2/XM
C DGAM1 = -C3/XM + C5*C1/XM + C5*C2/XM**2
C DF1 = DGAM1 - DBETA
C DO 400 I=1,400
C X = B1*(SW-SI) + B2*(SW**2-SI**2)
C      + B3*(SW**3-SI**3)
C      + B4*(SW**4-SI**4)
C Y = A1*(SM-SW) + A2*(SM**2-SW**2)
C      + A3*(SM**3-SW**3)
C      + A4*(SM**4-SW**4)
C Z = XM*X + Y
C F = XM*X/Z
C DKRW = B1 + SW*(2.0*B2 + SW*(3.0*B3 + 4.0*B4*SW))

```

```
DKRO = -A1-SW*(2.0*A2+SW*(3.0*A3+4.0*A4*SW))
XX=Y*DKRW-X*DKRO
GAMMA=XX/Z
BETA=B1+B2*(SW+SI)+
  * B3*(SW**2+SW*SI+SI**2)+
  * B4*(SW**3+SW**2*SI+SW*SI**2+SW**3)
FS=GAMMA-BETA
SWN=SW-FS/DF1
DIFF=DABS(SWN-SW)
IF (DIFF-TOL) 20,20,400
20  WRITE(6,23)I,SW,F
    GO TO 401
400  SW=SWN
     WRITE(6,24)I
24   FORMAT('SORRY, DOES NOT CONVERGE EVEN AFTER ',14,' ITERATIONS')
23   FORMAT('SOLN CONVERGES AT ITERATION ',14,' AND SWF IS ',
  * F6.3,2X,' AT FW = ',F6.3)
401  STOP
     END
```

APPENDIX E: Typical Routine for Use of BMDP Statistical Package

```
/PROB TITLE IS 'FITTING OF CUM. OIL RECOVERY VS TIME'.  
/INPUT VARIABLES ARE 2.  
MTSFILE IS 'DATAFILE'.  
FORMAT IS FREE.  
/VARIABLE NAMES ARE TIME,QO.  
/REGRESS DEPENDENT IS QO.  
PARAMETERS ARE 6.  
ITER=200.  
CONV=0.0001.  
TOL=0.0001.  
/PARAMETER NAMES ARE B,TM,A2,A3,A4,A5.  
INITIAL ARE .865,34284.,2457894.7,-1125.95,.2,.000003.  
MINIMUM ARE .69,30278.  
MAXIMUM ARE .95,48000.  
PRINT.  
/FUN F=PV*(3.*A2/TM**2-A2/TIME**2+2.*A3/TM-A3/TIME  
+A4*(1+LN(TIME)-LN(TM))-(2.*A2/TM**3+A3/TM**2+A5+A4/TM)*  
TIME+B+A5*(TM+TIME*(LN(TIME)-LN(TM)))).  
/PLOT RESIDUAL.  
VARIABLE ARE TIME,QO.  
NORMAL.  
DNORMAL.  
/END
```

Note: PV denotes pore volume of the sandpack in the coreholder in cubic centimetres. Exact numerical value of the pore volume must be used when running the program.

END

04.01.89

FIN